EFFECT OF NEARSHORE STRUCTURES ON REDUCTION OF WAVE ENERGY ALONG DIFFERENT LOCATON'S OF COASTLINE OF BANGLADESH

MD.TAWHIDUR RAHAMAN

DEPARTMENT OF WATER RESOURCES ENGINEERING
BANGLADESH UNIVERSITY OF ENGINEERING AND TECHNOLOGY
DHAKA-1000, BANGLADESH

SEPTEMBER 2019

EFFECT OF NEARSHORE STRUCTURES ON REDUCTION OF WAVE ENERGY ALONG DIFFERENT LOCATON'S OF COASTLINE OF BANGLADESH

Submitted By

Md.Tawhidur Rahaman

(Roll No. 0413162066 P)

In partial fulfillment of the requirements for the degree of

MASTER OF SCIENCE IN WATER RESOURCES ENGINEERING

DEPARTMENT OF WATER RESOURCES ENGINEERING

BANGLADESH UNIVERSITY OF ENGINEERING AND TECHNOLOGY

Dhaka-1000, Bangladesh

September 2019

CERTIFICATION OF APPROVAL

The thesis titled "Effect of nearshore structures on reduction of wave energy along different location's of coastline of Bangladesh" submitted by Md. Tawhidur Rahaman, Roll No: 0413162066 P, Session: April/2013, has been accepted as satisfactory in partial fulfillment of the requirements for the degree of **Master of Science in Water Resources Engineering** on 28th September,2019.

BOARD OF EXAMINERS

....

Dr.Umme Kulsum Navera Professor Department of WRE, BUET, Dhaka (Supervisor)	Chairman

....

Dr. Anika Yunus Professor & Head Department of WRE, BUET, Dhaka	Member (Ex-officio)

....

Dr. Md. Sabbir Mostafa Khan Professor Department of WRE, BUET, Dhaka	Member

....

Md. Zahirul Haque Khan Director Coast, Port & Estuary Division Institute of Water Modelling (IWM) House #496, Road #32, New DOHS, Mohakhali, Dhaka-1206	Member (External)

DECLARATION

I do hereby declare that this Thesis work entitled “Effect of nearshore structures on reduction of wave energy along different location’s of coastline of Bangladesh” has been done by me under the supervision of Dr. Umme Kulsum Navera, Professor, Department of Water Resources Engineering, Bangladesh University of Engineering and Technology, Dhaka. and any part of it has not been accepted elsewhere for the award of any degree or diploma from any other institution.

Signature of the Candidate

Md. Tawhidur Rahaman

TABLE OF CONTENTS

Page No.

TABLE OF CONTENTS	**IV**
LIST OF FIGURES	**VII**
LIST OF TABLES	**XI**
LIST OF ABBREVIATIONS	**XII**
ACRONYMS AND ABBREVIATIONS	**XIII**
ACKNOWLEDGEMENT	**XIV**
ABSTRACT	**XV**
CHAPTER ONE INTRODUCTION	
1.1 Background of the Study	1
1.2 Scope of the Study	2
1.3 Objective of the Study	3
1.4 Organization of the Thesis	4
CHAPTER TWO LITERATURE REVIEW	
2.1 General	5
2.2 Nearshore Hydrodynamic Related Study	5
2.3 Wave, Current and Sediment Related Study in Nearshore Area	7
2.4 Structural Intervention at Nearshore Related Study Around the World	9
2.5 Numerical Model-Based Study at Nearshore Area	13
2.6 Mathematical Modeling Based Study on the Bay of Bengal	14
2.7 Structural Intervention at Nearshore in the Bay of Bengal	18
2.8 Summary	20
CHAPTER THREE THEORY AND METHODOLOGY	
3.1 General	21
3.2 Nearshore Hydrodynamic	21
3.2.1 Waves in the Nearshore Area	21
3.2.2 Currents in the Nearshore Area	23
3.2.3 Sediment Transport in the Surf Zone	24

3.3 Theory of Hydrodynamics 29

3.3.1 Wave Hydrodynamics 29

3.3.2 Sediment Transport and Morphology 31

3.3.3 Nearshore Hydraulic Structures 32

3.3.4 Propagation through Breakwater and Groins 34

3.4 Governing Equation for Nearshore Hydrodynamics 35

3.5 Application of Mathematical Model 40

3.5.1 Application of Delft3D Model 40

3.5.2 Grid and Coordinates 40

3.5.3 Boundary Conditions 42

3.5.4 Stability and Accuracy 43

3.6 Methodology of the Study 44

3.6.1 Data collection 45

3.7 Summary 56

CHAPTER 4 STUDY AREA AND MODEL SETUP

4.1 General 57

4.2 Study Area 57

4.2.1 Site 1 along Cox-Bazar Marine Drive Road (Kalatoli to Hatchary Para) 61

4.2.2 Site 2 along Cox-Bazar Marine Drive Road (Near Himchari) 62

4.3 Development of FLOW-WAVE Coupled Bay of Bengal Model 63

4.4 Key variables of Breakwater during design consideration 64

4.5 Key variables of Groins during design consideration 65

4.6 Breakwater and Groins Parameters 65

4.7 Mathematical Model Setup 71

4.7.1 Hydrodynamic Model 73

4.7.2 Wave Model 77

4.8 Summary 79

CHAPTER 5 RESULTS AND DISCUSSIONS

5.1 General 80

5.2 Calibration and Validation of FLOW Model 80

5.3 Calibration and Validation of WAVE Model 94
5.4 Simulation of different structural options 99
5.4.1 Case 1 (Series of Breakwater in Site 1) 101
5.4.2 Case 2 (Series of Groin in Site 1) 105
5.4.3 Case 3 (Series of Breakwater in Site 2) 110
5.4.4 Case 4 (Series of Groin in Site 2) 115
5.5 Summary of the Results 120

CHAPTER 6 CONCLUSIONS AND RECOMMENDATIONS
6.1 General 122
6.2 Conclusions of the Study 122
6.3 Recommendations for Future Study 123

REFERENCES 125
APPENDIX A 133

LIST OF FIGURES

Figure No. **Title** **Page No.**

Figure 1.1: Location of Bay of Bengal (Source: Google Map) 1

Figure 3.1: Nearshore circulation system showing the rip currents 24

Figure 3.2: An example of a vertical grid 41

Figure 3.3: Staggered grid used in Delft3D (Source: Lesser et al. 2004) 41

Figure 3.4: m and n are the computation number of the grids 42

Figure 3.5: velocity (u, v & w) points and water level (Source: Lesser et al. 2004) 42

Figure 3.6: Delft3D FLOW-WAVE Coupled Model Flow chart for the study 44

Figure 3.7 : Data extraction location at Bay of Bengal 48

Figure 3.8 : Wind rose for the month of May,2007 for calibration 49

Figure 3.9: Wind rose for the month of October,2007 for calibration 49

Figure 3.10 : Wind rose for the month of May,2008 for validation 50

Figure 3.11: Wind rose for the month of October,2008 for validation 50

Figure 3.12: Wave rose for the month of May,2007 for calibration 51

Figure 3.13: Wave rose for the month of October,2007 for calibration 51

Figure 3 14: Wave rose for the month of May,2008 for validation 52

Figure 3.15: Wave rose for the month of October,2008 for validation 52

Figure 3.16: Annual wind rose of Cox's Bazar (Source: IWM, 2012) 53

Figure 3.17: Annual wave rose showing deep and shallow water wave height by 54

Figure 3.18: Annual wave rose to showing deep and shallow water 54

Figure 4.1: Bay of Bengal Model Boundary with Bathymetry 58

Figure 4.2: Study areas along the Cox-Bazar Marine Drive 59

Figure 4.3: Local protection measures due to erosion at Hatcharipara, Cox-Bazar 61

Figure 4.4: Selected location for study along Cox Bazar coastline (Site 1) 61

Figure 4.5: Damaged protection system at Himchari point, Cox-Bazar 62

Figure 4.6: Selected location for further investigation (Site 2) 62

Figure 4.7: Used Flow-Wave couple system in Delft3D 63

Figure 4.8: Plan view of nearshore breakwater scheme (Source: DEFRA, 2010) 64

Figure 4.9: Section view of nearshore breakwater scheme 64

LIST OF FIGURES

Figure No.	Title	Page No.
Figure 4.10:	Different key variable from the plan view	65
Figure 4.11:	Different key variable from section view in the functioning of groins	65
Figure 4.12:	Design parameters of Breakwaters at Site 1	69
Figure 4.13:	Design parameters of Groins at Site 1	70
Figure 4.14:	Design parameters of Breakwaters at Site 2	70
Figure 4.15:	Design parameters of Groins at Site 2	71
Figure 4.16:	Online modelling scheme at Delft3D (Source: Roelvink 2006)	72
Figure 4.17:	Grid and bathymetry of Bay of Bengal Model (1800m × 1800m)	73
Figure 4.18:	Grid and bathymetry of the study area (10m×10m) site-1	73
Figure 4.19:	Grid and bathymetry of the study area (10m×10m) site-2	74
Figure 4.20:	Bathymetry of Bay of Bengal from Delft3D model	74
Figure 5.1:	Calibration and validation Locations in Bay of Bengal	82
Figure 5.2:	Calibration point for Chattogram IHO at Bangladesh (May 2007)	83
Figure 5.3 :	Calibration point for Chattogram IHO at Bangladesh (October 2007)	83
Figure 5.4:	Calibration point for Passur river at Bangladesh (May 2007)	84
Figure 5.5:	Calibration point for Passur river at Bangladesh (October 2007)	84
Figure 5.6:	Calibrated point for Akyab at Myanmar (May 2007)	85
Figure 5.7:	Calibrated point for Akyab at Myanmar (October 2007)	85
Figure 5.8:	Calibrated point for Short Island at India (May 2007)	86
Figure 5.9:	Calibrated point for Short Island at India (October 2007)	86
Figure 5.10:	Calibrated point for Sibsa, Bangladesh (May 2007)	87
Figure 5.11:	Calibrated point for Sibsa, Bangladesh (October 2007)	87
Figure 5.12:	Validation for Chattogram IHO at Bangladesh (May 2008)	89
Figure 5.13:	Validation for Chattogram IHO at Bangladesh (October 2008)	89
Figure 5.14:	Validation for Passur river at Bangladesh (May 2008)	90
Figure 5.15:	Validation for Passur river at Bangladesh (October 2008)	90
Figure 5.16:	Validation for Akyab at Myanmar (May 2008)	91
Figure 5.17:	Validation for Akyab at Myanmar (October 2008)	91
Figure 5.18:	Validation for Short Island at India (May 2008)	92

LIST OF FIGURES

Figure No.	Title	Page No.
Figure 5.19:	Validation for Short Island at India (October 2008)	92
Figure 5.20:	Validation point for Sibsa at Bangladesh (May 2008)	93
Figure 5.21:	Validation point for Sibsa at Bangladesh (May 2008)	93
Figure 5.22:	Calibration and Validation point for wave model	94
Figure 5.23:	Wave calibration for point 1(May 2007)	95
Figure 5.24:	Wave calibration for point 1 (October 2007)	95
Figure 5.25:	Wave calibration for point 2 (May 2007)	96
Figure 5.26:	Wave calibration for point 2 (October 2007)	96
Figure 5.27:	Validation of wave model for Point 1 (May 2008)	97
Figure 5.28:	Validation of wave model for Point 1 (October 2008)	98
Figure 5.29:	Validation of wave model for Point 2 (May 2008)	98
Figure 5.30:	Validation of wave model for Point 2 (October 2008)	99
Figure 5.31:	Area map of site 1 and site 2 along the Cox-Bazar coastline	100
Figure 5.32:	Series of Breakwater at Site 1 along Cox-Bazar coast	101
Figure 5.33:	Wave Height Change Analysis for Site 1 with series of Breakwater	102
Figure 5.34:	Wave Energy Change Analysis for Site 1 with series of Breakwater	103
Figure 5.35:	Erosion and Sedimentation at Site 1 Breakwater (May 1- 7, 2008)	103
Figure 5.36:	Erosion and Sedimentation at Site 1 Breakwater (May 8-14,2008)	104
Figure 5.37:	Erosion and Sedimentation at Site 1 Breakwater (May15-21,2008)	104
Figure 5.38:	Erosion and Sedimentation at Site 1 Breakwater (May22-28,2008)	105
Figure 5.39:	Series of Groin at Site 1 along Cox-Bazar coast	106
Figure 5.40:	Wave Height Change Analysis for Site 1 with series of Groin	107
Figure 5.41:	Wave Energy Change Analysis for Site 1 with series of Groin	108
Figure 5.42:	Erosion and Sedimentation at Site 1 Groin (May 1- 7, 2008)	108
Figure 5.43:	Erosion and Sedimentation at Site 1 Groin (May 8-14,2008)	109
Figure 5.44:	Erosion and Sedimentation at Site 1 Groin (May15-21,2008)	109
Figure 5.45:	Erosion and Sedimentation at Site 1 Groin (May22-28,2008)	110
Figure 5.46:	Series of Breakwater at Site 2 along Cox-Bazar coast	111
Figure 5.47:	Wave Height Change Analysis for Site 2 with series of Breakwater	112

LIST OF FIGURES

Figure No. **Title** **Page No.**

Figure 5.48: Wave Energy Change Analysis for Site 2 with series of Breakwater 113

Figure 5.49: Erosion or Sedimentation at Site 2 Breakwater (May 1-7, 2008) 113

Figure 5.50: Erosion or Sedimentation at Site 2 Breakwater (May 8-14, 2008) 114

Figure 5.51: Erosion or Sedimentation at Site 2 Breakwater (May 15-21, 2008) 114

Figure 5.52: Erosion or Sedimentation at Site 2 Breakwater (May 22-28,2008) 115

Figure 5.53: Series of Groin at Site 2 along Cox-Bazar coast 116

Figure 5.54: Wave Height Change Analysis for Site 2 with series of Groin 117

Figure 5.55: Wave Energy Change Analysis for Site 2 with series of Groin 118

Figure 5.56: Erosion or Sedimentation at Site 2 Groin (May 1-7, 2008) 118

Figure 5.57: Erosion or Sedimentation at Site 2 Groin (May 8-14, 2008) 119

Figure 5.58: Erosion or Sedimentation at Site 2 Groin (May 15-21, 2008) 119

Figure 5.59: Erosion or Sedimentation at Site 2 Groin (May 22-28,2008) 120

LIST OF TABLES

Table No.	Title	Page No.
Table 3.1: Overview of types of hydraulic structures in Delft3D		33
Table 3.2: List of coefficients α, β value according to shape of the dam		35
Table 3.3: Data sources for generating the bathymetry		46
Table 3.4: shoreline data used for generating the model		46
Table 3.5: Tidal water level and Discharge data		47
Table 3.6: Latitude and Longitude of Boundary Station Locations		55
Table 3.7: Tidal Constituents at Vishakhapatnam		55
Table 3.8: Tidal Constituents at GWA Bay		55
Table 3.9: Properties of Sediments from the Bay of Bengal		56
Table 4.1: Changes in shoreline in different locations at Cox-Bazar marine drive		60
Table 4.2: Basic data for determining the breakwater parameters		66
Table 4.3: Physical parameters used in Delft3D Flow module		76
Table 4.4: Numerical parameters used in Delft3D Flow		77
Table 4.5: Physical parameters used in SWAN		78
Table 4.6: Summarizes the settings used for the numerical parameters in SWAN.		79
Table 5.1: Calibration and Validation Points along the Bay of Bengal		81
Table 5.2: Calibration and Validation point for wave model		94
Table 5.3: Wave Height Change along site 1 with series of Breakwater		101
Table 5.4: Wave Energy Change Analysis along site 1 with series of Breakwater		102
Table 5.5: Wave Height Change along the Site 1 with series of Groin		106
Table 5.6: Wave Energy Change Analysis along Site 1 with series of Groin		107
Table 5.7: Wave Height Change along the Site 2 with series of Breakwater		111
Table 5.8 :Wave Energy Change Analysis along Site 2 with series of Breakwater		112
Table 5.9 : Wave Height Change along Site 2 with series of Groin		116
Table 5.10: Wave Energy Change Analysis along Site 2 with series of Groin		117

LIST OF ABBREVIATIONS

K_s	Shoaling coefficient
C_{g0}	Deep-water wave height
α_0	Group velocity
ρ	Mass density of the water
ρ_s	Mass density of the sediment grains
U_c	Mean direction current
H_b	Breaking wave height
ε	Sea surface elevation
$\rho_w \& \rho_\sigma$	Air and water density respectively (kg /m3),
Ω	Coriolis parameter
C_w	Wind speed
H	Water depth (m).
H_s	Significant wave height
g	Acceleration due to gravity (9.81 m2/s)
L_0	Wave length at deep water
M	Manning number
C	Chezy number
P_0	Atmospheric pressure (kg/m/s2).
R_e	Reynolds‘s number
T	*t* Time (s), x and y (m) are Cartesian Co-ordinate (s).
W	Wind speed (m/s).

ACRONYMS AND ABBREVIATIONS

ADI	Alternate Direction Implicit
BBS	Bangladesh Bureau of Statistics
BoB	Bay of Bengal
BMD	Bangladesh Meteorological Department
BODC	British Oceanographic Data Centre
BTM	Bangladesh Transverse Mercator
BWDB	Bangladesh Water Development Board
BIWTA	Bangladesh Inland Water Transport Authority
BWDB	Bangladesh Water Development Board
CEM	Coastal Engineering Manual
CEIP	Coastal Embankment Improvement Project
CERP	Coastal Embankment Rehabilitation Project
CPP	Cyclone Protection Project
CSPS	Cyclone Shelter Preparatory Study
CFSR	Climate Forecast System Reanalysis
DIVAST	Depth Integrated Velocity and Solute Transport
DHI	DHI Water & Environment
DANIDA	Danish International Development Agency
DEFRA	Department for Environment, Food and Rural Affairs
DRR	Disaster Risk Reduction
DHI	Danish Hydraulic Institute
FVCOM	finite-volume community ocean model
FF&WC	Flood Forecasting and Warning Center
GBM	Ganges-Brahmaputra- Meghna
GIS	Geographic Information System
GEBCO	General bathymetric chart of the oceans
IHB	International Hydrographic Bureau
IWM	Institute of Water Modelling
IPCC	Intergovernmental Panel on Climate Change
IHO	International Hydrographic Organization
MoEF	Ministry of Environment, Forest and Climate Change
MSL	Meal Sea Level
NGA	National Geospatial-Intelligence Agency
NOAA	National Oceanic and Atmospheric Administration
NCEP	National Centers for Environmental Prediction
NDVI	Normalized Difference Vegetation Index
SWAN	Simulating WAves Nearshore
SLR	Sea Level Rise
SIDR	Cyclone Sidr
UTM	Universal Transverse Mercator
WVS	World Vector Shoreline

ACKNOWLEDGEMENT

The author would like to mention with gratitude Almighty Allah for giving him the ability to complete this research work.

The author expressed his sincere gratitude and thanks to his honorable supervisor, Dr. Umme Kulsum Navera, Professor, Department of Water Resources Engineering (WRE), Bangladesh University of Engineering and Technology (BUET), Dhaka, for her continuous guidance, constant support, supervision, inspiration, advice, infinite patience and enthusiastic encouragement throughout this research work.

The author is also indebted to the member of the Board of Examination namely Dr. Anika Yunus, Professor and Head, Department of WRE, BUET, Dr. Md. Sabbir Mostafa Khan, Professor, Department of WRE, BUET and Mr. Md. Zahirul Haque Khan, Director, Coast Port and Estuary Management Division, Institute of Water Modelling (IWM) for their valuable comments and constructive suggestions regarding this study.

The author is highly gratitude to Dr. Md. Khairul Islam, Regional Country Director, WaterAid; Hasin Jahan, Country Director, WaterAid; Md. Saiful Islam, Associate Specialist, Coast, Port & Estuary Management Division, IWM for their motivation, constants encouragement and appreciation. Additionally, the author is thankful to IWM, BWDB, DHI for providing the necessary data for this study.

The author would like to express a very special indebtedness to his parents and his family whose encouragement and support was a continuous source of inspiration for this work.

Finally, the author likes to express his sincere gratitude to all other teachers and members of the Water Resources Engineering Department, BUET, for their cooperation and help in the successful completion of the work.

ABSTRACT

The natural shape of Bangladesh coastal and marine areas is controlled by dynamic processes such as tides, wave actions, strong winds and it faces continuous land erosion and accretion. This study prioritizes the most vulnerable locations on the Bangladesh coast and finally selected the two most erosion-prone areas at the Cox Bazar coastline along the marine drive. Although there are few measures have been taken by the local authority using geotubes, tetrapods, and concrete block, but this does not stand appropriately against wave action; as a result, all previous measures are futile. This study is based on mathematical modeling to simulate the nearshore complex hydrodynamic and wave conditions. To analysis, the real-world nearshore scenarios, a two-dimensional model named Delft3D is used to set up the Bay of Bengal model. The coupled model is fully calibrated and validated to simulate the nearshore structures to examine the wave height, wave energy reduction rate with associated sediment transport patterns in the structures' vicinity. A series of Breakwater and Groins have been used at two different sites along the Cox Bazar coastline.

The analysis shows that at site one, which is 1.7 km, Breakwaters are less capable of trapping sediment. The intervened series of Breakwater has a wave height reduction rate between 27 % - 53 %, wave energy reduction rate between 47%-78% and two of the Breakwater shows continuous erosion among three. On the other hand, series of Groin has wave height reduction rate between 9 % - 76 %, wave energy reduction rate between 17%-91%, and six groins shows continuous sedimentation within seven where one Groin shows continuous erosion. The analysis from site two, which is about 3 km shows, Groins are more capable of trapping sediment compare to Breakwater. The series of Breakwater at site two has a wave height reduction rate between 30 % -53 %, wave energy reduction rate 51% -78%, and all the eleven Breakwater shows continuous erosion; whereas, a series of Groin has wave height reduction rate between 15% - 53 %, wave energy reduction rate 51% -78%, and eleven groins show continuous sedimentation within thirteen where two Groin shows erosion. Moreover, the beach and sea view are also very important for the study areas, and Groins can be the best solution where no sand nourishment is required for long-term sustainability. This study is one of the first in Bangladesh to examine the nearshore structural intervention with Breakwater and Groin, can be used as a reference for field implementation or further research work.

CHAPTER ONE

INTRODUCTION

1.1 Background of the Study

The 710 km coastline of Bangladesh is very dynamic with estuarine and sandy beaches. The country is also vulnerable to sea-level rise due to climate change, natural disasters like cyclones, and storm surges (Nasreen et al.,2013). Understanding the fundamentals of the complex phenomena is of the greatest importance for near-shore hydrodynamics and shoreline protection. The coastal area represents 47,201 km², which is about 32% of Bangladesh's total geographical area (BBS, 2011; MoEF, 2007. In terms of administrative consideration, 19 districts out of 64 are considered coastal districts (BBS, 2011; MoEF, 2007). About 10% of the country is 1 m above the mean sea level, and one-third is under tidal excursions (Ali, 1999). The country covers three discrete coastal regions - western, central, and eastern coastal zones. The western part is known as the Ganges tidal plain, where the average land elevation is below 1.5 m of MSL. The southwestern part of the region is covered by the world's largest mangrove forest (6017 km²), popularly known as Sundarbans. The central region is the most active one, and this area suffers from continuous erosion and accretion (Karim and Mimura, 2006).

Figure 1.1: Location of Bay of Bengal (Source: Google Map)

The natural shape of Bangladesh coastal and marine areas is controlled by dynamic processes such as tides, wave actions, strong winds, and sea-level variations. Over the last two centuries, enormous changes have taken place due to continuous land erosion and accretion along the coastline. Most of the erosion of the Bay of Bengal front was due to storm surges and continuous wave actions (Ahmed, 1999). The people in the coastal area are increasing, and they are the worst victims of these phenomena.

A recent study by (Mahamud and Takewaka, 2018) analyzed the erosion problem at Cox Bazar coast with digitalizing Landsat images of the shoreline positions for a 44-year (1972–2016) period and found sand spit growing in a northward direction from 2000 to 2015; the adjacent erosion area extended in the same direction. Another study was done by IWM (2012) for the planning and design of protective work of the Cox Bazar marine drive, which experienced severe erosion due to sea wave action. In that study, it is found that the significant reason for the erosion of marine drive due to wave action. It is also evident from their model result that the net sediment transport along the Marine Drive is about 500,000 m^3/yr towards the North. Another evidence-based study was done by (Navera and Ahmed, 2018), where they analyzed the remote sensing data to find out shoreline shifting in the Cox Bazar marine drive through open-source Landsat images from 1980 to 2017. They found an average change of shoreline up to 120 m erosion and 100 m deposition in different locations. To reduce the wave energy by placing nearshore structure is the most significant importance for coastal protection. At the same time, it also associates with the reduction of wave height and sediment change patterns. This study will focus on the most significant location in the coastline of Bangladesh for observing nearshore complex coastal systems.

1.2 Scope of the Study

Among the three coastal regions, the most significant location due to coastal erosion is Cox Bazar which located at south eastern part of Bangladesh. The longest uninterrupted sea beach is facing continuous erosion due to high wave action and the marine drive road is under vulnerable situation. This road has enormous importance because of livelihood of the local people is mostly depending on sea fishing, salt cultivation, aquaculture, and tourism where all of these activities lies around that area. The socio-economic condition of the area solely depends on the connectivity of the road. Few points like Harchery para, Himchari and Inani beach area is under continuous threat due to continuous erosion problem. Nearly one kilometer in length road was completely washed out near Kalatoli due to severe wave action during a storm surge event. Different structural intervention like revetment and concrete blocks are the only protecting measures taken earlier along the shoreline but after long time it shows no improvement where the functionality of the protection systems damaged every year due to high wave action. It is very much important to understand the nearshore flow wave conditions before intervening any structural measures. In this work, a coupled Delft3D-Flow Wave model has been used to simulate different nearshore structures on reduction of wave energy along with the changes of wave height and sediment transport. The Delft3D-Flow Wave model is tested by different research works (Vlijm, 2011; James and Dykes, 2008) and also widely used in large coastal projects. A fully calibrated and validated Bay of Bengal model has been developed and different nearshore structures (Breakwater and Groin) also incorporated in the model for observing the wave energy reduction trend with explore the erosion control measures. There is huge knowledge gap of structural interventional work in a calibrated model where very few works have been done worldwide. Finally, this work can contribute to the decision maker for resolving the erosion problem at Cox Bazar marine drive as well as it can be a valuable reference work for other erosion prone coastal part of Bangladesh.

1.3 Objective of the Study

The main objective of this study is to develop a Delft3D Coupled hydrodynamic and wave model for the Bay of Bengal that is capable of simulating nearshore wave height and sediment transport patterns from deep water condition.

The specific objectives are:

1. To set up the Bay of Bengal Model by using Delft3D model with proper calibration and validation
2. To assess the decrease in wave height and wave energy by placing different hydraulic structures at different location of Cox’s Bazar coast in Bangladesh
3. To observe the changes in sediment transport in the vicinity of the hydraulic structures at different location of Cox’s Bazar coast in Bangladesh

Based on the above objectives of the study the possible outcomes of the research work are as follows:

1. Generated wave heights from the Delft3D (Bay of Bengal) model at different location of Cox's Bazar coast in Bangladesh;
2. Wave height reduction by placing different structures at different points along Cox's Bazar coastline;
3. Changes in sediment transport pattern by placing different structures at different points along Cox's Bazar coastline.

1.4 Organization of the Thesis

Considering literature review, location of the study area, theories related to the nearshore hydrodynamic, wave hydrodynamics, mathematical modeling, data analysis, model calibration, results and discussions the thesis has been organized under six chapters which are described below:

Chapter One describes the background, highlights the objectives of the study and contains organization of the thesis.

Chapter Two explain the literature review on nearshore hydrodynamics, nearshore waves, sediment transport, and coastal protection-related study.

Chapter Three delineate the basic theory of hydrodynamic for the near-shore zone, wave hydrodynamics, sediment transport, hydraulic structure, wave transformations and structure of the model. Additionally, methodology of the total work, development of the Bay of Bengal model has been also included in this chapter.

Chapter Four outline the study area, mathematical model setup (flow and wave model), development of structural intervention scenarios.

Chapter Five depict the model calibration and validation for hydrodynamic and wave modeling. Simulation of different options for marine drive protection, breakwater, and groins at different location considering nearshore environment at the vicinity of the breakwaters and groins are included in this chapter.

Chapter Six provides the overall conclusions of the study, research gaps, and recommendations for further study.

CHAPTER TWO

LITERATURE REVIEW

2.1 General

The Bay of Bengal (BoB) is a semi-enclosed tropical basin in the northern Indian Ocean (Nasreen, et al.,2013). It experiences seasonal changes in circulation and weather due to the seasonally reversing monsoons. The Bay of Bengal is activated by the cyclonic winds and storms, which causes damages in nearshore coastal areas during and after the events. Coastal erosion and accretion in nearshore areas are the major phenomena. On the other hand, sea-level rise because of climate warming, and the greenhouse effect is extremely severe for low-lying coastal areas. Bangladesh is lying in the most vulnerable low laying areas in this region, and the projected worldwide rise of sea level can cause a severe threat to the coastal areas. The increase in the sea level would inundate Bangladesh's low-lying areas, destroy coastal marshes and swamps, erode shoreline, cause coastal flooding, and increase the rivers' salinity, bay, and aquifers. It is important to know the nearshore coastal hydrodynamics before applying any measures in coastal protection. Several studies have been carried worldwide to explore the nearshore hydrodynamic, wave, current, sediment characteristics, and numerical models. In this chapter, some previous studies have been reviewed, which are related to the present research work.

2.2 Nearshore Hydrodynamic Related Study

Linta (2015) examined the tidal prediction for the intricate waterways in Bangladesh. The region of interest is the head Bay of Bengal region located along the east coast of India. Preliminary analysis of measured sea-level data indicates that tide gauges located along Bangladesh have research quality data, and therefore that data was used for the study. Station data from seven locations viz; Hiron Point, Khepupara, Charchanga, Chittagong, Khal No.10, Cox's Bazaar, and Teknaf all located in Bangladesh were used for tidal analysis, and thereafter the predictive capability of SLPR2 for one-year period was investigated. There are exceptions at two stations, Teknaf (comprising of 87% observed data) and Khal No.10 (99% of observed data), and the remaining five stations are free from data gaps. In a hydrographic perspective, the Bangladesh region has a complex waterways network, and bottom topography has several detached shoals. Tides enter the Bangladesh coast through two submarine canyons, reaching Hiron Point and Cox Bazaar at almost the same time. Amongst the principal constituents, dominant modes are exhibited by M2 and S2, whose natural oscillation periods are 12 h 25 min, and 12 h, respectively. This study indicates considerable seasonal variation in water level prediction during the monsoon season, attributable to meteorological reasons and excess river discharge, at stations Cox Bazaar and Charchanga. The locations Hiron Point and Khepupara show elevated predicted tides after monsoon onset, indicating the presence of seasonal signature resulting from the large amplitude of the annual tidal component 'Sa.' Residual time series produces the de-tidal water level variations attributed to meteorological effects such as wind, atmospheric pressure, and river discharge.

Alam (2003) studied the tides on the Bangladesh coast, originating in the Indian Ocean. It enters the Bay of Bengal through the two submarine canyons named 'Swatch of No Ground' and 'Burma Trench' and arrives near the 10-fathom contour line at Hiron point Cox's Bazar respectively, at about the same time. The most dominant principle constituents are M2 and S2, whose natural periods of oscillations are 12 hours, 25 minutes, and 12 hours respectively. The north-eastern bay's extensive shallowness gives rise to partial reflections and thereby increases the tidal range and friction distortions concurrently. Large seasonal effects of meteorological origin and the complexity of the non-linear shallow water interaction give rise to a considerable number of higher harmonics. All such higher harmonic terms are needed in predicting tide to make it as nearly representative as possible. Besides numerous inlets, there are six major entrances through which tidal waves penetrate the Bangladesh's waterways system. The major entrances are Pussur entrance, Harin Ghata entrance; Tetulia entrance; Shahbazpur entrance; Hatia river entrance, and Sandwip channel entrance. The strong tide is caused at the north of Sandwip by the shallowness and funnel effect in the Hatia River. The spring range noticed here is more than 7 meters during vernal equinoxes, and at upstream of Sandwip the tidal wave entering the channel sometimes deforms into a bore.

Akhtar (2015), carried out a nearshore hydrodynamic model to simulate the maximum wave height in the nearshore coastline of the Cox's Bazar area in Bangladesh. In this study a two-dimensional hydrodynamic model DIVAST (Depth Integrated Velocity and Solute Transport) has been established based on different parameters like co-efficient of eddy viscosity, Manning roughness coefficient, advective and diffusion co-efficient etc. The DIVAST model is based on FORTRAN programming, and it has a number of modules for different purposes with different sets of equations. The model output consists of wave height, wave direction, celerity, group velocity, and water velocity at a different grid point in the study area of Bay of Bengal. The output from the mathematical model DIVAST showed very good agreement with the measured data. These simulated results can be used for the nearshore wave climate around the area.

Hossain (2001) observed that the tides in the coastal and estuarine areas are semidiurnal with two high and two low periods per day and have a maximum amplitude of 3-4 m at spring tide. The tidal activity is an important mechanism for the movement of water and nutrients especially in the estuarine areas, and this is probably a reason for the wide range of biodiversity in the estuarine water. The tidal range and river discharge are responsible for the extension of the estuarine environment in the sea. The variation of tide level in the coastal areas may be attributed to the depth of the bay and varying topography of coastal water. It is found from the study that, the tide penetrates up to 170 km in the south-west and 0-50 km in the south-east area of Bangladesh during lean period (April-May) depending on the topography and channels in the area.

Noda (1974), studied the phenomenon of wave-induced nearshore circulation. The most visually evident characteristic of nearshore circulation patterns is the phenomenon of rip currents. The driving mechanism for circulation patterns in the nearshore region was assumed to be due to alongshore variation in the radiation stress field. Herein is presented a theoretical analysis of nearshore wave-induced circulation patterns produced by the interaction of incoming waves and local bottom topography. This interaction results in a spatial variation of wave characteristics that produce a possible driving mechanism for nearshore circulation patterns. Both normal and oblique wave incidence are considered with the imposed beach profiles developed from an examination of prototype data. The analytical model results are compared with field measurements and yield optimal results.

2.3 Wave, Current, and Sediment Related Study in Nearshore Area

Upal (2018), analyzed the erosional problem around a river delta on Cox's Bazar coast. The coastline extends from south to north. Rapid erosion has affected some portions of a 24 km road along the coast, and local authorities have attempted to protect the road via revetment. However, the structure was soon buried with sediment because of a growing sand spit along the river delta, and a new area was eroded. Shoreline positions for a 44-

year (1972–2016) period were digitized using Landsat images to observe the real scenarios. From the time stack images, it observed a sand spit growing in a northward direction from 2000 to 2015, and the adjacent erosion area extended in the same direction. This study employed a numerical model (MIKE21FM SM) for the computation of wave-driven currents and sediment transport along the coast and attempted to reproduce recent erosional processes. The numerical result shows that net littoral drift is dominant in the northward direction along the coast, which is the same direction of the spit growth observed in the satellite images. A higher amplitude spit induces higher sediment transport compared to a low amplitude spit because of the difference in local incident wave angles resulting in a greater positive gradient of the longshore sediment flux distribution, causing erosion in the downcoast.

Navera and Ahmad (2018), examined the shoreline changes in Cox Bazar coast by using Remote Sensing and GIS techniques. From this study, it is found that Cox's Bazar-Teknaf shoreline has been experiencing severe erosion at a number of places due to wave action. Wave and wind-induced motion results in sediment distribution and shaping of nearshore morphology in these zones. The shoreline shifting analysis has been performed by the process of open-source Landsat images from 1980 to 2017. Satellite-derived band algebra; Normalized Difference Vegetation Index (NDVI) has been utilized to identify the vegetation cover. Based on the coastline shifting, the erosion behavior and the vulnerable areas are identified in this study. From the analysis, it is found that at different locations, the average change in shoreline goes up to 120 m in erosion and 100m in the deposition.

Ahmmed (2013), estimated the major wave parameter design wave height along Marine Drive Road form Kalatali to Inani. The proposed 80 km long road from Cox's Bazar to Teknaf along the sandy beach was originally conceptualized in 1993. In the first phase, a 24 km road from Kalatali to Inani had been constructed. Shore protection work was also initiated, completed in 2008 but started to fail at some points started from Kalatali. A previous study prevails that the design wave height used by the designers in Marine Drive shore protection is inappropriate. Therefore, design wave height is calculated for different return periods after wind analysis using the Gumbel method, and later wind stress factor calculation has also been done. The result shows at Cox's Bazar wind blows dominantly from South (S), Southwest (SW), and West (W) direction during pre-monsoon or monsoon period with 3.55 m, 4.13 m, and 4.74 m wave height for 25, 50, and 100 years of return period respectively. This study also includes calculation of design wave height for Teknaf, which will significantly contribute to the design of the coastal engineering projects, including redesigning the Marine Drive shore protection in the future.

Ahmed (2012), studied the effect of sediment erosion and deposition on the bathymetry of the Yangtze River in the Renmin island region. The study area was selected because of the presence of large quantities of sediment transported and deposited on this island reach and thus, increases the area of the island yearly. These encroachments can trace back to the evolution of the island. In that study, Delft3D-Flow, with an application of two-dimensional models, was used to simulate and evaluate the hydrodynamics and morphodynamics of the Renmin island region. Data on the discharge, water level and sediment concentration from June 1986 to June 1992 were used for the hydrodynamic and morphodynamical models. Comparisons were made between the computed model results and the observed data. The overall results revealed that the sediment deposition in the left branch side was larger than that in the right branch side, where continuous erosion and the tail part of the island increased in the deposition. The hydrodynamic and sediment transport model has been calibrated and applied successfully with the Delft3DFlow sediment-online model.

2.4 Structural Intervention at Nearshore Related Study Around the World

Amelia (2016), investigated wave propagation from an open lake environment to a small craft harbor protected by a breakwater at Lake Ontario by a surface wave model. The Simulating WAves Nearshore (SWAN) spectral wave model, coupled with the Delft3D hydrodynamic model, is applied to simulate a series of storms in November 2013. The model results are compared to observations from two pressure sensors and used to quantify wave properties around existing and future breakwaters to evaluate the bulk changes to the harbor configuration. Overall, the results indicate that the rubble mound breakwater reduces wave heights in the existing harbor by 63% compared to no breakwater and that the addition of a surface breakwater extension could reduce wave heights by an additional 54%. Wave height attenuation was found to be highly dependent on the incident wave direction relative to breakwater orientation. The spectral wave model is useful for simulating wave transformation for broad directional spectra in wind-sea conditions over large scales to semi-protected areas such as small craft harbors.

Chien (2016), set out a model to analyze the shoreline changes behind emerged detached breakwaters under varying geometrical layouts and conditions. This study able to identify where and when the presence of this structure along the shoreline shows accretion and erosion. This study is established as a rational and motivation for shore protection. The equilibrium shoreline has been observed and measured through the aerial images series at four important positions. Consequently, the empirical relationships have been developed between the impact parameters and the equilibrium shoreline parameters, and thereby, the magnitude of the shoreline changes behind the breakwater is quantified under specific conditions. Detached breakwaters reduced the wave height but did not eliminate erosion in the field of the structures. Evaluation of the shoreline showed that of the three positions at the opposite gap, the up-drift, and the down-drift, at least one of them is always eroded. The chances of erosion in the tombolo formation presented the possibility of erosion at the down-drift, might a chance of erosion at the up-drift, and rare erosion at opposite the gap. The chance of erosion in the salient formation showed that in these three positions, there is not much difference; both situations of erosion and accretion exist. However, the down-drift has more potential for erosion than the other positions.

Afroz (2015), investigated experimentally the interaction between waves and horizontal slotted submerged porous breakwater using a numerical model. To investigate the performance of proposed horizontal slotted submerged breakwater, experimental studies are carried out in a two-dimensional wave flume (21.3 m long, 0.76 m wide and 0.74 m deep) at the Hydraulics and River Engineering Laboratory of the Bangladesh University of Engineering and Technology. A set of experiments are carried out at 50 cm still water depth with fixed horizontal slotted submerged breakwaters of three different porosities (n = 0.4, 0.5, and 0.6) for interaction with regular waves of four different wave periods (T = 1.6 sec, 1.7 sec, 1.8 sec and 2.0 sec) in the wave flume. This study is expected to serve as a useful model to analyze wave deformation due to horizontal slotted submerged porous breakwater and will be important for designing submerged porous breakwater as a coastal protection measure.

Akter (2013), investigated the hydrodynamic performance of rectangular porous breakwater(s), both submerged and emerged as a shore protection structure. Experimental studies were carried out in a two-dimensional flume (21.3 m long, 0.76 m wide, and 0.74 m deep) of the Hydraulics and River Engineering Laboratory of Bangladesh University of

Engineering and Technology. A set of experiments were carried out at h= 50 cm water depth with fixed vertical porous breakwaters of three different porosity (n= 0.45, 0.51, and 0.7) and with three different heights (hb= 40 cm, 50 cm, and 60 cm). It is found from the study that wave energy loss co-efficient (KL) increases with increasing porosity. This study can provide engineers with useful information for designing coastal structures.

Womera (2011). In her research work, she investigated the interaction between waves and rectangular submerged breakwater. To investigate the performance of proposed rectangular type submerged breakwater, experimental studies carried out in a two-dimensional wave flume (21.3 m long, 0.76 m wide, and 0.74 m deep) at the Hydraulics and River Engineering Laboratory of Bangladesh University of Engineering and Technology. A set of experiments was carried out at 50 cm still water depth with fixed submerged breakwaters of three different heights (30 cm, 35 cm, and 40 cm) for five different wave periods (1.5 sec, 1.6 sec, 1.7 sec, 1.8 sec, and 2.0 sec) in the same wave flume. The effects of breakwater height and length along the wave direction on wave height reduction are analyzed. A two-dimensional numerical model is based on the SOLA-VOF method developed for wave interaction with a floating breakwater. The SOLA-VOF model allows efficient tracking of the free surface. The basic equations used for VOF method are the continuity equation, the Navier Stokes equation for incompressible fluid and the advection equation representing the behavior of the free surface. Because the wave generation source is placed within the computational domain, these equations involve the wave generation source. This study can be used as a future reference to design different breakwater.

Ahammed (2010), Investigate the embankments alongside the coastline and analyzed the effect of the dynamic loading due to waves associated with submerged, floating breakwater, and CC block condition on the coastal embankment. The coastal embankment is a structural measure usually taken near the coastline to protect inland habitat and crops. This research work considers only those embankments which are located along the coastline directly facing the sea. The general practices in Bangladesh for the design of coastal embankment normally consider high tide level as the design high water. Based on the design criteria, it can be said that the consideration of periodicity of small waves while designing an embankment is one of the most important parameters. For accurate design consideration, the main parameters are wave height, wave direction, current, and soil properties. An experimental investigation was conducted to study the behavior of wave parameters with different loading conditions in the laboratory flumes of Hydraulics and River Engineering Laboratory of the Department of Water Resources Engineering, BUET. The study shows that the presence of breakwater in front of the coastal embankment resulted in a change in the loading distribution. Breakwater position (submerged or floating) individually affects the wave loads furthermore.

Arab (2009), studied the T groin with the help of Delft3D model. In this research work, Delft3D was verified against a field case in Trabzon province of Turkey, on the Black Sea coast. Two T-head groins were placed on a bed with a constant slope, and the bathymetry was measured after 6 months. The main purpose of the study was to find the best way to represent the T-Head groins in the model from both Hydrodynamic and Morphological point of view. The model tends to overestimate eddies in the shadow zone of the structure and to overcome the problem some alternatives were tested. Increased bed roughness along the trunk of the structure is an effective way to damp these eddies but finding the proper values that do not result in instability of the model makes it hard to be a universal choice. Wall roughness is another effective tool, but it has upstream boundary effects that need a sufficiently large model domain to avoid these effects, and consequently, longer simulation time. It was shown from the study that the actual body of the groins as a high unerodable bed level results in the best Hydrodynamic pattern and Morphological response in comparison to the measurements.

Ahmed (1997), In his study he developed a morpho dynamic model named DELFI'2D-MOR, which is a two-dimensional horizontal model, and an on-line model UNIBEST to examine the influence of the breakwater. From the model, he found that the breakwater geometry affects the hydrodynamic processes as well as the morphological evolution (salient or tombolo). Based on sensitivity analysis, the wave-current interaction was found to affect the morphological evolutions. The agreement between the results of the model and the literature results was quite satisfactory. After getting insight into the validity of the DELFI'2D-MOR model, a case study of a single detached breakwater situated at the northern coast of Egypt was carried out. The wave climate was analyzed to get the morphological equivalent one-wave condition and two-wave condition. It was found that the longshore current was higher due to the longshore current formulation and this, in turn, affects the sediment transport rate.

Kraus et al. (1994), conducted research on functional design of groins. According to the study, there is a number of cases, in which usage of groins is not effective; including, (a) if there is a large tidal range, allowing to bypass the structures at low tide or to overpass at high tide, (b) if cross-shore sediments transport is dominant, such as is typical in shallow bays and lagoons, and sometimes along the great lakes, where strong winds relatively small fetches make steep waves (erosive) dominant over swell. Undesirable updrift buildup and offshore transport of sediment may be promoted if groins extend too offshore in relation to the wave average breaker line or if they are not sufficiently permeable, potentially causing sand to be jetted seaward.

2.5 Numerical Model-Based Study at Nearshore Area

Bricheno (2016), examined the tidal hydrodynamics and freshwater flow in a complex river system in Ganges-Brahmaputra- Meghna (GBM) delta in the northern part of the Bay of Bengal by finite-volume community ocean model (FVCOM). The delta region is data-poor in observations of both bathymetry and water level; making it a challenge for accurate hydrodynamic models be configured for and validated in this area. This work is the first 3D baroclinic model covering the whole GBM delta from deep water beyond the shelf break to 250 km inland, the limit of tidal penetration. This study examines what controls tidal penetration from the open coast into an intricate system of river channels. Tidal penetration is controlled by a combination of bathymetry, channel geometry, bottom friction, and river flow. The performance of FVCOM tidal model configuration is evaluated at a range of sites in order to assess its ability to capture water levels which vary over both a tidal and seasonal cycle. From this study, it is found that when the river discharge is particularly strong, the tidal range can be reduced as the tide and river are in direct competition. The bathymetry is found to be the most influential control on water levels within the delta, though tidal penetration can be significantly affected by the model's bottom roughness and the inclusion of large river discharge.

Anindita (2016), studied the assessment and evaluation of the impact of climate change on coastal belts in Bangladesh, which is thickly populated and highly vulnerable to threats from sea-level rise and extreme weather events. In that study, the wave climatology for the north Indian Ocean, specifically covering the head Bay region, was examined, utilizing the past 21 years of satellite altimeter data for the period ranging from 1992 to 2012. In addition, the study also examines the significant wave heights obtained from the

WAVEWATCH-III (WW3) model to substantiate and evaluate the findings of the observed variability from altimeter records. The study establishes the fact that the responsible mechanism for this contrasting trend is the variations in mean sea level pressure over the head Bay region. In addition, a comprehensive analysis using the empirical orthogonal function (EOF) shows that the second mode that represents the inter-seasonal variations substantiates the trend observed in the percentage distribution of these parameters. Interestingly, the study clearly signifies that trends in both wind speed and significant wave height was lower for the western side, unlike that noticed over the eastern portions in the head Bay of Bengal region.

Tazkia (2016), studied the low-frequency modulation of tides for the Northern Bay of Bengal (BoB). This research work focused on the seasonal changes in the amplitude of the semi-diurnal lunar tide, M2. It is found that M2 amplitude shows marked changes between winter and summer seasons (of order 10 cm), incommensurate with most of the world's coastal ocean. They had observed contrasted patterns from the open areas of the coastal ocean to the inner part of the GBM estuary. In the coastal ocean and over most of the GBM delta, M2 amplitude is stronger during summer and decreases until winter. Conversely, in the far northern part of GBM estuary, M2 amplitude is stronger during winter and weaker during summer. A hydrodynamic tidal model has been incorporated to decipher the processes responsible for this evolution. It was found that throughout the coastal ocean and over most of the GBM delta, this evolution is driven by frictional effects, with a seasonal modulation of the bottom dissipation of tidal energy.

2.6 Mathematical Modeling Based Study on the Bay of Bengal

Rahman (2014), studied the coastal resilience by coastal bio shield. His work focused on storm surges generated by cyclones, which causes devastating damage to property and loss of life in coastal areas of Bangladesh with the Bay of Bengal. Bio-shield in wetlands can reduce the energy of storm surges and cyclones. In his study, historical storm surges were analyzed, and existing bio-shield protection is evaluated along the coastal belt of Bangladesh. It is also found that there are only 60 km or 6% of forest belts of the 957 km total length of embankment of 49 sea-facing polders, much of which is already degraded. A two-dimensional numerical model named Bay of Bengal model developed by the Institute of Water Modeling is used to simulate the effect of coastal bio-shield in reducing the energy of storm surge SIDR along the Kuakata beach of Bangladesh. The model results demonstrate that up to 2 cm of surge height and 0.48 *mls* or 62 % of current speed are reduced by 200 m width of bio-shield when SLR is not considered. Again, the surge height and current speed are reduced by 3 cm and 0.46 *mls* or 59 % respectively by 200 m width of bio-shield when 74 cm of SLR is considered for the year 2100 according to 5_{th} IPCC report. It is anticipated that these results will find broad application in coastal management and planning for areas with existing coastal bio-shield as well as for bio-shield restoration and establishment efforts.

Hossain (2012), carried out a mathematical model to simulate the tidal flow velocity in the nearshore coastline of Bangladesh. In his study, a two-dimensional hydrodynamic model DIVAST (Depth Integrated Velocity and Solute Transport) has been used considering the different parameters like the coefficient of eddy viscosity, Manning roughness, advective and diffusion coefficient, etc. of the Bay of Bengal. In this study hydrodynamic module has been used. The hydrodynamics of the selected area of the Bay of Bengal has been simulated by solving two-dimensional depth-integrated momentum and continuity equations numerically with the finite difference method. Consequently, the water elevation η with respect to mean sea level and the respective velocity components U, V in the x and y directions are calculated across the selected coastal domain for a prescribed set of initial and boundary conditions. Simulated velocity has been verified at selected locations of coastal area with the measured field data and compared with the other study carried out in the coastal region of Bangladesh. Viewing over the DIVAST simulated results very good agreement is found between the measured data as well as to the other study. This encouraging good result justifies that the DIVAST model works reasonably well for the selected domain of the Bay of Bengal.

Hossain (2012), studied the storm surges and coastal erosion hazard in Bangladesh with their adaptation measures considering the impact of current and future states of climate. Data has been collected from different internet sources and the Bangladesh Meteorological Department (BMD) to model the coastal erosion by SWAN (Simulating of Waves Nearshore). The study concluded that Bangladesh has seriously addressed the Disaster Risk Reduction (DRR) and climate change issue there is still some commitment and capacities required to achieve DRR due to lack of resources and research work. Modeling by SWAN shows that the rate of erosion along the coast of Bangladesh increases with the increasing wind speed. The study also shows that the rate of erosion in 2030 and 2050 will be increased due to sea level rise, but it will not be increased significantly. However, new areas on the coast will be inundated and affected by erosion.

Komol (2011), set up a two-dimensional hydrodynamic Depth Integrated Velocity and Solute Transport (DIVAST) model based on FORTRAN program. The tides in the coastal and estuarine areas of Bangladesh are semidiurnal in nature. Determination of the tidal level for understanding the hydraulic behavior of the coastal region is very important and crucial for taking any decision of coastal area development. It is found from the study that the simulated tidal ranges have been observed as micro-tidal at Daulatkhan, meso-tidal at Tazumuddin, and Hiron Point, macro-tidal at Hatiya, Sandwip, Feni River, and Rangadia. The simulated tidal levels have also been compared with the simulated tidal levels of two other studies, and results have been found in good agreement.

IWM (2007), has made a detailed assessment of the potential impacts of relative sea-level rise on coastal livelihoods of Bangladesh. The study considered the sea level rise for both low (B1) and high (A2) greenhouse gas emission scenarios according to the 3rd IPCC predictions. The study shows that about 13% more area (551,000 ha) in the coastal region will be inundated in monsoon due to 62 cm sea-level rise The study also examine that if 1991 cyclone will come with 27 cm SLR and increased intensity, Chittagong district will be affected more and about 99,000 ha more area (18%) will be exposed to severe inundation (>100cm) compared to 1991 cyclone inundation. Moreover, about 35,000 ha area of Cox ‘s Bazar district will be inundated severely (>100cm) compared to 1991 cyclone inundation.

IWM (2005), has made a detailed impact assessment of sea-level rise on inundation, drainage congestion, salinity intrusion, and change of surge level in the coastal zone of Bangladesh. The potential effects of climate change were studied for a different sea-level rise i.e.14 cm, 32 cm, and 88 cm for the projected years 2030, 2050, and 2100. Mathematical models of the Bay of Bangle have been used to transfer the sea level rise in the deep sea along the southwest region rivers and the Meghna Estuary. The study shows that about 11% more area (4,107 sq.km) will be inundated due to 88 cm sea level rise in addition to the existing (the year 2000) inundation area under the same upstream flow. About 84% of the Sundarbans area becomes deeply inundated due to 32 cm sea-level rise, and for 88 cm sea level rise Sundarbans will be completely lost. Due to a 32 cm sea-level rise, surge level increase in the range of 5 to 15% on the eastern coast. It also observed that 10% increase in wind speed of 1991 cyclone along with 32 cm sea-level rise would produce 7.8-to 9.5 m high storm near Kutubdia- Cox ‘s Bazar coast.

Jakobsen et al. (2002), studied the hydrodynamics of the Bay of Bengal in detail using a calibrated and validated the two-dimensional numerical hydrodynamic model. The Flood Forecasting and Warning Center (FF&WC) of Bangladesh, supported by the Institute of Water Modeling (IWM) in Dhaka and DHI has developed an operational salinity intrusion forecast model enabling both short term and long-term forecasting of salinity conditions in the delta. The Bay of Bengal model was transferred to the FF&WC during a DANIDA supported project from 2000 to 2006 in order to test the feasibility of carrying out operational cyclone forecasting. Later on, the Bay of Bengal model was transferred into a flexible mesh model technology based on the finite element method. This has allowed for a more detailed resolution in the deltaic region and up into the river systems and thereby enhancing the accuracy of modeling of saline intrusion. An advection-dispersion model is coupled to the hydrodynamic model describing the transport and mixing of the freshwater outflows from the river with the saline Bay of Bengal waters. The combined hydrodynamic and advection-dispersion model is referred to as the Bay of Bengal model. The Bay of Bengal model was originally developed by IWM and used in a number of projects where it has been updated, recalibrated, and verified used in a number of projects where it has been updated, re-calibrated and verified.

CEIP (2017), is focused on the strategy to protect the coastal area against high tides and frequent storm surges. In this study, a hydro morphological model was used to simulate the different condition along the Bay of Bengal. The main objective of the study was to increase the resilience of the entire coastal population to tidal flooding and natural disasters by upgrading the whole embankment system by different mathematical models. With an existing network of the embankment of nearly 5,700 km long with 139 polders, the magnitude of this work is very crucial. This is a multi-phased approach to embankment improvement, and rehabilitation has been adopted over a period of 15 to 20 years. The Coastal Embankment Improvement Project – Phase 1 (CEIP-1) is the first phase of this long-term program CEIP.

CERP (2000), carried out the storm surge modeling study based on the two-dimensional Bay of Bengal Model. Since 1991, IWM is maintaining the two-dimensional Bay of Bengal Model. The first version of the model was applied in Cyclone Protection Project

(CPP, 1991) and was further developed as a part of the Cyclone Shelter Preparatory Study (CSPS, 1998). The model was further updated as a part of the second Coastal Embankment Rehabilitation Project (CERP, 2000). In this study, the model has been updated with existing data and upgraded in 200 m grid resolution incorporating Sundarban area, and it has been extended to the sea up to 16º latitude. The storm surge model is the combination of Cyclone and Hydrodynamic models. For simulating the storm surge and associated flooding, the Bay of Bengal model based on MIKE21 hydrodynamic modelling system has been adopted. In the hydrodynamic model simulations meteorological forcing like cyclone is given by wind and pressure field derived from the analytical cyclone model. The MIKE 21 modelling system includes dynamical simulation of flooding and drying processes, which is very important for a realistic simulation of flooding in the coastal area and inundation.

Ali et al. (1997), studied that one of the important reasons for disastrous floods in Bangladesh was the back-water effect from the Bay of Bengal on the floodwater outflow. A two dimensional vertically integrated hydrodynamic model of the northern Bay of Bengal was used to study the back-water effect due to storm surges and astronomical tides in the Meghna estuarine region of Bangladesh. The model also investigated the impact of flood water discharge on tides and storm surges. It has been found that a significant amount of water was held up inside the country by the backwater effect. Not only that, a huge amount of water penetrates inside Bangladesh particularly due to storm surge and astronomical tides.

2.7 Structural Intervention at Nearshore in the Bay of Bengal

IWM (2010), carry out the coastal, hydraulic, and morphological study for the proposed Deep-Sea Port at Sonadia Island under Moheshkhali Upazila in Cox's Bazar district in order to assess the probable risk from erosion-accretion, maximum cyclonic surge level, wave condition, and harbor calmness. The complex interaction of tides, waves, storm surges, river discharges, and sediment transport were studied in relation to safe and cost-effective planning and design of the Deep-Sea Port applying numerical modelling technology. The shallow water wave heights and directions estimated in the wave analysis were used to measure the harbor calmness in the proposed deep-sea port at Sonadia Island. Shallow water waves from NW, W, and SW directions entered into the harbor through breakwater opening and went under diffraction and reflection effects before reaching the harbor basins. Historical satellite images (1989-2008) were analyzed to find out the bankline shifting and erosion-deposition pattern around the island. In order to find the morphological behavior of the project area with and without the proposed north breakwater and south breakwater, sediment transport model was simulated for 15 days in dry period and another 15days in monsoon period covering spring and neap tide. Model results showed that the construction of the breakwaters in the changed orientation decreased deposition slightly along the south breakwater and increased scouring very slightly along the north breakwater. The breakwater also resulted in the deposition in between them, which was slightly increased in this orientation compared to the previous one. One of the important findings of the morphological model was the sedimentation of approximately 3.4 million m^3 per year in between two breakwaters and a half to one-third of its volume may deposit in the approach channel and dredging should be carried out to keep the channel navigable.

IWM (2012), carried out the study for planning and design of protective works in Cox Bazar marine drive. The project components include road, cross drainage structures, and coastline protection works. The project area falls under Ecologically Critical Area declared in 1997. Over the years the Road has experienced severe erosion and damaged at few locations mainly due to sea wave action. Extensive work was carried out to finalize the design parameter using past experience, existing condition of Marine Drive and different model results. The erosion vulnerability of the Marine Drive was assessed considering severity of erosion in the past, present, and future, longshore sediment transport characteristics, wave dynamics, and place of importance based on model results, field visits, satellite image analysis, and consultation with various stakeholders. A number of potential erosion protection measures such as breakwater, revetment, beach nourishment, groins, and sleeping defense were considered and analyzed to select the best suited protective measures from the perspective of long-term solution. This study has recommended a few reasonable solutions for protecting the marine drive, ensuring sea view, attractive beach, and easy access to the beach, which can be sustained for the long term.

2.8 Summary

Several studies have been carried out worldwide and also in Bangladesh, to understand the nearshore hydrodynamic conditions like wave, current, and sediment transport. In this chapter, different numerical and mathematical modeling-based research is reviewed for constructing the ground of the study. There is a limited amount of work done in Bangladesh for shoreline protection through hydraulic structures . Especially, study on coastal protection through Breakwater and Groin is rarely available in Bangladesh context. Coastal erosion is a major phenomenon for Bangladesh, where most coastal districts are under vulnerable conditions for long-term erosion problems. At the same time, the southeast part of the coastline of Bangladesh facing high tide and high wave action around the year. There is a need to examine the nearshore complex system to protect the coastline from long-term erosion problems. For this study, a fully calibrated and validated model is needed for simulating the nearshore conditions with different structural interventions. This study's main focus is to protect shoreline due to erosion with structural interventions and oversee the wave height, wave energy reduction with associated sediment movement in the vicinity of the structure. The significance of the study will carry value addition in the scientific world and future reference of similar kinds of research in Bangladesh.

CHAPTER THREE

THEORY AND METHODOLOGY

3.1 General

In this section, relevant studies are reviewed. This includes published works regarding the nearshore coastal hydrodynamics. Tides and waves in nearshore area are two of the most important aspects which are discussed here to understand their effects. Additionally, nearshore currents, hydraulic structures, and sediment transport have also been discussed for understanding the physics of the study. Simulating Waves Nearshore (SWAN), a spectral wave model, coupled with the Delft3D hydrodynamic model, is applied to this study to simulate the Bay of Bengal model. Delft3D has a number of modules for a different purpose, and each module has different sets of equations, which is also discussed in this chapter for selecting nearshore conditions.

3.2 Nearshore Hydrodynamic

The dynamic processes that exist in the nearshore region are generated by a number of different drivers. Under the influence of these external forces, the fluid motion of the water manifests itself as coastal currents, tides and tidal currents, internal and surface waves, storm surges, tsunamis, and others (Horikawa, 1988). This section provides a brief description of waves and current in nearshore and sediment transport in the surf zone.

3.2.1 Waves in the Nearshore Area

Wind waves are generated by the wind blowing over the water surface. In deep water where the ratio of water depth (h) and wavelength (L_0) is bigger than 0.5; it is generally assumed that there is no effect of the seabed on the waves. However, shallow water waves may be subject to shoaling, refraction, and the breaking of waves. In the following section, the phenomena are illustrated.

(i) Refraction and shoaling wave

When waves propagate toward the coastline, the water depth reduction leads to the wavelength decreasing, and refraction and shoaling waves occur. Refraction can only occur if the waves approach underwater contours at an angle while shoaling will occur when waves approach the contours perpendicular. A convenient formula of wave height that expresses both effects of wave shoaling and refraction is,

$$H=H_0 K_s K_r \tag{3.1}$$

Where: H_0 is the deep-water wave height, K_s is the shoaling coefficient.

$$K_s = \sqrt{\frac{C_{g0}}{c_g}} \tag{3.2}$$

and *K*r is the refraction coefficient, which for straight and parallel shoreline contours can be expressed in terms of the wave angles as follows:

$$K_r = \sqrt{\frac{\cos \alpha_0}{\cos \alpha}} \tag{3.3}$$

Given the deep-water wave height is C_{g0} and the group velocity is α_0

(ii) Breaking wave

Wave breaking is one of the most important subjects to coastal engineers because it highly influences both the sediment behavior on beaches and the magnitudes of the forces on coastal structures. Breaking is difficult to describe mathematically because it is the most complicated wave phenomenon. Unfortunately, at present, only limited properties of breaking waves can be predicted accurately.

Waves may break in several different ways: spilling, plunging, surging, and collapsing. Spilling breakers are usually found along flat beaches. Spilling is a very small reflection of wave energy back towards the sea. Plunging breakers are forms that are often found in mid-slope beaches. Some energy of plunging waves is reflected back to the sea, and some are transmitted to the coast. Surging breakers occur along steep coasts for relatively long swell waves. The energy of the surging breaker zone is more than half reflected back into deeper water. A collapsing breaker is a breaker between a plunging and a surging breaker.

In general, the maximum wave height at any particular location depends on the wavelength, L; the water depth, h; and the slope of seabed, tanβ. Based on Stokes wave theory, Miche (1944) gave the limiting wave steepness as:

$$\left[\frac{H}{L}\right]_{max} = 0.142 \tanh\left(\frac{2\pi h}{L}\right) \tag{3.4}$$

However, in the case of deep water (h/L ≥ 0.5) only the wavelength is important and breaking occurs when the wave steepness H/L is approximately 0.142. In shallow water depths, the breaking wave is relative to both water depth and wavelength; the conditions are h/L ≤ 0.05, and the maximum wave height $H_{max}/h \approx 0.88$, but the largest number of waves are breaking when $H_S/h \approx 0.4\text{-}0.5$.

3.2.2 Currents in the Nearshore Area

The current in the surf zone is a combination of currents driven by breaking waves, the tidal current, the wind-driven current, and the oscillatory flows due to wind waves and infra-gravity waves.

(i) Longshore current

When oblique incoming waves are breaking, the radiation shear stress component shoreward decreases as a result of which alongshore current can develop. This longshore current can only occur there, where energy dissipation happens, this means in the surf zone. The wave height (H) and the oblique wave angle (α) are the main effect on the strength of the longshore current. If they decrease, the longshore current decreases as well. (Eq. 3.5)

$$S_{xy} = nE sin\alpha \cos\alpha = \frac{n}{8}\rho g H^2 sin\alpha \; cos\alpha \tag{3.5}$$

Where: n is the ratio of wave group speed and phase speed.

(ii) Cross-shore current

A cross-shore current is not constant over depth. The mass transport carried shoreward due to waves is concentrated between the wave trough and the crest elevations because the beach forms a barrier for mass flux landward movement, and in a balanced situation, the mean directed flow onshore should equal to zero. Therefore, to compensate for the wave-induced mass movement in the upper layers, an opposite flow or undertow follows in the lower layers. The undertow current may be strong close to the bottom. The vertical profile of the undertow is determined as a balance between radiation stresses, the pressure gradient from the sloping mean water surface, and vertical mixing.

(iii) Rip current

The nearshore circulation system happening at the beach often includes non-uniform longshore currents, rip currents, and cross-shore flows. Rip currents are narrow jets of water issuing from the inner surf zone out through the breaker line that carries sand offshore. Rip currents on a long straight beach have been observed from one horizon to the other with roughly a uniform spacing, with approximate wavelength. Figure 3.1 shows rip currents and feeder currents.

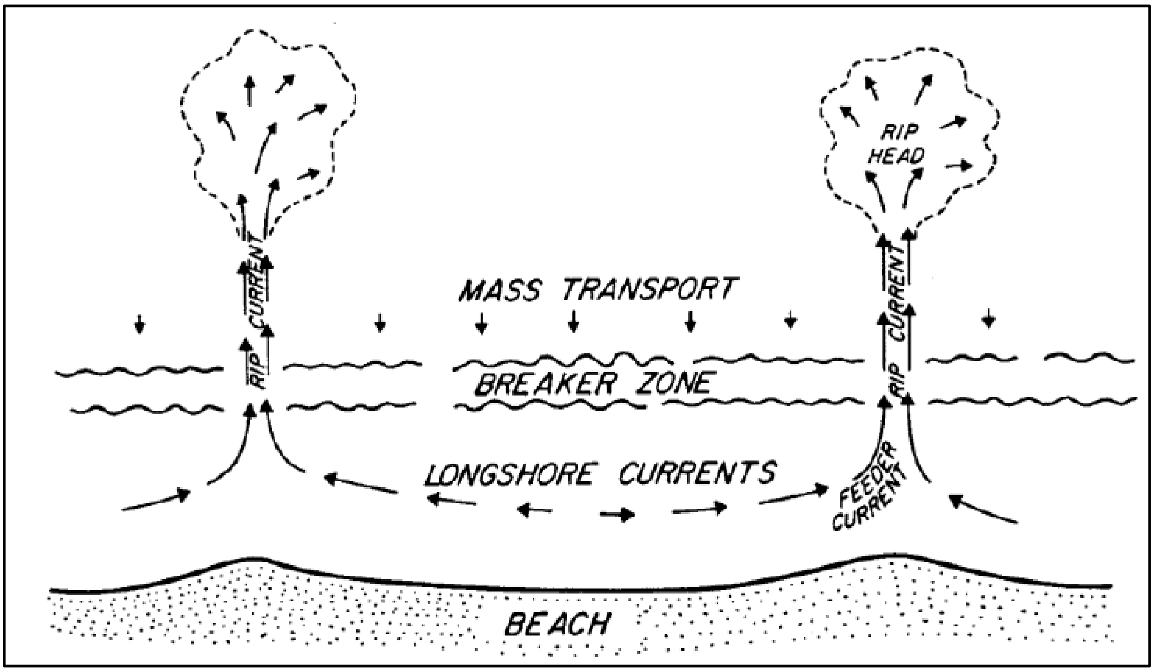

Figure 3.1: Nearshore circulation system showing the rip currents and the feeder currents (Source: Shepard and Inman, 1951).

3.2.3 Sediment Transport in the Surf Zone

In this section, a brief description of Longshore transport and Cross-shore transport have been carried out where several sediment transport formulation model under these transport systems also been summarized for the proper understanding of the physics of nearshore sediment transport.

(i) Longshore transport

Under the action of the waves and the longshore currents, the sediment moved along a shoreline. In general, three modes of sediment transport are recognized: bedload transport suspended load, and swash load. In the bed load mode, the particles are rolled, shifted, or have a small jump over in the seabed. In the suspended load mode, the particles are lifted up from the seabed within the fluid column and moved in suspension by currents. And in the swash load mode, the particles are moved on the surface of the beach by the swash. It is difficult to fully understand which of these predominant motions for various wave conditions, sediment types, and the profile of locations or even whether it is important to identify the different mechanisms. Several of sediment transport formulations of these modes are illustrated below:

Energy flux model*:* Inman and Bagnold (1963), showed that the total amount of material moved along the shoreline was related to the amount of energy available in the waves arriving at the shoreline:

$$Q = \frac{KP_1}{(P_S - p)g\,(1-p)} \tag{3.6}$$

$$F\cos\theta\sin\theta \equiv P_l = EC_g \sin\theta\cos\theta = \frac{1}{16}\rho g H^2 C_g \sin 2\theta \tag{3.7}$$

Where,

θ : is the angle the wave ray makes with the onshore;

H: wave height;

E: the energy per unit surface area;

C_g : the group velocity;

F=EC_g: the energy flux per unit width;

K: the dimensionless parameter (K=0.77) by Komar and Inman (1970); K=0.2 to 0.22 by Kraus et al. (1982); K= 1.23 by Dean et al. (1982).

g: gravity;

ρ: mass density of the water;

ρ_s: mass density of the sediment grains;

P: in-place sediment porosity (p=0.4)

Energetics model: Bagnold (1963), created a model for sediment transport based on the amount of the flow energy uses to transport of the sediment. Inman and Bagnold (1963) then adapted the theory for oscillatory flow within the surf zone. They demonstrated that the final expression for the dynamic transport rate for the wave-induced sediment transport is:

$$I_c = KEC_g \frac{U_c}{U} \tag{3.8}$$

Where U: the near-bed velocity of the fluid;
U_c: mean direction current.

Suspended transport model: Dean (1973), developed the model of the suspended load for sediment transport within the surf zone. As in the suspended sediment model, Inman and Bagnold (1963) supposed that the falling sand grains dissipate a part of the available energy flux into the surf zone. They expressed that the dissipation *D* for a single sand grain is due to the loss of potential energy by the particle and is related to the submerged weight of the particle and the fall velocity ω

$$D=(\rho_s - \rho)g\frac{\pi d^3}{6}\omega \tag{3.9}$$

where the grain is roughly spherical with diameter d, as it is assumed.

Dean calculated the number of suspended grains per unit length in the surf zone and then obtained the final longshore current formula is:

$$Q=CP_l \tag{3.10}$$

$$C= 34.3 \times 10^3 \epsilon \frac{\sqrt{H_b / k tan\beta cos\theta_b}}{C_f\sqrt{g}(\rho_s-\rho)(1-\rho)\omega} \tag{3.11}$$

Traction models: Another class of sediment transport models outside the surf zone has been created, which is based on the information about traction models created for open channel flow. An important variable is the Shields parameter. The sediment will move when its critical value is lower than the bottom shear stress.

Madsen and Grant (1976), calculated a mean transport rate over half a wave period for the time that the oscillatory flow in one direction starts to the time when it stops to change direction, which is

$$\overline{\emptyset} = \frac{2}{T}\int_{t_1}^{\frac{T}{2}-t_2} 40\psi(t)^3\, dt \tag{3.12}$$

Where: t_1 is the time at which the beginning motion criterion is exceeded and (T/2-t_2) is the time when the transport finishes.

Other relationship transport: Kamphuis (1991), showed that the results of the sediment transport rate are a function of wave, fluid, sediment, and beach profile based on three-dimensional hydraulic model experiments. The Kamphuis relationship is:

$$Q=2.27\, H_b^2 T_p^{1.5} tan\alpha_b^{0.75} d^{-0.25} sin^{0.6}(2\theta_b) \tag{3.13}$$

In which Q is the total longshore sediment in kg/s, α_b is the beach slope of the breakpoint seaward, and all other variables expresses in metric units. In this equation, the longshore sediment is related to the breaking wave characteristics, the beach slope, and the median sediment size d.

(ii) Cross-shore transport

The breaking of oblique incoming waves induces a longshore current, which is the main cause of longshore transport. However, the action of waves and the return flow (or undertow) lead to the sediment transport in the cross-shore. Various models of the cross-shore will be shown below.

Fall time model: Dean (1973), developed a model for cross-shore transport in the surf zone, in which he supposed that breaking waves suspend the sand grains in the water column and the eventual settling of sand to the bottom. Dean showed that the time that it will take for the sand to fall back to the bottom is: $t = \frac{s}{\omega}, in\ which\ S = \beta H_b$ an average distance wave breaking in the surf zone lifting sand from the bottom up into the water column, ω is the fall velocity of the sand; $H_b$is the breaking wave height and β is a constant. If the fall time of a sand grain is smaller than T/2, where T is the wave period, the sand grain should move shoreward. Alternatively, if the fall time is bigger the T/2, the sand grain will be carried shoreward.

Simple cross-shore transport model: Moore (1982), proposed a simple cross-shore model first and later Kriebel (1983) and Kriebel and Dean (1985) improved this model. The initial definition is that, if sediment across the profile is a uniform size and in an equilibrium beach, the energy dissipation rate per unit volume is constant, then they supposed to obtain the $A\ y^{2/3}$ profile. If the beach profile is different from this equilibrium state, then the energy dissipation rate is different from the constant value too. It is assumed that the amount of sediment moved will depend on the difference between the dissipation energy of the two states. Therefore, the volumetric cross-shore sediment transport rate per unit width in the seaward direction is

$$q_s = K(D - D_*) \tag{3.14}$$

In which, K *is a new dimensional constant;*

The equilibrium energy dissipation per unit volume D_* determined by the profile scale factor A, for:

$$A = \left(\frac{24D_*}{5\rho g k^2 \sqrt{g}}\right)^{\frac{2}{3}} \tag{3.15}$$

Energetics model: Stive (1986) and Roelvink and Stive (1989) investigated the Bailard's formula sediment transport by cross-shore flows.

$$\overline{t(y)} = \rho C_f \frac{\epsilon_b}{cos\beta tan\phi}\left(\overline{|u|^2}u - \frac{tan\beta}{tan\phi}\overline{|u|^3}j\right) + \rho C_f \frac{\epsilon_s}{\omega}\left(\overline{|u|^2 u}\right) - \frac{\epsilon_s}{\omega} tan\beta\overline{|u|^5}j \tag{3.16}$$

Stive successfully investigated the evolution of offshore shoals that were a result of wave activity. Roelvink and Stive investigated Bailard's formula coupled with a conservation of sand formula $\frac{\partial h}{\partial t} = \frac{\partial_{qs}}{\partial y}$ to model the behavior of beach profiles. They used a model of a random wave breaking (Battjes and Janssen, 1978) and combined nonlinear waves, groups of waves, undertow, and wave-induced turbulence. They came to the conclusion that their model predicted the wave hydrodynamics well; however, the Bailard formulation might have been insufficient for locations outside the surf zone because of the strong vertical variation of the flow. They were able to create sandbars with their model, but not in the same regions as the experiment results.

Ripple model: The bed of an offshore breaker line is often rippled, and the ripples influence the sediment transport in this location. As the wave-induced motion increases over a ripple, the flow separates from the crest of the ripple and forms a vortex in the trough before the next ripple. This vortex captures and carries sediment.

Dingler and Inman (1976) and Jette (1997), found that the mobility number is significant to the dynamics of ripples. The mobility number $\psi_m$is the shields parameter with the near-bottom orbital velocity replacing the shear velocity as,

$$\psi_m = \frac{(A\sigma)^2}{gd(s-1)} \tag{3.17}$$

where A is one-half the near bottom water particle excursion, and σ is the angular frequency of the wave.

If $\psi_m > 150$, ripples tend to be obliterated; 50<$\psi_m < 100$, ripples can from rapidly, $\psi_m < 50$, ripples can from slowly.

3.3 Theory of Hydrodynamics

Numerical techniques have been applied in this thesis to simulate the flow model and the wave model. The hydrodynamic model has been simulated to calculate the tidal level, and the wave model simulated to calculate the significant wave height. The mathematical calculations have been done based on some basic equations which are described below separately.

3.3.1 Wave Hydrodynamics

When a wave is a driving force in the model, and in our case, the only driving force, energy dissipation in the wave field results in radiation stresses gradient that runs the body of water; this phenomenon is modeled in Delft-3D-Wave module, which is an interface for the well-known third-generation spectrum model of SWAN (Simulating WAves Nearshore).

SWAN, in fact, solves the conservation of action density over the wave grid. Usually, the spectrum wave models determine the evolution of the action density N($\underset{x}{\rightarrow}$,t;$\sigma, \theta$) in space,$\underset{x}{\rightarrow}$, and in time t, where,$\sigma$ is the wave direction normal to the wave crest of each spectral component. The action density is a realization of energy density E$(\sigma, \theta), while\ N = E/\sigma$. The advantage of the action density is based upon its conservation during propagation in the absence of ambient current, whereas energy density is not (Whitman,1974).In the Cartesian coordinates, the action balance equation reads,

$$\frac{\partial N}{\partial t} + \frac{\partial c_x}{\partial x} N + \frac{\partial c_y}{\partial y} N + \frac{\partial c_\sigma}{\partial \sigma} N + \frac{\partial c_\theta}{\partial \theta} N = \frac{S_{tot}}{\sigma} \quad (3.18)$$

$$c_x = c_{gx} + U_x \ \& \ c_y = c_{gy} + U_y \quad (3.19)$$

In circumstances like in the current study where velocity field and bathymetry change during the simulation, it is often desirable to call the wave module more than once. At each call to the wave module, the latest bed elevation, water elevations, and current velocities are transferred from the FLOW module to the wave module.

Wave action on the coastal seas may influence morphology for the following reasons:

(i) Wave forcing due to breaking, by radiation stress gradients, modeled as shear stress at the water surface (Dingemans et al. 1987) $\overline{\mathrm{M}} = \frac{\mathrm{D}}{\omega} \bar{k}$
   a. In where $\overline{\mathrm{M}}$=Forcing due to radiation stress gradients= Dissipation due to wave
   b. breaking (W/m²),ω = Angular wave frequency $\left(\frac{rad}{s}\right)$, and $\underset{k}{\rightarrow}$=Wave number
   c. vector (rad/m)

(ii) The effect of enhanced bed shear stress on the flow simulations, using the wave-current interaction of Fredsoe (1984)

(iii) Wave-induced mass flux, adjusted for the vertically non-uniform Stokes drift (Walstra 2000)

(iv) Additional turbulence production due to dissipation in the bottom wave boundary and due to wave white capping and breaking at the surface, which is included in the k-ε turbulence closure model (Walstra et al. 2000)

(v) Streaming, a wave induces a current in the bottom boundary layer directed in the direction of wave propagation, modeled as additional shear stress acting across the thickness of the bottom wave boundary layer (Walstra et al. 2000). In other words, a time-averaged shear stress, which results from the fact that the horizontal and vertical orbital velocities are not exactly 90 degrees out of phase.

3.3.2 Sediment Transport and Morphology

Delft3D supports both bed-load transport and suspended-load transport for non-cohesive material. Complications, if compared to modeling of constituents like heat, are, for example the exchange of sediment with the sediment bed and the settling velocity caused by gravity. Exchange of sediment with the sediment bed causes changes in bed level, which results in changes in hydrodynamic behavior. In this way, the interaction between flow, sediment transport, and morphology is taken into account.

Three-dimensional *suspended-load transport* is calculated using a three-dimensional advection diffusion equation. When using Delft3D in depth-averaged mode, also three-dimensional advection diffusion equation is averaged over the water depth. The flow velocities and eddy diffusivities are based on the results of the hydrodynamic calculation. The settling velocity is determined by the formulations of Van Rijn (1993) by default. The transport equation is not used when sediment type "bedload" is defined or when a transport formula is chosen that calculates a total transport, for instance Engelund & Hansen or Meyer-Peter-Müller.

Bed-load transport is calculated by transport formulas. These formulas give the magnitude of the transport. Subsequently, the sediment transport rates at the cell interfaces are determined, and corrected for slope effects, bed composition, and sediment availability. Several bed-load formulations are available in Delft3D, varying in complexity and applicability. Bed-load transport is corrected for slope effects by a rotation of the transport vector. At the boundaries, morphological boundary conditions should be defined. Sediment transports, bed levels, and bed level changes can be prescribed. An alternative approach is the use of a Neumann boundary condition, which sets the inflow sediment concentration equal to the concentration calculated in the interior.

A number of standard sediment transport formulas are available in Delft3D, including Engelund & Hansen, Meyer-Peter-Müller (which both give a total transport rate) and Van Rijn (1993), which gives both suspended-load and bed-load transport rates. The more advanced formulas in Delft3D also include the effects of, for instance waves. Because morphological processes take place at significantly larger time scales than the flow, a morphological acceleration factor can be used. The calculated bed level change within one-time step is simply multiplied with this factor. In this way, computation times are decreased.

3.3.3 Nearshore Hydraulic Structures

In Civil Engineering practice, the domain of interest often has dimensions in the order of kilometers. To limit computation demands, a computational coarse grid is often chosen. The consequence is that not all details of the hydraulic structures present in the domain can be resolved onto the horizontal grid. That is why the structures are treated as sub-grid features in Delft3D. A parameterization is applied to account for the force on the flow generated by the structure. The hydraulic structures are placed on the velocity points of the staggered grid. The width of the hydraulic structures is set to zero. In this section, the different types of hydraulic structures in Delft3D are described.

Four types of parameterization are possible; they are:

Partial blockage of the flow by a *3D gate*. The velocities and transport fluxes perpendicular to the hydraulic structure are set to zero. Both movable and fixed gates can be selected.

The second type of parameterization is *quadratic friction*. The flow through a hydraulic structure is related to the difference between the upstream and downstream water levels h by a Q-H relationship (3.38), in which μ is a dimensionless contraction coefficient, depending on the kind of hydraulic structure and A is the wet cross-section. A local equilibrium between the force on the flow due to the obstruction and the local water level gradient is assumed. An additional quadratic friction term is inserted into the momentum equations, depending on the contraction coefficient.

$$Q = \mu A \sqrt{2g|h_u - h_d|} \tag{3.20}$$

Thirdly, Delft3D offers the possibility of adding a linear friction term to the momentum equations, to reduce the flow rate through a certain cross-section. This kind of hydraulic structure is also known as a rigid sheet. The user should define the loss coefficients manually.

Finally, floating structures can be defined. All energy loss formulations assume subcritical flow, except for the 2D-weir, for which an empirical formulation for supercritical flow has been implemented. The table below gives an overview of the relevant types of hydraulic structures. For a complete overview, reference is made to the Delft3D-FLOW user manual (DELTARES, 2014).

Table 3.1: Overview of types of hydraulic structures in Delft3D

3 D-gate	Represents small obstacles in the flow by inserting a vertical plate in one of the grid directions over one or more computational layer (3D)
Barrier	A barrier restricts the flow area from above by blocking a part of the water depth. Combination of a movable gate and a quadratic friction term (3D) or only quadratic friction (2D)
Current deflection wall	Combination of a fixed gate and a quadratic friction term. A current deflection wall can be seen as a "plate on piles" in the flow. (3D)
Thin Dam	All the velocities and transport fluxes perpendicular to this type of hydraulic structure are set to zero over the complete water depth. (2D and 3D)
Weir	Weirs are fixed structures, causing a local energy loss to the flow. They are commonly used to model sudden depth changes due to the presence of, for example roads, dikes and groins.2D-weirs are used in 2D horizontal mode, local weir in 3D mode

(Table 3. 1 continues)

2D-weir	The user-defined crest level is only used to determine whether the weir is emerged or submerged in the drying and flooding algorithm. When the weir emerges, it acts as a thin dam. In a submerged state, a quadratic friction formula is used. For supercritical flow, the discharge is completely determined by upstream energy head. For subcritical flow, the energy loss is determined by a Carnot loss or using experimental data from tables. The choice is depending on the local flow velocity. (2D)
Local weir	The water depth at the weir point is decreased, depending on the crest height. A part of the energy loss is computed directly by the discretization of the convection terms in the momentum equations and the bottom friction term. (3D)
Culvert	Intake/outlet coupling structure. The discharge through the culvert depends on the water level difference over the culvert. A quadratic friction term is applied. (3D)

3.3.4 Propagation through Breakwater and Groins

In the Wave model of Delft3D, SWAN can estimate wave transmission through a (line-) structure such as a breakwater and groin. Such an obstacle will affect the wave field in two ways; First, it will reduce the wave height locally all along its length, and second, it will cause diffraction around its end(s). The model is not able to account for diffraction. In irregular, short-crested wave fields, however, it seems that the effect of diffraction is small, except in region less than one or two wavelengths away from the tip of the obstacle (Booij *et al.*, 1992). Therefore, the model can reasonably account for waves around an obstacle if the directional spectrum of incoming waves is not too narrow. Since obstacles usually have a transversal area that is too small to be resolved by the bathymetry grid in SWAN, an obstacle is modelled as a line. If the crest of the breakwater is at a level where (at least part of the) waves can pass over, the transmission coefficient Kt (defined as the ratio of the (significant) wave height at the down-wave side of the dam over the (significant) wave height at the up-wave side) is a function of wave height and the difference in crest level and water level. The expression is taken from Goda *et al.* (1967):

$$K_t = 0.5\ [\ 1\text{-}\ sin\ (\frac{\pi}{2\alpha}(\frac{F}{H_i}+\beta))]\ for\ -\beta-\alpha<\frac{F}{H_i}<\alpha-\beta \qquad (3.21)$$

where $F = h - d$ is the freeboard of the dam and where Hi is the incident (significant) wave height at the up-wave side of the obstacle (dam), h is the crest level of the dam above the reference level (same as reference level of the bottom), d the mean water level relative to the reference level, and the coefficients α, β depends on the shape of the dam (Seelig, 1979):

Table 3.2: List of coefficients α, β value according to shape of the dam

Case	α	β
Vertical thin wall	1:8	0.1
Caisson	2.2	0.4
Dam with slope 1:3/2	2.6	0.15

The above expression is based on experiments in a wave flume, so strictly speaking it is only valid for normal incidence waves. Since there is no data available on oblique waves it is assumed that the transmission coefficient does not depend on direction. Another phenomenon that is to be expected is a change in wave frequency since often, the process above the dam is highly non-linear. Again, there is little information available, so in the model, it is assumed that the frequencies remain unchanged over an obstacle (only the energy scale of the spectrum is affected and not the spectral shape).

3.4 Governing Equation for Nearshore Hydrodynamics

The flow model is two-dimensional hydrodynamic simulation program which calculates non-steady flow resulting from tidal and meteorological forcing on rectilinear grid. The model solves the non-linear shallow water equations on a dynamically coupled system of nested grid using a finite difference numerical scheme. It simulates unsteady two-dimensional flows taking into account density variations, bathymetry, and external forcing such as metrology, tidal elevations, currents, and other hydrographical conditions. The basic partial differential equations are the depth-integrated continuity and momentum equations; shallow water equations have been presented by Equation (3.22), (3.23), and (3.24). The governing equations of hydrodynamics solving hydraulic problems in coastal areas are:

Conservation of Mass Equation:

$$\frac{\partial \varepsilon}{\partial t}+\frac{\partial p}{\partial x}+\frac{\partial q}{\partial y}=0 \tag{3.22}$$

Conservation of momentum equation:

The momentum equation in the x-direction is given by,

$$\frac{\partial P}{\partial t}+\frac{\partial P^2/h}{\partial x}+\frac{\partial Pq/h}{\partial y}+gh\frac{\partial \varepsilon}{\partial x}+\frac{f}{2}\frac{\sqrt{p^2+q^2}}{h^2}P-\frac{1}{p}\frac{\partial \tau_{xy}h}{\partial y} - \Omega q-\frac{\rho_a}{\rho}C_wWW_x+\frac{h}{\rho}\frac{\partial P_a}{\partial x}=0 \tag{3.23}$$

The momentum equation in the y-direction is given by:

$$\frac{\partial q}{\partial t}+\frac{\partial q^2/h}{\partial y}+\frac{\partial Pq/h}{\partial x}+gh\frac{\partial \varepsilon}{\partial y}+\frac{f}{2}\frac{\sqrt{p^2+q^2}}{h^2}q-\frac{1}{p}\frac{\partial \tau_{yx}h}{\partial x} - \Omega p-\frac{\rho_a}{\rho}C_wWW_x+\frac{h}{\rho}\frac{\partial P_a}{\partial y}=0 \tag{3.24}$$

Where,

P and q flux in x and y directions respectively ($m^3/s/m$)
t time (s),x and y (m) are Cartesian Co-ordinate (s).
h water depth (m)
g acceleration due to gravity (9.81 m^2/s)
ε sea surface elevation (m)
ρ_w *and* ρ_a air and water density respectively (kg/m^3)
C_w wind speed (m/s)
Ω *Coriolis parameter*
ρ_a atmospheric pressure ($kg/m/s^2$)

Resistance term:

The bed resistance in the Hydrodynamic: either as a Chezy number or as a Manning number in Equation (3.25).

$$\text{Bed Resistance} = \frac{g*u*|u|}{C^2} \tag{3.25}$$

Where g is gravity, u is velocity and C is the Chezy number. Manning numbers are converted to Chezy numbers as follows by Equation (3.26).

$$C=M*h^{\frac{1}{6}} \tag{3.26}$$

Where M is the Manning number and h is the water depth.

Eddy Viscosity:

The eddy viscosity E has been specified in the model as a time-varying function of the local gradients in the velocity field. This formulation is based on the so-called Smagorinsky concept, which yields the Equation (3.27).

$$E = C_s^2 \Delta^2 \sqrt{\left(\frac{\partial U}{\partial x}\right)^2 + \frac{1}{2}\left(\frac{\partial U}{\partial y} + \frac{\partial U}{\partial x}\right) + \left(\frac{\partial V}{\partial y}\right)} \tag{3.27}$$

Deldt3D-Flow simulates two-dimensional (2D, depth-averaged) unsteady flow and transport phenomena resulting from tidal, density difference, or wave forcing. If the flow variation in the vertical direction is negligible, then a 2D approach is suitable for simulations, while 3D modeling is of particular interest when the horizontal flow field shows significant variation in the vertical direction.

The Navier Stokes equation for an incompressible fluid, under the shallow water and Boussinesq assumptions are solved, and vertical momentum accelerations are neglected which results in hydrostatic pressure equations, due to the fact that these accelerations are negligible comparing to gravitational acceleration. In the horizontal direction, Delft3D-Flow uses orthogonal curvilinear coordinates. For the sake of clarity, the equations are presented only in their Cartesian rectangular form.

The continuity equation is given by:

$$\frac{\partial \xi}{\partial t}+\frac{\partial[(d+\xi)U]}{\partial X}+\frac{\partial[d+\xi)V}{\partial y}+\frac{\partial[(d+\xi)]}{\partial z}=Q \tag{3.28}$$

U=u+u_s and V= v+v_s

Where,

ξ= Water level above a reference level (datum)
T= Time
D=Depth below a frame of reference
U=GLM (Generalized Lagrangian Mean, see Walstra et al. 2000 and Groeneweg,1999) velocity component in the x-direction
V= GLM velocity component in the y-direction
Q= Contribution per unit area due to the discharge or withdrawal of water

u and v are Eulerian velocity components, while us and vs are stoking drift components. The momentum balance equation in the x-direction is as follows:

$$\frac{\partial U}{\partial t} + U\frac{\partial V}{\partial x} + V\frac{\partial V}{\partial y} + w\frac{\partial V}{\partial x} \quad - fv =$$

$$M_x + \frac{1}{\rho}\frac{\partial p}{\partial x} + \frac{1}{h^2}v_v\frac{\partial^2 v}{\partial \sigma^2} + \quad v_h\left(\frac{\partial^2 U}{\partial x^2} + \frac{\partial^2 U}{\partial y^2}\right) \tag{3.29}$$

The corresponding momentum balance equation in the y direction is given below:

$$\frac{\partial U}{\partial t} + U\frac{\partial V}{\partial x} + V\frac{\partial V}{\partial y} + w\frac{\partial v}{\partial z} + fv = M_y - \frac{1}{\rho}\frac{\partial p}{\partial y} + \frac{1}{h^2}v_h\left(\frac{\partial^2 V}{\partial x^2} + \frac{\partial^2 V}{\partial y^2}\right) \tag{3.30}$$

The imbalance of horizontal Reynold's stresses is modeled using the eddy viscosity concept. This concept expresses the Reynolds stress component as the product between a flow as well as grid-dependent eddy viscosity coefficient and the corresponding component of the mean rate of deformation tensor, for further details refer to Delft3D-Flow manual.

The Hydrostatic pressure balance equation under "shallow water assumption" is given as:

$$\frac{1}{\rho}\frac{\partial p}{\partial \sigma} = -\rho g h \tag{3.31}$$

Moreover, the horizontal pressure gradients are given by Boussinesq approximation as:

$$\frac{1}{\rho_o}\frac{\partial P}{\partial x} = g\frac{\partial \xi}{\partial x} g\frac{h}{\rho_o}\int_{\sigma}^{0}\left(\frac{\partial \rho}{\partial x} + \frac{\partial \sigma'}{\partial x}\frac{\partial \rho}{\partial \sigma'}\right).d\sigma' \qquad (3.32)$$

$$\frac{1}{\rho_o}\frac{\partial P}{\partial y} = g\frac{\partial \xi}{\partial y} g\frac{h}{\rho_o}\int_{\sigma}^{0}\left(\frac{\partial \rho}{\partial y} + \frac{\partial \sigma'}{\partial y}\frac{\partial \rho}{\partial \sigma'}\right).d\sigma' \qquad (3.33)$$

Transport Equation: Suspended sediment transport is governed by advection-diffusion equation, which reads:

Transient Term Horizontal Advection Term Vertical Advection Term Horizontal Diffusion Term

$$\frac{\partial[hc]}{\partial t} + \quad \frac{\partial[hUc]}{\partial x} + \frac{\partial[hVc]}{\partial y} + \frac{\partial[\omega c]}{\partial \sigma} = \quad h[\frac{\partial}{\partial x}(D_H\frac{\partial C}{\partial y})] +$$

Vertical Diffusion Term Source or Sink of Material

$$\frac{1}{h}\frac{\partial}{\partial \sigma}(D_V\frac{\partial C}{\partial \sigma}) + hs$$

C= Concentration of material (in this case suspended sediment)

D_H= Horizontal eddy diffusivity

D_v=Vertical eddy discursivity

h=Depth

The vertical velocity,ω,in the σcoordinate system, is computed from the continuity equation

$$\frac{\partial \omega}{\partial \sigma} = -\frac{\partial \xi}{\partial t} - \frac{\partial[hU]}{\partial x}\frac{\partial[hV]}{\partial y} \qquad (3.35)$$

To solve the equations above, the horizontal and vertical viscosity and diffusivity need to be prescribed. In Delft3D-FLOW, the horizontal viscosity and diffusivity are assumed to be a superposition of three parts: (1) molecular viscosity, (2) “3D turbulence”, and (3) ”2D turbulence” which is a measure of the horizontal mixing that is not resolved by advection on the horizontal computational grid. “2D turbulence” values may either be specified by the user as a constant or as a space-varying parameter. The vertical eddy diffusivity is scaled from the vertical eddy viscosity according to:

$$D_V = \frac{v^V}{\sigma_c} \tag{3.36}$$

Where,σ_c is the Prandtl-Schmidt number

3.5 Application of Mathematical Model

The hydrodynamic module of Delft3D, which is called Delft3D-Flow, is a fully integrated computer software suite for a multidisciplinary approach and 3D computations in rivers, estuarine environment, and coastal seas. The model is capable of simulating different phenomena, including wave-driven currents, Non-hydrostatic flows, Transport of dissolved material and pollutants, Online sediment transport and morphology, etc. For more information, see Delft3D Flow Manual.

3.5.1 Application of Delft3D Model

Delft3D-Flow module solves the nonlinear unsteady shallow water equations derived from the three-dimensional Navier Stokes equations for incompressible free surface flow, under the Boussinesq assumption, in two (depth-averaged) or in three dimensions. This system of equation consists of horizontal equation of motion, continuity equation and conservation of constituent for sediment.

3.5.2 Grid and Coordinates

The numerical method of Delft3D-FLOW is based on finite differences. To discretise the 3D shallow water equations in space, the model area, is covered by a curvilinear grid. In 3D simulations, a boundary fitted approach (σ -coordinate) is used for the vertical grid direction (Figure 3.2), and for 2D simulation, the boundary fitted approach is not used.

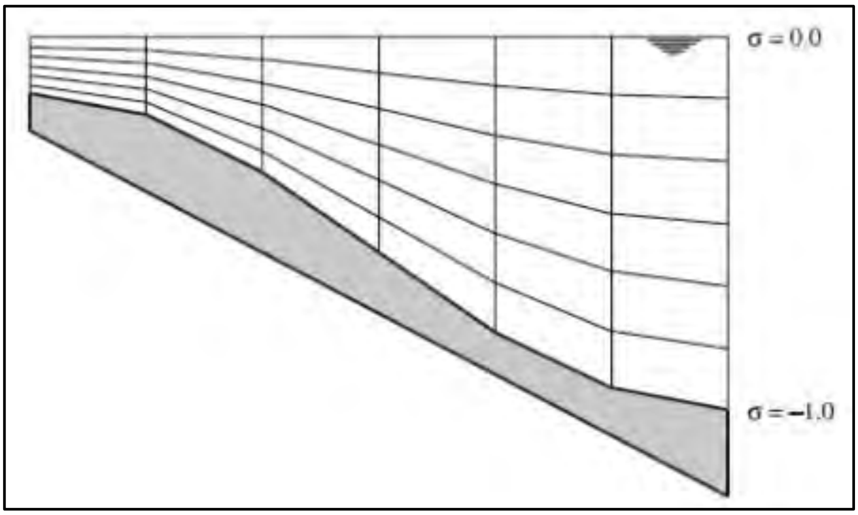

Figure 3.2: An example of a vertical grid consisting of six equal thicknesses σ -layers (Source: Lesser et al. 2004)

The vertical σ-coordinate is scaled as (-1< σ< 0) ; σ= (z-ζ)/h. The primitive variables, water level and velocities (u, v, w) describe the flow. To discretise the 3D shallow water equations, the variables are arranged in a special way on the grid. The pattern is called a staggered grid. This particular arrangement of the variables is called the Arakawa C-grid (Figure 3.3, 3.4 & 3.5). The water level points (pressure points) are defined in the Centre of a (continuity) cell. The velocity components are perpendicular to the grid cell faces where they are situated.

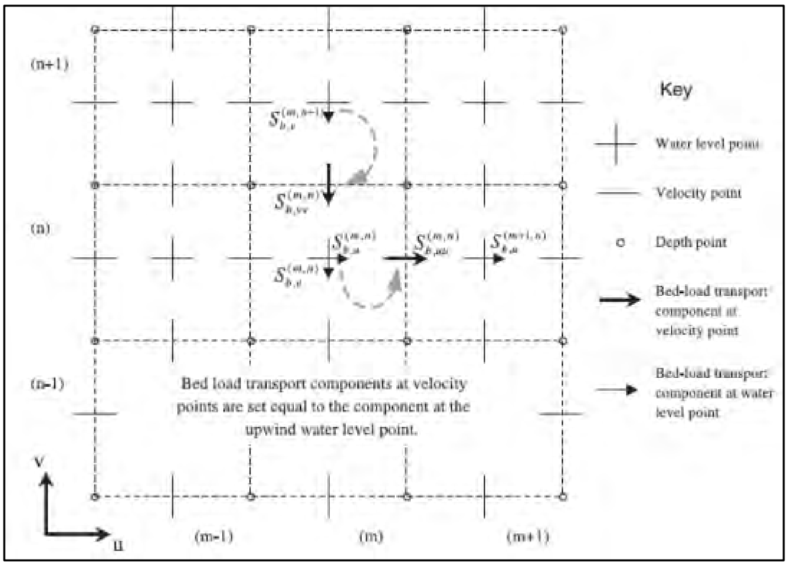

Figure 3.3: $Staggered\ grid\ used\ in\ Delft3D$ ($Source$: $Lesser\ et\ al.$ 2004)

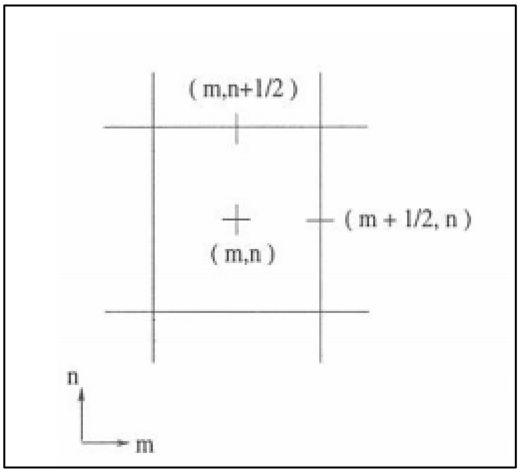

Figure 3.4: m and n are the computation number of the grids (Source: Lesser et al. 2004)

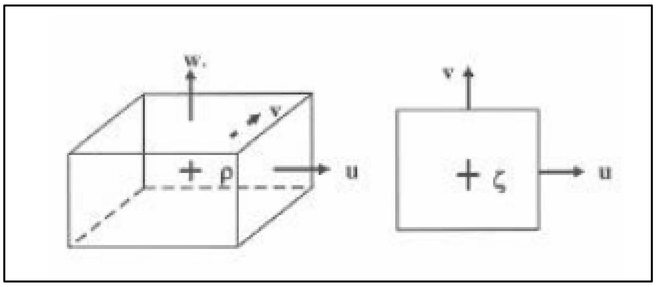

Figure 3.5: velocity (u, v & w) points and water level (Source: Lesser et al. 2004)

3.5.3 Boundary Conditions

Bed and free surface boundary conditions: In the σ coordinate system,the bed and the free surface correspond with the σ planes. Therefore, the vertical velocities at these boundaries are simply:

$$\omega(-1) = 0 \; and \; \omega(0) = 0$$

Friction is applied at the bed as:

$$\frac{v_v}{h}\frac{\partial u}{\partial \sigma}|\sigma = -1 = \frac{\tau_{bx}}{\rho} \; \& \; \frac{v_v}{h}\frac{\partial u}{\partial \sigma}|\sigma = -1 = \frac{\tau_{by}}{\rho} \qquad (3.37)$$

Where τ_{bx} and τ_{by} are bed shear stress components that include the effects of wave current interaction.At the lateral boundaries of the model, since the longshore water level surface gradient does not change (steady wave field), water level gradients are imposed as zero and the model determines the correct solution (so-called Neumann boundaries):

$\frac{\partial \xi}{\partial x}$=0

These two lateral boundaries combined with a water level boundary (seaward) outline the boundary conditions of the model. The important assumption lying behind the transport equation is that the horizontal transport of dissolved substances is dominated by advection; meaning, at the open inflow boundary the entering concentration of sediment must be given (in our case, equilibrium sediment concentration at the inflow boundary, calculated within the model), and at the outflow boundary the sediment concentration must be free.

3.5.4 Stability and Accuracy

The Delft3D code uses an implicit numerical scheme, resulting in unconditional stability. However, too large time steps cause inaccurate results. This can be checked using the *Courant wave number* and the *Courant advection number* (Courant and Hilbert,1962). The Courant wave number is related to the propagation of energy through the system. During one time step Δt , energy is moved over a distance $c\Delta t$. The Courant wave number,

$$c\frac{\Delta t}{\Delta x}, \tag{3.38}$$

gives the number of cells over which the energy is moved within one-time step. When the wave celerity c= $\sqrt{gd}$ changes gradually, large Courant wave numbers can be applied in the order of 60. When sudden depth changes occur, the Courant wave number should be decreased.

The Courant advection number is related to the advection of water with the flow velocity *U*. The main importance of this number is the accuracy of the drying and flooding algorithm. During one time step Δt , water is moved over a distance $U\Delta t$. The Courant advection number,

$$u\frac{\Delta t}{\Delta x}, \tag{3.39}$$

gives the number of cells per time step that is skipped during drying or flooding with a velocity *U*.

3.6 Methodology of the Study

A coupled system of Delft3D Flow-Wave is needed for developing the Bay of Bengal model. For the process, proper calibration and validation are needed to justify its functionality in the nearshore environment. In this study, General bathymetric chart of the Oceans (GEBCO) used for generating Bathymetry and valid through survey data. A Matlab tool (Delft Dashboard), which is a part of the OpenEarth Toolbox used for extracting the bathymetry initially, it also used for setting up the model. Furthermore, manual inputs are provided to setup different datasets for the development of the model. The calibration and validation will be done through setting up the boundary data with different climatic parameters such as wind speed, wind direction, wave height, wave period, wave direction, sediment properties, the roughness of the sea, etc. A detailed literature review has been carried out to decipher the wind-wave complex system development in Delft3D model. The total methodology has been discussed below step by step,

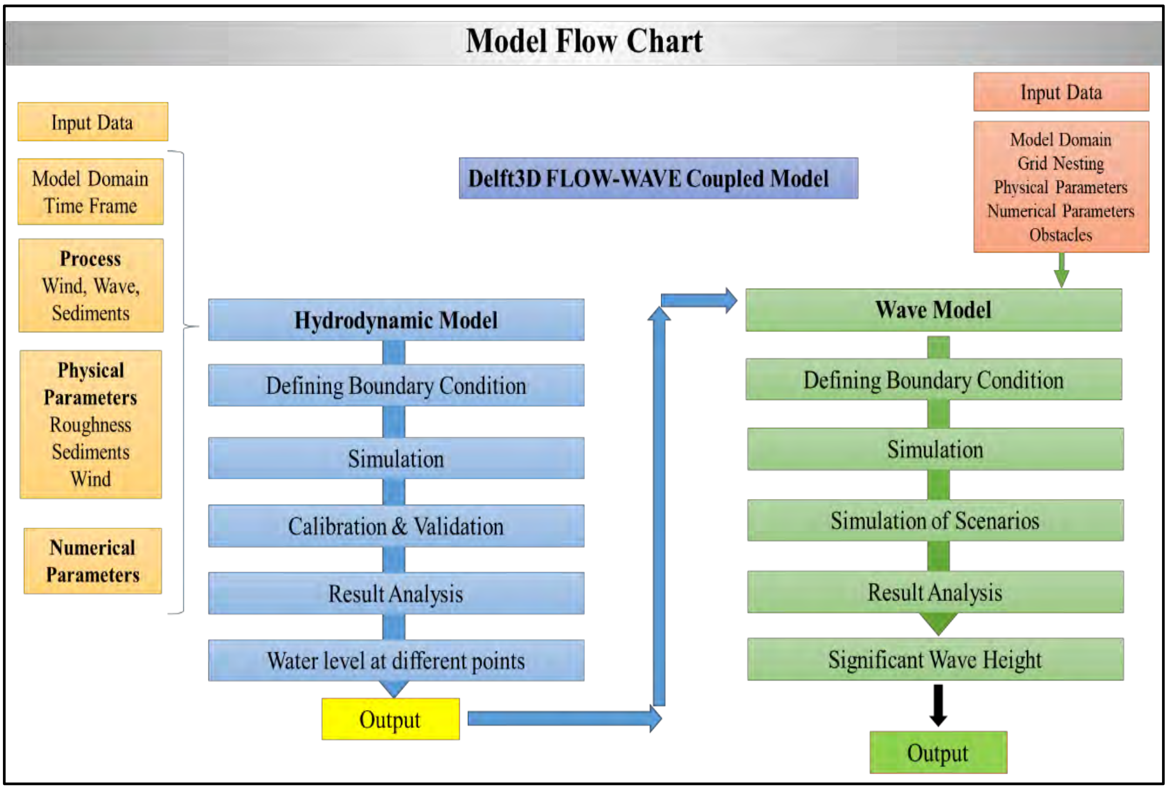

Figure 3.6: Delft3D FLOW-WAVE Coupled Model Flow chart for the study

3.6.1 Data collection

In this study, a different dataset has been used to set up the model for proper calibration and validation. The bathymetry and grid data were extracted from the General Bathymetric Chart of the Oceans (GEBCO) and British Oceanographic Data Centre (BODC) and validated by field survey data from the Institute of Water Modelling (IWM). Shoreline data has been collected from the world vector shoreline of the National Geospatial-Intelligence Agency (NGA). Tidal water level and discharge data have been collected from the Bangladesh Water Development Board, Bangladesh Inland Water Transport Authority, and International Hydrographic Organization. Following are the list of data used for the study,

(i) Bathymetry Data (GEBCO_08)
(ii) Shoreline Data
(iii) Tidal Water level and Discharge Data
(iv) Wind and Wave Data
(v) Boundary Data
(vi) Sediment Data

(i) Bathymetry Data

Bathymetric data have been collected from the General Bathymetric Chart of the Oceans (GEBCO)_08, which is a continuous terrain model for ocean and land with a spatial resolution of 30 arc second, and the grids are download from the British Oceanographic Data Centre (BODC) through the Delft Dashboard. The GEBCO_08 Grid was first released in 2009, and final updates available to the year 2014 from GEBCO_14. In the latest release of Bathymetry data for the Indian Ocean, Bathymetric survey carried out by HMS Scott in 2005, which is the same as for GEBCO_08 and GEBCO_14 version. For validating the GEBCO data, different survey data from the Institute of Water Modelling (IWM) have been used. Data sources for bathymetry preparation are given in Table 3.3

Table 3.3: Data sources for generating the bathymetry for the Bay of Bengal model

Water Body (Rivers, Estuary, Sea)	Source of Data
Bay of Bengal	General Bathymetric Chart of the Oceans (GEBCO), British Oceanographic Data Centre (BODC) and International Hydrographic Organization (Last updated on 2010)
Bay of Bengal	British Admiralty Chart Nos. 814, 829 and 859
Along Cox-bazar Marine drive	Institute of Water Modeling (IWM) surveyed data

The surveyed bathymetry data has been collected from the Institute of Water Modelling (IWM) in BTM (Bangladesh Transverse Mercator) coordinate system. Then these data have been converted from BTM co-ordinate system to UTM (Universal Transverse Mercator) co-ordinate system and finally it has been converted into corresponding latitude-longitude for validating the bathymetry of the Bay of Bengal model.

(ii) Shoreline Data

Shoreline data is collected from the world vector shoreline. The original World Vector Shoreline (WVS) was a digital data file containing the shorelines, international boundaries, and country names of the world. WVS data were processed into NGA's Vector Product Format in 1995, resulting in the highest resolution demarcation of coastline globally available, the World Vector Shoreline Plus. Information of the shoreline data used for generating the model has been presented in Table 3.4

Table 3.4: shoreline data used for generating the model

Model Component	Type of Data Source	
	Land	Land-Water Boundary
1800 m grid		Delft Dashboard
10 m grid	Digital Elevation Model	Delft Dashboard and LANDSAT

(iii) Tidal Water Level and Discharge Data

The tidal water level and discharge data are collected from International Hydrographic Organization (IHO), Bangladesh Water Development Board (BWDB), and used to generate boundary conditions, observation points for calibration, and validation purposes. Calibration and validation are done for the selected month of pre-monsoon (May) and post-monsoon (October) for 2007 and 2008 in the Bay of Bengal model. The following table shows the calibrated and validated data points,

Table 3.5: Tidal water level and Discharge data for model calibration and validation

Gauge Station Authority	Station Name	Latitude (Degree)	Longitude (Degree)
Water Level Data			
IHO	CTG IHO, Bangladesh	22.23	91.83
	Pasur river, Bangladesh	21.97	89.52
	Akyab, Myanmar	20.13	92.83
	Short Island, India	20.75	87.08
Discharge Data			
BWDB	Barurua	23.46	89.48
	Pasur River	21.97	89.52

(iv) Wind and Wave Data

The Bay of Bengal basin experiences three different types of weather systems, fair weather or the pre-monsoon period (February–May), the southwest or the summer monsoon period (June–September), and northeast or post-monsoon season (October–January). In this study, calibrated and validated was done for pre-monsoon (May) and post-monsoon (October) for 2007 and 2008. All the relevant data were collected from the Danish Hydraulic Institute (DHI) open data portal.

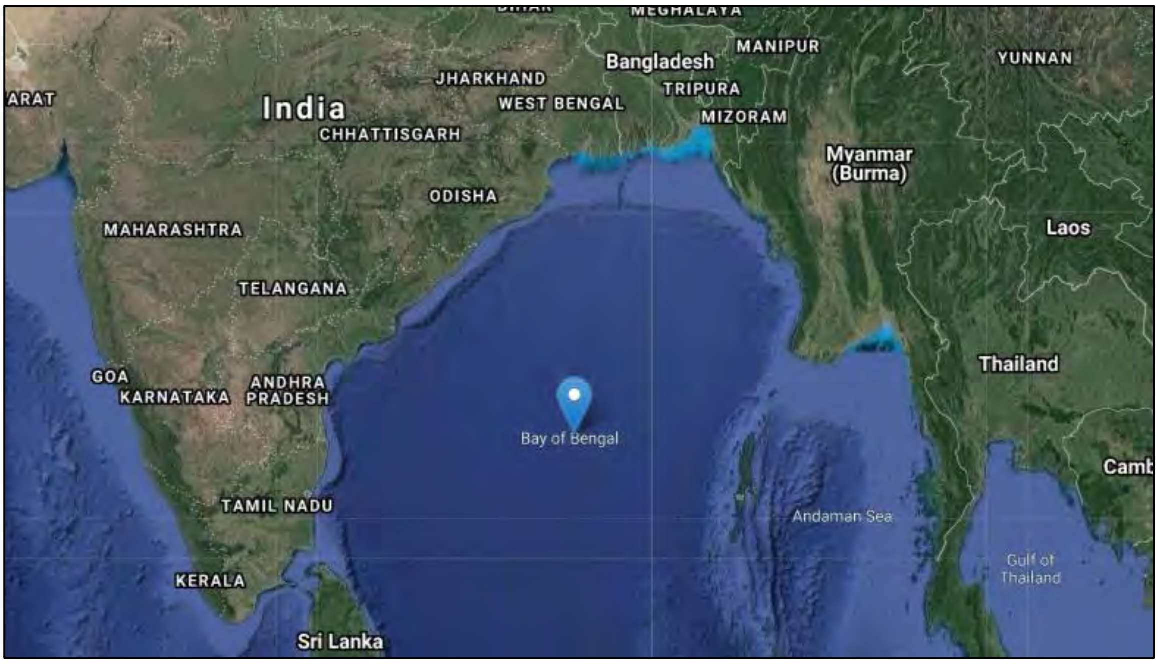

Figure 3 7: Data extraction location at Bay of Bengal (Latitude: 13°60′, Longitude: 87°65′)

Wind Data:

Wind data has been collected from Global, Met. Parameters (incl. 10m wind) at 0.2 deg., Climate Forecast System Reanalysis (CFSR), from NCEP NOAA. A global high accuracy wind dataset for the period from 1979 until present with hourly values at a spatial resolution of 0.3° during 1979 to 2010, and 0.2° from 2011 and onwards is available at DHI open data portal. A dataset for the year of 2007 (calibration period) and 2008 (validation period) has been extracted. The followings are the wind rose and wind direction used for calibration and validation of the model in the pre-monsoon period (May) and post-monsoon period (October)

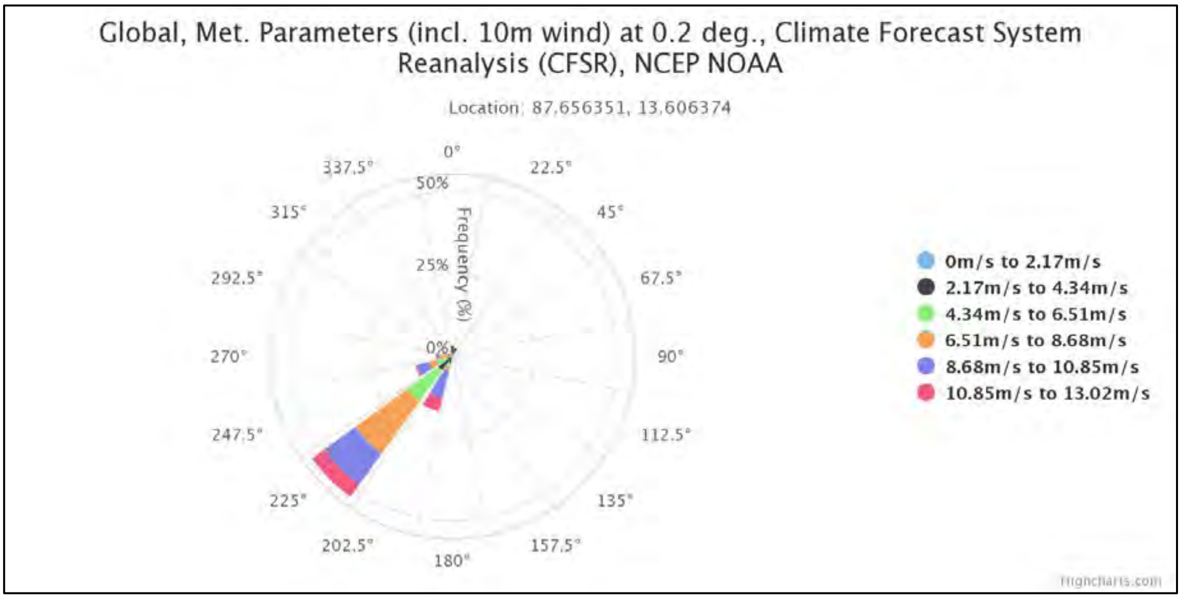

Figure 3 8 : Wind rose for May 2007 for calibration (Latitude: 13°60´, Longitude: 87°65´)

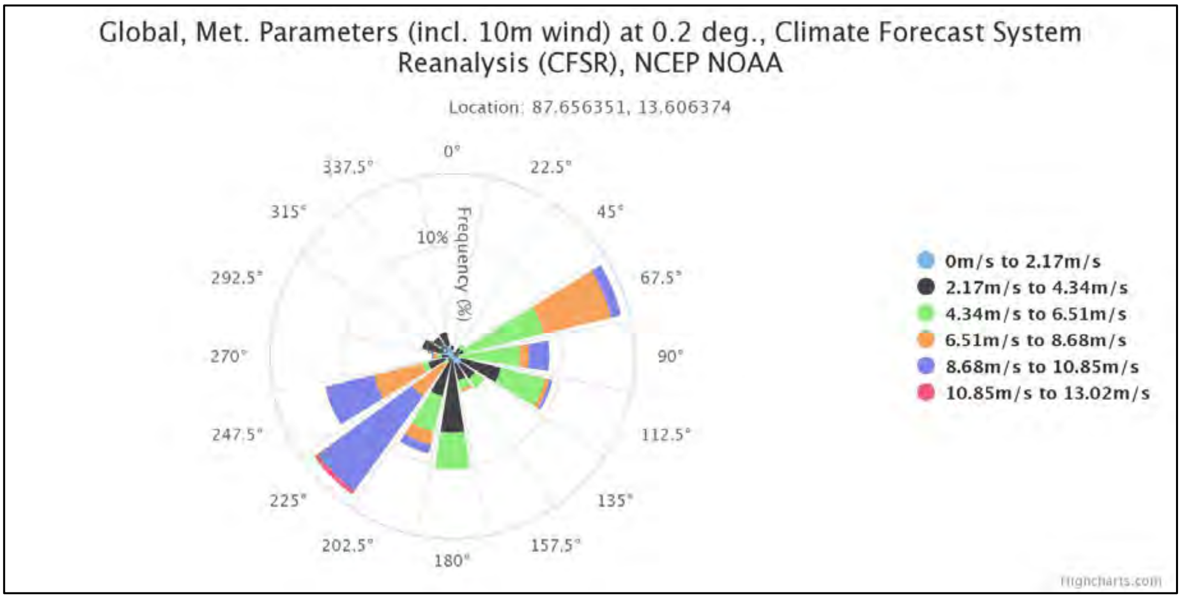

Figure 3 9: Wind rose for October 2007 for calibration (Latitude: 13°60´, Longitude: 87°65´)

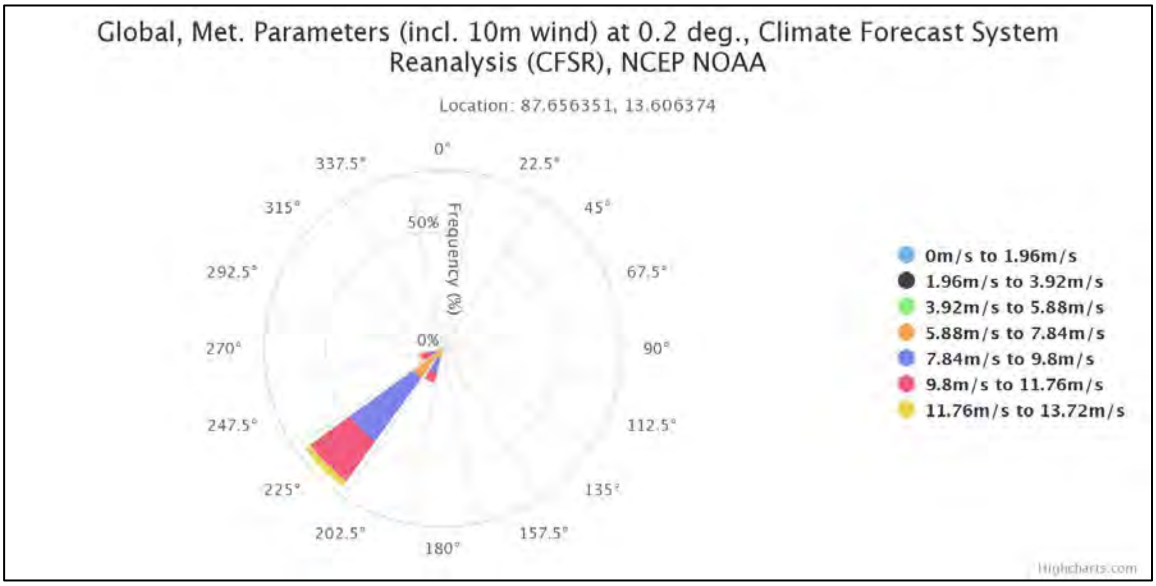

Figure 3 10: Wind rose for May 2008 for validation (Latitude: 13°60´, Longitude: 87°65´)

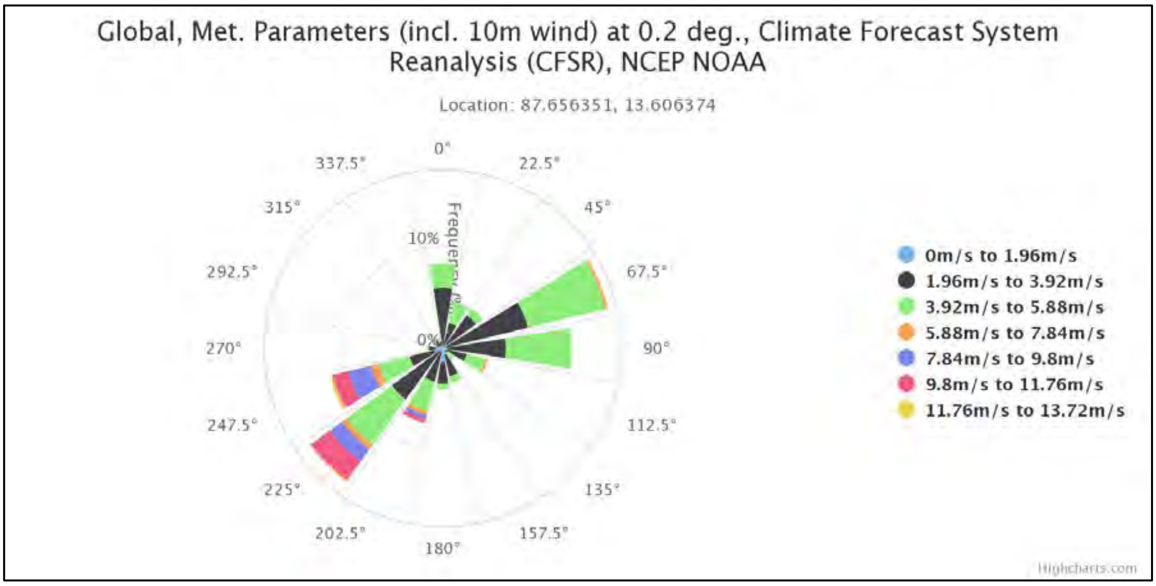

Figure 3 11: Wind rose for October 2008 for validation (Latitude: 13°60´, Longitude: 87°65´)

Wave data:

Wave data used for this study collected from the Bay of Bengal MIKE 21 Spectral Wave Model (SW) by DHI. The dataset is generated by DHI's MIKE 21 SW wave model based on the high accuracy global CFSR wind data. Wave conditions are available for a 36 years period at hourly interval at a few kilometers interval and with fully spectral information at a slightly lower spatial resolution 0.1° or 0.5°, depending on focus area. These data have been extracted from DHI open data portal. Following are the used data for calibration and validation of the model,

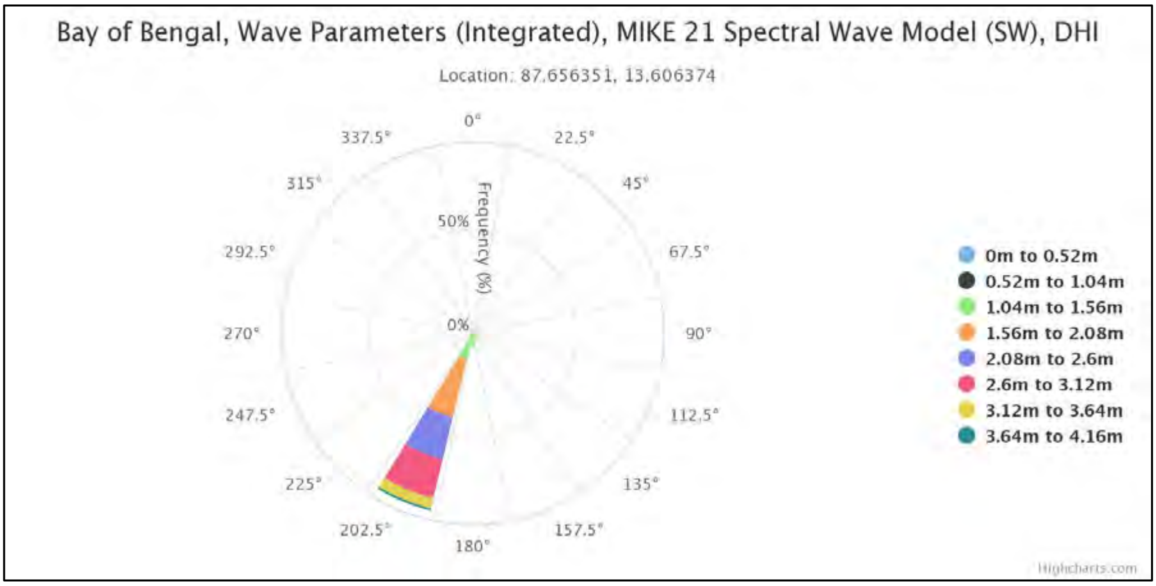

Figure 3 12: Wave rose for May 2007 for calibration (Latitude: 13°60′, Longitude: 87°65′)

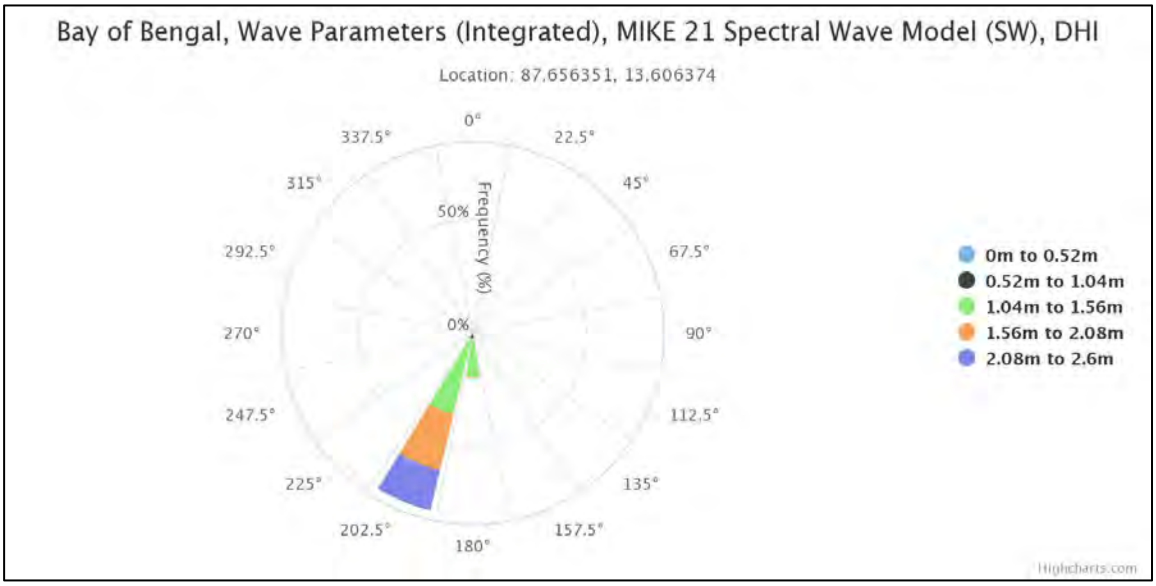

Figure 3 13: Wave rose for October 2007 for calibration (Latitude: 13°60′, Longitude: 87°65′)

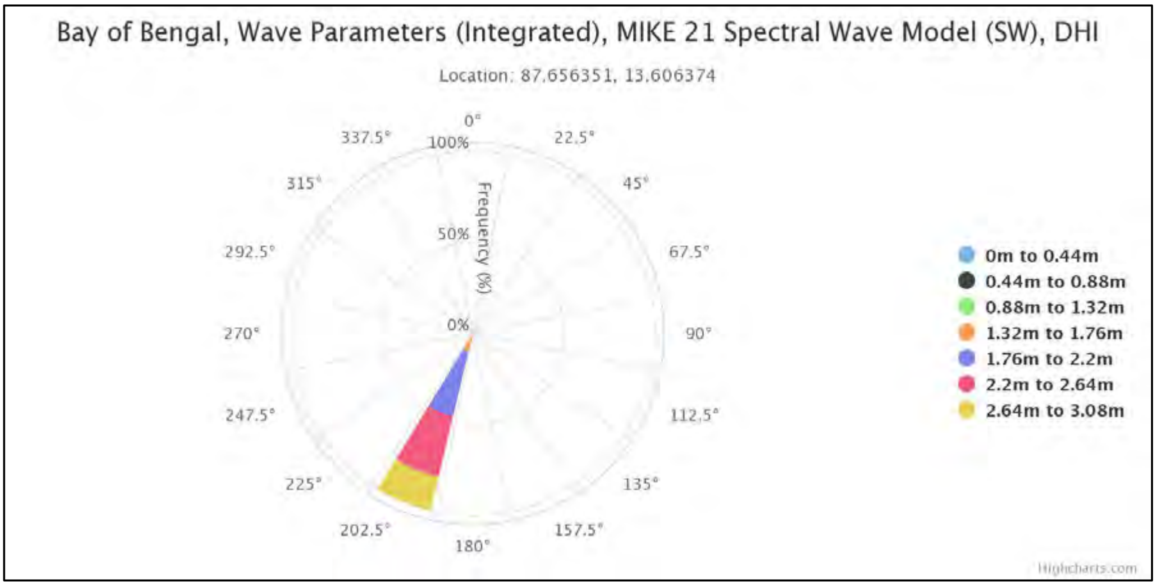

Figure 3 14: Wave rose for May 2008 for validation (Latitude: 13°60´, Longitude: 87°65´)

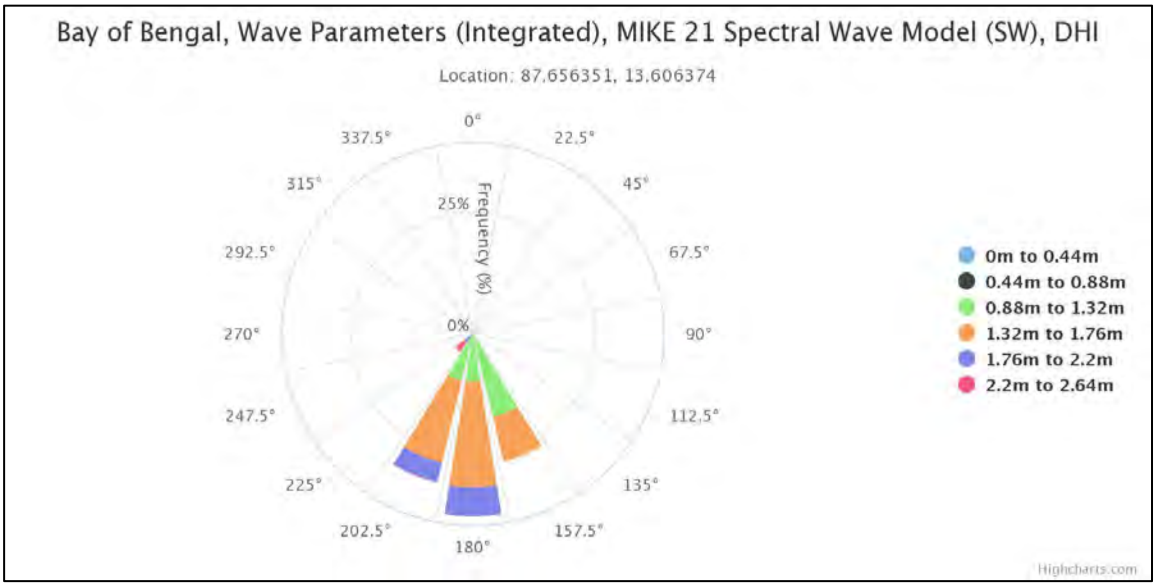

Figure 3 15: Wave rose for October 2008 for validation (Latitude: 13°60´, Longitude: 87°65´)

For calibration and validation of the wave model, measured wave data have been collected from the Institute of Water Modeling (IWM) for their surveyed data along the cox-Bazar marine drive.

Additionally, the Bangladesh Meteorological Department (BMD) has a wind speed observation station at Cox's Bazar. Wind analysis shows a strong seasonal cycle, lowest in the winter and highest in the summer. During dry season, the winds are predominantly from the north northeast whereas during monsoon they are from south southeast. The annual wind rose of Cox's Bazar is shown in Figure 3.16

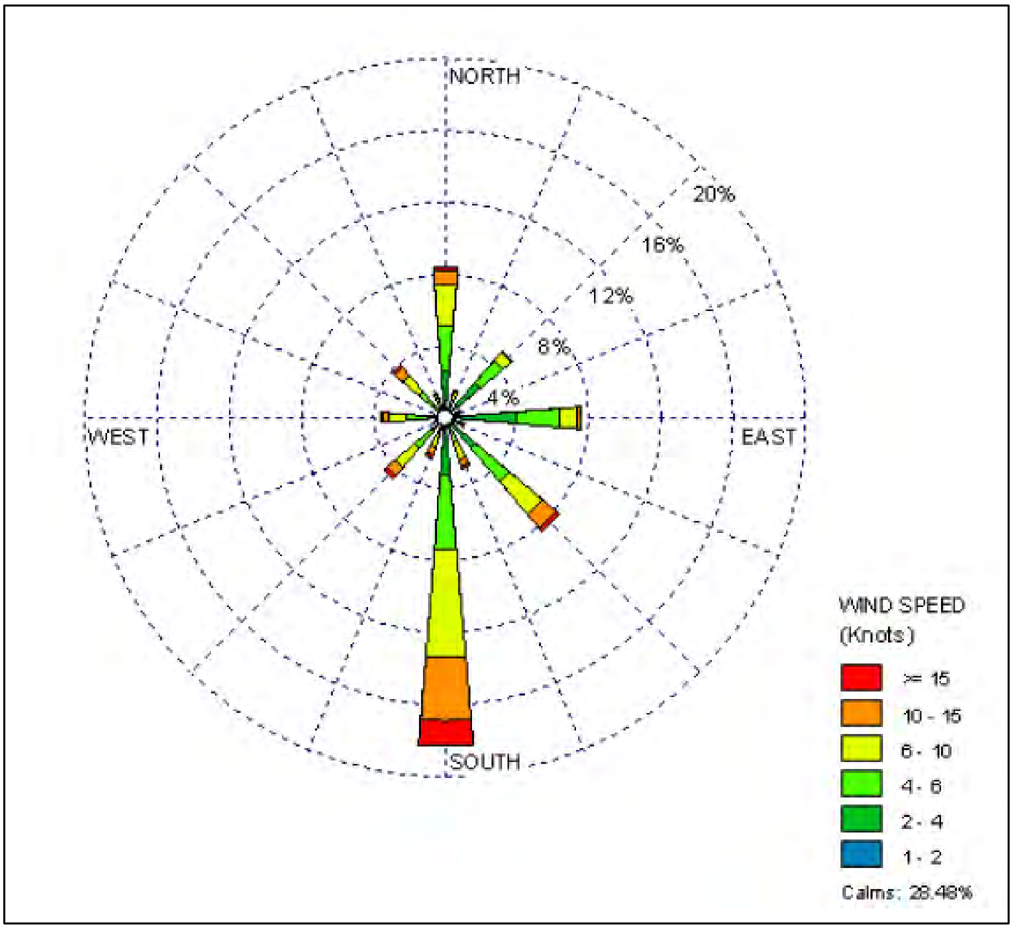

Figure 3.16: Annual wind rose of Cox's Bazar (Source: IWM, 2012)

There are two types of wave namely short waves and long waves. There is a typical difference between short waves, which are waves with periods less than approximately 20s, and long waves or long-period oscillations, which are oscillations with periods between 20-30s and 40 min. But short waves are the single most important parameter in coastal morphology. Wave conditions vary considerably from site to site, depending mainly on the wind climate and on the type of water area. Annual wave roses for deep and shallow water near Cox's Bazar from BMD and Bangladesh Navy are shown in Figure 3.17 and Figure 3.18 respectively.

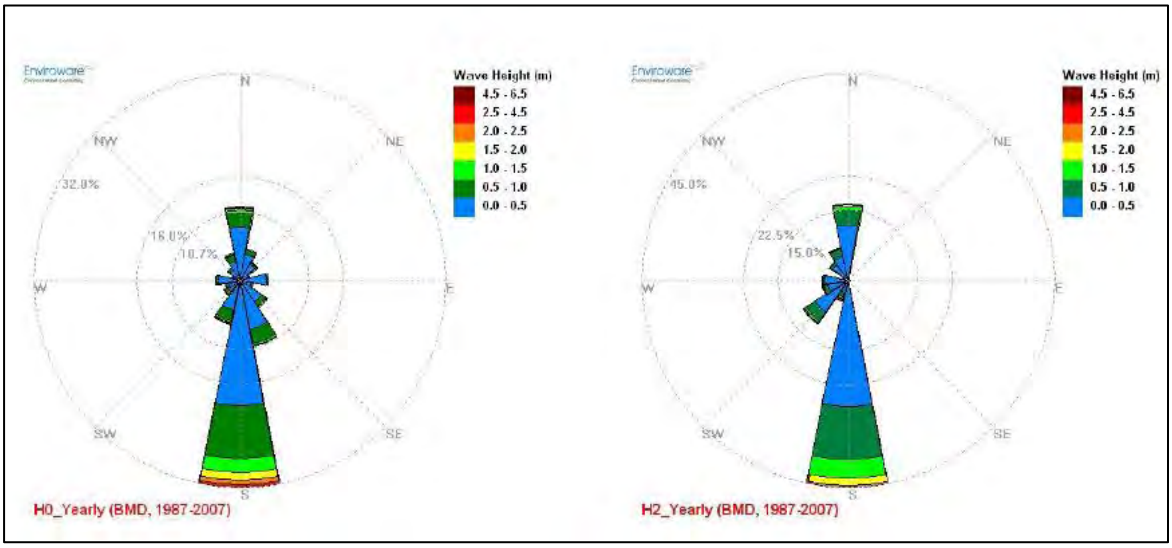

Figure 3.17: Annual wave rose showing deep and shallow water wave height by direction from Bangladesh Meteorological Department data. (Source: IWM,2012)

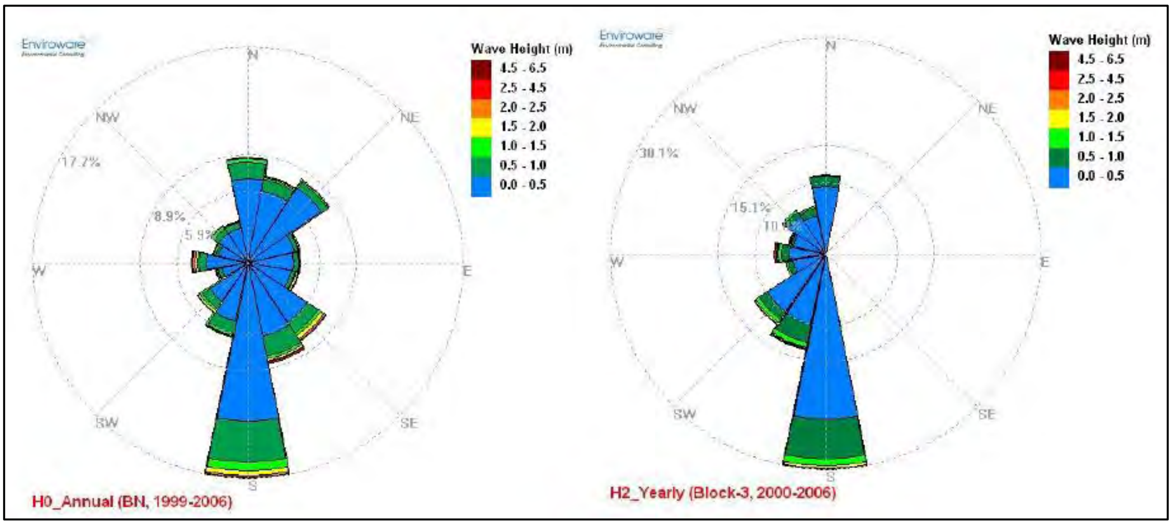

Figure 3.18: Annual wave rose to showing deep and shallow water wave height by direction from Bangladesh Navy's Block-3 data, (Source: IWM, 2012)

(v) Boundary Data

At upstream from Visakhapatnam (Latitude: 18.904°, Longitude : 93.865°) to Gwa (Latitude: 17.686°, Longitude : 83.299°) a time series data has been generated in Delft3D by the tidal constituent's and downstream at Barurua in upper meghna river (Table 3.8, Table 3.9 and Table 3.10) shows the details:

Table 3.6: Latitude and Longitude of Boundary Station Locations

Boundary	Station Name	Latitude (Degree)	Longitude (Degree)
Northern	Barurua	23.46	89.48
Southern	Vishakhapatnam	18.904	93.865
	Gwa Bay	17.686	83.299

Table 3.7: Tidal Constituents at Vishakhapatnam (Latitude: 18.904 Longitude: 93.865)

No.	Tidal Constituents	Amplitude	Phase (Degree)	No.	Tidal Constituents	Amplitude	Phase (Degree)
1.	M2	0.2519	79.92	8.	Q1	0.0014	313.54
2.	S2	0.1112	109.59	9.	Mf	0.0061	12.62
3.	N2	0.0547	72.60	10.	Mm	0.0031	5.53
4.	K2	0.0303	106.85	11.	M4	0.0012	54.74
5.	K1	0.0592	251.12	12.	MS4	0.000095	216.84
6.	O1	0.0218	242.43	13.	MN4	0.00016	185.14
7.	P1	0.0179	246.04				

(Source: TPXO Global Tidal Model, Data Extracted for the year 2018)

Table 3.8: Tidal Constituents at GWA Bay (Latitude: 17.686 Longitude: 83.299)

No.	Tidal Constituents	Amplitude	Phase (Degree)	No.	Tidal Constituents	Amplitude	Phase (Degree)
1.	M2	0.8841	78.550	8.	Q1	0.0022	265.007
2.	S2	0.3541	106.215	9.	Mf	0.0097	13.2207
3.	N2	0.1414	80.521	10.	Mm	0.0048	5.841
4.	K2	0.0913	115.053	11.	M4	0.0192	75.294
5.	K1	0.1224	249.579	12.	MS4	0.0167	108.399
6.	O1	0.4831	237.804	13.	MN4	0.0063	72.312
7.	P1	0.0371	244.639				

(Source: TPXO Global Tidal Model, Data extracted for the year 2018)

(vi) Sediment Data

The sediment value for the Bay of Bengal is collected from the study of Krishna et al. (1989). The research shows sediment velocities vary between 1,482 and 1,679 m/s, with on average of 1,583 m/s, and the great majority of the samples show's a velocity in the range of 1,550 to 1,625 m/s. The densities of the sediments range from 1,338 to 1,757 kg/m³, with an average value of 1,527 kg/m³. The following table shows the different sediment types according to the density and velocity,

Table 3.9: Properties of Sediments from the Bay of Bengal

Sediment Type	Density (Kg/m³)			Velocity (m/sec)		
	Min	Max	Avg.	Min	Max	Avg.
Clay	1338	1649	1491	1509	1679	1579
Sandy clay	1556	1756	1666	1482	1658	1590

(Source: Krishna et al.,1989)

3.7 Summary

In this chapter, the theories of waves and currents in nearshore, sediment transport in the surf zone have been outlined. The basic theory of hydrodynamics in the nearshore zone, governing equations, stability, the accuracy of the model, wave hydrodynamics, sediment transport, hydraulic structures, and propagation through obstacles is summarized. Additionally, the flow model's description, the grid and coordinate systems, and boundary conditions for the model have also been discussed. The methodology adopted for the study outlined here step by step with the subsection of data collection, development of the Bay of Bengal model.

CHAPTER 4

STUDY AREA AND MODEL SETUP

4.1 General

In this study, we developed a fully calibrated and validated model for the Bay of Bengal with an open-source software distributed by Deltares (Delft3D) to simulate nearshore hydrodynamic systems. This study's main objective is to oversee the changes of the wave height, wave energy, and sediment transport by placing Breakwater and Groins in nearshore coastline of Cox-Bazar for protecting it against erosion. As a background of the study, a vigorous literature review has been done to understand the complex coastal system. Additionally, different studies related to nearshore hydrodynamics, shoreline changes, and relevant study on the Bay of Bengal have also been reviewed. This chapter explains the selection of study area, data collection, and mathematical model setup for further case development with Breakwater and Groins.

4.2 Study Area

The Bay of Bengal, including the Andaman Sea and Malacca Strait, lies roughly between latitudes 5°N and 23°N and longitude 79.8°E and 102°E. It is boarded by the eastern coast of Srilanka and India on the west, Bangladesh coast to the north, western coast of Myanmar and north western part of Malay Peninsula to the east. According to the limits defined by International Hydrographic Bureau (IHB), the Andaman and Nicobar Island separates the water eastward of it from the Bay of Bengal to form the Andaman Sea. The boundary of the Andaman Sea is considered to be line running from Cape Negrais (16°03’N) through Andaman Island to a point (10°48’N,92°24’E) in Little Andaman Island. The bay is triangular with the width decreasing from approximately 1600 km at the southern boundary to as narrow as 500 km at the northern end, which is commonly known as head bay where Bangladesh coast located.

In our study of the Bay of Bengal model, the upstream boundary is from Vishakhapatnam (Latitude:18.904° Longitude:93.865°) in Odisha coast in India to Gwa Bay (Latitude:17.686° Longitude: 83.299°) near sittwe in Myanmar, where the downstream boundary is at Barurua (Latitude:23.46°; Longitude : 89.48°) in the confluence of lower Jamuna river and Padma river.

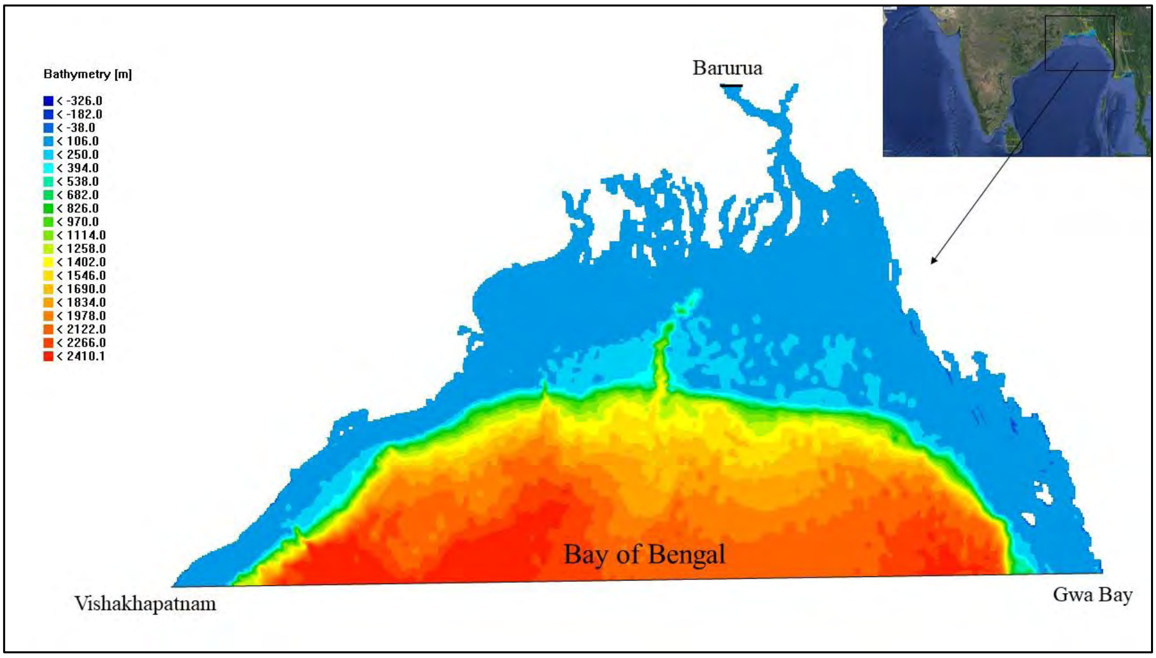

Figure 4.1: Bay of Bengal Model Boundary with Bathymetry

Over the last two centuries, huge changes have taken place due to continuous land erosion and accretion along the coastline of Bangladesh. Most of the erosion of the Bay of Bengal front was due to storm surges and continuous wave actions. One of the studies by (IWM-BUET-DHI-EML, 2012) has been carried out for planning and design of protective work of the Cox Bazar marine drive where historical satellite images analyzed along Marine drive road. According to the study, they have found five different sub-reaches which are vulnerable to erosion. Among them, sub-reach-I (0 to 2 kilometer) and sub-reach-III (7 to 10 kilometer) are most vulnerable along the marine drive (Table 4.1). In this study, these two sub reaches have been selected for further investigation. The courser Bay of Bengal model consists of 1800 m × 1800 m grid, and the finer model consists of 10 m× 10 m grid for further hydrodynamic investigation.

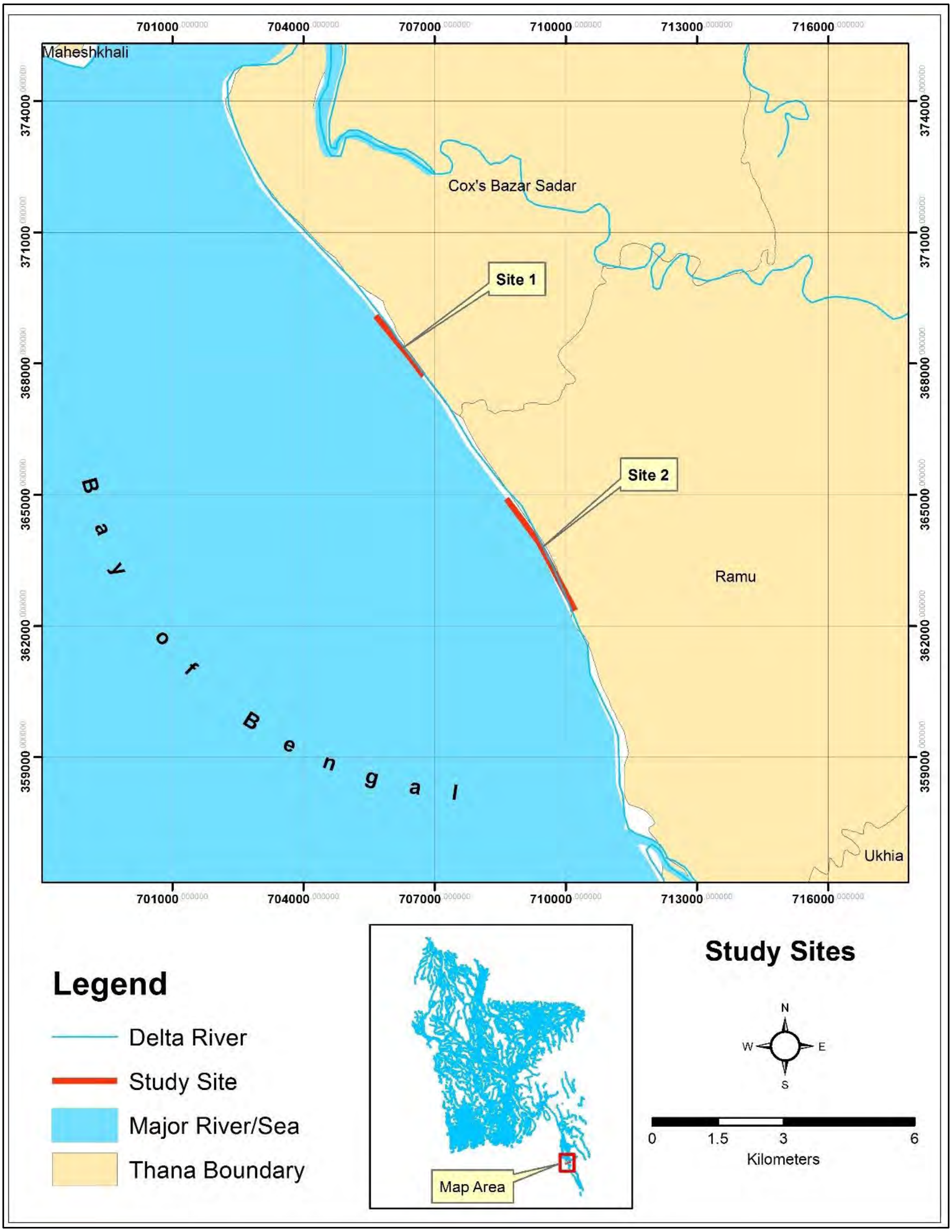

Figure 4.2: Study areas along the Cox-Bazar Marine Drive

Table 4.1: Changes in shoreline in different locations at Cox-Bazar marine drive

Chainage (Km)	Change (m) (1972-1980)	Change (m) (1980-1989)	Change (m) (1989-2000)	Change(m) (2000-2012)	Change (m) (1972-2012)
0 =Kalatali start of Phase-1	58.31	-233	93	-202	-283.69
1	230	-202	113	-137	4
2	5	-150	201	-144	-88
3	55	-170	158	-72	-29
4	52	-108	118	52	114
5	63	-108	149	-101	3
6	44	-295	274	-268	-245
7	-70	-124	208	-200	-186
8	-	-155	99	-224	-280
9	96	-77	-41	-246	-268
10	-223	46	-101	30	-248
11	-102	326	125	-57	292
12	67	-	256	-286	37
13	-	-46	73	-154	-127
14	76	-139	200	-211	-74
15	-137	-	130	-136	-143
16	180	-170	95	-114	-9
17	200	-170	77	-48	59
18	-86	-93	160	-39	-58
19	-	-	136	-101	35
20	-74	46	42	-105	-91
21	-5	-108	107	-140	-146
22	-	-281	119	-75	-237
23	-118	77	26	-88	-103

Note: Positive value denotes deposition, and negative value denotes erosion. (Source: IWM, 2012)

4.2.1 Site 1 along Cox-Bazar Marine Drive Road (Kalatoli to Hatchary Para)

Along with the historical changes (1972-2012) data, a field visit was also carried out to examine the current condition at Cox Bazar marine drive. At the location of Latitude: 21°24’13 N; Longitude : 91°59’28 E near the Hatcharipara, which is continuously eroded by high wave action. During a storm surge event, one kilometer of marine drive road was totally washed out near the kolatoli beach area. Now, the fragile geo-tube protection system faces challenges on its sustainability. Figure 4.3 shows the erosion-prone vulnerable place, and Figure 4.4 shows the selected site 1 (Kalatoli to Hatcharipara), which is 1.7 km in length for further investigation.

Figure 4.3: Local protection measures due to erosion at Hatcharipara, Cox-Bazar

Figure 4.4: Selected location for study along Cox Bazar coastline (Site 1)

4.2.2 Site 2 along Cox-Bazar Marine Drive Road (Near Himchari)

Severe erosion is ongoing due to high wave action near the Himchari point (IWM, 2012). In this study, site 2 is selected nearby the Himchari area (Latitude: 21°18’5 N , Longitude: 92°2’54 E), which is 3 km in length. Temporary protection work is done in recent days by placing tetrapod alongside the marine drive with geo-bags, which is a short-term solution and facing difficulty protecting that area. Figure 4.5 shows the fragile protection system, and Figure 4. 6 shows the full site 2 location for further investigation.

Figure 4.5: Damaged protection system at Himchari point, Cox-Bazar

Figure 4.6: Selected location for further investigation (Site 2)

4.3 Development of FLOW-WAVE Coupled Bay of Bengal Model

In this section, different steps have been discussed to develop the Bay of Bengal model. Simultaneously, a finer model was set up from the courser model to simulate the nearshore hydrodynamics for the Cox Bazar coast in Bangladesh.

Development of Delft Flow model:

For setting up the Flow model, which consists of the hydrodynamic part, a boundary condition needs to define by generating the staggered curvilinear grid. The boundary condition consists of upstream data, which is the Tidal Constituents collected from the global tidal model (TPXO), and downstream discharge data, which are collected from BIWTA for 2007 and 2008. The courser model consists of a grid size 1800 m ×1800 m and the finer model consist of the grid size of 10m×10m for the study area. Model calibration period is May 2007, October 2007, and the validated period is May 2008 and October 2008 due to the availability of bathymetry, tide, water level, discharge, and measured wave data.

Development of Delft Wave model:

The Delft3D wave model known as SWAN is used in this work, which is a part of the Delft3D software platform. The water level data generated through the hydrodynamic (Flow) part and shared with the SWAN wave model as input data. In this work, seasonal wind, wave data have been collected from DHI open data portal and surveyed data from the Institute of Water Modeling (IWM) for May 2007, October 2007, and May 2008, October 2008.

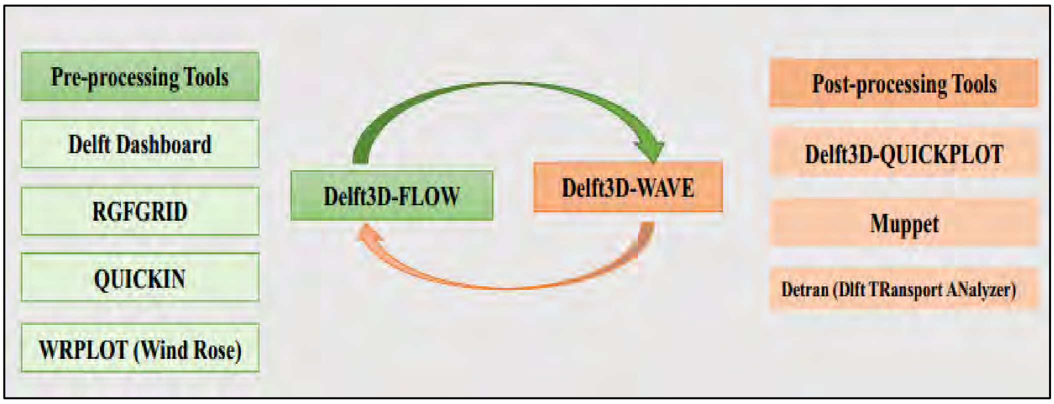

Figure 4.7: Used Flow-Wave couple system in Delft3D with different pre and post processing tools

4.4 Key variables of Breakwater during design consideration

In this study, two erosion-prone points have been selected (Fig 4.4 and Fig 4.6) alongside the Cox Bazar marine drive. There are few considerations to placing the structural intervention. The first step in designing a nearshore detached breakwater scheme, or other infrastructural beach control option, is to consider what change is required to the existing shoreline. This study considers governing parameters during selection of Breakwater length, distance from the shoreline, and gaps between two breakwaters. Figure 4.8 Illustrate the key variables during Breakwater parameter selection,

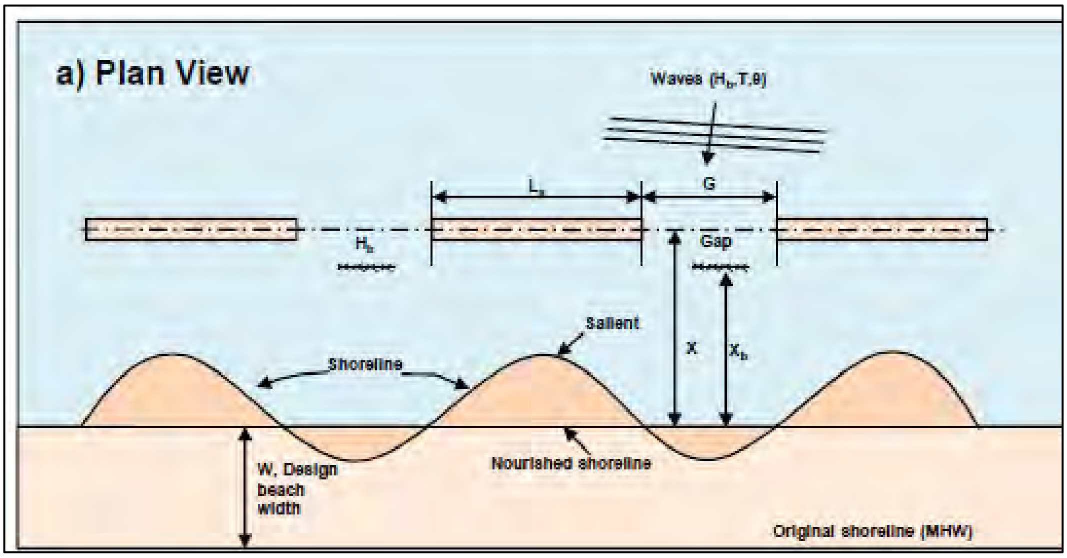

Figure 4. 8: Plan view of nearshore breakwater scheme (Source: DEFRA, 2010)

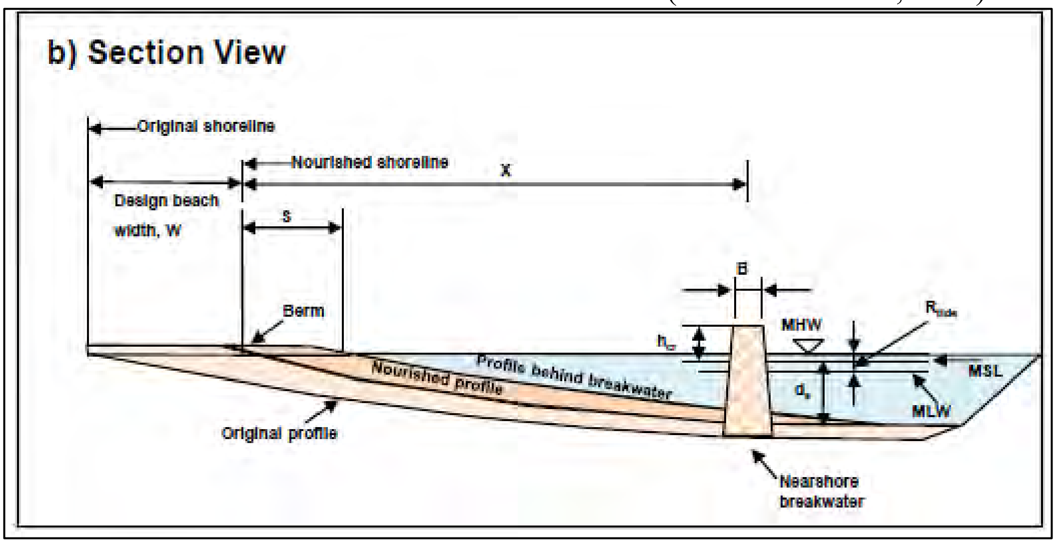

Figure 4.9: Section view of nearshore breakwater scheme (Source: DEFRA, 2010)

4.5 Key variables of Groins during design consideration

Groins are a widely used structure that is used to protect beaches from erosion. Groins are shore-perpendicular structures aimed at either (1) maintaining the beach behind them, or (2) controlling the amount of sand moving alongshore. Kraus et al. (1994) provide a comprehensive overview of parameters governing the effect of groins. Parameters related to groin structure are such as Length; Spacing between groins, angle to the shoreline; Shape (as straight, angled, T-head, spurred, etc.). In this study, a thumb rule (Yincan et al, 2017) applied to find out key variables for the selection of groin.

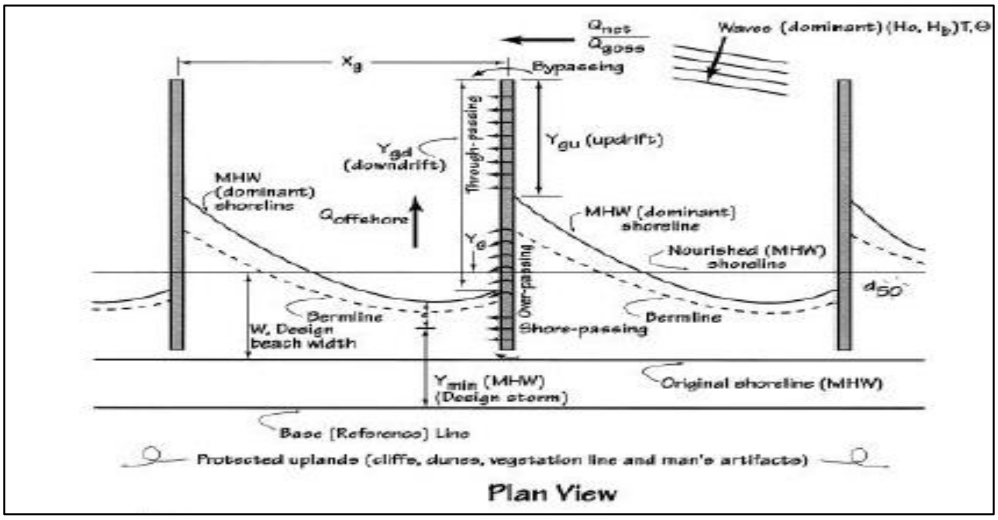

Figure 4.10: Different key variable from the plan view in the functioning of groins (Source: CEM, 2006)

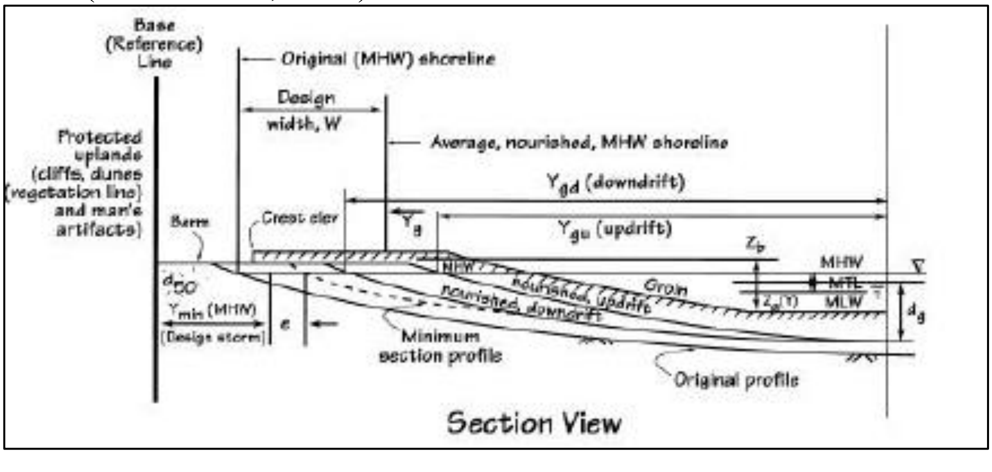

Figure 4.11: Different key variable from section view in the functioning of groins (Source: CEM, 2006)

4.6 Breakwater and Groins Parameters

In this section, Breakwater and Groin's key variables have been calculated on the basis of secondary data. This Breakwater calculation is followed by Department for Environment, Food and Rural Affairs, UK (DEFRA, 2010) and Coastal Engineering Manual. These key parameters are used for calculation of the design specification for nearshore structures. Table 4.2 shows the design parameters for Breakwaters,

Table 4.2: Basic data for determining the breakwater parameters at Cox- Bazar coastline in Bangladesh

Parameter	Basic data
MHWS *	3.77 relative to MSL
1-year surge	2.5 m
Beach slope	1:272 (Site 1) 1:33 (Site 2)
Estimated depth of closure	6 m relative to MSL
Percentage of incoming longshore transport	50 % of incoming longshore transport is desired to be bypassed to downdrift beaches and a salient response or minimum response is desired at the breakwater. This implied that the salient or minimul response in the leeward side of the breakwater would be formed by the 50 per cent of the incoming longshore that is trapped in the leeward side of the breakwater

(Source: ICWFM ,2013 and IWM ,2018)

According to the calculation procedure by DEFRA (2010), Geometric parameters of the breakwater have been considered. Followings are the steps for selecting the geometric parameters for Breakwater,

Breakwater location calculations:

Estimate, X_b (Distance from baseline to closure depth):

X_b= Closure depth/ Beach Slope=350 m

At site 1, the beach slope is= 1:272
And, at site 2, the beach slope is= 1:99

Therefore,
X_{b1} = Closure depth/Beach slope at site 1= 1667 m
X_{b2} = Closure depth/Beach slope at site 1= 600 m

Determine X (Distance from baseline to breakwater centerline) based on percentage of longshore transport to be bypassed:

Assuming that $X/_{X_b} = 0.5$, gives 50 per cent bypassing:

X_1 (Distance from baseline to breakwater centerline at site 1) = 0.5× X_{b1}= 833 m

X_2 (Distance from baseline to breakwater centerline at site 2) = 0.5× X_{b1}= 300 m

Breakwater length calculations:

Determine Ls (Length of Breakwater),

Conditions for the Formation of Tombolos:

i. Ls/X>1; Tombolo for shallow Water (Gourlay 1981),
Therefore,
L_{S1}> 833 m
L_{S2}> 300 m

ii. Ls/X> 1.5; Tombolo for Multiple Breakwater (Dallay and Pope 1986)
Therefore,
L_{S1}> 1250 m
L_{S2}> 450 m

Condition for the Formation of Salients:

i. Ls/X=0.67; Salient Creation (Dally and Pope 1986)
Therefore,
L_{S1}=558 m
L_{S2}= 200 m

ii. Ls/X < 1.5; Well-developed Salient (Ahrens and Cox 1990)
Therefore,
L_{S1}< 1250 m
L_{S2}< 450 m

Conditions for Miminal Shoreline Response:

i. Ls/X≤ 0.27; No Sinuosity (Ahrens and Cox 1990)
Therefore,
$L_{S1} \leq$ 225 m
$L_{S2} \leq$ 81 m

ii. Ls/X≤0.125; Uniform Protection (Noble 1978)
Therefore,
$L_{S1} \leq$ 105 m (In this study 100 m long Breakwater is selected for site 1 and 2)
$L_{S2} \leq$ 38 m

Crest level calculation:

Breakwater crest level, h_{cr} = MHWS + 1-year surge

≈ 6 m MSL

Breakwater crest level, h_{cr}= 6 m (MSL)

Gap width and Crest width:

Determine G (gap width) based on erosion in breakwater bays, G/X=0.5

G= X (Distance from Baseline to Breakwater Center Line) x 0.5

G_{S1} ≈ 400 m at site 1
G_{S2} $= 150$ m at site 2

Crest width of a rubble mound breakwater (For operation and movement of Construction equipment and repair)

B$\geq 3K_{\Delta}\left(\frac{w}{\gamma r}\right)^{1/3}$

W=$\frac{\gamma_r \times H^3}{\mathrm{K_D} \times (s-1)^3 \times cotg(\alpha)}$

Where,
B= Crest width
KΔ= Form coefficient=1.15 (Irregular Rockfill)
w= Weight of Block
$\gamma_{r=Specific\,Weight\,of\,Granite\;\;Rock} = 26\ KN/M^3$
K_D= Empirical stability coefficient
H=Incident design wave height
S= Specific gravity of Block

$$\gamma_{w=Specific\,Weight\,of\,Sea\,Water} = 10.25\ KN/M^3$$

B$\geq 3\times\ 1.5\left(\frac{w}{26}\right)^{1/3}$

W=$\frac{26\ \times 6.64^3}{2\times\left(\frac{26}{10.25}-1\right)^3 \times 2} = 524.50\ kN$

B$\geq 3\times\ 1.5\left(\frac{w524.50}{26}\right)^{1/3}$

B≥ 9.40

Thus, the crest width considered for this work is B= 10 m

Groins Parameters:

Yincan et al (2017), developed a thumb rule for developing key parameters for groin. In this study, this simple technique has been used for determining key parameters for model development.

Site 1: Area Coverage 1.75 km (Figure: 4.4)

- Groin Length= 100 m
- Gap =200 m
- n= 7 nos.

Site 2: Area Coverage 3 km (Figure: 4.6)

- Groin Length=100 m
- Gap=200m
- n= 13 nos.

Following figures shows the Design parameters of Breakwaters and Groins at site 1 and site 2 at Cox-Bazar coastline,

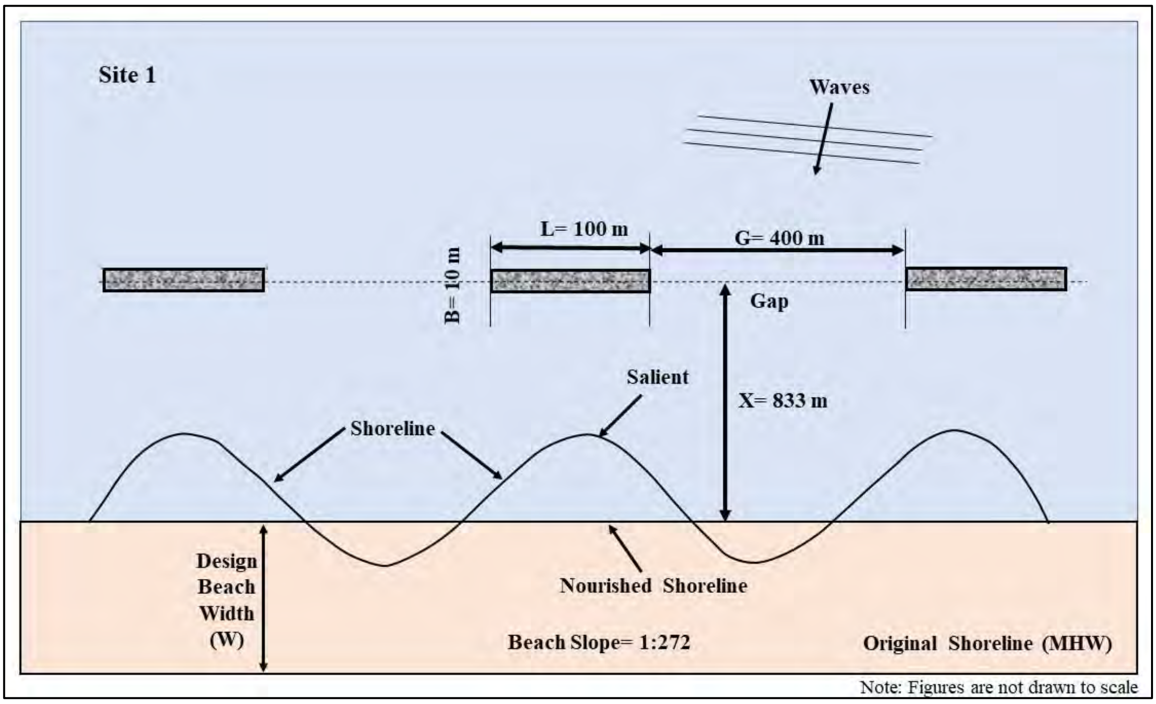

Figure 4 12: Design parameters of Breakwaters at Site 1,Cox-Bazar coastline

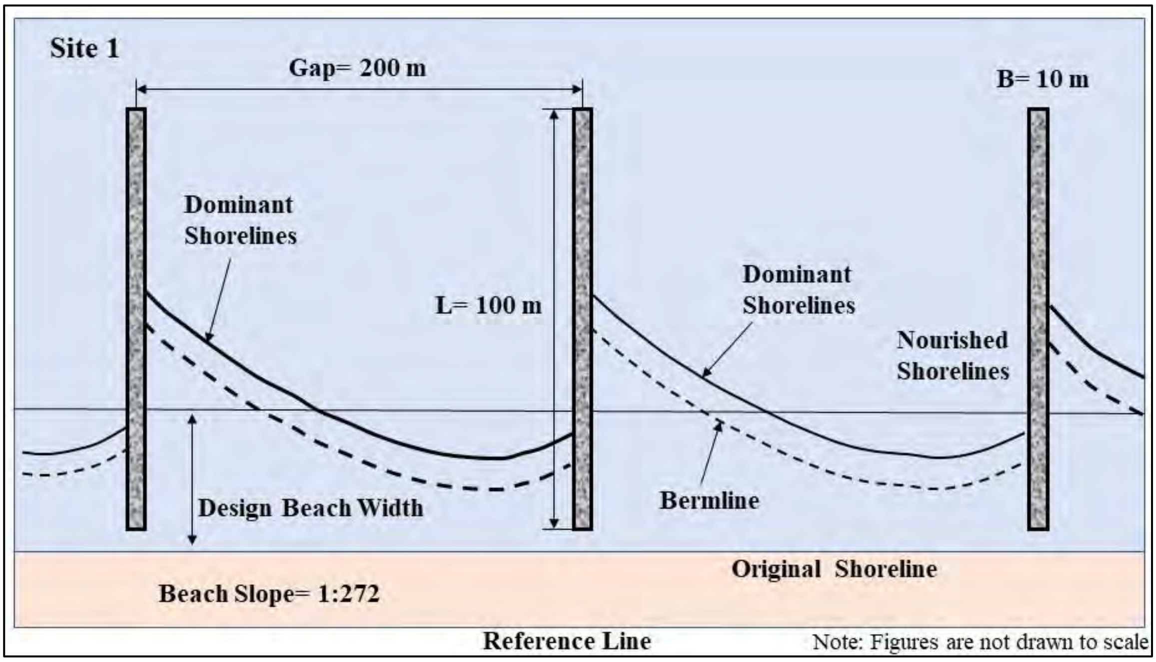

Figure 4 13: Design parameters of Groins at Site 1, Cox-Bazar coastline

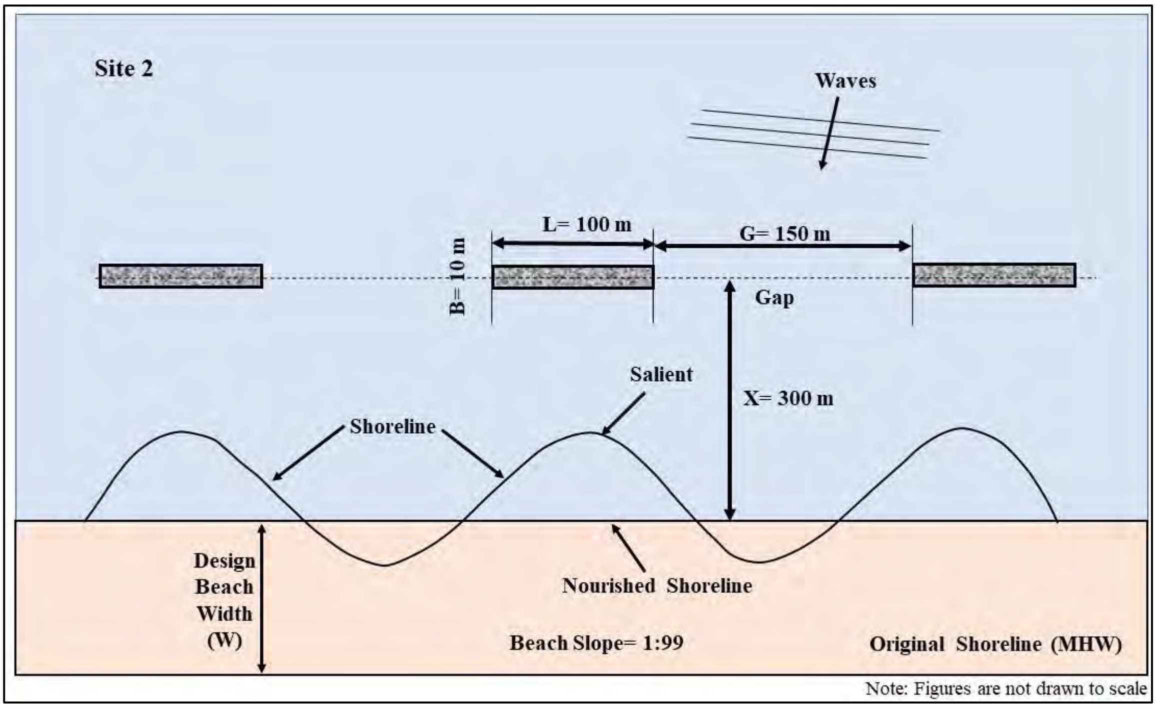

Figure 4 14: Design parameters of Breakwaters at Site 2, Cox-Bazar coastline

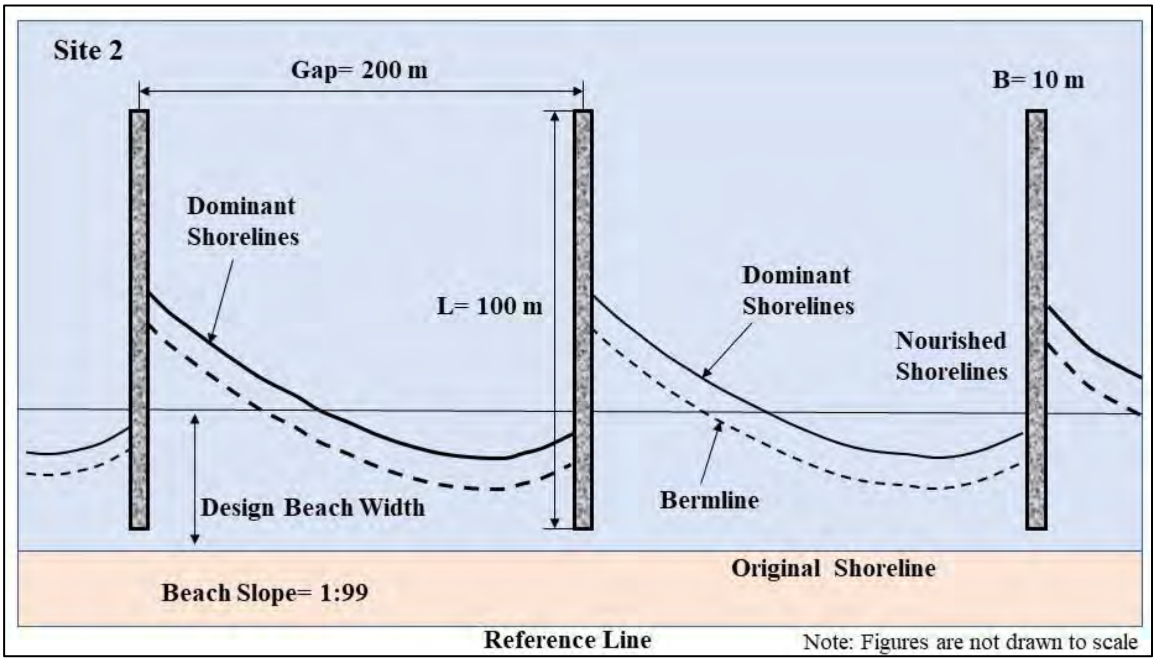

Figure 4 15: Design parameters of Groins at Site 2, Cox-Bazar coastline

4.7 Mathematical Model Setup

In order to study the hydrodynamic processes, numerical modelling can be a powerful tool. Numerical modelling is relative cheap compared to conducting extensive field- or scale model measurements and allows studying individual processes or individual design parameters relatively easy for idealized conditions.

Based on (Burcharth et al. 2007), several considerations contribute to the choice of which numerical model to use, for example the required accuracy of wave/flow conditions, the dominant physical processes to be reproduced, budget, time/computational efficiency etc. Because of these considerations, the software package Delft3D is used, developed by Deltares. Delft3D is capable of representing all the important hydrodynamic and morphologic processes accurately in a limited amount of computational time for longer (morphological) time scales. In addition, Delft3D has proven to be a robust model in a variety of coastal problems (Lesser et al. 2004). To reduce the computational time, but still reproduce accurate results, a depth-averaged approached is used (Johnson et al. 2005). In this chapter, a brief description of Delft3D is illustrated for model set up.

Delft3D:

The Delft3D software package is a modelling system that consists of a number of integrated modules in a shared user interface, which together allows to simulate a variety of physical processes. The main module is the Delft3D-Flow module. In this work, the Delft3Dflow module is online-coupled with the SWAN wave model which is a part of Delft 3D wave model to accurately simulate near-shore hydrodynamics. A schematic overview of this coupled system is shown in Figure 4.16.

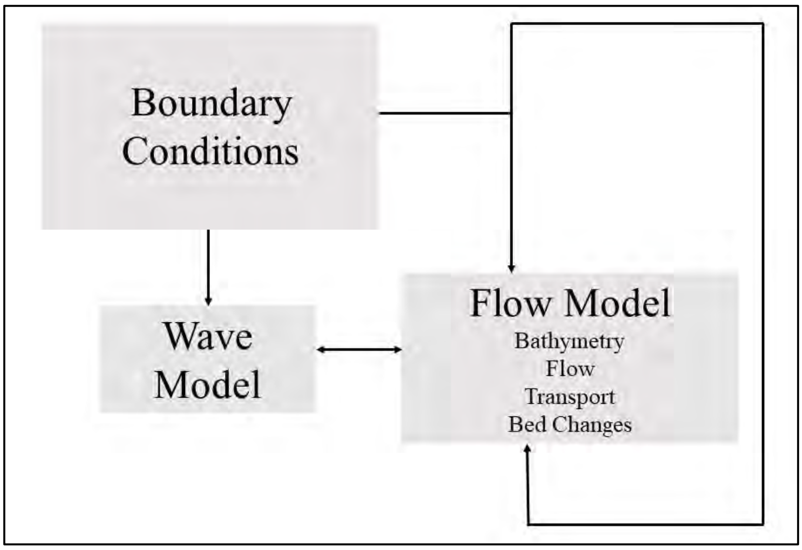

Figure 4.16: Online modelling scheme at Delft3D (Source: Roelvink 2006)

Delft3D-Flow is a non-stationary process based numerical model, which solves the Navier- Stokes equations for an incompressible fluid under the shallow water and bousinesq assumptions. In the vertical, the Navier-Stokes equations reduce to the hydrostatic pressure assumption, so vertical accelerations are neglected. For the computation of the suspended sediment transport, an advection-diffusion equation is used.

SWAN:

Delft3D-WAVE, or better known as SWAN (Booij et al. 1999; Deltares 2010b), is a third-generation spectral wave model using an Eulerian approach. In SWAN, the evolution of wind-generated waves is based on a two-dimensional wave action-density spectrum and is calculated simultaneously for each point in space. SWAN is capable of simulating wave propagation, wave generation by wind, non-linear wave-wave interactions and wave energy dissipation for given conditions like bathymetry, wind, flow, and water level.

4.7.1 Hydrodynamic Model

Grid:

The numerical model of Delft3D-FLOW is based on finite differences. In order to solve the mathematical formulations of Delft3D-FLOW, the shallow water equations are discretized in time and space. For the spatial discretization based on the finite differences approach, a staggered grid is used. For the simulation of Bay of Bengal model, a courser grid of 1800 m × 1800 m is used and the simulation of different structural interventions (Breakwater & Groins) at different location of Cox Bazar coastile a finer grid of 10m×10m is used (Figure 4.17, Figure 4.18 and Figure 4.19).

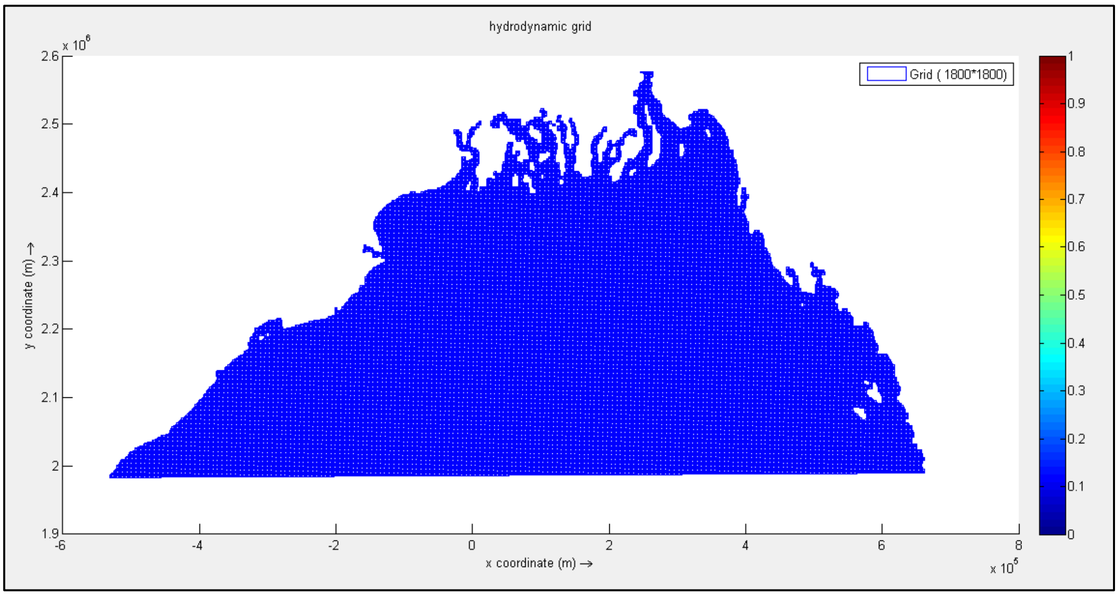

Figure 4.17: Courser Grid of Bay of Bengal Model (1800 m × 1800 m)

Figure 4.18: Finer Grid at Cox Bazar coastline site-1 (10m×10m)

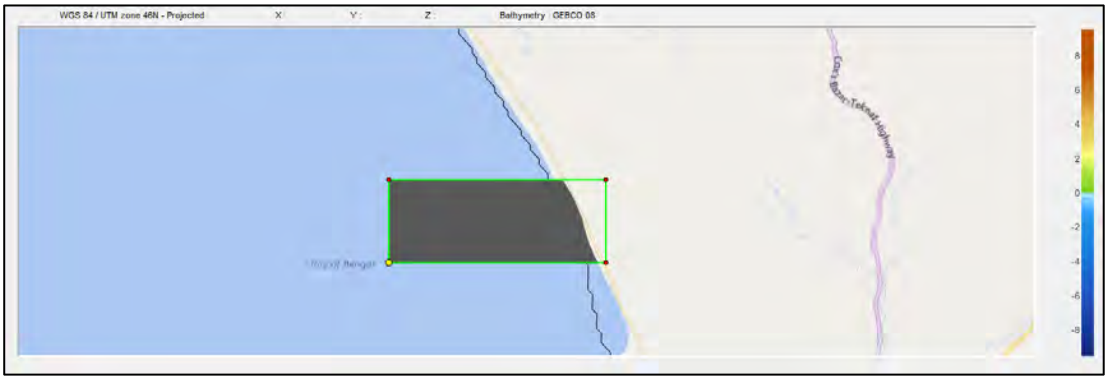

Figure 4.19: Finer Grid at Cox Bazar coastline site-2 (10m×10m)

Bathymetry:

In this study, the bathymetry of Bay of Bengal has been developed by Global Bathymetric Chart of the Oceans (GEBCO), which obtained from the British Oceanographic Data Centre (BODC). This bathymetry data is also validated through British Admiralty Chart and surveyed bathymetry data by Institute of Water Modeling (IWM). Figure 4.20 shows the bathymetry of the Bay of Bengal.

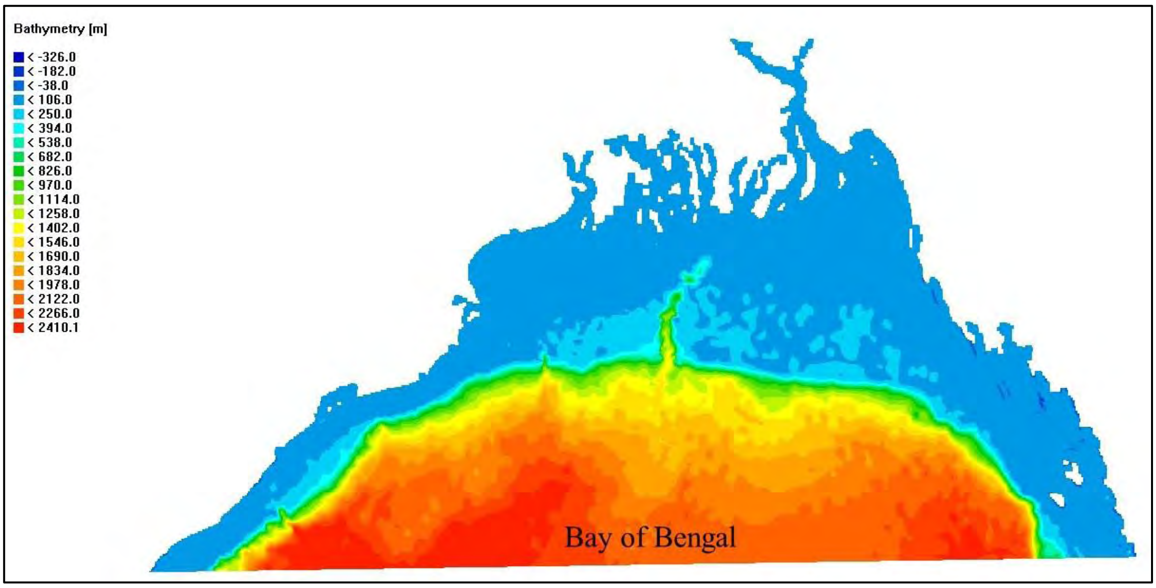

Figure 4.20: Bathymetry of the Bay of Bengal from Delft3D model

Time Frame:

As discussed, the numerical model of Delft3D-Flow is based on finite differences. To discretize the equations in time, different schemes can be used. Explicit schemes are preferred in numerical modelling when it comes to computational efficiency. In contrast to implicit schemes, explicit schemes are fast but require a limited time step to maintain stable. To improve computational efficiency of implicit schemes, the Alternate Direction

Implicit (ADI) method is used. The ADI method splits one-time step into two stages. For both stages all the equations within Delft3D have solved in such a consistent way that the accuracy in space is at least second order. Despite the fact that the implicit scheme is unconditionally stable, for accuracy constrictions the Courant number should be less than:

$$C_f=2\Delta t\sqrt{gH\left(\frac{1}{\Delta x^2}+\frac{1}{\Delta y^2}\right)}<4\sqrt{2}$$

Based on this time step limitation, a time step of 0.5 minutes or 30 seconds is used. The total simulated time for the courser Bay of Bengal model is 60 tidal cycles or a total 744 hours for calibration and another 60 tidal cycles or 744 hours for validation. In the finer model at Cox Bazar coastline, the total simulation time is 120 tidal cycles or 1,488 hours for each case with Breakwater and Groins.

Processes and initial conditions:

To obtain a universal idealized approach as much as possible, only sediments and waves by online coupling with SWAN are taken into account. The initial conditions, water level, and initial sediment concentration remain zero.

Boundary conditions:

The Southern offshore boundary conditions for the flow grid consist of tidal constituents of Vishakapatnam and Gwa, which creates time-series data, and the northern boundary is an open water level boundary at Barurua point. During the simulation of Flow-Wave model at the nearshore Cox Bazar coast, all of the boundary data were extracted from the calibrated and validated Bay of Bengal model.

Physical parameters:

The physical parameters for Delft3D-Flow used are defined in Table 4.3. The following considerations have been undertaken during model setup,

i. Bottom roughness to account for the differences in bottom roughness in Delft3D-Flow between a sandy bottom and the rough structures (Breakwater and Groins), a spatial varying Manning coefficient is used.

ii. Horizontal eddy viscosity only have a small effect, so a constant horizontal eddy viscosity will suffice for accurate results (Apotsos et al. 2007).

iii. The median sediment diameter is kept constant, despite its influence it has on hydrodynamic and morphologic processes. The reference density taken from secondary data.

iv. Locally an initial sediment layer thickness is considered zero. For the surrounding bathymetry, the bottom consists of a sediment layer of 5 m, enabling no restrictions on morphological changes.

Table 4.3: Physical parameters used in Delft3D Flow module

Subject	Parameter	Settings
Constants	Gravity	9.81 m/s²
	Water density	1025 kg/m³
Roughness	Bottom roughness formula	Manning
	Stress formulation due to wave forcing	Fredsoe
	Slip condition (wall roughness)	Free
Viscosity	Background horizontal viscosity/diffusivity	Uniform
	Horizontal eddy viscosity	1m²/s
	Horizontal eddy diffusivity	10 m²/s
Sediment	Sediment sand	
	Reference density for hindered setting	1527 kg/m³
	Specific Density	2650 kg/m³
	Dry bed density	1600 kg/m³
	Median sediment diameter d_{50}	200 µm
	Initial sediment layer thickness at bed	5m
Morphology	Update bathymetry during FLOW simulation	True
	Include effect of sediment on fluid density	False
	Equilibrium sand concentration profile at inflow boundaries	True
	Morphological scale factor	1
	Minimum depth for sediment calculation	0.1m

(Continue Table 4.3)

	Vab Rijn's reference height factor	1
	Threshold sediment thickness	0.05m
	Estimated ripple height factor	2
	Factor for erosion of adjacent dry cells	0
	Current-related reference concentration factor	1
	Wave-related suspended transport	1
	Wave-related bed load transport factor	1

Numerical parameters:

The numerical parameters used in Delft3D-Flow, are presented in Table 4.4. Following under-mentioned comments on these parameters: Advection scheme for momentum; for the numerical scheme of the advection terms of the momentum balance several options are available. Based on the description of these schemes, the Flood scheme may be the preferred choice for steep slopes. The default option in Delft3D-Flow, a cyclic scheme is used in this study.

Table 4.4: Numerical parameters used in Delft3D Flow

Subject	Parameter	Settings
Numerical Parameters	Drying and flooding check	Grid cell centers and faces
	Depth specified at:	Grid cell corners
	Depth at grid cell faces	Mor
	Threshold depth	0.1m
	Marginal depth	-999 m
	Smoothing time	60 m
	Advection scheme for momentum	Cyclic
	Forester filter horizontal	On

4.7.2 Wave Model

Grid and bathymetry:

The wave model consists of a courser grid cell of 1800m ×1800 m for the Bay of Bengal model and 10m ×10m finer grid cell for the nearshore coastline at Cox-Bazar. The bathymetry used in the wave computations results from the flow grid coupling and it incorporated all boundary values. To account for the flow-wave coupling, the water level, current, and bathymetry from the Delft3D Flow results are used in SWAN.

Boundaries:

For the southern boundary at Vishakhapatnam and Gwa , the JONSWAP spectrum is used. For the directional spreading, the cosine and gamma function is used. The uniform and stationary boundary conditions in time and space can be defined by Hs=2 m, Tp=7s, shore normal wave direction (θ=220°) and a directional spreading of m=4, but it vary throughout this work in case for study area in smaller model, as these parameters are important for a diversity of hydrodynamic processes, Physical parameters: Table 4.5 summarizes the physical parameters used for SWAN.

Table 4.5: Physical parameters used in SWAN

Subject	**Parameter**	**Settings**
Constants	Gravity	9.81 m/s^2
	Water density	1025 kg/m^3
	North w.r.t. x-axis	90 degrees
	Minimum depth	0.05 m
	Forces	Radiation stresses
Processes	Depth-induce wave breaking	[Battjes and Janssen 1978] model
	Alpha	1
	Gamma	0.73
	Non-linear triad interactions	Off
	Bottom friction	On
	Bottom friction type	JONSWAP
	Bottom friction coefficient	0.067 m^2s^{-3}
Various	White capping	On
	Refraction	On
	Wind growth	
	Frequency shift	On

Numerical parameters:

Table 4.6: Summarizes the settings used for the numerical parameters in SWAN.

Subject	Parameter	Settings
Spectral space	Directional space	0.5
	Frequency space	0.5
Accuracy criteria	Relative changes H_S T_{m01}	0.02
	Percentage of wet grid points	98 %
	Relative changes w.r.t. mean value H_S and T_{m01}	0.02
	Maximum number of iterations	15

4.8 Summary

This chapter summarizes the significance of the study area and the selection of two sites based on its current threat or vulnerabilities . These two sites are along the Bay of Bengal at the Cox-Bazar coastline, and continuous erosion has taken place over the years. The justification of selecting these sites lies not only for the vulnerability but also the socio-economic factors as that area is very much important for tourism and fisheries industries. Moreover, this chapter also describes the process of developing a fully functional mathematical model with Delft3D. The full methodology for Flow-Wave coupling with proper calibration and validation of the hydrodynamic and wave model also describes in this chapter. Additionally, the key variable and design parameters are also defined for Breakwater and Groins, where a schematic diagram illustrates the proposed location for Breakwater and Groins. Necessary Bathymetry data, shoreline data, tidal water level, discharge data, wind-wave data, and sediment data have been collected from IWM, BIWTA, IHO, GEBCO, and DHI open data portal. This chapter also illustrates the model setup, especially the physical and numerical inputs for model development.

CHAPTER 5

RESULTS AND DISCUSSIONS

5.1 General

A fully calibrated and validated couple Flow-wave model is required to achieve the objective of the study. To achieve the proposed objectives, it is necessary to understand the model functionality in a complex system where each parameter has its own role in achieving its sensitivity to simulate real-world scenarios. This chapter describes the calibration and validation of flow wave model and different cases with Breakwater and Groins in two different locations along the Bay of Bengal at Cox-Bazar shoreline.

5.2 Calibration and Validation of FLOW Model

Calibration means iterative adjustment of the model parameters so that simulated and observed responses of the system match within the desired level of accuracy. Model parameters require adjustment due to a number of reasons. In reality, all models require some degree of calibration to fine-tune the predictive ability of the model. In a hydrodynamic model, errors may creep in from four potential sources (Abramowitz and Stengun, 2003).

(i) Random or systematic error in input data,

(ii) Random or systematic error in output data,

(iii) Error due to incorrect parameter values and

(iv) Error due to incomplete or incorrect model formulation.

During the calibration process, only errors from source (iii) are minimized whereas the disagreement between the simulated and observed outputs is due to all the four sources. Errors related to (i) and (ii) serve as the 'background noise' and determine the minimum level of mismatch between the observed and simulated outputs. Therefore, the objective of model calibration is to minimize the errors from source (iii) until they become insignificant compared to the errors from sources (i) and (ii). As far as the fourth source is concerned, every effort has to be made to ascertain that the state equation, initial condition, and boundary condition have been specified correctly.

The modeler should not blindly attempt to minimize the deviations between the observed and recorded output values by adjusting the parameters through some optimization algorithm. This is likely to produce physically unrealistic parameter values. Usually, parameter values are adjusted through ‘trial and error’ by running the model repeatedly. Sound understanding of physics of the phenomenon and experience with similar real-world systems can be of great help in determining the correct parameter values. For a large number of parameters, it is not realistic to try and adjust all the parameters one by one or in combination. A more sensible approach is to attempt a coarser simulation using only a few parameters whose values are least well known or to which the model shows maximum sensitivity (Abramowitz and Stengun, 2003).

In this study, the model calibration has been accomplished against measured water level and discharge data at five different locations in the Bay of Bengal. Among the five locations, four are from the International Hydrographic Organization (IHO) stations and one from Bangladesh Water Development Board (BWDB) station. The calibration periods are selected considering the pre-monsoon period from 01 May 2007 at 0000 hours to 15 May 2007 and post-monsoon period from 01 October 2007 at 0000 hours to 15 October 2007. The validation periods are selected considering the pre-monsoon period from 01 May 2008 at 0000 hours to 15 May 2008 and post-monsoon period from 01 October 2008 at 0000 hours to 15 October 2008. The hourly tidal data has been collected from the International Hydrographic Organization (IHO) and discharge data collected from Bangladesh Water Development Board (BWDB). The locations of all the tidal gauge stations are listed in Table 5.1

Table 5.1: Calibration and Validation Points along the Bay of Bengal

Gauge Station Authority	Station Name	Latitude (Degree)	Longitude (Degree)
IHO	CTG IHO, Bangladesh	22.23	91.83
	Pasur River, Bangladesh	21.97	89.52
	Akyab, Myanmar	20.13	92.83
	Short Island, India	20.75	87.08
BWDB	Sibsa River, Bangladesh	21.59	89.30

Hydrodynamic model calibration has been accomplished against water level and discharge of all the selected locations by fine-tuning the important variable input parameters of higher sensitivity like Minimum Renolds number, value of roughness coefficient k, absolute wind speed through the calibration process after different trial.

The numerical model Delft3D simulates the tidal level for continuous sixty tidal cycles, where each tidal cycle consists of 12.4 tide hours. So, the time of simulation of the model is set for 744 hours for all the locations. The time step of 30 seconds is considered to ensure the stability of the numerical scheme. The model has attained stability by maintaining the courant number $(g1/2h1/2\Delta t/\Delta s)$ less than or equal to 1, in which Δt is the computational time step (=30 s) and Δs is the grid spacing of 1800 m.

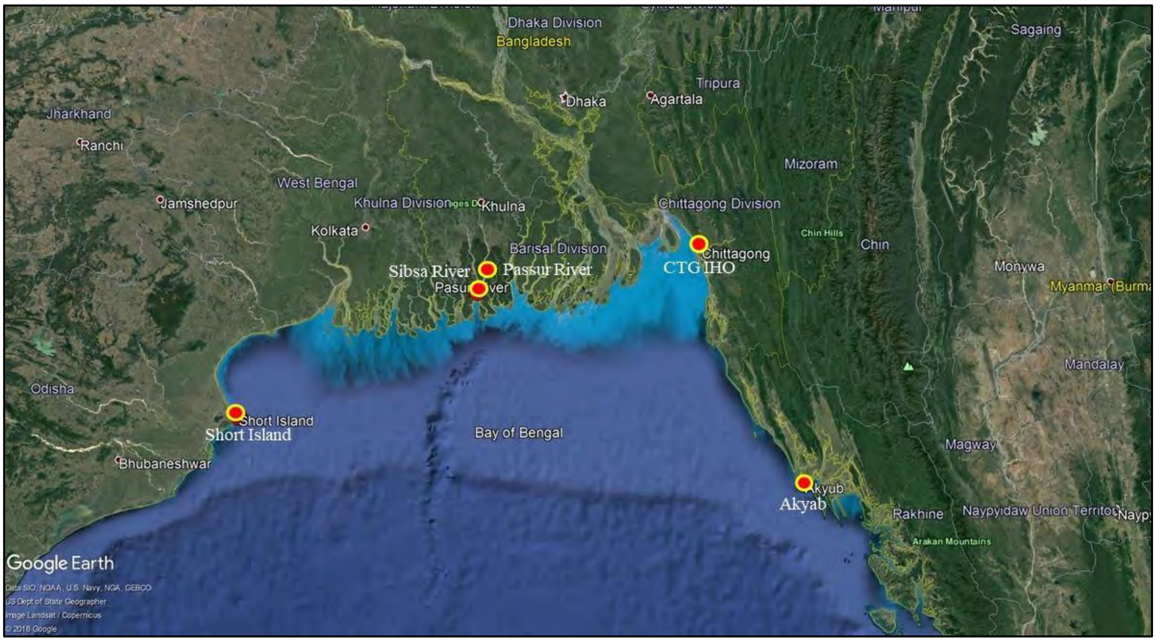

Figure 5. 1: Calibration and validation Locations in Bay of Bengal

Calibration Results:

The simulation periods of calibration have been considered for continuous thirty tidal cycles of 372 hours duration from 01 May 2007 at 0000 hrs to 15 May 2007 at 0000 hrs and another thirty tidal cycle of 372 hours duration from 01 October 2007 at 0000 to 15 October 2007 at 0000 hrs. The simulated sixty tidal cycles of the model are compared with the measured tidal levels and discharge measuring stations located at different points shown in followings,

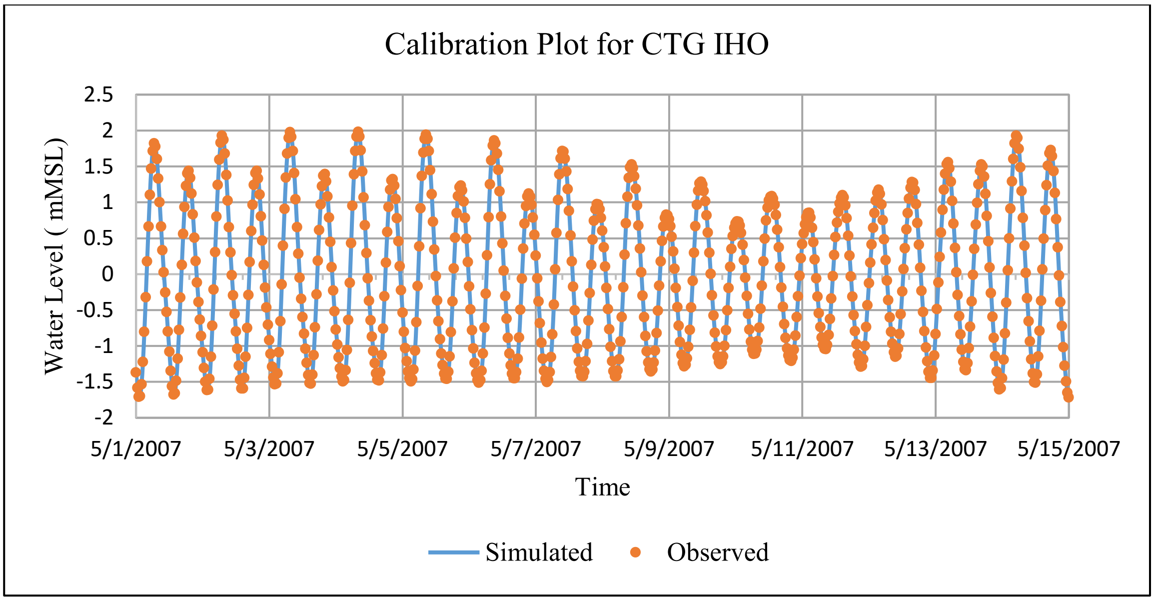

Figure 5.2: Calibration point for Chattogram IHO at Bangladesh (May 2007)

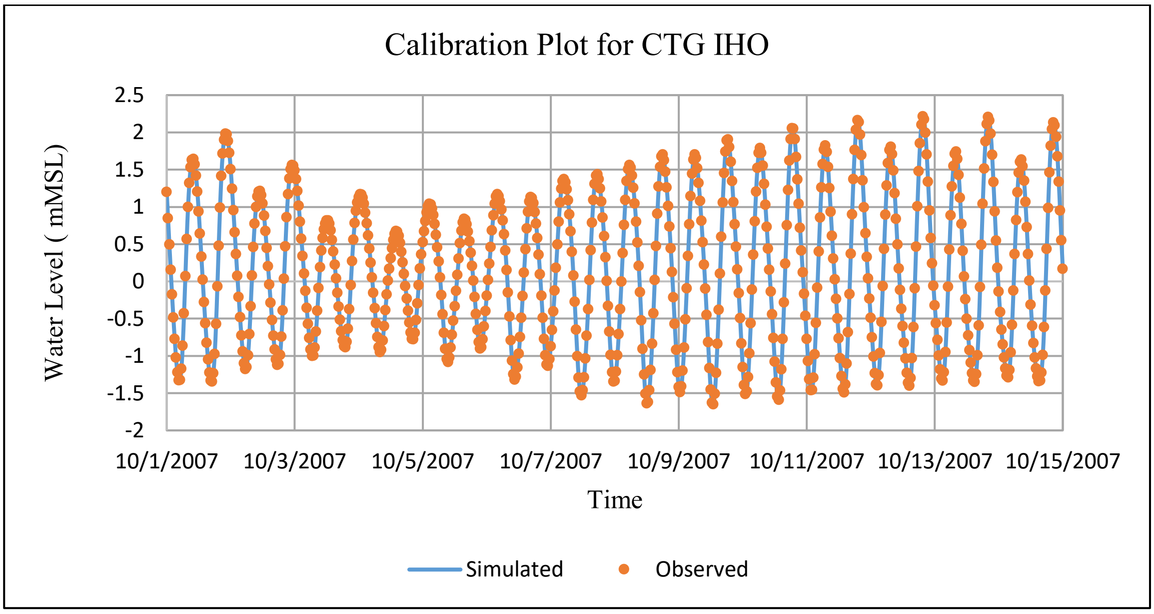

Figure 5 3: Calibration point for Chattogram IHO at Bangladesh (October 2007)

It is observed from the above graph that both the measured and simulated tidal levels of continuous sixty tidal cycles are very close and similar in tidal patterns with each other and have no deviations. The tidal patterns of both the observed and simulated tidal levels show the semi-diurnal tidal environment at this place.

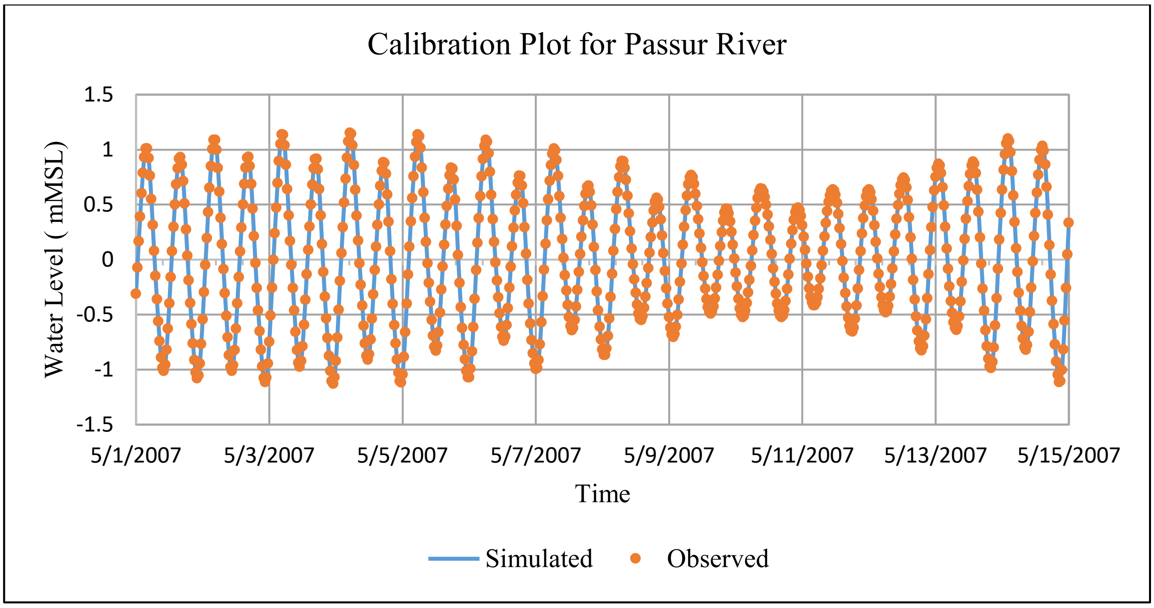

Figure 5.4: Calibration point for Passur River at Bangladesh (May 2007)

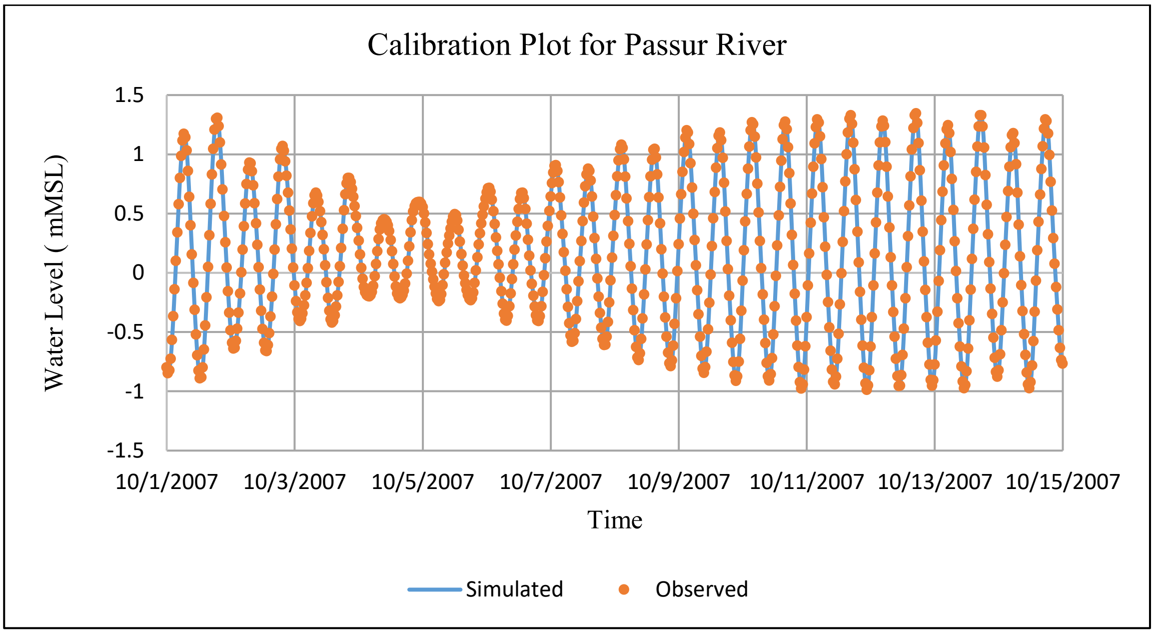

Figure 5 5: Calibration point for Passur River at Bangladesh (October 2007)

Figures 5.4 and 5.5 shows that both the measured and simulated tidal levels of continuous sixty tidal cycles are very close and similar in tidal patterns with each other. However, the simulated tidal levels do not precisely coincide with observed tidal levels but show good agreement with negligible deviation (less than 1 %). The tidal patterns of both the observed and simulated tidal levels show the semi-diurnal tidal environment at this place.

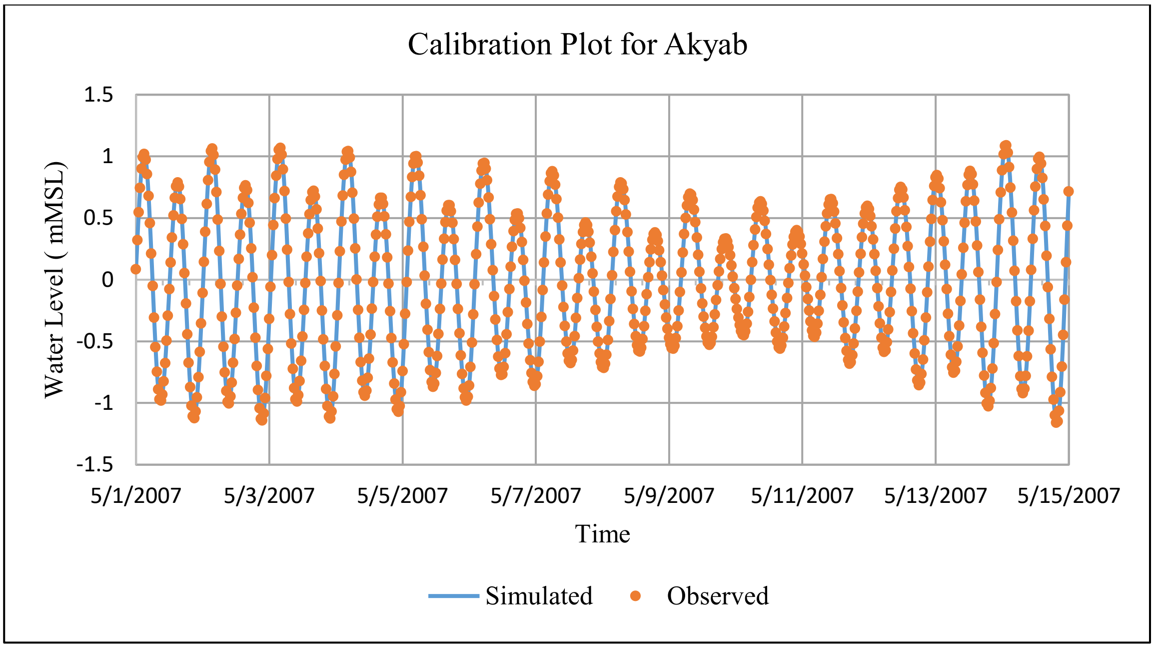

Figure 5.6: Calibrated point for Akyab at Myanmar (May 2007)

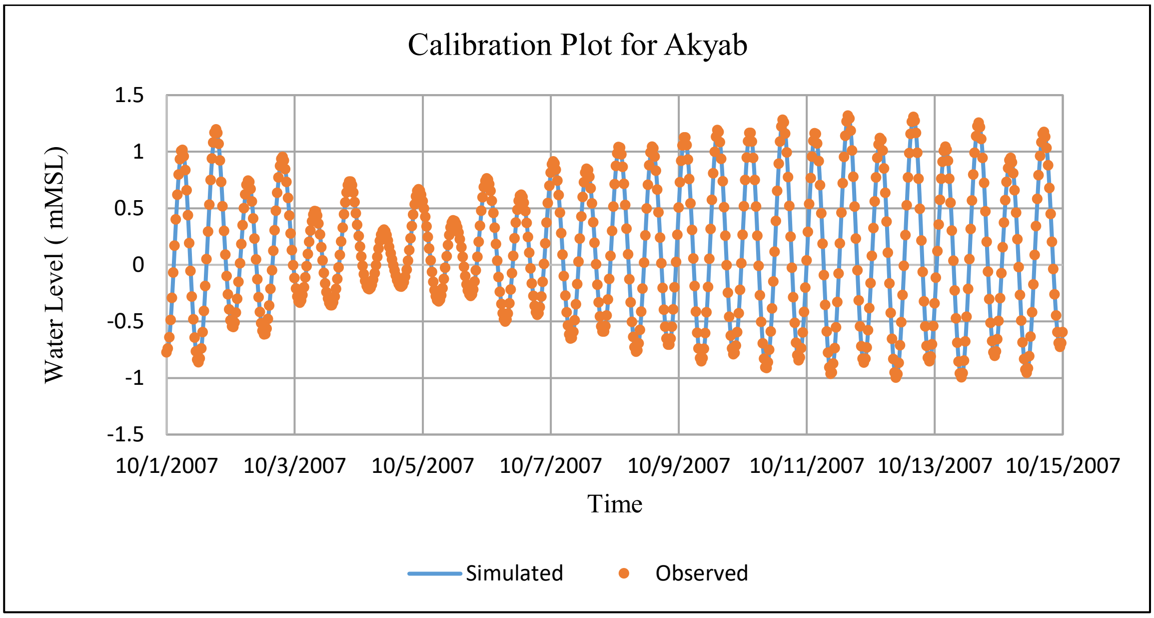

Figure 5 7: Calibrated point for Akyab at Myanmar (October 2007)

It is observed from the above figure that both the measured and simulated tidal levels of continuous sixty tidal cycles are very close and similar in tidal patterns with each other. The tidal patterns of both the observed and simulated tidal levels show the semi-diurnal tidal environment at this place.

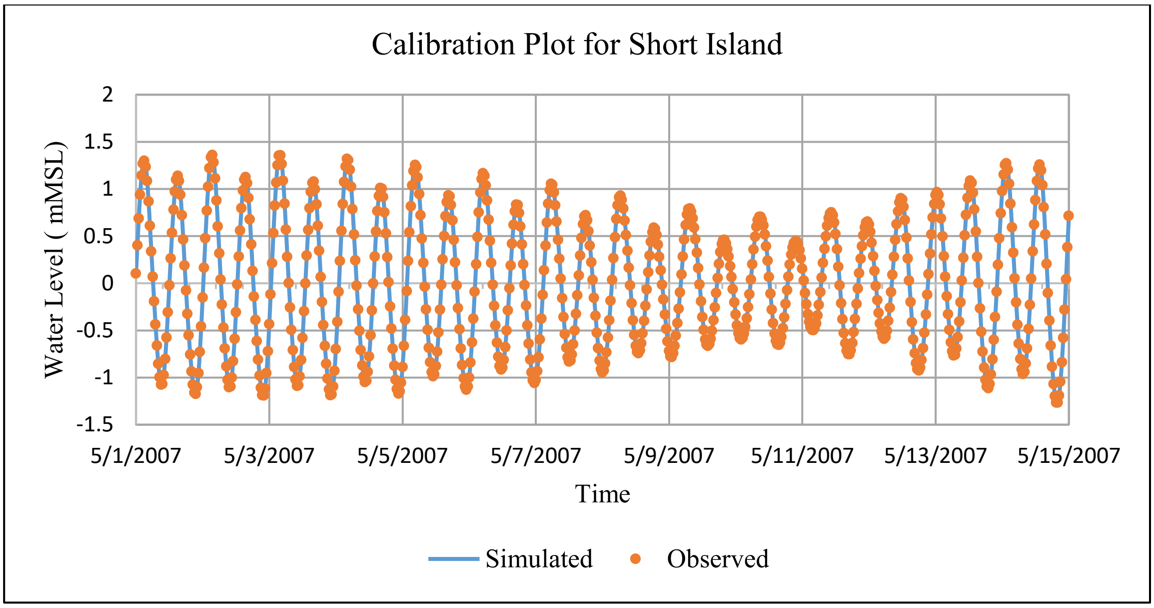

Figure 5 8: Calibrated point for Short Island at India (May 2007)

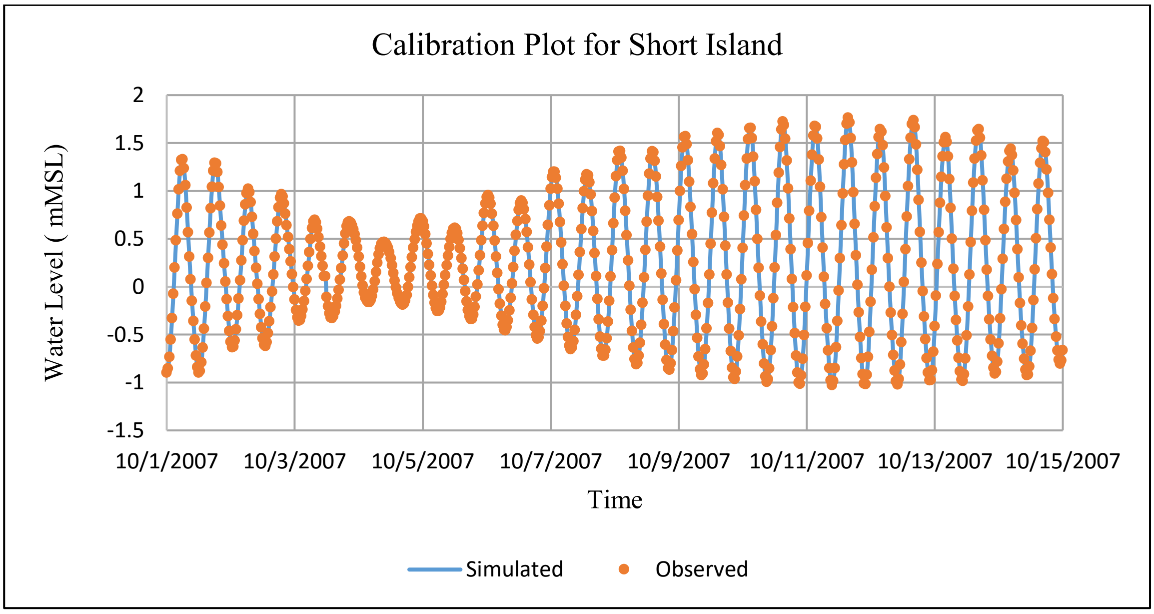

Figure 5 9: Calibrated point for Short Island at India (October 2007)

The followings above figure 5.8 and 5.9 shows both the measured and simulated tidal levels of continuous sixty tidal cycles which are very close and similar in tidal patterns with each other. However, the simulated tidal levels do not precisely coincide with observed tidal levels due to the model's initial stability but show good agreement with negligible deviation. The small variation (less than 2%) of tidal levels, as mentioned above, does not have a significant percentage of errors, and as a whole, the results show good agreement.

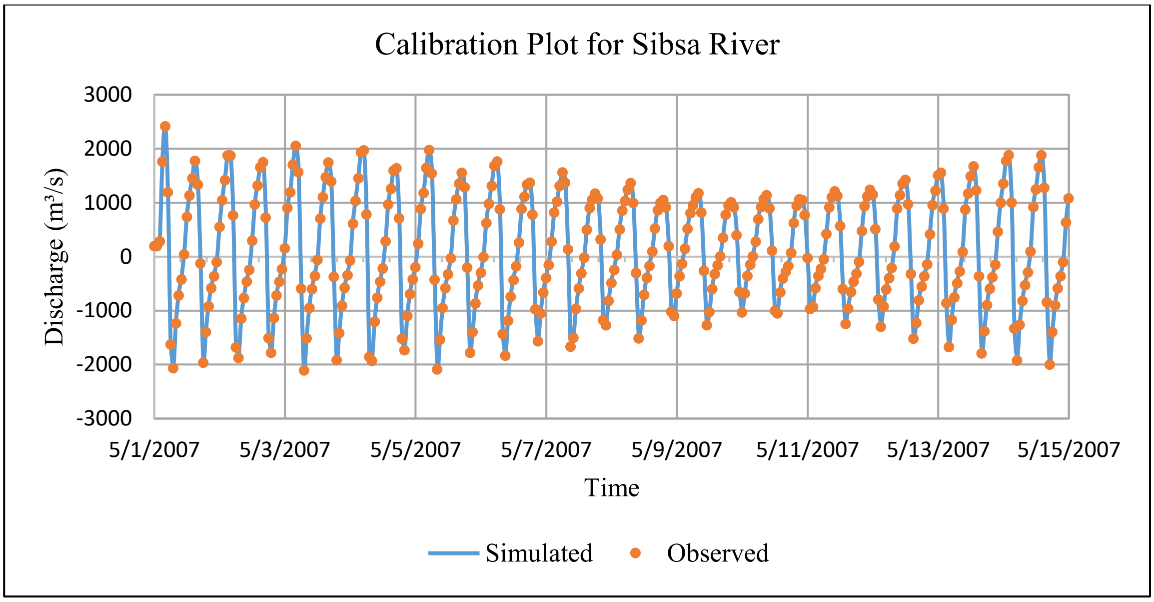

Figure 5 10: Calibrated point for Sibsa River at Bangladesh (May 2007)

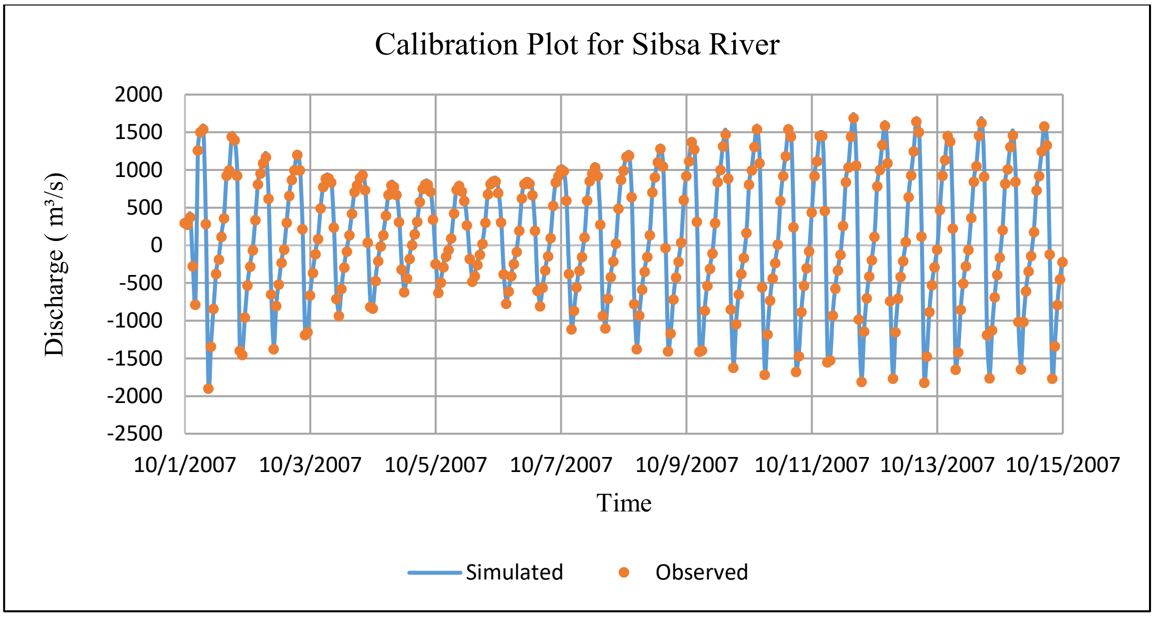

Figure 5 11: Calibrated point for Sibsa, River at Bangladesh (October 2007)

It is observed from the above figure that both the measured and simulated discharge are very close and similar in patterns with each other. However, the simulated discharge does not exactly coincide with observed discharge due to the initial stability of the model but shows good agreement with negligible deviation. The small variation (less than 2%) of the discharge, as mentioned above, does not have a significant percentage of errors, and as a whole, the results show good agreement.

Validation of FLOW Model:

Since most real-world models contain a large number of parameters, it is not always possible to produce a combination of parameter values that replicate the recorded data satisfactorily. However, this does not ensure an adequate model formulation or optimal parameter values. The calibration may have been achieved purely by numerical curve fitting without considering whether the parameter values so obtained are physically reasonable. Moreover, it might be possible to achieve multiple calibrations or apparently equally satisfactory calibrations based on a different combination of parameter values. Therefore, it is important to find out if a particular calibration is satisfactory or which of the several calibrations is the best one by testing (verifying) the model with a different set of data not used during calibration (Halim and Faisal, 1995).

According to Klemes (1986), a simulation model should be tested to show how well it can perform the task for which it is intended. Performance characteristics derived from the calibration data set are insufficient as evidence of satisfactory model operation. Thus, the verified or validated data must not be the same as those used for calibration but must represent a situation similar to that to which the model will be applied operationally.

A model should be tested for both steady and unsteady conditions (when applicable). The basic model structure could be validated by solving simple test problems for which analytical solutions exist. A common practice during the calibration-validation phase is to conduct a 'split sample test.' This means dividing the data into two and using one part to calibrate the model and the other part to validate it. The final model should also be transferable to a great extent to another problem area having similar characteristics.

In this study, the simulation time periods of validation have been considered for continuous thirty tidal cycles of 372 hours duration from 01 May 2008 at 0000 hrs to 15 May 2008 at 0000 hrs and another thirty tidal cycles of 372 hours duration from 01 October 2008 at 0000 to 15 October 2008 at 0000 hrs. The simulated sixty tidal cycles of the model are compared with the measured tidal levels of tidal gauge station, and discharge of water located at different location showed in the followings figures, Validation Results:

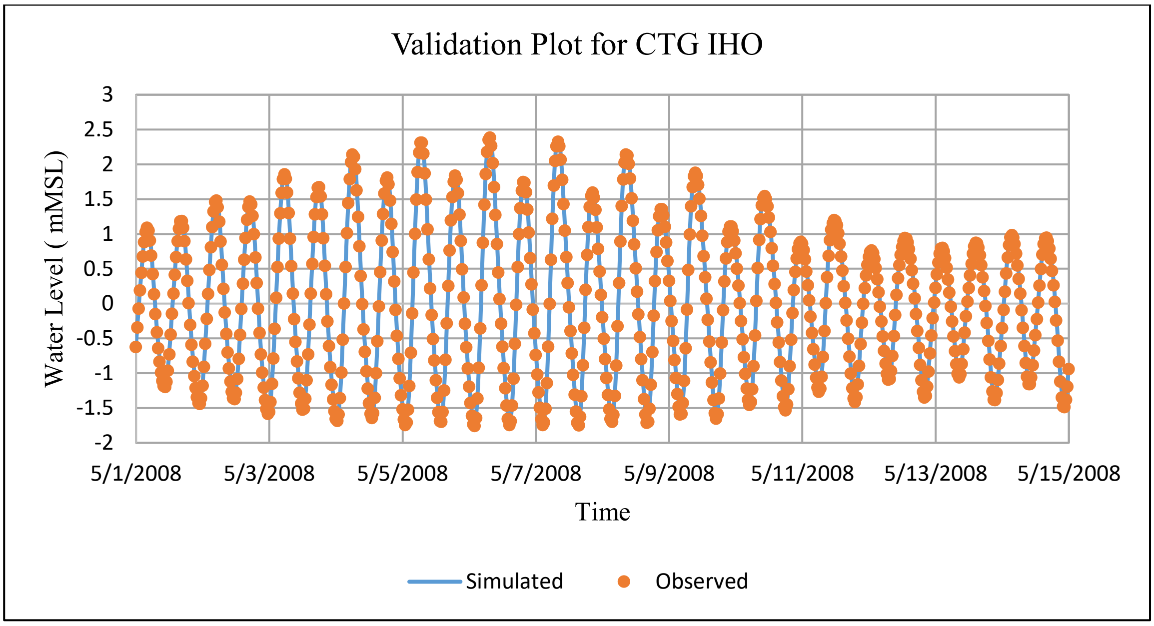

Figure 5.12: Validation for Chattogram IHO at Bangladesh (May 2008)

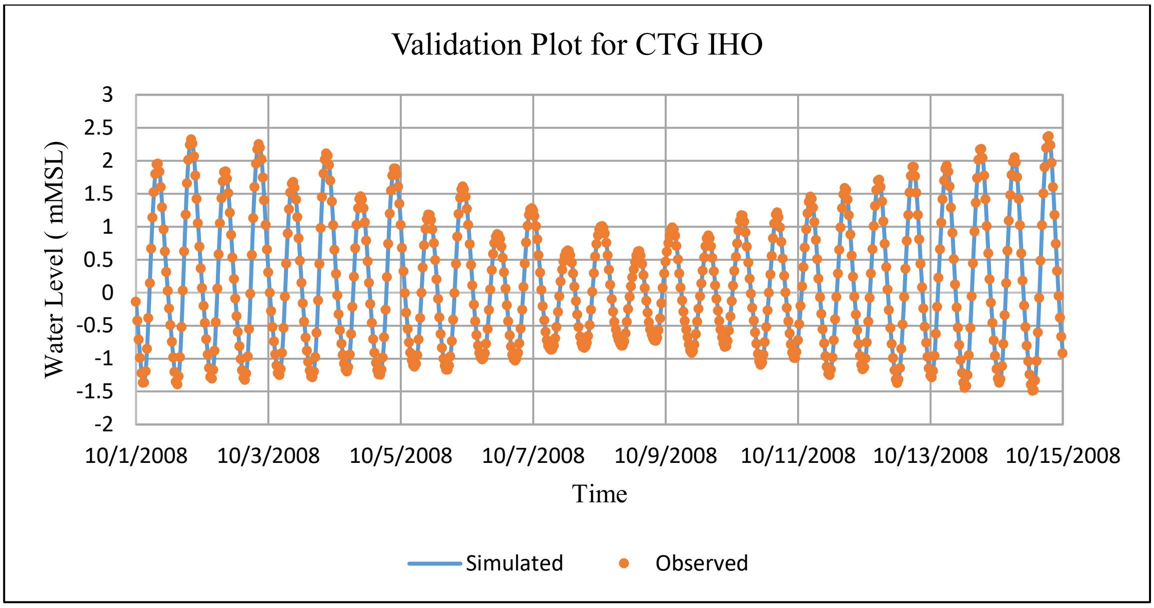

Figure 5 13: Validation for Chattogram IHO at Bangladesh (October 2008)

It is observed from the above figures that both the measured and simulated tidal levels of sixty tidal cycles are very close and similar in tidal patterns with each other and have no deviations. The tidal patterns of both the observed and simulated tidal levels show the semi-diurnal tidal environment at that place.

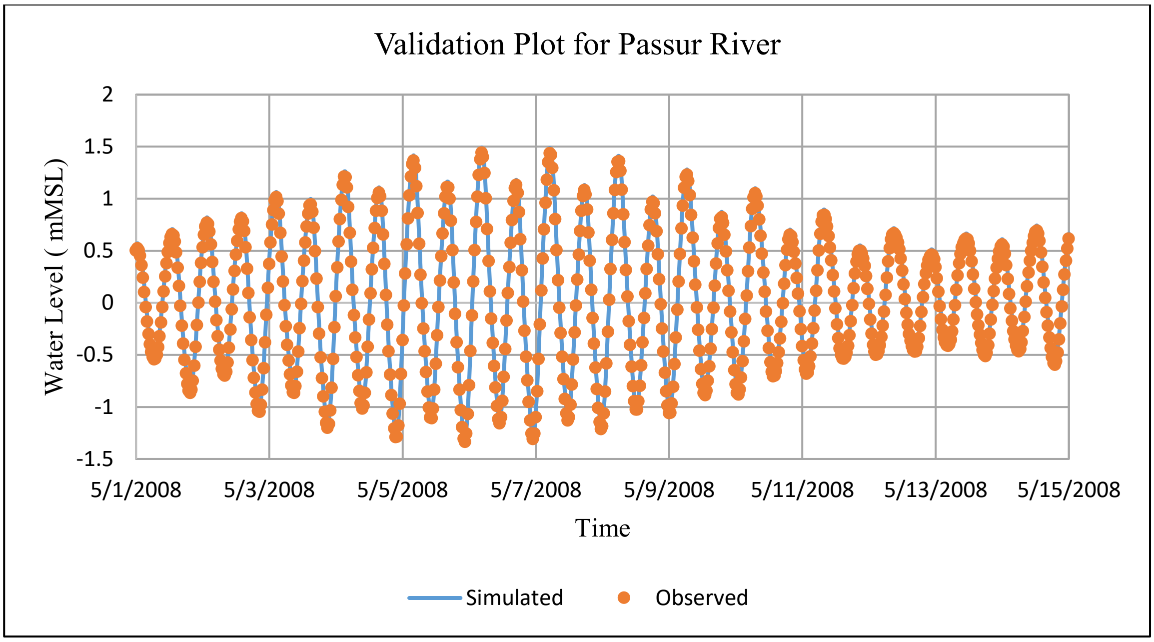

Figure 5.14: Validation for Passur River at Bangladesh (May 2008)

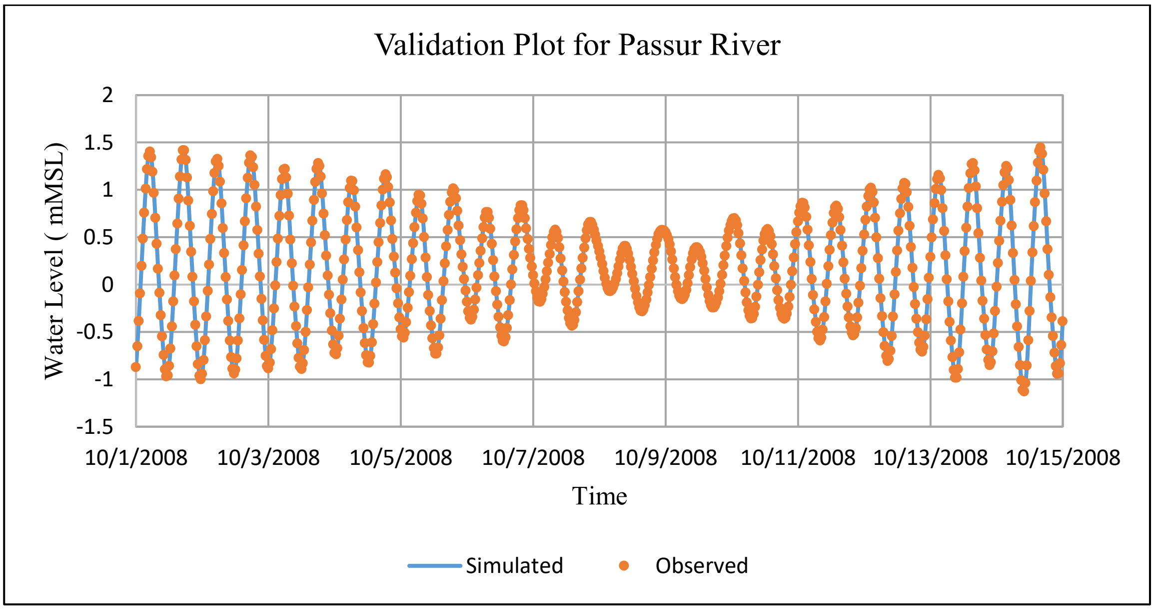

Figure 5 15: Validation for Passur River at Bangladesh (October 2008)

The above figures 5.14 and 5.15 show that both the measured and simulated tidal levels of sixty tidal cycles are very close and similar in tidal patterns and have no deviations. The tidal patterns of both the observed and simulated tidal levels show very good agreement.

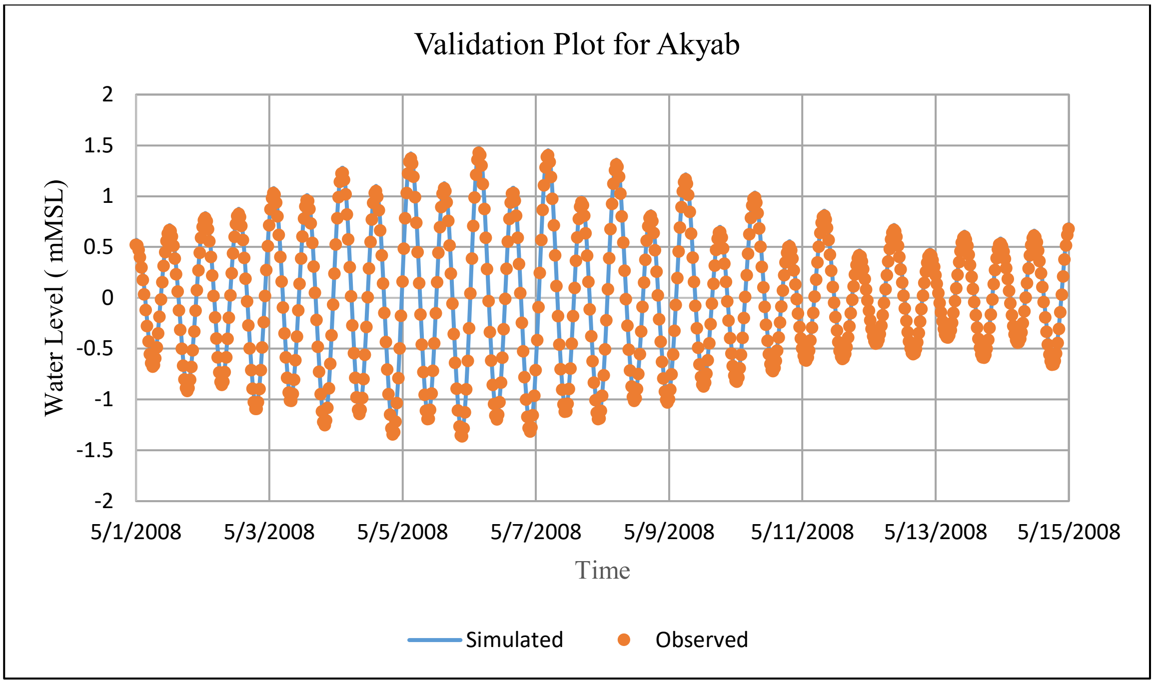

Figure 5.16: Validation for Akyab at Myanmar (May 2008)

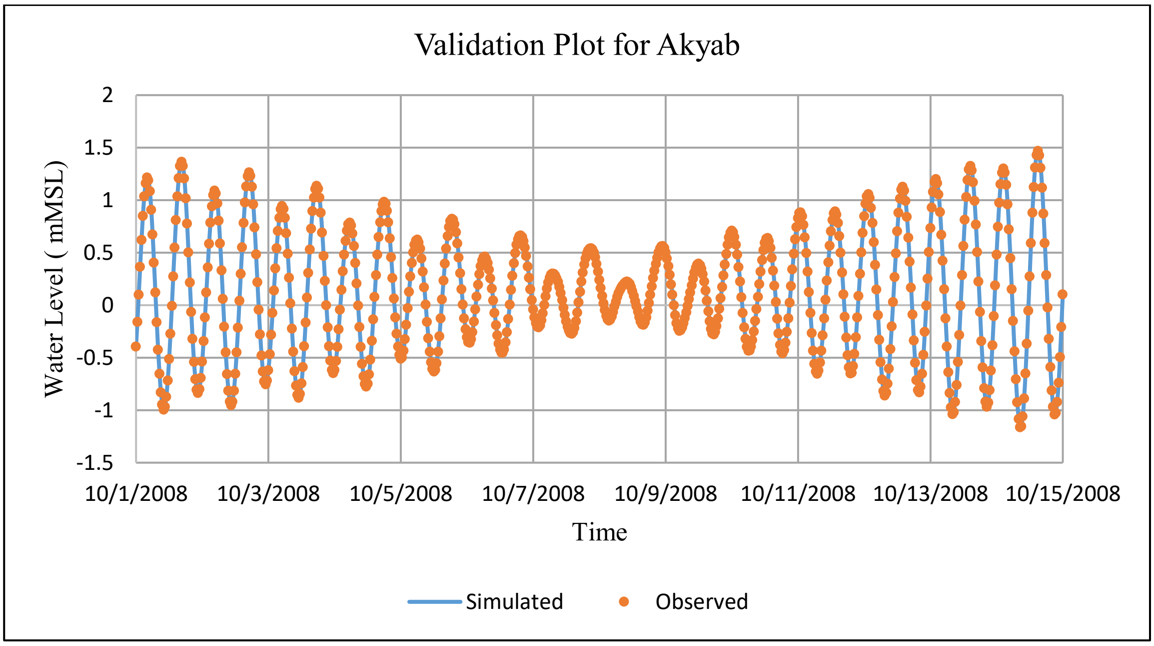

Figure 5 17: Validation for Akyab at Myanmar (October 2008)

Figures 5.16 and 5.17 shows that the simulated tidal levels peaks and troughs at different time periods during the flood and ebb tides have a very similar result with the observed tidal levels. The tidal patterns of both the observed and simulated tidal levels show the semi-diurnal tidal environment for the total sixty tidal cycles.

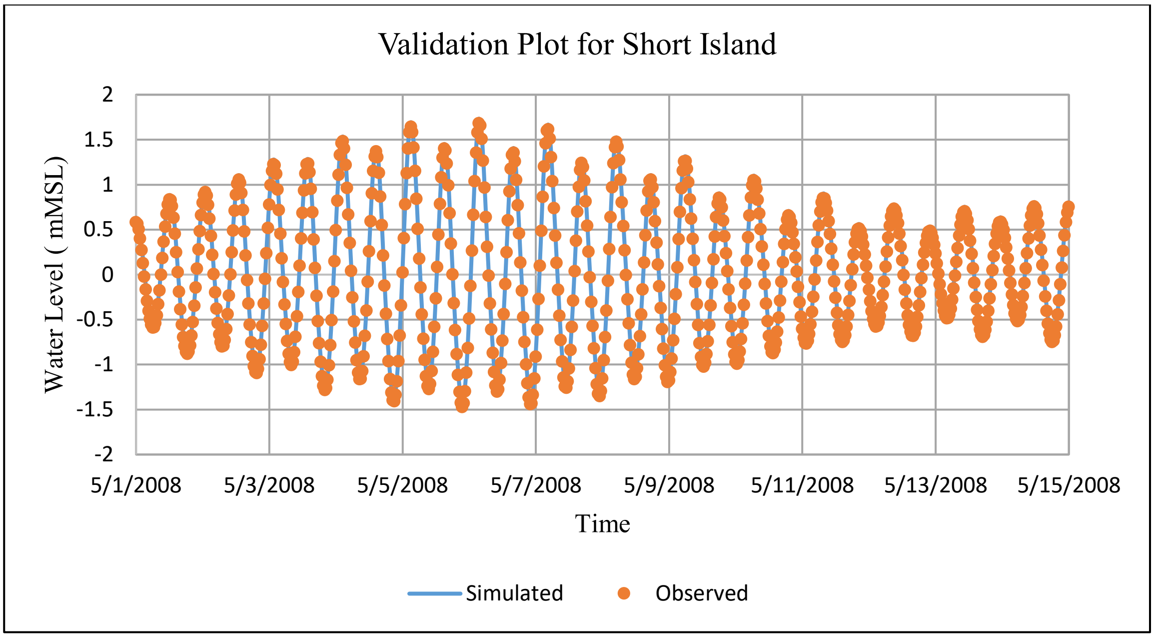

Figure 5.18: Validation for Short Island at India (May 2008)

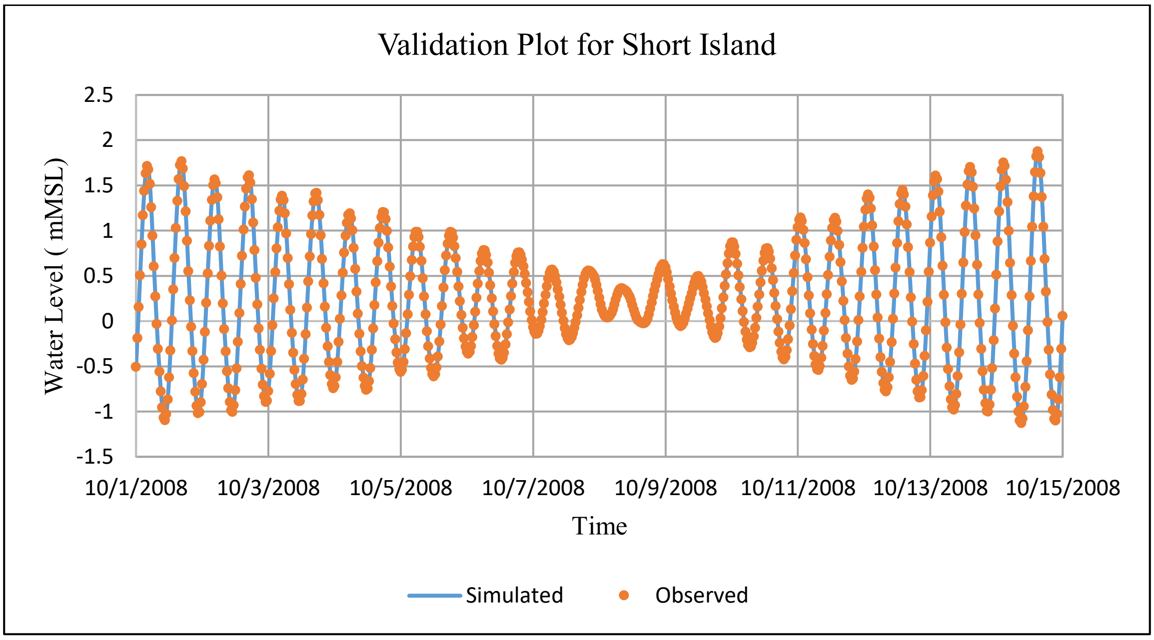

Figure 5 19: Validation for Short Island at India (October 2008)

It is observed from the above figure that both the measured and simulated tidal levels of continuous sixty tidal cycles are very close and similar in tidal patterns with each other. However, the simulated tidal levels do not precisely coincide with observed tidal levels in few cases but show good agreement with negligible deviation (less than 1 %). The tidal patterns of both the observed and simulated tidal levels show the semi-diurnal tidal environment at that place.

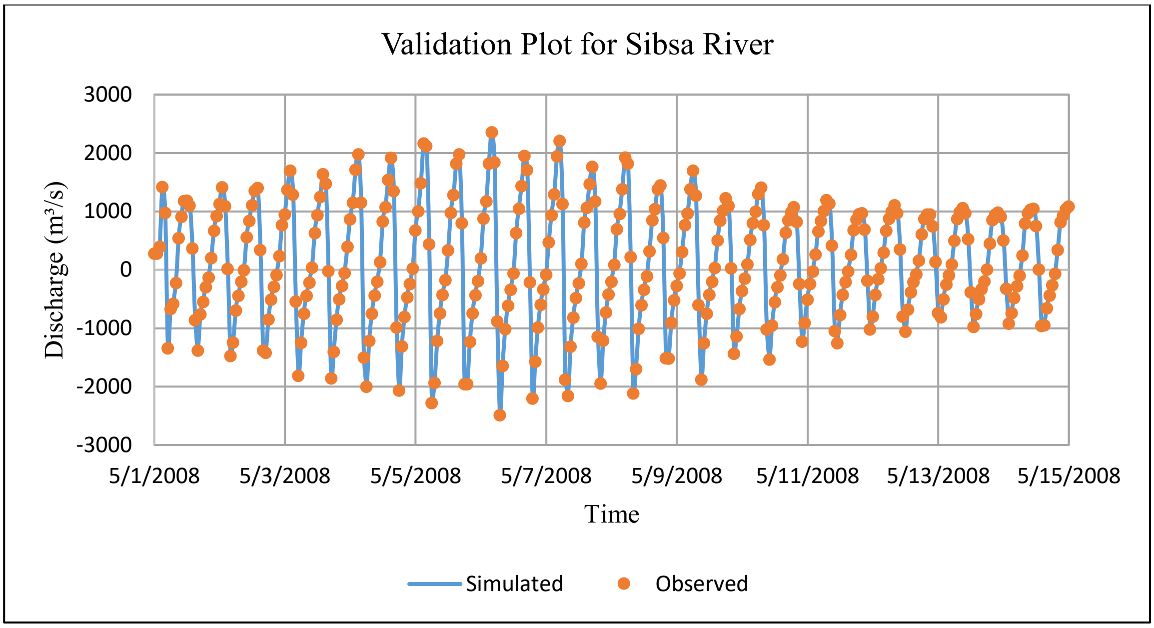

Figure 5 20: Validation point for Sibsa River at Bangladesh (May 2008)

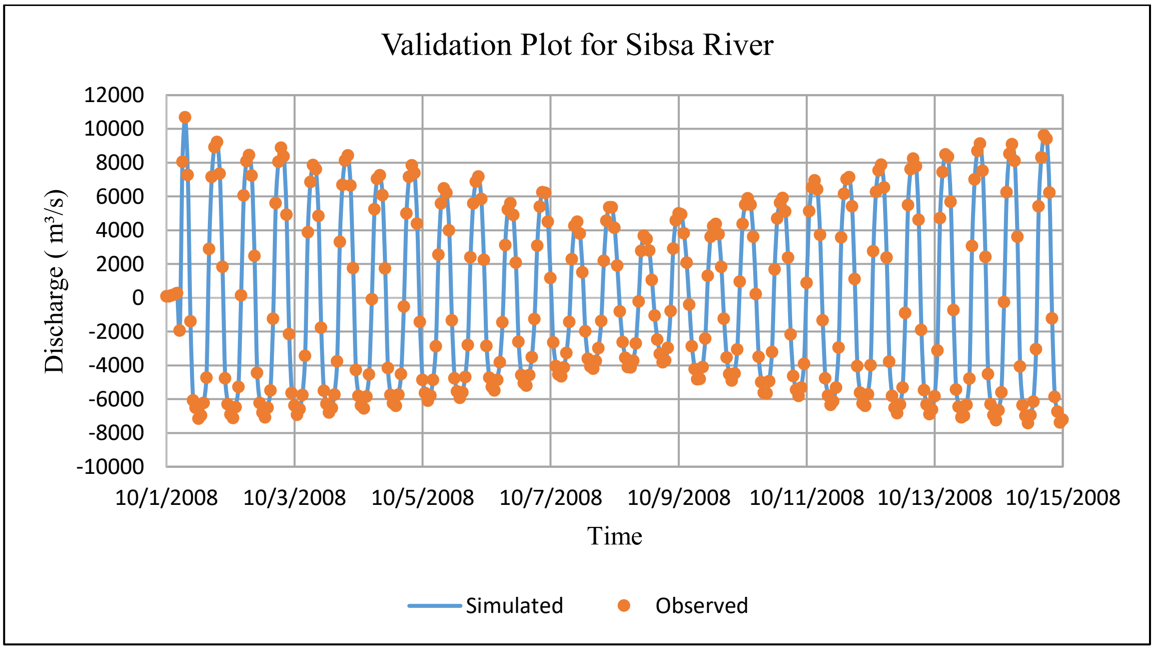

Figure 5 21: Validation point for Sibsa River at Bangladesh (October 2008)

The above figures 5.20 and 5.21 shows that both the measured and simulated discharge are very close and similar in patterns with each other. However, the simulated discharge does not exactly coincide with observed discharge due to the model's initial stability but shows good agreement with negligible deviation. The small variation (less than 1%) of discharge, as mentioned above, does not have a significant percentage of errors, and as a whole, the results show good agreement.

5.3 Calibration and Validation of WAVE Model

The wave model's calibration was achieved with the measured wave height at two different points in the Bay of Bengal alongside Cox Bazar shoreline, presented in Figure 5.22. The predicted wave height is generated using the coupled FLOW-WAVE model, where the WAVE part is simulated through SWAN (Simulating Waves Nearshore). The measured wave height has been collected from the Institute of Water Modeling (IWM). The calibration plot against the simulated wave height for the period of 01 May 2007 to 15 May 2007 and 01 October 2007 to 15 October 2007 is presented in Figure 5.23, Figure 5.24, Figure 5.25, and Figure 5.26 respectively,

Table 5 2:Calibration and Validation points for wave model (Data Source: IWM, for May 2007, October 2007 and May 2008, October 2008)

Gauge Station Authority	Station Name	Latitude (Degree)	Longitude (Degree)
IWM	Point 1	21.13°	91.83°
	Point 2	21.25°	91.85°

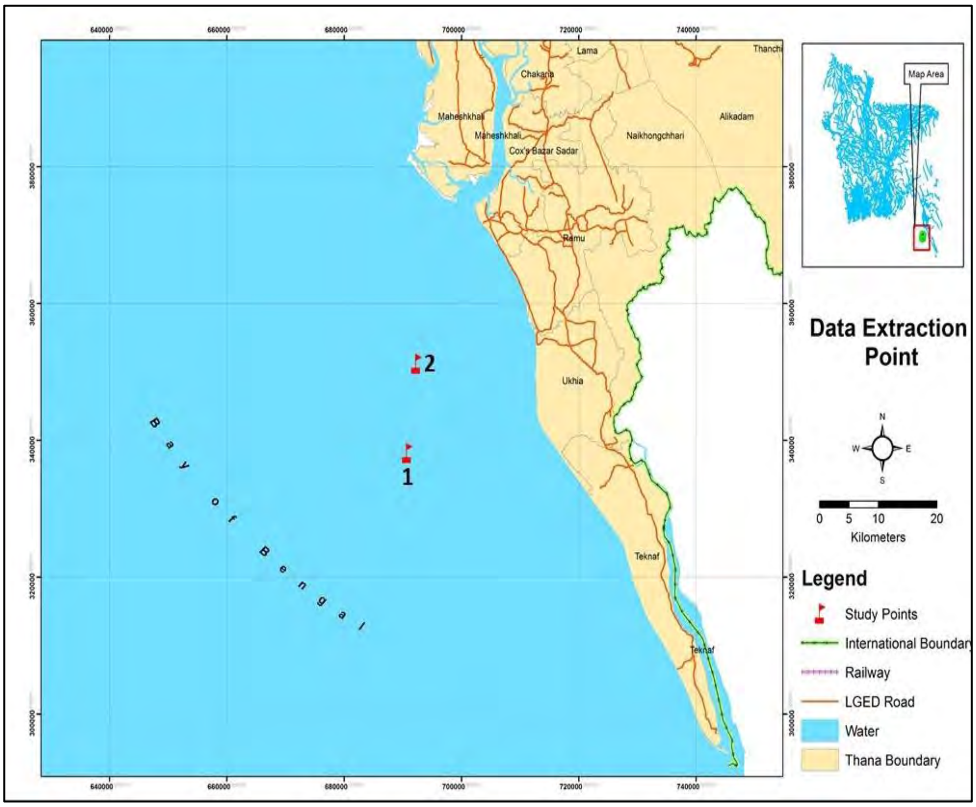

Figure 5.22: Calibration and Validation point for wave model

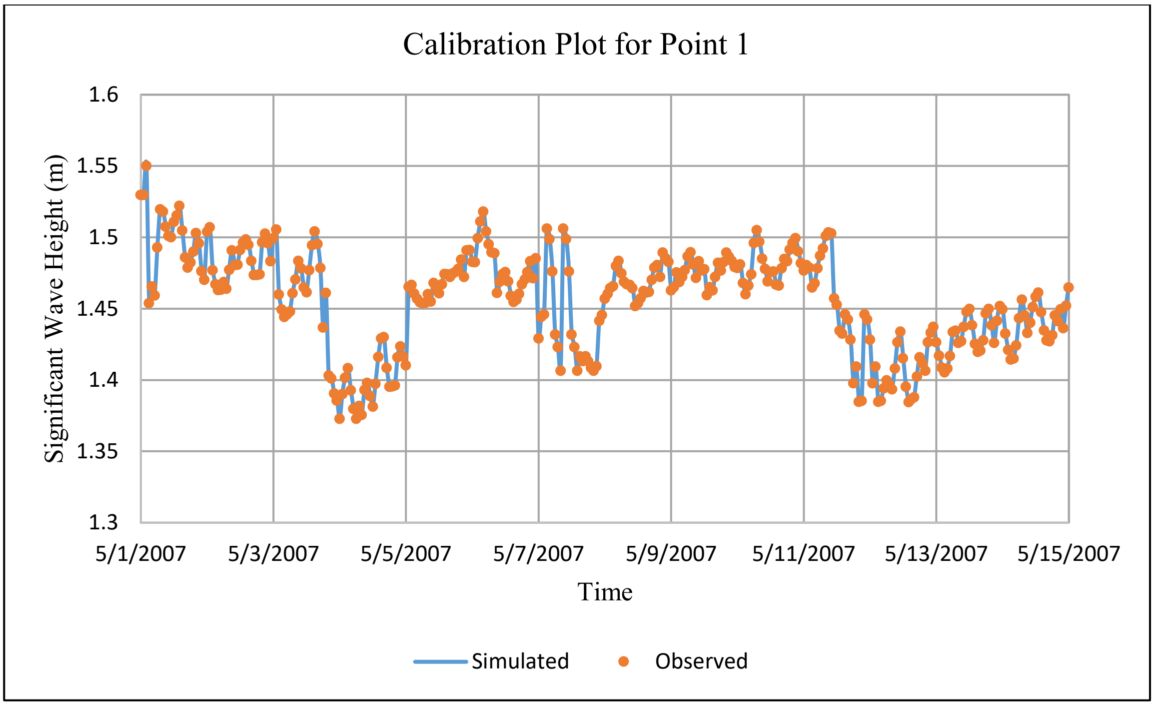

Figure 5.23: Wave calibration for point 1 near Cox-Bazar coastline in the Bay of Bengal (May 2007)

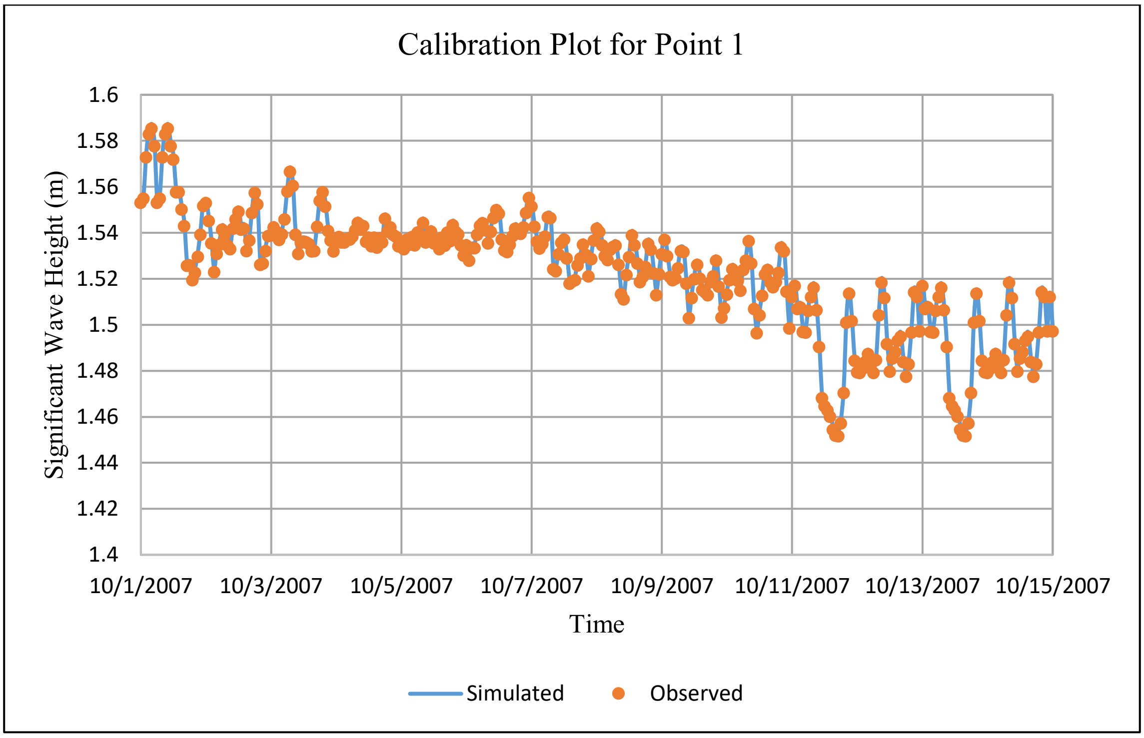

Figure 5 24: Wave calibration for point 1 near Cox-Bazar coastline in the Bay of Bengal (October 2007)

It is observed from the above analysis that the simulated wave height at different periods has a very similar result with the observed wave height. The coupled-wave model has calibration periods from 01 May 2007 at 0000 hours to 15 May 2007 at 0000 hours and 1

October 2007 at 0000 hours to 15 October 2007 at 0000 hours. This point shows an excellent result for calibrating the model, and the range of the wave height varies from 1.37m to 1.55 m for May 2007 and 1.45 m to 1.58m for October 2007.

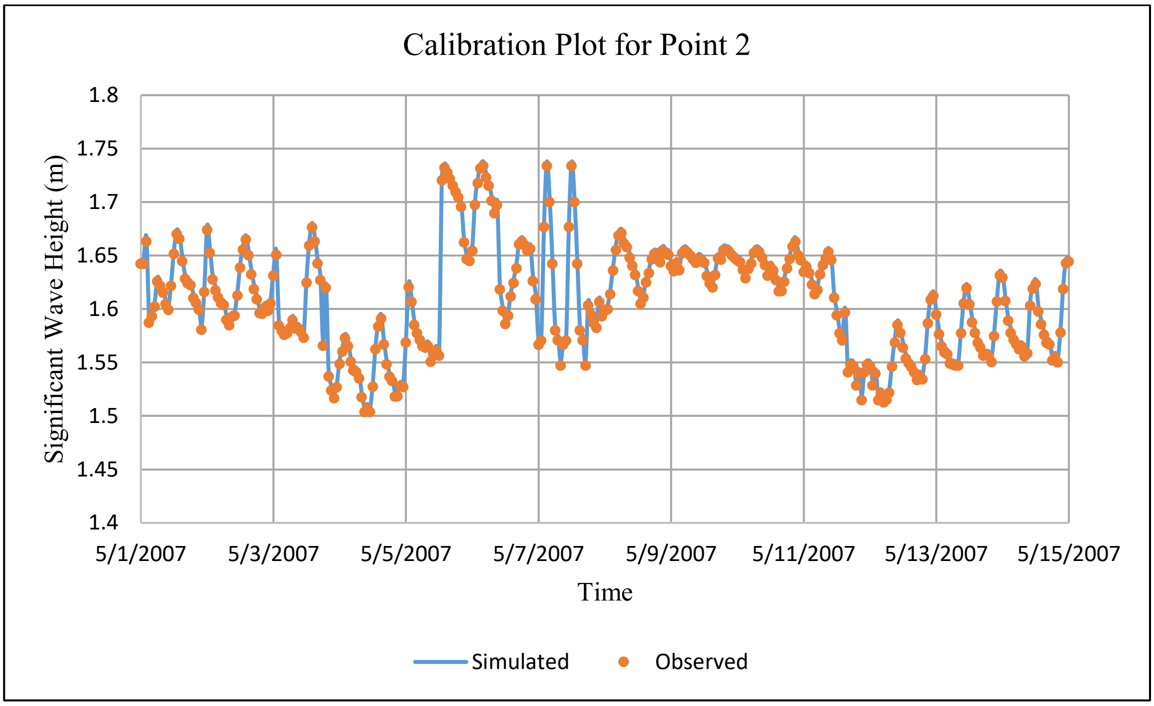

Figure 5.25: Wave calibration for point 2 near Cox-Bazar coastline in Bay of Bengal (May 2007)

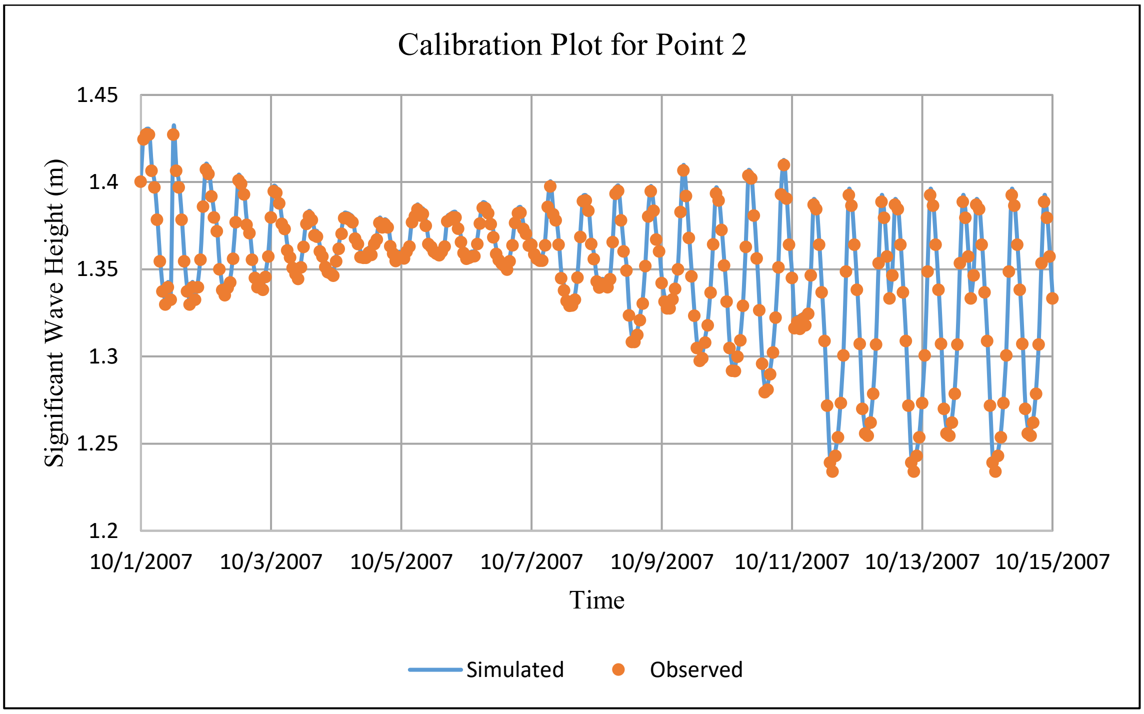

Figure 5 26: Wave calibration for point 2 near Cox-Bazar coastline in the Bay of Bengal (October 2007)

It is observed from the above analysis that the simulated wave height at different periods has a very similar result with the observed wave height. The coupled-wave model has calibration periods from 01 May 2007 at 0000 hours to 15 May 2007 at 0000 hours and 1 October 2007 at 0000 hours to 15 October 2007 at 0000 hours. This point also shows very good results for calibrating the model, and the range of the wave height varies from 1.50 m to 1.73 m for May 2007 and 1.23 m to 1.42 m for October 2007.

Validation of WAVE Model:

The validation has also been done with the measured wave height at two different points alongside Cox Bazar, presented in Figure 5.22. The predicted wave height has been generated using the coupled FLOW-WAVE model, where the WAVE part is simulated through SWAN (Simulating WAves Nearshore). The measured wave height has been collected from the Institute of Water Modeling (IWM). The validation plot against the simulated wave height for the period of 01 May 2008 to 15 May 2008 and 01 October 2008 to 15 October 2008 is presented in the Figure 5.27, Figure 5.28, Figure 5.29, and Figure 5.30 respectively,

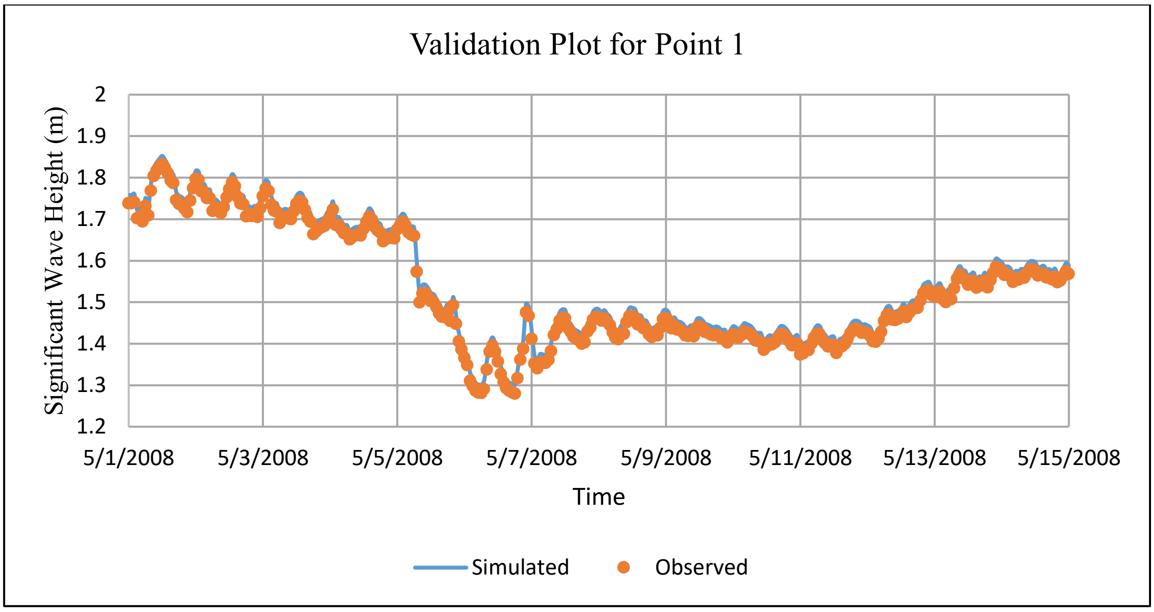

Figure 5.27: Validation of wave model for Point 1 near Cox-Bazar coastline (May 2008)

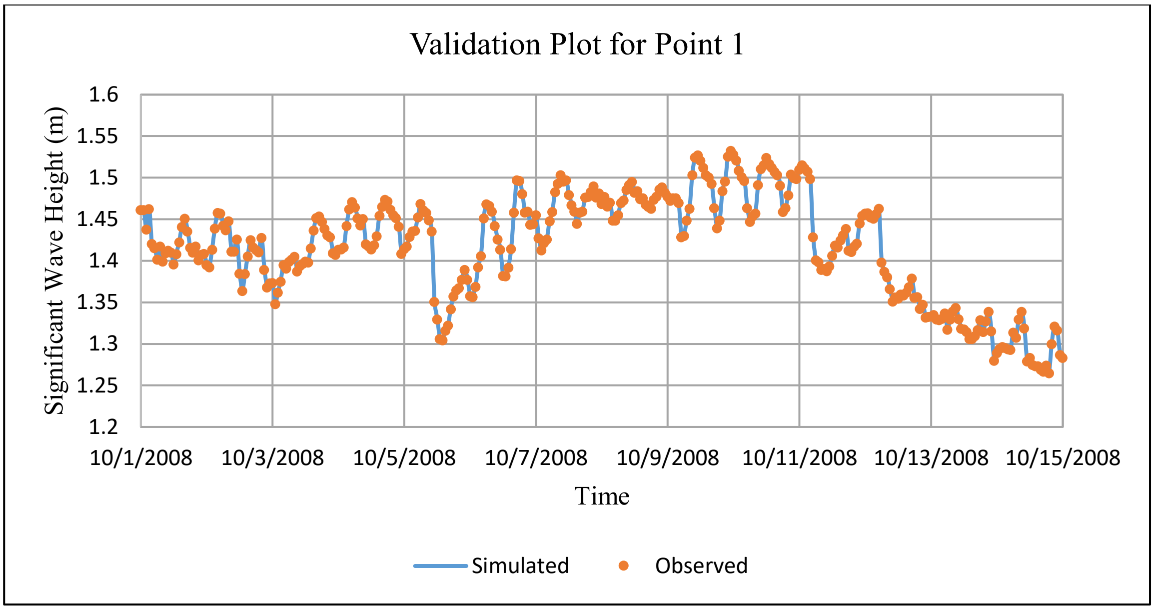

Figure 5 28: Validation of wave model for Point 1 near Cox-Bazar coastline (October 2008)

It is observed from the above analysis that the simulated wave height at different time periods has a very similar result with the observed wave height. The coupled-wave model has validation periods from 1 May 2008 at 0000 hours to 15 May 2008 at 0000 hours and 1 October 2008 at 0000 hours to 15 October 2008 at 0000 hours. This point shows very good results for validating the model, and the range of the wave height varies from 1.28 m to 1.83 m for May 2008 and 1.26 m to 1.52 m for October 2008.

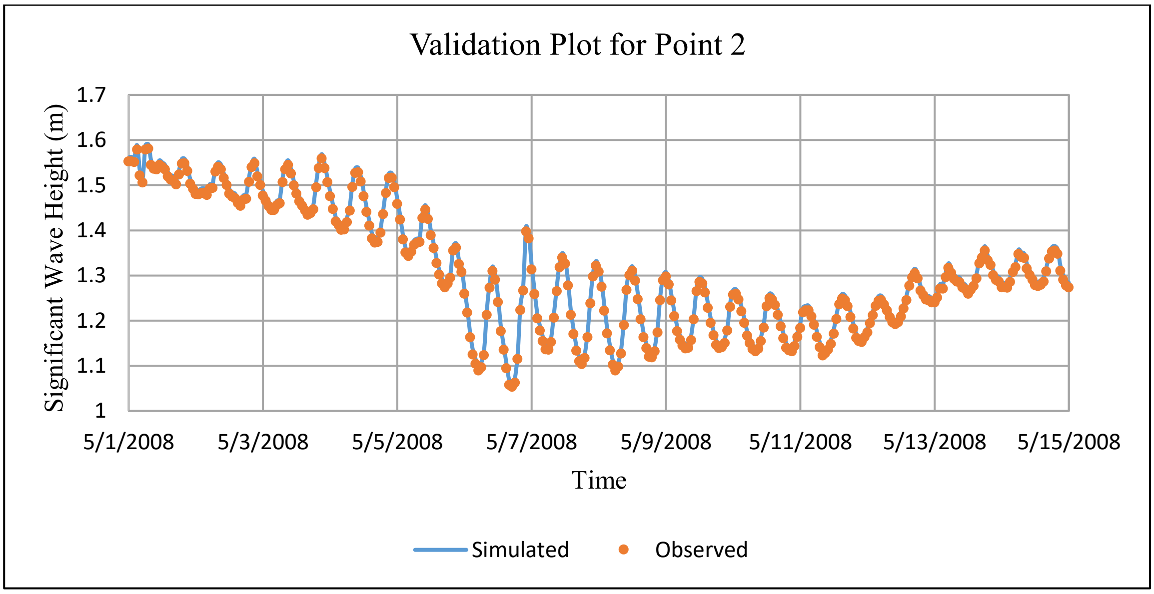

Figure 5.29: Validation of wave model for Point 2 near Cox-Bazar coastline (May 2008)

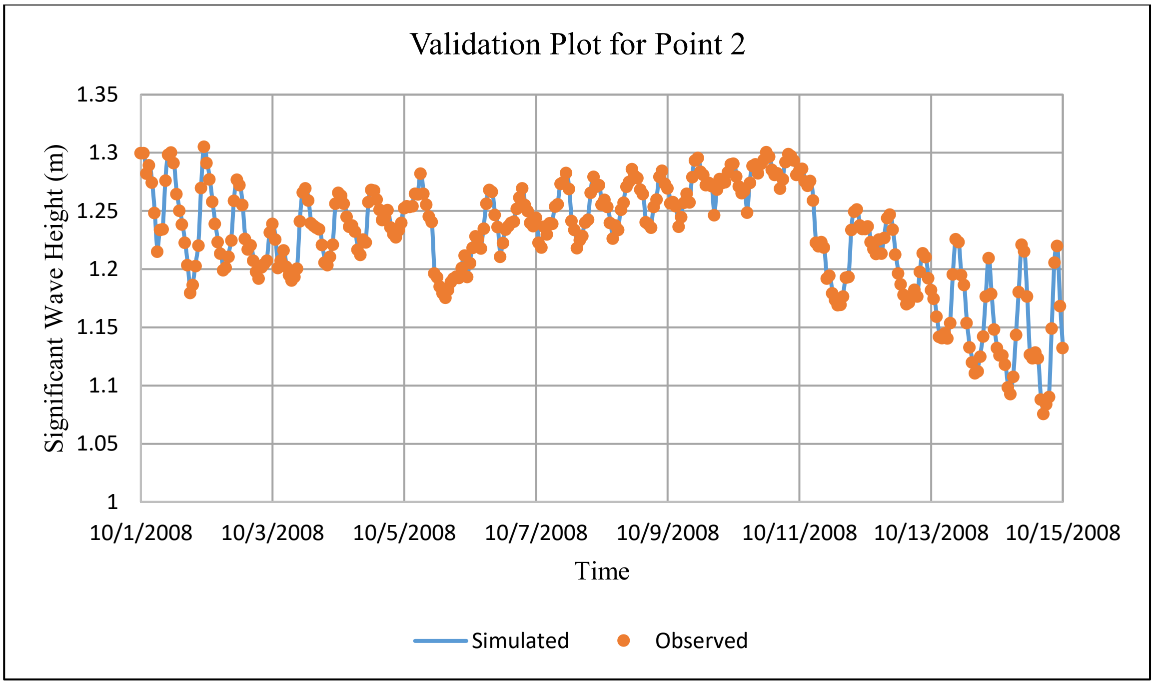

Figure 5 30: Validation of wave model for Point 2 near Cox-Bazar coastline (October 2008)

It is observed from the above analysis that the simulated wave height at different time periods has a very similar result with the observed wave height. The coupled-wave model has validated periods from 1 May 2008 at 0000 hours to 15 May 2008 at 0000 hours and 1 October 2008 at 0000 hours to 15 October 2008 at 0000 hours. This point also shows very good results for validating the model, and the range of the wave height varies from 1.05 m to 1.58 m for May 2008 and 1.07 m to 1.30 m for October 2008

5.4 Simulation of different structural options

The calibrated and validated model outputs are applied to the finer model of study sites. To protect the study area from continuous erosion, two types of hard solutions are considered. Breakwater and Groins applied to the finer model considering the proper length and distance from the shoreline. At the finer model, Breakwater is considered parallel to the coastline, and Groins considered along the coastline. During the design procedure, DEFRA and CEM manual have been followed. Two different sites are considered for the simulation, and all the nearshore hydrodynamic parameters are incorporated with the Bay of Bengal model. Four scenarios were considered to understand Breakwater and Groin's influence in the nearshore area.

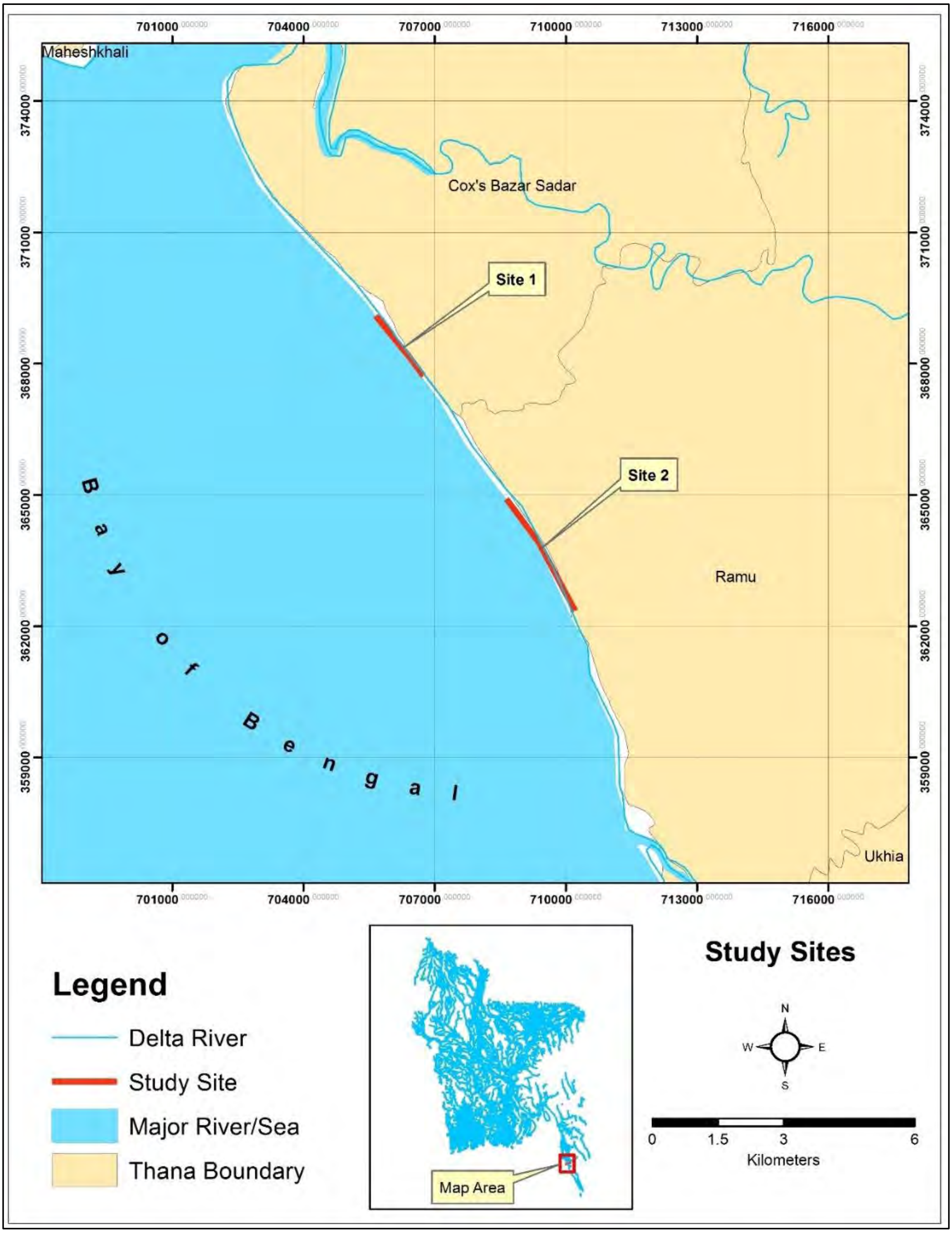

Figure 5.31: Area map of site 1 and site 2 along the Cox-Bazar coastline

5.4.1 Case 1 (Series of Breakwater in Site 1)

At site 1, from Kolatoli to Hatcharipara, a total of 1.7 km has been selected for the study. In the finer model 10 m × 10 m grid is generated with all the hydrodynamic and wave outputs from the Bay of Bengal model for simulating the Breakwaters. For protecting the 1.7 km area with Breakwater at site 1, (Starting Point: Latitude : 21.41°, Longitude : 91.98°; Ending point: Latitude : 21.40°, Longitude : 91.99°), a total of three Breakwaters considered as per DEFRA design guideline and incorporated at the finer model as per design specification. The Breakwater's total length is 100 m, the distance from the shoreline is 800 m, and gaps between the two Breakwater are 400 m, according to the beach slope. Finally, the model runs without the intervention and with the intervention for the 60 tidal cycles from May 1, 2008 - May 31, 2008. Individual analysis of erosion and sedimentation for Breakwaters at site 1 is attached in Appendix A.

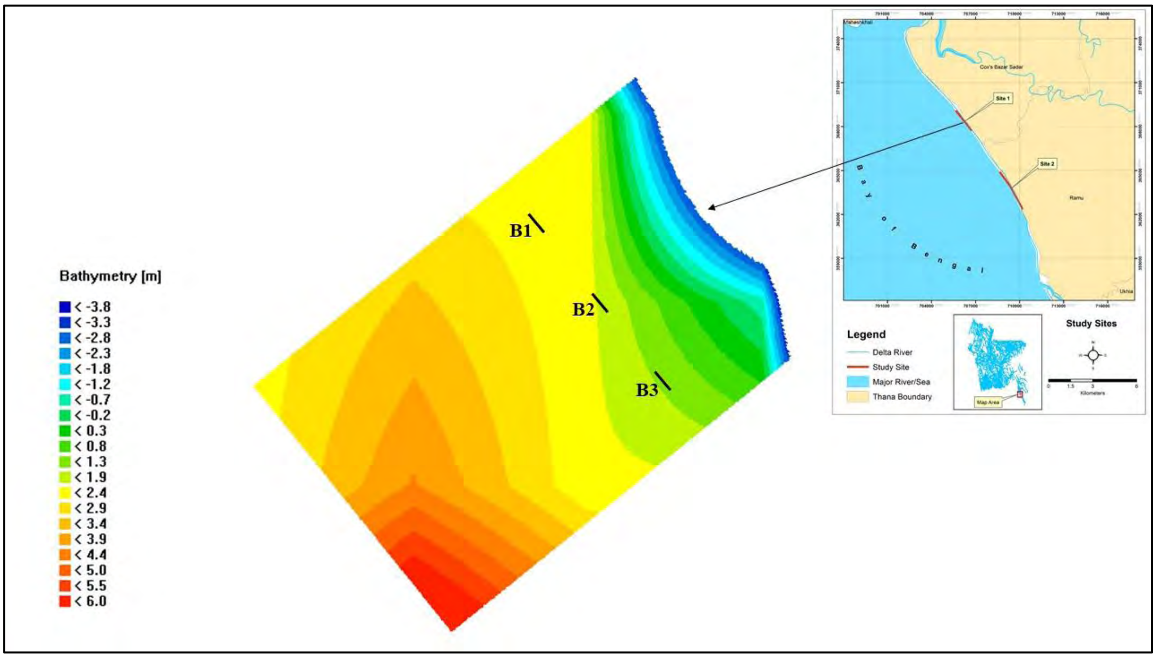

Figure 5.32: Series of Breakwater at Site 1 along Cox-Bazar coast

Table 5 3: Wave Height Change along site 1 with series of Breakwater (May 1, 2008- May 31, 2008)

Breakwater No.	Before Intervention (m)	After Intervention (m)	% Change
B1	0.49	0.36	27
B2	0.49	0.35	28
B3	0.31	0.15	53

From the above table, wave height changes along site 1 are summarized. It is seen from the analysis that there are significant changes in wave height due to placing the Breakwater parallel to the shoreline. At site 1, Breakwater (B3) has the maximum wave height reduction percentage (53%), where the other Breakwater shows changes between 27 % - 28 %. However, the total arrangement shows a very good result to reduce the wave height. The following figure shows the wave height changes along site 1:

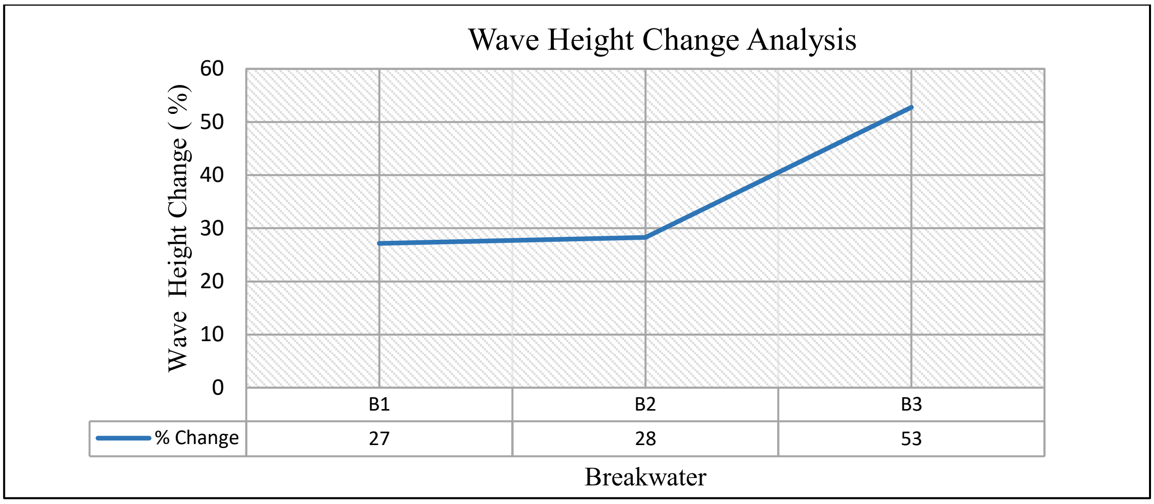

Figure 5.33: Wave Height Change Analysis for Site 1 with series of Breakwater

Table 5 4: Wave Energy Change Analysis along site 1 with series of Breakwater (May 1, 2008- May 31, 2008)

Breakwater No.	Before Intervention (J/m2)	After Intervention (J/m2)	% Change
B1	150.04	79.62	47
B2	145.54	74.84	49
B3	59.16	13.20	78

From the above table wave energy change along site 1 is summarized. It is seen from the analysis that there are significant changes in wave energy due to placing the Breakwater parallel to the shoreline. At site 1, Breakwater (B3) has the maximum wave energy reduction percentage (78%), where the other Breakwater shows changes between 47 % - 49 %. However, the total arrangement shows a very good result to reduce the wave energy. The following figure shows the wave energy changes along site 1:

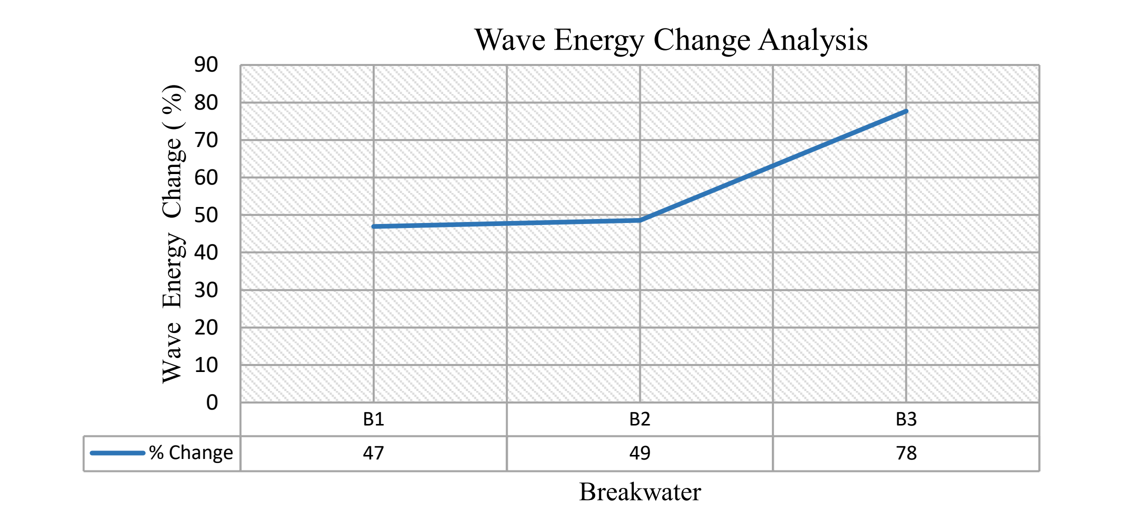

Figure 5 34: Wave Energy Change Analysis for Site 1 with a series of Breakwater

Erosion and sedimentation Analysis:

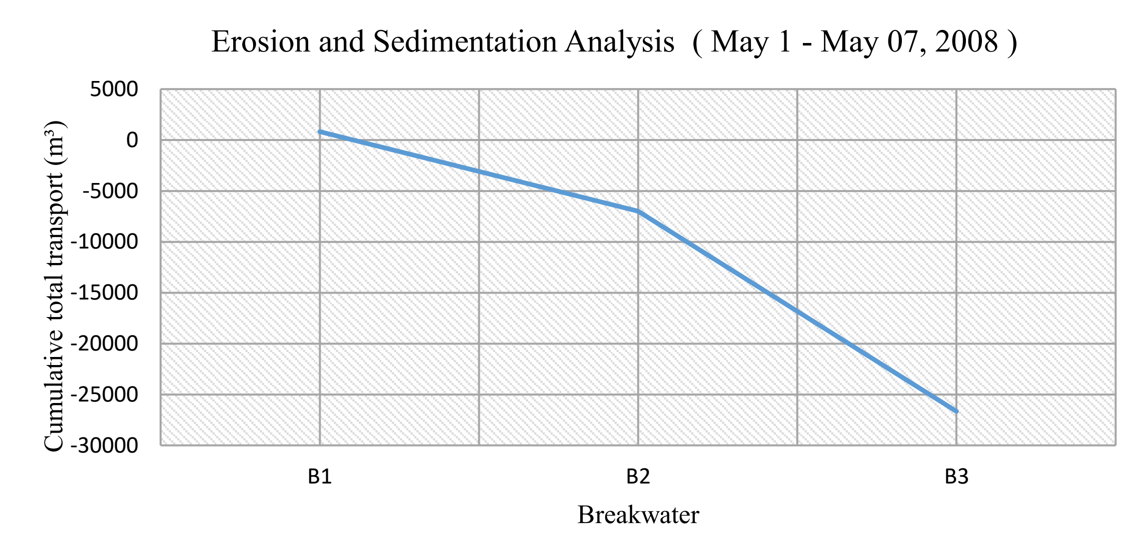

Figure 5. 35: Erosion and Sedimentation at Site 1 with series of Breakwater (May 1 - May 07, 2008)

Figure 5.35 shows, among the three Breakwater, two of them showing continuous erosion at the vicinity of the structure where the others one shows sedimentation. The maximum erosion occurs at Breakwater (B3) with total transport of -26659 m^3, and Breakwater (B1) shows sedimentation at a rate of 818 m^3 from May 1- May 07, 2008.

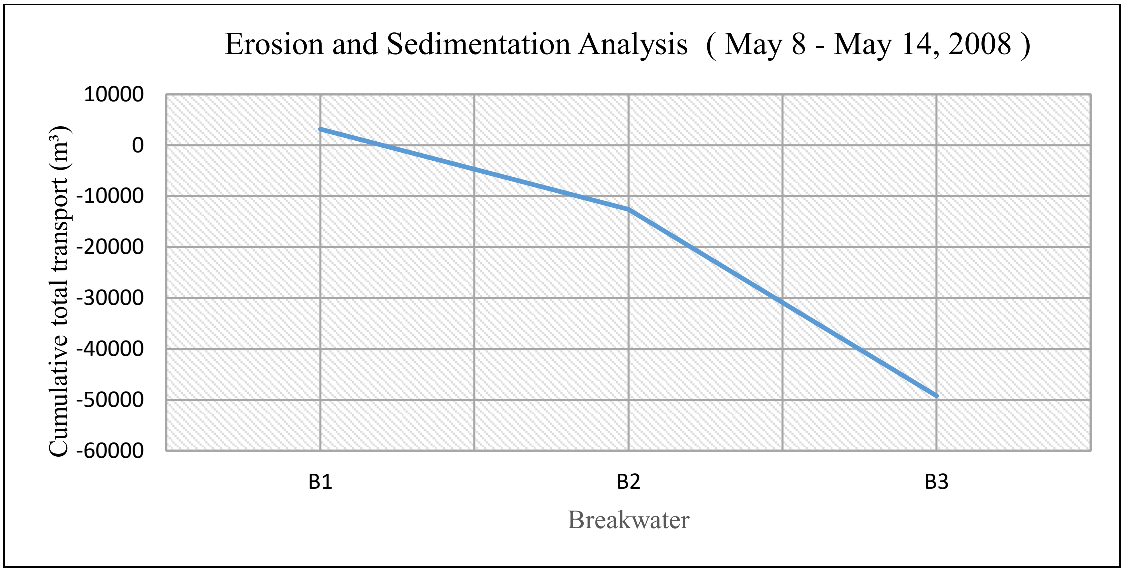

Figure 5.36: Erosion and Sedimentation at Site 1 with series of Breakwater (May 8 – May 14, 2008)

Figure 5.36 shows, among the three Breakwater, two of them showing continuous erosion at the vicinity of the structure where the others one shows sedimentation. The maximum erosion occurs at Breakwater (B3) with total transport of -49233 m^3, and Breakwater (B1) shows sedimentation at a rate of 3173 m^3 from May 8 - May 14, 2008.

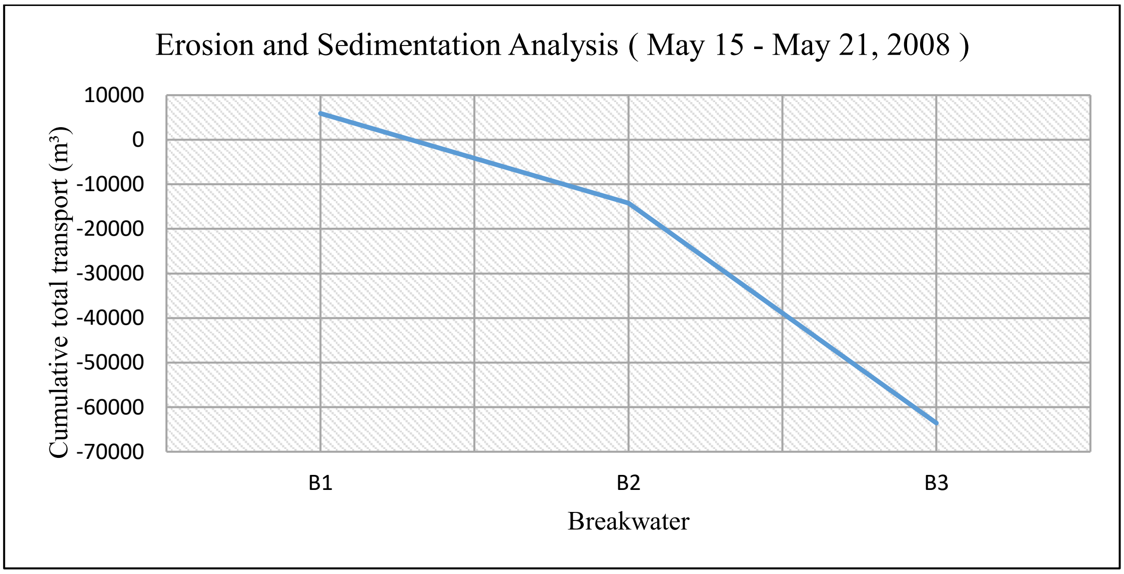

Figure 5.37: Erosion and Sedimentation at Site 1 with series of Breakwater (May 15 – May 21,2008)

Figure 5.37 shows, among the three Breakwater, two of them showing continuous erosion at the vicinity of the structure where the others one shows sedimentation. The maximum erosion occurs at Breakwater (B3) with total transport of -63567 m^3, and Breakwater (B1) shows sedimentation at a rate of 5910 m^3 from May 15 - May 21, 2008.

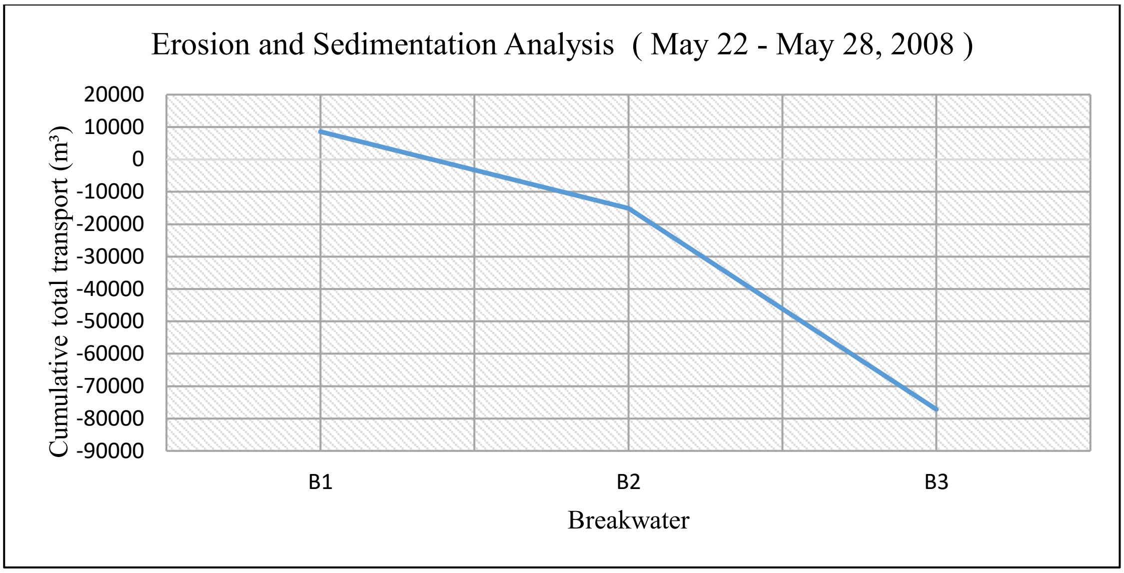

Figure 5.38: Erosion and Sedimentation at Site 1 with series of Breakwater (May 22 - May 28, 2008)

Figure 5.38 shows, among the three Breakwater, two of them showing continuous erosion at the vicinity of the structure where the others one shows sedimentation. The maximum erosion occurs at Breakwater (B3) with total transport of -77185 m^3, and Breakwater (B1) shows sedimentation at a rate of 8564 m^3 from May 22 - May 28, 2008.

5.4.2 Case 2 (Series of Groin in Site 1)

For protecting the 1.7 km area with Groins at site 1, (Starting Point: Latitude: 21.41°, Longitude : 91.98°; Ending point: Latitude : 21.40°, Longitude: 91.99), a total of seven Groins considered as per DEFRA design guideline and incorporated at the finer model as per design specification. In the finer model 10 m × 10 m grid is generated with all the hydrodynamic and wave outputs from the Bay of Bengal model for simulating the Groins. The total length of the Groin is 100 m and gaps between two Groin is 200 m. Finally, the model run without the intervention and with the intervention for 60 tidal cycle from May 1, 2008 - May 31, 2008. Individual analysis of erosion and sedimentation for Groin at site 1 is attached in Appendix A.

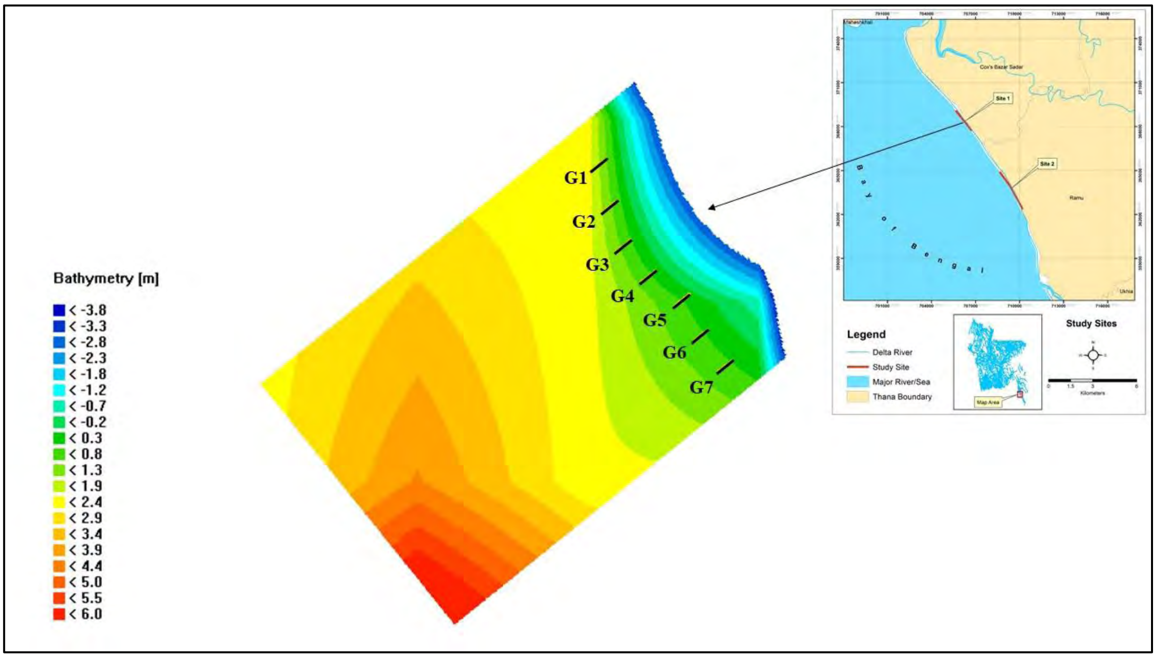

Figure 5.39: Series of Groin at Site 1 along Cox-Bazar coast

Table 5.5: Wave Height Change along the Site 1 with series of Groin
(May 1, 2008- May 31, 2008)

Groin No.	Before Intervention (m)	After Intervention (m)	% Change
G1	0.36	0.30	17
G2	0.42	0.38	9
G3	0.43	0.39	9
G4	0.39	0.09	76
G5	0.14	0.05	75
G6	0.24	0.08	69
G7	0.30	0.08	74

From the above table wave height changes along site 1 are summarized. It is seen from the analysis that there are significant changes in wave height due to placing the groins along the shoreline. At site 1, Groin G4 has the maximum wave height reduction percentage (76%), where the other groin shows changes between 9 % - 75 %. However, the total arrangement shows a relatively mixed performance to reduce the wave height. The following figure shows the wave height changes along site 1:

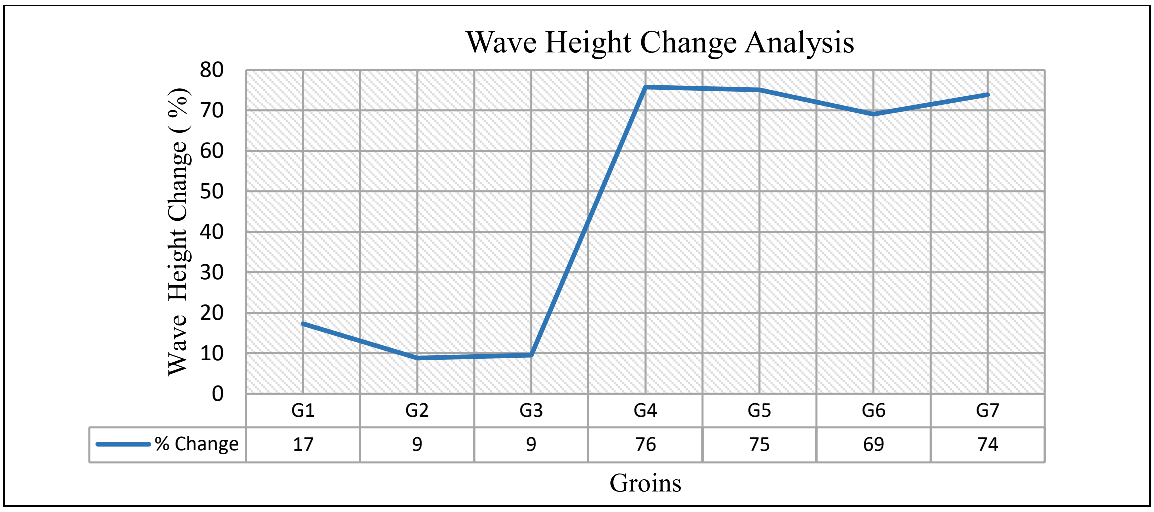

Figure 5.40: Wave Height Change Analysis for Site 1 with series of Groin

Table 5 6: Wave Energy Change Analysis along Site 1 with series of Groin (May 1, 2008- May 31, 2008)

Groin No.	Before Intervention (J/m2)	After Intervention (J/m2)	% Change
G1	79.51	54.36	32
G2	107.16	89.14	17
G3	115.66	94.86	18
G4	93.34	9.13	90
G5	19.45	3.90	90
G6	38.81	7.45	83
G7	54.16	4.85	91

From the above table wave energy change along site 1 is summarized. It is seen from the analysis that there are significant changes in wave energy due to placing the Groins along the shoreline. At site 1, Groin G7 has the maximum wave energy reduction percentage (91%), where the other Groin shows changes between 17 % - 90 %. However, the total arrangement shows a very good result to reduce the wave energy. The following figure shows the wave energy changes along with the site 1:

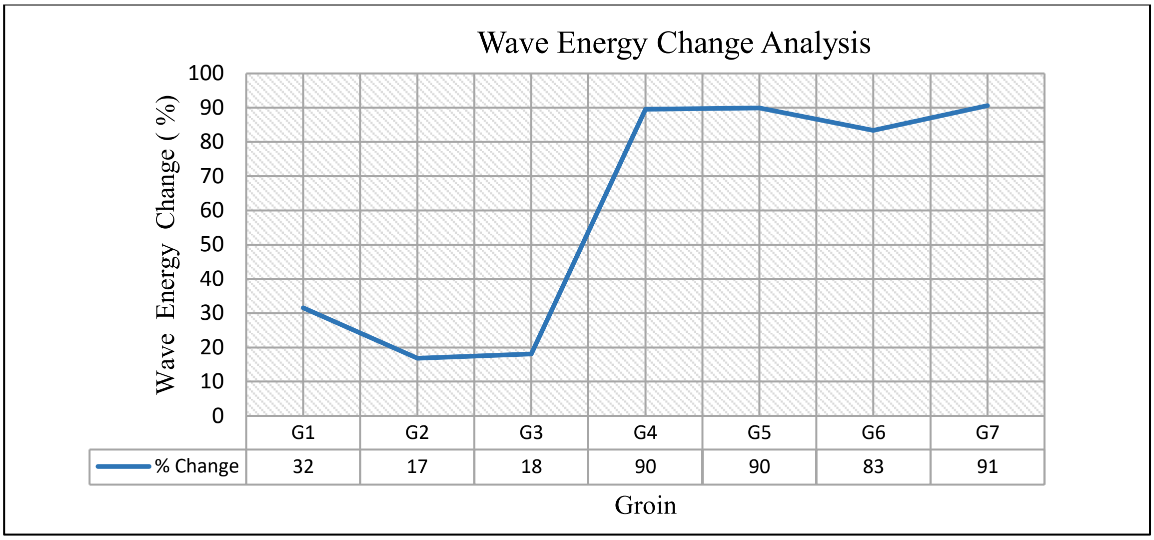

Figure 5 41: Wave Energy Change Analysis for Site 1 with series of Groin

Erosion and sedimentation Analysis:

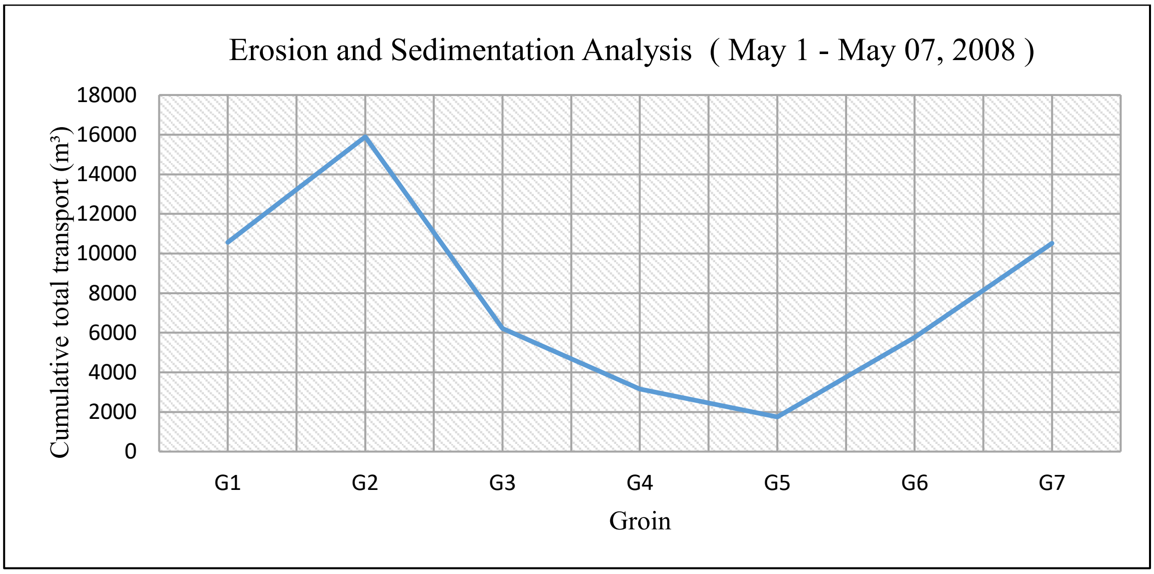

Figure 5.42: Erosion and Sedimentation at Site 1 with series of Groin
(May 1 - May 7, 2008)

Figure 5.42 shows, among the seven Groin, all of them showing sedimentation in nearby areas. The maximum sedimentation occurs at Groin (G2) with total transport of 15891 m^3, and Groin (G5) shows the lowest sedimentation accumulation at a rate of 1749 m^3 from May 1- May 7, 2008.

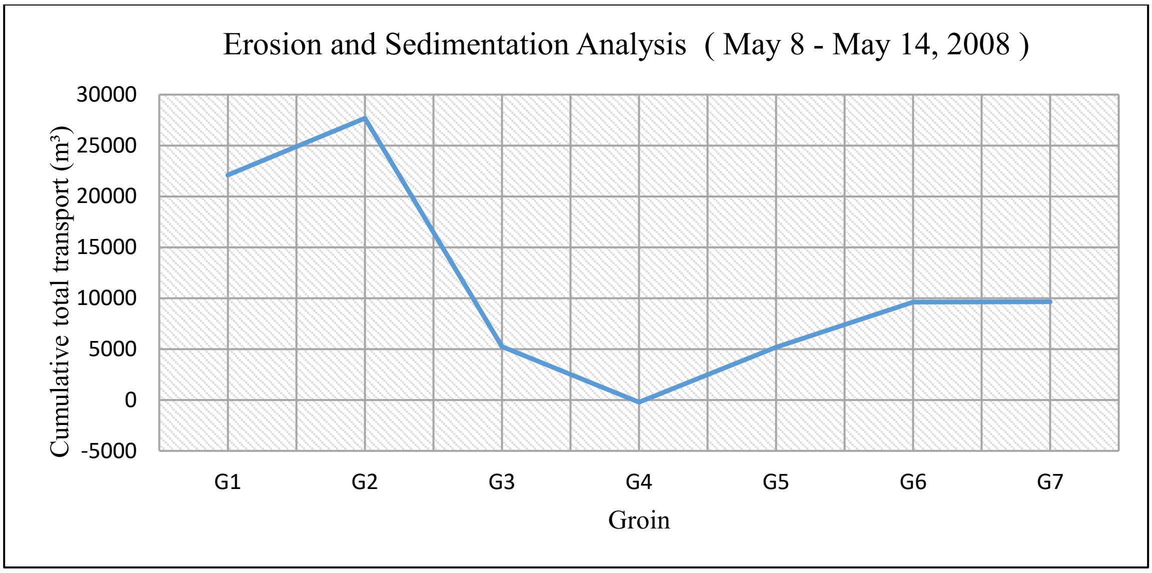

Figure 5.43: Erosion and Sedimentation at Site 1 with series of Groin (May 8 - May 14, 2008)

Figure 5.43 shows, among the seven Groin, all of them showing sedimentation in nearby areas. The maximum sedimentation occurs at Groin (G2) with total transport of 27681 m^3, and Groin (G4) shows the lowest sedimentation accumulation at a rate of -214 m^3 from May 8 - May 14, 2008.

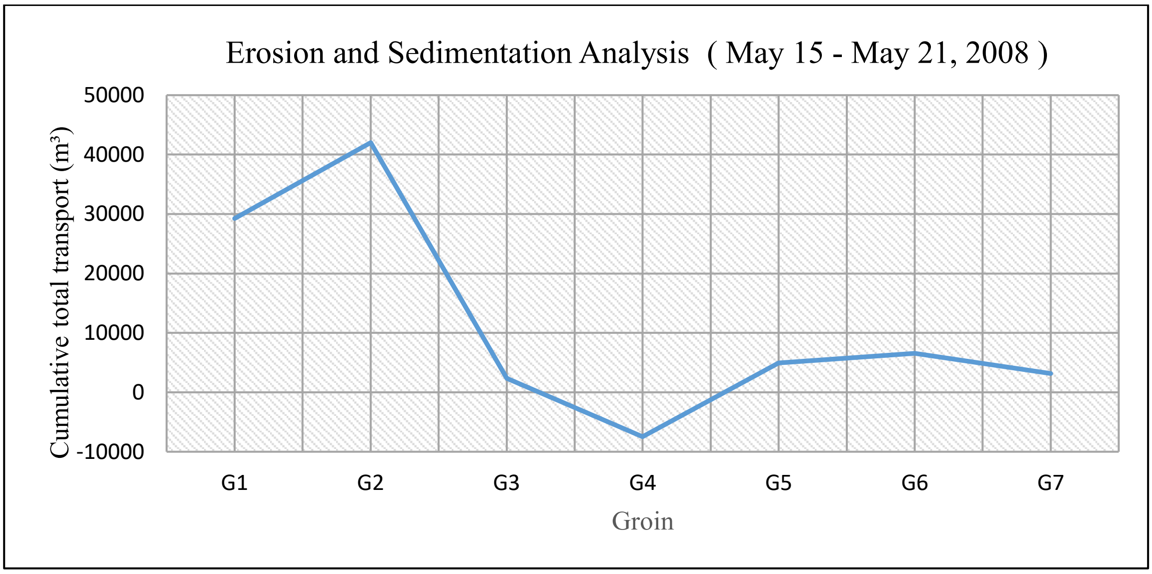

Figure 5.44: Erosion and Sedimentation at Site 1 with series of Groin (May 15 – May 21, 2008)

Figure 5.44 shows, among the seven Groin, all of them showing sedimentation in nearby areas. The maximum sedimentation occurs at Groin (G2) with total transport of 42013 m^3, and Groin (G4) shows the lowest sedimentation accumulation at a rate of -7471 m^3 from May 15 - May 21, 2008.

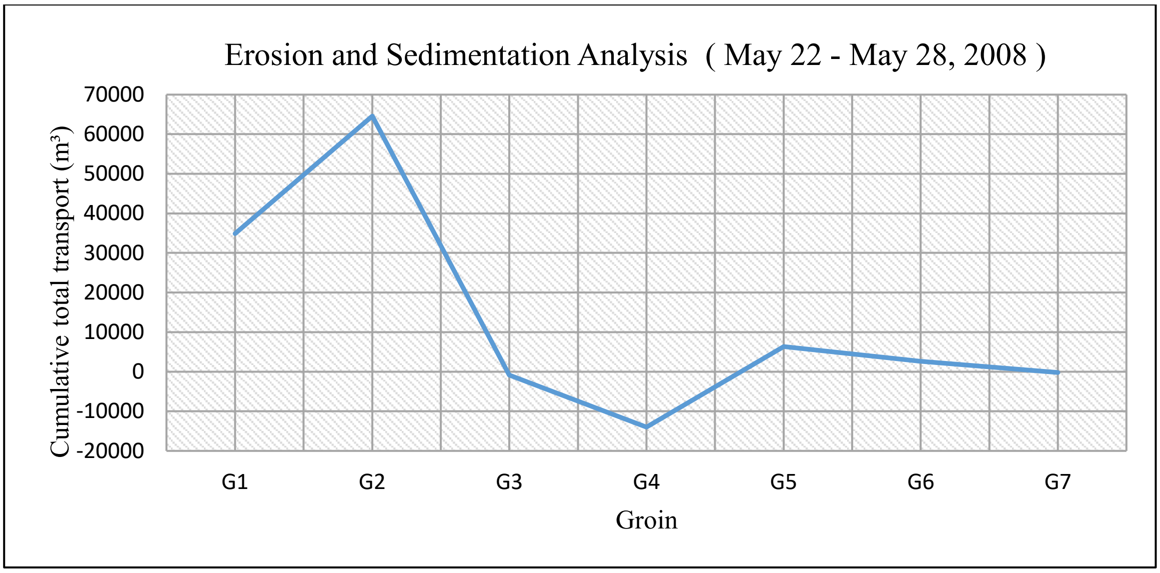

Figure 5.45: Erosion and Sedimentation at Site 1 with series of Groin (May 22 – May 28, 2008)

Figure 5.45 shows, among the seven Groin, all of them showing sedimentation in nearby areas. The maximum sedimentation occurs at Groin (G2) with total transport of 64581 m^3, and Groin (G4) shows the lowest sedimentation accumulation at a rate of -13992 m^3 from May 22 - May 28,2008.

5.4.3 Case 3 (Series of Breakwater in Site 2)

At site 2, which is near to the Himchari area, around 3 km has been selected for the study. In the finer model 10 m × 10 m grid is generated with all the hydrodynamic and wave outputs from the Bay of Bengal model for simulating the Breakwaters. For protecting the 3 km area with Breakwater at site 2, (starting Point: Latitude : 21.37°, Longitude : 92.00°; Ending point: Latitude : 21.35°, Longitude : 92.02°), a total of eleven Breakwaters considered as per DEFRA design guideline and incorporated at the finer model as per design specification. The Breakwater's total length is 100 m, the distance from the shoreline is 300 m, and gaps between the two Breakwater is 150 m, according to the beach slope. Finally, the model runs without the intervention and with the intervention for the 60 tidal cycles from May 1, 2008 - May 31, 2008. Individual analysis of erosion and sedimentation for Breakwaters at site 1 is attached in Appendix A.

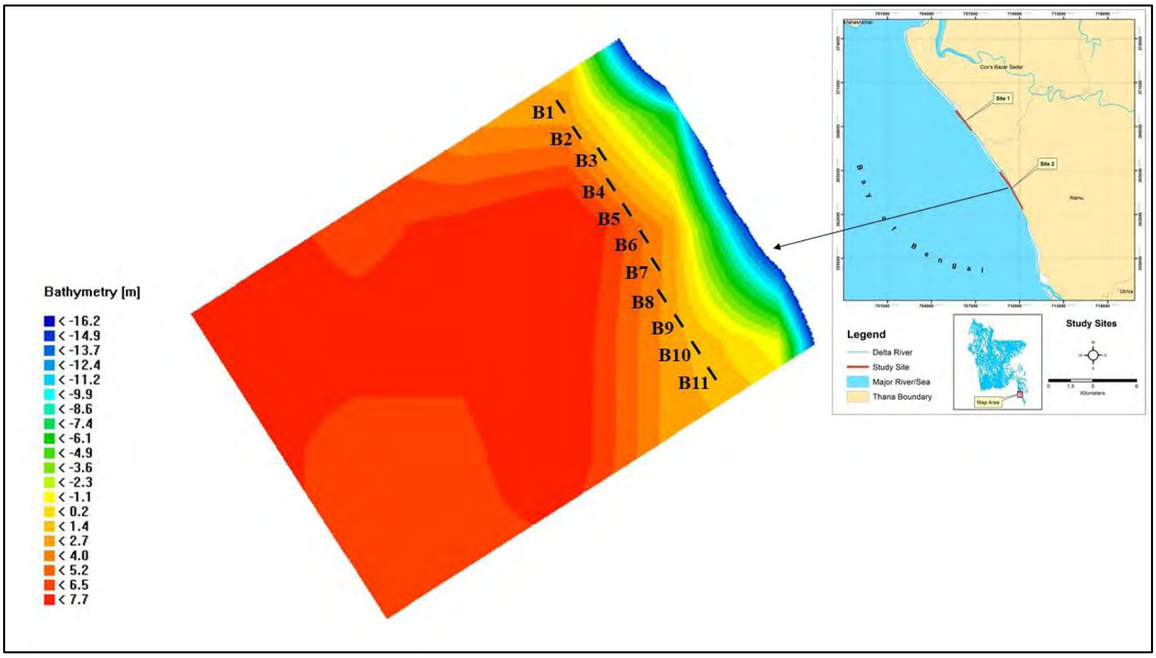

Figure 5.46: Series of Breakwater at Site 2 along Cox-Bazar coast

Table 5.7: Wave Height Change along the Site 2 with series of Breakwater (May 1, 2008- May 31, 2008)

Breakwater No.	Before Intervention (m)	After Intervention (m)	% Change
B1	0.40	0.28	30
B2	0.37	0.20	47
B3	0.47	0.28	40
B4	0.41	0.21	48
B5	0.42	0.22	47
B6	0.42	0.22	48
B7	0.46	0.27	41
B8	0.47	0.27	41
B9	0.39	0.25	37
B10	0.34	0.16	53
B11	0.27	0.14	50

From the above table wave height change along site 2 is summarized. It is seen from the analysis that there are significant changes in wave height due to placing the breakwater parallel to the shoreline. At site 2, Breakwater (B10) has the maximum wave height reduction percentage (53 %), where the other Breakwater shows changes between 30 % - 50 %. However, the total arrangement shows a very good result to reduce the wave height along the area. The following figure shows the wave height changes along the site 2:

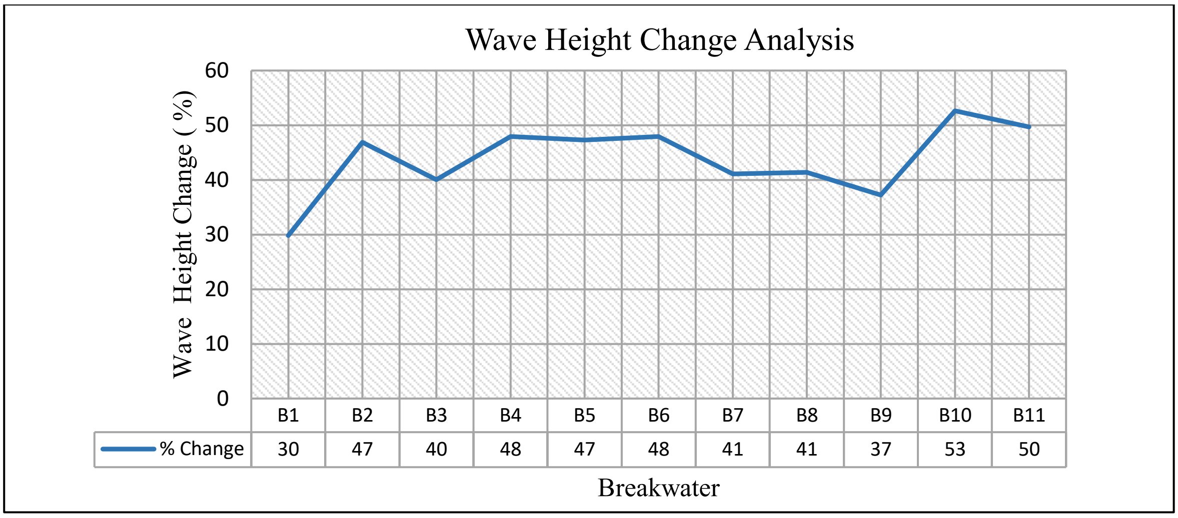

Figure 5.47: Wave Height Change Analysis for Site 2 with series of Breakwater

Table 5 8:Wave Energy Change Analysis along Site 2 with series of Breakwater (May 1, 2008- May 31, 2008)

Breakwater No.	Before Intervention (J/m2)	After Intervention (J/m2)	% Change
B1	98.10	48.32	51
B2	84.49	23.82	72
B3	137.60	49.51	64
B4	100.68	27.27	73
B5	107.38	29.85	72
B6	107.81	29.21	73
B7	131.13	45.52	65
B8	132.92	45.67	66
B9	95.27	37.51	61
B10	71.47	16.04	78
B11	44.60	11.30	75

From the above table wave energy change along site 2 is summarized. It is seen from the analysis that there are significant changes in wave energy due to placing the breakwater parallel to the shoreline. At site 2, Breakwater (B10) has the maximum wave energy reduction percentage (78%), where the other Breakwater shows changes between 51 % - 75 %. However, the total arrangement shows a very good result to reduce the wave energy. The following figure shows the wave energy changes along the site 2:

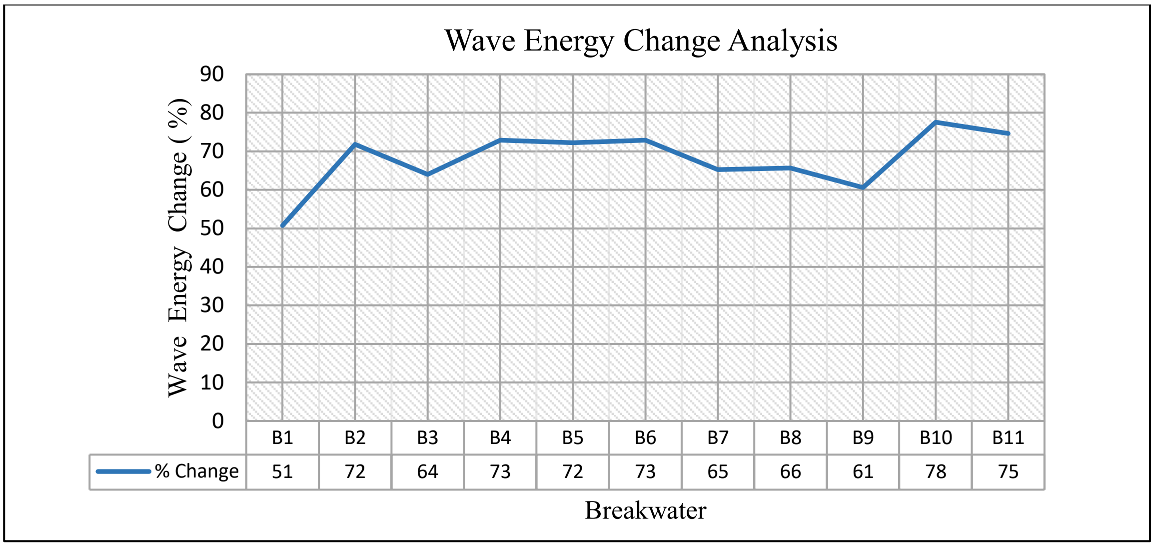

Figure 5 48: Wave Energy Change Analysis for Site 2 with series of Breakwater

Erosion or sedimentation Analysis:

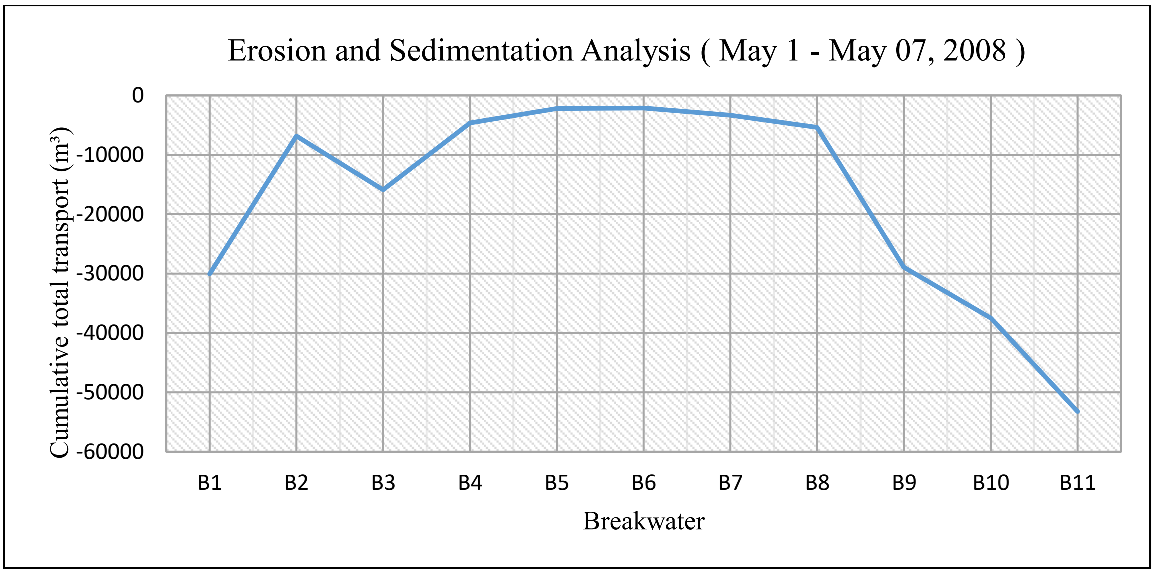

Figure 5.49: Erosion or Sedimentation at Site 2 with series of Breakwater
(May 1 - May 07, 2008)

Figure 5.49 shows, among the eleven Breakwater, all of them showing continuous erosion in the vicinity of the structure. The maximum erosion occurs at Breakwater (B11) with total transport of -53225 m^3, and Breakwater (B6) shows a minimum erosion rate of -2125 m^3 from May 1 - May 07, 2008.

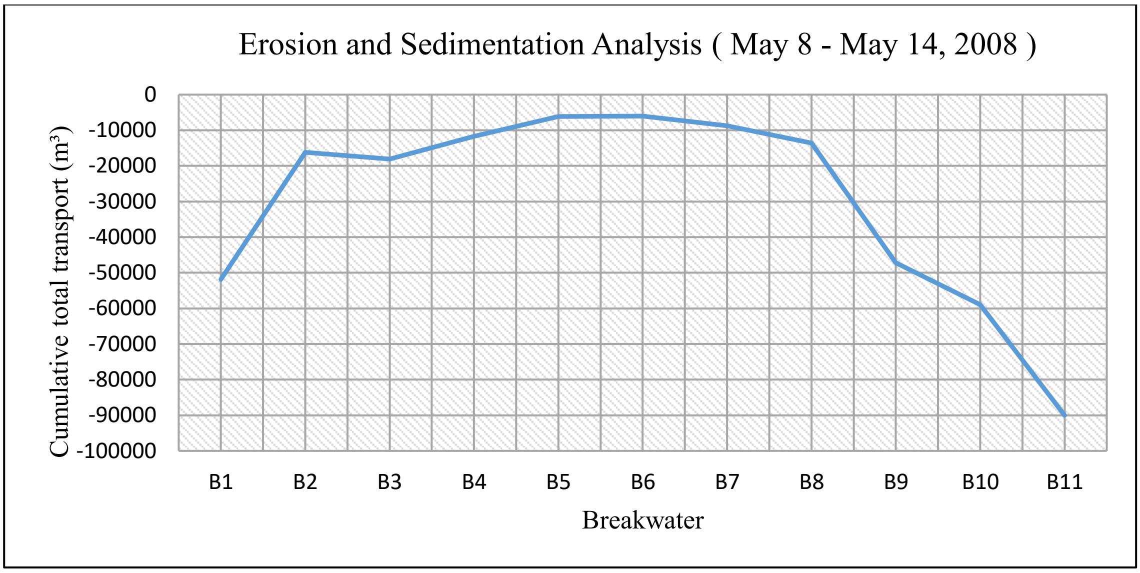

Figure 5.50: Erosion or Sedimentation at Site 2 with series of Breakwater (May8 - May 14, 2008)

Figure 5.50 shows, among the eleven Breakwater, all of them showing continuous erosion at the structure's vicinity. The maximum erosion occurs at Breakwater (B11) with total transport of -90005 m³, and Breakwater (B5) shows minimum erosion at a rate of -6139 m³ from May 8 - May 14, 2008.

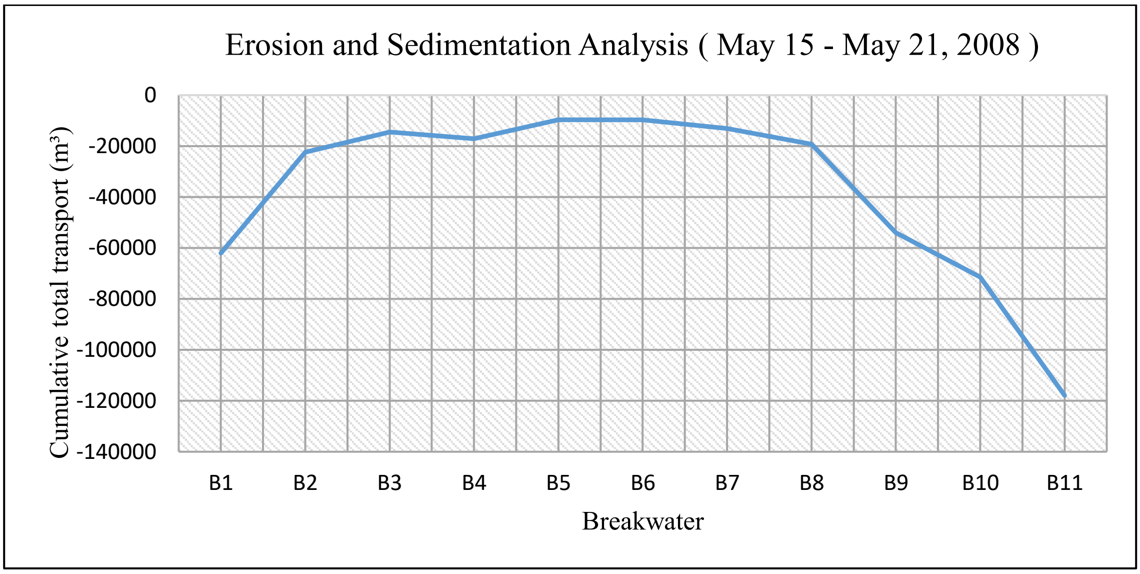

Figure 5.51: Erosion or Sedimentation at Site 2 with series of Breakwater (May 15 – May 21, 2008)

Figure 5.51 shows, among the eleven Breakwater, all of them showing continuous erosion in the vicinity of the structure. The maximum erosion occurs at Breakwater (B11) with total transport of -117858 m³, and Breakwater (B6) shows minimum erosion at a rate of -9697 m³ from May 15 - May 21,2008.

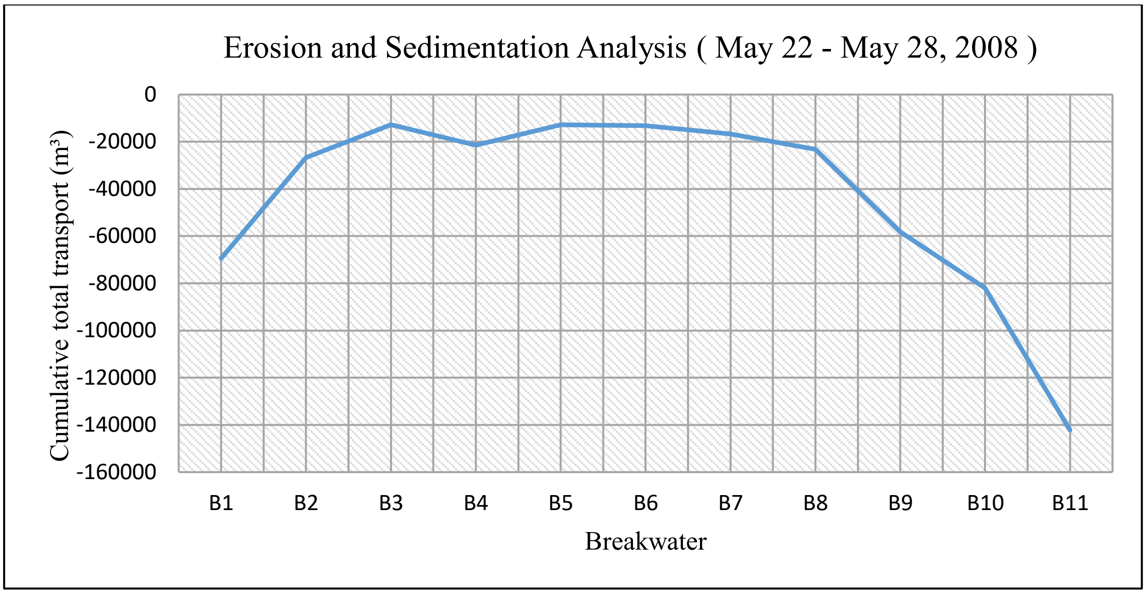

Figure 5.52: Erosion or Sedimentation at Site 2 with series of Breakwater (May 22 – May 28, 2008)

Figure 5.52 shows, among the eleven Breakwater, all of them showing continuous erosion in the vicinity of the structure. The maximum erosion occurs at Breakwater (B11) with total transport of -142205 m^3, and Breakwater (B3) shows minimum erosion at a rate of -12842 m^3.

5.4.4 Case 4 (Series of Groin in Site 2)

For protecting the 3 km area with Groins at site 2, (starting Point: Latitude : 21.37°, Longitude : 92.00°; Ending point: Latitude : 21.35°, Longitude : 92.02°), a total of thirteen Groins considered as per DEFRA design guideline and incorporated at the finer model as per design specification. In the finer model 10 m × 10 m grid is generated with all the hydrodynamic and wave outputs from the Bay of Bengal model for simulating the Groins. The total length of the Groin is 100 m and gaps between two Groin is 200 m. Finally, the model run without the intervention and with the intervention for 60 tidal cycle from May 1, 2008 - May 31, 2008. Individual analysis of erosion and sedimentation for Groin at site 1 is attached in Appendix A.

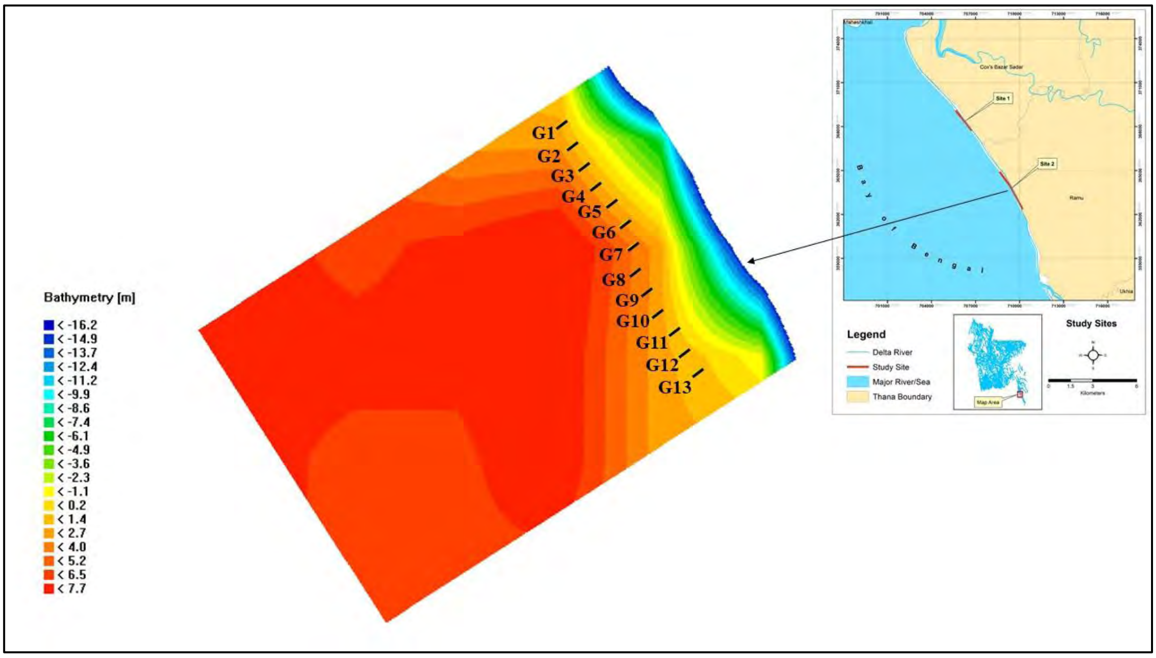

Figure 5.53: Series of Groin at Site 2 along Cox-Bazar coast

Table 5.9: Wave Height Change along Site 2 with series of Groin
(May 1, 2008- May 31, 2008)

Groin No.	Before Intervention (m)	After Intervention (m)	% Change
G1	0.48	0.23	53
G2	0.48	0.38	21
G3	0.51	0.43	16
G4	0.49	0.28	43
G5	0.50	0.42	15
G6	0.49	0.38	22
G7	0.51	0.44	14
G8	0.47	0.29	38
G9	0.44	0.28	35
G10	0.43	0.28	34
G11	0.40	0.26	35
G12	0.36	0.30	15
G13	0.49	0.25	50

From the above table wave height change along site 2 is summarized. It is seen from the analysis that there are significant changes in wave height due to placing the groin along the shoreline. At site 2, Groin G1 has the maximum wave height reduction percentage (53%), where the other groin shows changes between 15 % - 50 %. However, the total arrangement shows relatively good performance to reduce the wave height. The following figure shows the wave height changes along the site 2:

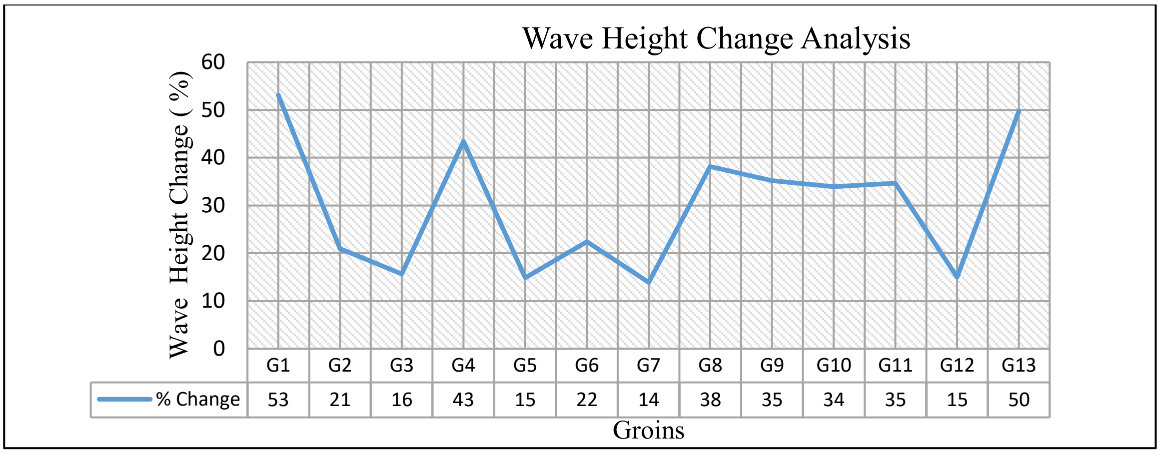

Figure 5.54: Wave Height Change Analysis for Site 2 with series of Groin

Table 5 10: Wave Energy Change Analysis along Site 2 with series of Groin (May 1, 2008- May 31, 2008)

Groin No.	Before Intervention (J/m2)	After Intervention (J/m2)	% Change
G1	143.93	31.65	78
G2	143.01	89.36	38
G3	156.90	111.63	29
G4	146.98	47.06	68
G5	151.74	109.98	28
G6	145.85	87.75	40
G7	159.11	117.97	26
G8	136.37	52.13	62
G9	115.94	48.68	58
G10	112.65	49.19	56
G11	99.36	42.41	57
G12	78.40	56.63	28
G13	141.12	35.28	75

From the above table wave energy change along site 2 is summarized. It is seen from the analysis that there are significant changes in wave energy due to placing the Groin along the shoreline. At site 2, Groin (G1) has the maximum wave energy reduction percentage (78%), where the other Groin shows changes between 28 % - 75 %. However, the total arrangement shows a very good result to reduce the wave energy. The following figure shows the wave energy changes along site 2:

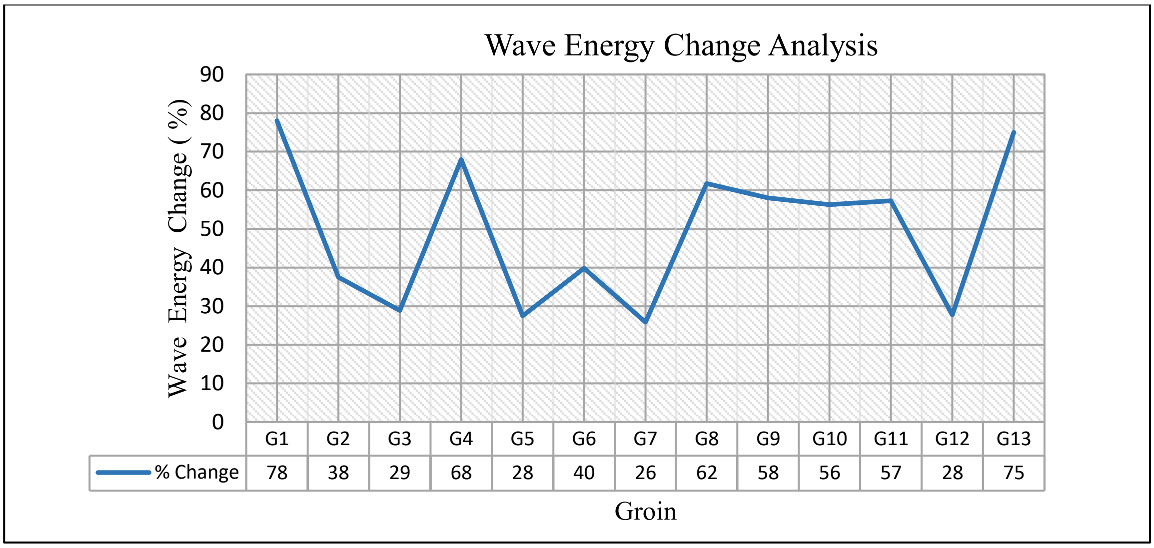

Figure 5 55: Wave Energy Change Analysis for Site 2 with series of Groin

Erosion or sedimentation Analysis:

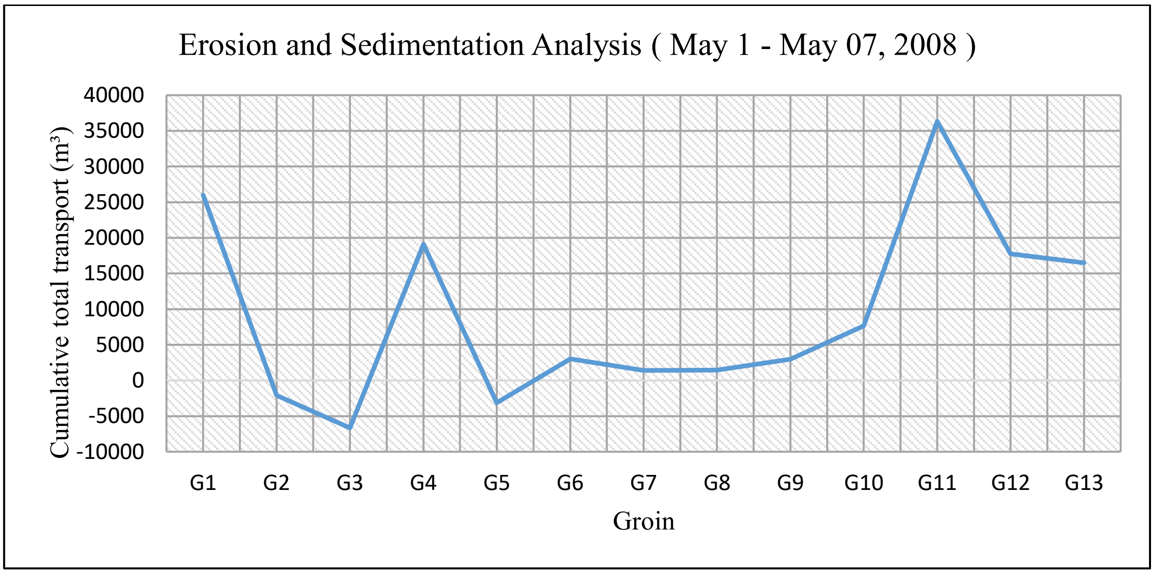

Figure 5.56: Erosion or Sedimentation at Site 2 with series of Groin
(May 1 - May 07, 2008)

Figure 5.56 shows, among the thirteen Groin, three of them showing erosion and all other accumulating sediments in nearby areas. The maximum sedimentation occurs at the groin (G11) with total transport of 36316 m^3, and Groin (G3) shows erosion at a rate of -6655 m^3 from May1- May 07,2008.

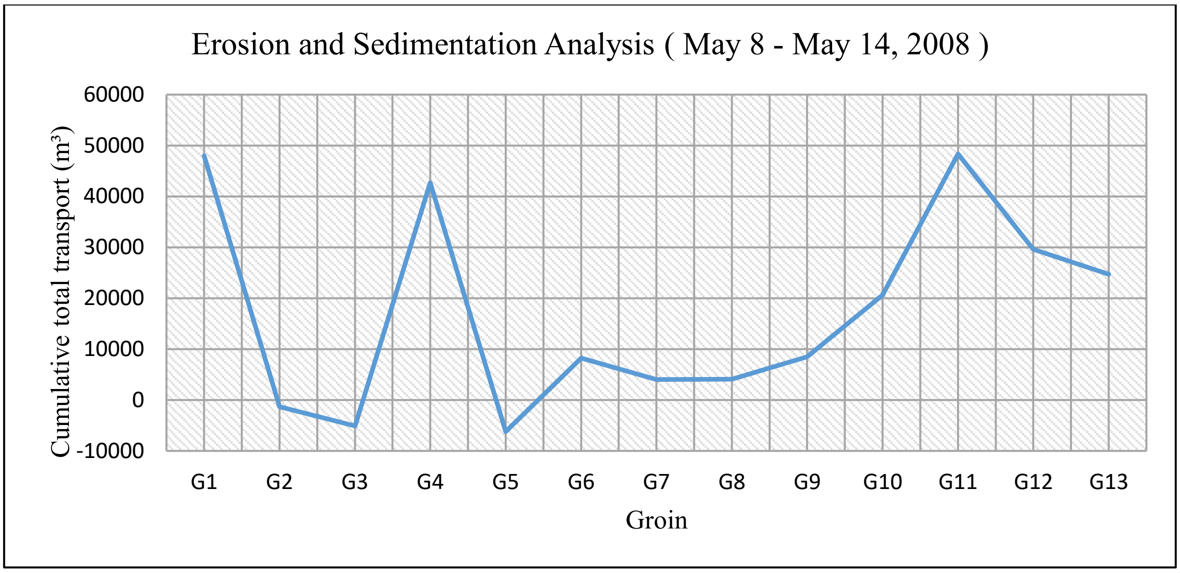

Figure 5.57: Erosion or Sedimentation at Site 2 with series of Groin (May 8 - May 14, 2008)

Figure 5.57 shows, among the thirteen Groin, three of them showing erosion and all other accumulating sediments in nearby areas. The maximum sedimentation occurs at the groin (G11) with total transport of 48349 m^3, and Groin (G5) shows erosion at a rate of -6208 m^3 from May 8- May 14, 2008.

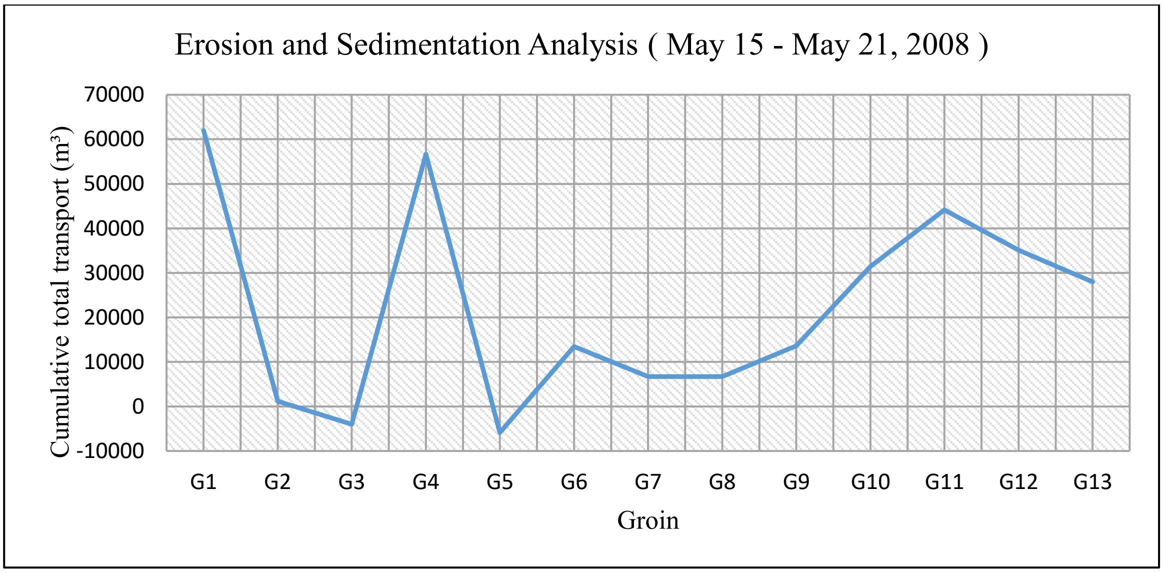

Figure 5.58: Erosion or Sedimentation at Site 2 with series of Groin (May 15 - May 21, 2008)

Figure 5.58 shows, among the thirteen Groin, two of them showing erosion and all other accumulating sediments in nearby areas. The maximum sedimentation occurs at Groin (G1) with total transport of 61983 m^3, and Groin (G5) shows erosion at a rate of -5857 m^3 from May15-May21,2008.

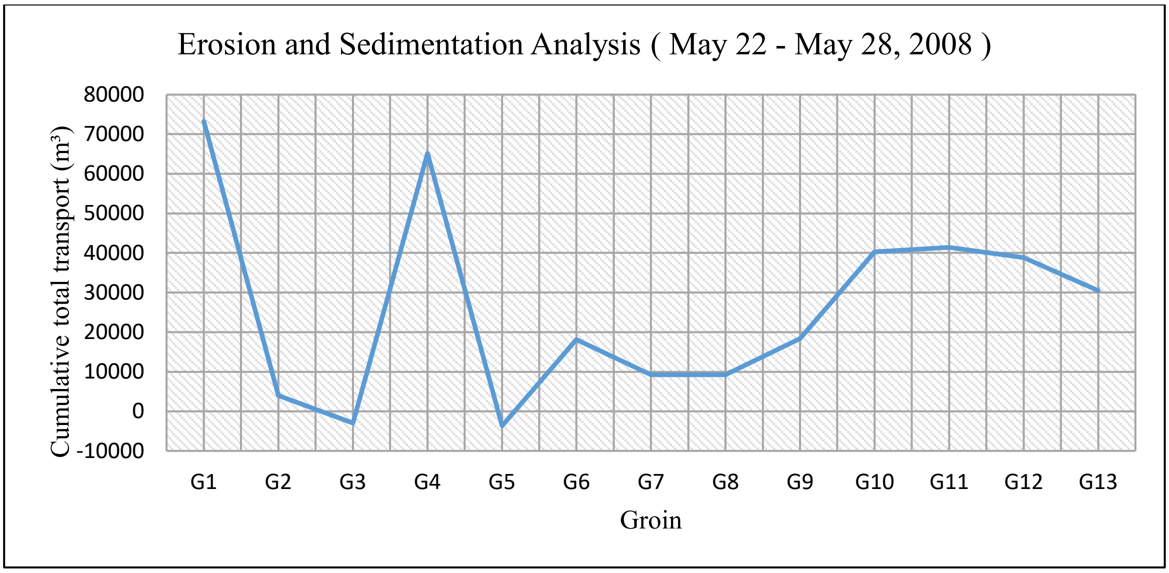

Figure 5.59: Erosion or Sedimentation at Site 2 with series of Groin (May 22 – May 28, 2008)

Figure 5.59 shows, among the thirteen Groin, two of them showing erosion, and all the other showing sedimentation in nearby areas. The maximum sedimentation occurs at Groin (G1) with total transport of 73243 m³, and Groin (G5) shows the lowest sedimentation accumulation at a rate of -3659 m³ from May22-May 28,2008.

5.5 Summary of the Results

This study deciphers the complex nearshore behavior with fully calibrated and validated couple model with Breakwater and Groins. Four scenarios simulated to protect the area against erosion and examine the wave height, wave energy reduction rate with sediment movement at the vicinity of the structures; results are described below,

a) Results from the simulation of Breakwater in Site 1:

From the simulation of series of Breakwaters at site 1 it has been found that the significant wave height reduced to a great extent to make the beach stable due to regular wave action. The range of wave height reduction from all of the three intervened Breakwater is between 27 % - 53 %, which is good enough to reduce the wave height. In extent, the energy reduction rate varies between 47% -78%, which also changes the sediment dynamics. The final simulation shows sedimentation at Breakwater (B1) 18467 m³ and continuous erosion at Breakwater (B2) -48947 m³ and Breakwater (B3) -216645 m³ for a continuous sixty tidal cycle. This pattern shows sedimentation in one place and continuous erosion in other places at the Breakwater vicinity.

b) Results from the simulation of Groin in Site 1:

The results show a mixed proportion of significant wave height reduction rate from series of Groins at site 1. The range of wave height reduction from all seven intervened Groin is between 9 % - 76 %, which is good enough to reduce the wave height. In extent, the energy reduction rate varies between 17% -91%, which also changes the sediment dynamics. The final simulation shows sedimentation at Groin (G1) 96794 m^3, (G2)150167 m^3,(G3)12971 m^3,(G5)18271 m^3,(G6)24528 m^3,(G7)23147 m^3 and erosion at Groin (G4)-18522 m^3 for a continuous sixty tidal cycle. This pattern shows sedimentation in the alongshore of all of the Groins, where one Groin (G4) shows erosion only.

c) Results from the simulation of Breakwater in Site 2:

The significant wave height reduced in a great extent to make the beach stable due to regular wave action at site 2 with series of Breakwater. The range of wave height reduction from all eleven intervened Breakwater is between 30 % - 53 %, which is good enough to reduce the wave height. In extent, the energy reduction rate varies between 51% -78%, which also changes the sediment dynamics. The final simulation shows erosion at Breakwater (B1) -213310 m^3, (B2) -72096 m^3,-61230 (B3) m^3,-54921 (B4) m^3,-30827 (B5) m^3,-31005(B6) m^3,-41782 (B7) m^3,-61339 (B8) m^3,-188148 (B9) m^3,-249947 (B10) m^3,(B11) -403293 m^3 for continuous sixty tidal cycle. This pattern shows continuous erosion in the vicinity of the Breakwater.

d) Results from the simulation of Groin in Site 2:

From the above analysis at site 2, the results show good changes of significant wave height with series of Groins. The range of wave height reduction from all of the thirteen intervened Groin is between 15% - 53 %, which is good enough to reduce the wave height. In extent, the energy reduction rate varies between 51% -78%, which also changes the sediment dynamics. The final simulation shows sedimentation at Groin (G1) 209169 m^3, (G2) 1730 m^3,(G4) 183561 m^3,(G6)42830 m^3,(G7) 21405 m^3,(G8)21449m^3, (G9) 43384 m^3,(G10) 99926 m^3,(G11)170195 m^3,G (12)121322 m^3, (G13) 99663 and erosion at (G3) -18772 m^3, (G5)-18873 m^3 for sixty tidal cycles. This pattern shows sedimentation in the alongshore of all of the Groins where Groin(G2) and Groin (5) shows erosion only.

CHAPTER 6

CONCLUSIONS AND RECOMMENDATIONS

6.1 General

In this study Bay of Bengal model has been developed with Delft3D with proper calibration and validation. The effect of nearshore structures has been analyzed to protect two different locations at Cox-Bazar coastline. Moreover, the reduction of wave energy and associate wave height reduction rate with sediment movement pattern also been examine here. The two locations are between Cox's Bazar-Himchari Marine Drive Road and this area is very significant for tourism and fishing industry. Over the years this area has experienced severe erosion and damage in few locations mainly because of sea wave action. Due to the priority of economic activity and tourist attraction this long road strip was protected by geotextile bags with tetrapod which is short term solution. In most of the location geotextile bags are damaged due to high tide and wave action. In this study a real-world scenario has been simulated with different nearshore structures. A well-established flow wave coupled model (Delft3D) used to find out the best fit solution for the study areas.

6.2 Conclusions of the Study

A fully calibrated and validated Bay of Bengal model used to run four cases with Breakwater and Groin in two different locations at the Cox-Bazar coastline. It is observed from the analysis that to protect site 1, which is 1.7 km long with series of Breakwater, the wave height reduction rate is 27 % - 53 %, and the wave energy reduction rate is 47% - 78%. It shows good results to reduce wave height and energy at those interventions. The further analysis illustrates a mixed result, where two of the Breakwater shows continuous erosion, and one Breakwater shows continuous sedimentation in the vicinity of the structure. To protect the site1 with series of Breakwater is not a feasible option because it requires additional maintenance work with sand nourishment to make the beach stable.

The analysis from case 2 shows to protect site 1, which is 1.7 km long with series of Groin, the wave height reduction rate is 9 % - 76 % and wave energy reduction rate is 17% -91%, which also shows low to moderate reduction rate of the wave height and energy. The sediment analysis depicts positive results, where six Groins shows continuous sedimentation, and one shows erosion. To protect site 1 with series of Groin is a good option because six groins among seven show positive results to accumulate sediment along the shoreline to make the beach stable.

It is observed from the case 3 analysis that to protect site 2, which is 3 km long with series of Breakwater, the wave height reduction rate is 30 % - 53 %, and wave energy reduction rate is 51% -78%, which illustrates good results to reduce the wave height and energy. Further analysis shows continuous erosion in the vicinity of all eleven Breakwater. To protect site 2 with series of Breakwater is not a feasible option because of its erosion trend.

Moreover, the analysis from case 4 shows that to protect site 2, which is 3 km long with series of Groin, the wave height reduction rate 15% - 53 %, and wave energy reduction rate 51% -78% which shows excellent results to reduce the wave height and energy. The sediment analysis shows positive results, where eleven Groins show continuous sedimentation, and two shows erosion. To protect site 2 with series of Groin is a good option because eleven groins among thirteen show positive results to accumulate sediment along the shoreline.

Finally, from the above analysis, we can conclude that Groins are more capable of trapping sediment than Breakwater. In most cases, Breakwater shows a continuous erosion where Groins trap sediment in a different direction. Although, the wave height and wave energy reduction rate are higher for the Breakwaters where Groins has a moderate wave height and energy reduction rate. In both cases for site 1 and site 2, Breakwater has a high potential for wave height and wave energy reduction rate, but it shows a continuous erosion in all structures' vicinity. At the same time, Groins shows more potentiality to trap sediment, and it has a moderate wave height and energy reduction rate. The beach and sea view are very important for the study area, and Groins can be the best solution where minimum or no sand nourishment is required for long term sustainability.

6.3 Recommendations for Future Study

1. To protect the erosion-prone shorelines in Bangladesh, it is also essential to examine the effect of different structural combinations in one site with Breakwater and Groin. Other factors like different structural lengths, distance from the shoreline, and sea-level rise scenarios are recommended for future study.

2. Structural measures like Detached Breakwater creates an obstacle to the sea view, and it required huge investment for construction. Further investigation is needed with a flexible and robust economic solution like low crested vertical slotted breakwater.
3. Groins are helpful for beach formation, and it does not restrict the sea view. Further investigation is required with different types of groin, which can trap sand and does not require any sand nourishment.

REFERENCES

Ahammed, M. U. (2010), Experimental and Numerical Investigation on Wave Interaction with Submerged Breakwater. MSc Thesis, Department of Water Resource Engineering, BUET.

Akter, A. (2013), Experimental Study on Hydrodynamic performance of vertical thick porous breakwater. MSc Thesis, Department of Water Resource Engineering, BUET.

Afroz, R. (2015), Experimental and Numerical Investigation on Wave Interaction with Horizontal Slotted Submerged Porous Breakwater. MSc Thesis, Department of Water Resource Engineering, BUET.

Akhtar (2015), Assessment of nearshore hydrodynamic process along the coast of Cox Bazar

Ali, A., (1999), Climate change impacts and adaptation assessment in Bangladesh, Vol. 12: 109–116.

Anindita P. and Bhaskaran, P. K. (2016), Trends in wind-wave climate over the head Bay of Bengal region, International Journal of Climatology, DOI: 10.1002/joc.4627

Alam, M. (2003), Bangladesh Country Case Study with climate change. National Adaptation Programme of Action (NAPA) Workshop, Bhutan.

Ahmed et al. (2012), Application of Two-Dimensional Models to Simulate the Flow and Sediment Transport. J Am Sci 2012; 8(12):778-784, ISSN: 1545-1003

Allison, M. A. (1998), Historical changes in the Ganges- Brahmaputra delta front. Journal of Coastal Research, Vol-14, pp 1269-1275.

Ali, A., Rahman, H., Sazzad, S., Choudhary, S. S. H. and Begum, Q. N. (1997) , Back water effect of tides and storm surges on fresh water discharge through the Meghna estuary. Journal of Remote Sensing & Environment, Vol-1, pp 85-95.

Ahmmed and Rahman (2013), Estimation of design wave height along marine drive road from kalatali to inani at Cox-Bazar, 4th International Conference on Water & Flood Management (ICWFM-2013)

Amelia, H. C. and Mulligan, R. P. (2016), Application of a Spectral Wave Model to Assess Breakwater Configurations at a Small Craft Harbour on Lake Ontario, J. Mar. Sci. Eng., doi:10.3390/jmse4030046

Apotsos, A., B. et al. (2007), "Effects of wave rollers and bottom stress on wave setup." Journal of Geophysical research Vol. 112.

Ahmed (1997), 2D and 1D numerical model simulation for the effect of single detached breakwater, MSc Thesis, Delft Hydraulics

Abramowitz, M. and Stengun, I.A., (2003) , Handbook of Mathmatical Modeling.Ninth printing, Dover Publishing, New York.

Bangladesh Bureau of Statistics, (2011), Bangladesh Population and Housing Census 2011, Final Result.

Booij, N., L. H. and de Lange, P. H. M. (1992), The penetration of short-crested waves through a gap. In Proceedings 23rd International Conference Coastal Engineering, Venice 4-9 Oct., 1992, New York, 1993, pages 1044–1052. 129

Battjes, J. A. et al. (1978), Energy loss and set-up due to breaking of random waves. Coastal Engineering, 19.

Booij, N., N. C. and Holthuijsen L. H. (1999), A third-generation wave model for coastal regions, part 1, model description and validation. Journal of Geophysical research 104: 7649-7666.

Burcharth, H. F., Hawkins, S. J., B. et al. (2007), Environmental Design Guidelines for Low Crested Coastal Structures Elsevier Ltd.

Battjes, J. A. and. Stive, M. J. F (1995), Calibration and verification of a dissipation model for random breaking waves. Journal of Geophysical research vol. 90(NO. C5): 9159-9167.

Battjes, J. A. and Janssen, J. P. F. M. (1978), Energy loss and set-up due to breaking of random waves. Proc. 16th Int. Conf. Coastal Engineering, ASCE. pp 1993-2004

CERP, (2000), Second Coastal Embankment Rehabilitation Project. Hydraulic modeling study prepared by IWM/DHI.

CEIP (2017), Coastal Embankment Improvement Project,Phase-1, Bangladesh Water Development Board.

Courant, R. and Hilbert, D. (1962), "Methods of mathematical physics", Interscience, New York.

C.E.M. (2008), Shore protection projects. Coastal engineering manual. Vol. 1100. U.S. Army Corps of Engineers.

Dean, R. G. (1973), Heuristic models of sand transport in the surf zone. Conferences on engineering dynamics in the surf zone, Sydney, NSW, Proceeding, 208-214.

Dean, R. et al., (1982), Longshore transport determined by an efficient trap. Coastal Engineering Proceedings

DEFRA (2010), Department for Environment Food and Rural Affairs. Guidance for outline design of nearshore detached breakwaters on sandy macro-tidal coasts. Environment Agency of United Kingdom.

Deltares (2010b), Delft3D-Wave, Simulation of short-crested waves with SWAN, user manual

Eldeberky, Y. and Battjes, J. A. (1995), Parameterization of triad interactions in wave energy models. Coastal Dynamics Conference '95 Gdansk, Poland.

Fredsoe, J. (1984), Turbulent boundary layer in wave–current interaction. ASCE Journal of Hydraulic Engineering 110, 1103–1120.

Goda, Y., Takeda, H. and Moriya, Y. (1967), Laboratory investigation of wave transmission over breakwaters. Tech. Rep. 13, Rep. port and Harbour Res. Institution.

Hossain, D.(2012), Application of 2D Mathematical Model for Verification of Water Velocity at Coastal Area of Bangladesh, MSc Thesis, Department of Water Resource Engineering, BUET.

Hossain, M.H.(2012), Storm surges and coastal erosion in Bangladesh - State of the system, Climate change impacts and 'low regret' adaptation measures, MSc Thesis, Faculty of Civil Engineering and Geodetic Science, Leibniz Universität Hannover.

Horikawa K. (1988), Nearshore dynamics and coastal processes, Univ. of Tokyo Press, Japan

Hossain, M. S. (2001) , Biological aspects of the coastal and marine environment of Bangladesh, Journal of Ocean Coast Management, Vol-44, pp 261-282.

Islam, S. (2015), Modelling the effects of cyclonic storm surge and wave action on selected coastal embankments. MSc Thesis, Department of Water Resource Engineering, BUET.

Islam, M.S.N. (2008), Cultural Landscape Changing due to Anthropogenic Influences on Surface Water and Threats to Mangrove Wetland Ecosystems: A Case Study on the Sundarbans, Bangladesh, PhD thesis, Brandenburg University of Technology, Cottbus.

IWM (2005), Impact Assessment of Climate Change Zone of Bangladesh‖, submitted to WARPO, GoB.

IWM and CEGIS (2007), Investigating the Impact of Relative Sea-Level Rise on Coastal Communities and their Livelihoods in Bangladesh, submitted to UK Department for Environment Food and Rural Affairs.

IWM (2013), Analyzing the trend of Water level time series at the coastal area of Bangladesh.

IWM, 2010, Coastal and Hydraulic Study for Deep Sea Port, Final Report

IWM-BUET-DHI-EML (2012), Coastal Hydraulic and Morphological Study and Design of Protection Measures for Marine Drive Road.

Inman, D. L. and Bagnold, R. (1963), Littoral processes. The sea, 3, 529-553.

Johnson, H. K., Karambas, T. V. et al. (2005), Modelling of waves and currents around submerged breakwaters. Coastal Engineering 52(10-11): 949-969.

Janssen, T. T. and Battjes, J. A. (2007). "A note on wave energy dissipation over steep beaches." Coastal Engineering 54(9): 711-716.

Jakobsen, F., Azam, M. H. and Kabir, M. M., (2002), Residual flow in the Meghna Estuary on the coastline of Bangladesh. Estuarine, Coastal and Shelf Science, Vol-55, Issue-4, pp 587-597.

James, D. Dykes, J. D., Hsu, L. Y. and Kaihatu, J. M. (2008), Application of Delft3D in near shore zone, Naval Research Laboratory, Stennis Space Center, Mississippi.

Kraus, N. C., Hanson, H., and Blomgren, S. H. (1995), Modern functional design of groin systems. In Coastal Engineering 1994 (pp. 1327-1342).

Karim, M.F. and Mimura, N., (2006), Sea Level Rise in the Bay of Bengal: Its Impacts and Adaptations in Bangladesh. Center for Water Environment Studies, Ibaraki University, Hitachi, Ibaraki 316-8511, Japan. Microsoft PowerPoint – Poster for IOC_02June06_Karim

Komol, K. M. (2011), Numerical Simulation of Tidal Level at Selected Coastal Area of Bangladesh, MSc Thesis, Department of Water Resource Engineering, BUET, 2011.

Kraus, N. C., et al. (1982), Field experiments on longshore sand transport in the surf zone. Coastal Engineering Proceedings

Komar, P. D. et al. (1970), Longshore sand transport on beaches. Journal of geophysical research, 75, 5914-5927

Kamphuis, J. W. (1996), Alongshore sediment transport rate. Journal of Waterway, Port, Coastal, and Ocean Engineering, 117, 17.

Kriebel, D. L. (1983), Beach and dune response to hurricanes. University of Delaware

Kriebel, D. L and Dean, R. G. (1985), Numerical simulation of time-dependent beach and dune erosion. Coastal Engineering, 9, 221-245.

K. S. Krishna et. al. (1989), Sound Velocity, Density, and Related Properties along a Transect across the Bay of Bengal, Geo-Marine Letters (1989) 9:95-102

Khuong T. C. (2016), Shoreline response to detached breakwaters in prototype. Ph.D dissertation, Delft University of Technology.

Lucy M. B., Wolf, J. and Islam, S, (2016) , Tidal intrusion within a mega delta: An unstructured grid modelling approach, Estuarine, Coastal and Shelf Science 182 (2016), http://dx.doi.org/10.1016/j.ecss.2016.09.014

Linta, R. and Bhaskara, P. K. (2015), Tidal Prediction for Complex Waterways in the Bangladesh Region, ICWRCOE 2015, Aquatic Procedia 4 (2015) 532 – 539

Lesser, G. R., Roelvink, J. A., et al. (2004), Development and validation of a three-dimensional morphological model. Coastal Engineering 51(8-9): 883-915.

Miche, R. (1944), Mouvement ondulatoires de la mer en profondeur constante ou decroissante. Annales des Ponts et Chaussees.

Mole, S. (2012), Numerical modelling of tides and storm surges in the Bay of Bengal, Ph.D. Thesis, Goa University.

Madsen, O. S. et al., (1976), Quantitative description of sediment transport by waves. Coastal Engineering Proceedings.

Moore, B. D. (1982), Beach profile evolution in response to changes in water level and wave height. University of Delaware.

Mahamud and Takewaka (2018), Shoreline Change around a River Delta on the Cox's Bazar Coast of Bangladesh,Journal of Marine Science and Engineering J. Mar. Sci. Eng. 2018, 6, 80; doi:10.3390/jmse6030080

Nasreen, M., Khan, Z. H. and Nazibur. R (2013), Impact of Sea level Rise on Coastal Rivers of Bangladesh, Coast, Port & Estuary Division, Institute of Water Modelling (IWM), Dhaka, Bangladesh.

Navera, U.K and Ahmed,S. (2018), Application of Landsat imagery and vegetation indes property to assess the shoreline changes along Cox'bazar- Teknaf coast, Proceedings of the 4th International Conference on Civil Engineering for Sustainable Development (ICCESD 2018), 9~11 February 2018, KUET, Khulna, Bangladesh (ISBN-978-984-34-3502-6)

Noda, E. K., (1974), "Wave Induced Nearshore Circulation", 27 Journal of Geophysical Research, Vol. 79, No. September 20, 1974.

Rahman, A. (2014), Study on Effectiveness of Coastal Bio-Shield for Reduction of the Energy of High Frequency Surges. MSc Thesis, Department of Water Resource Engineering, BUET, 2014.

Rezaie, A. M , Jisan, M.A, Haque, A. and Rahman, M., (2015),Assessing Performance of Polders under Storm Surges in the Coastal Regions of Bangladesh for Current and Future Climate Scenarios Using the Delft 3D Model, The Gobeshona Conference for Research on Climate Change in Bangladesh (Gobeshona.net)7th to 11th January 2015.

Roelvink, J. and Stive, M. (1989), Bar-generating cross-shore flow mechanisms on a beach. Journal of Geophysical Research: Oceans (1978–2012), 94, 4785-4800.

Roelvink, J. A. (2006), Coastal morphodynamic evolution techniques. Coastal Engineering 53(2-3): 277-287.

Sepehr Eslami Arab (2009), A Numerical Study on Design of Normal & T-Head Groins.

Stive, M. (1986), A model for cross-shore sediment transport. Coastal Engineering Proceedings, 1.

Seelig, W., (1979), Effects of breakwaters on waves: laboratory tests of wave transmission by overtopping. In Proceedings Conference Coastal Structures, vol. 79:2, pages 941–961. 129

Shepard, F. P. and Inman, D. L. (1951), Sand movement on the shallow inter-canyon shelf at La Jolla, California, US Beach Erosion Board.

Tazkia, A. R. er.al (2016), Seasonal modulation of M2 tide in the northern Bay of Bengal, Continental Shelf Research, DOI: http://dx.doi.org/10.1016/j.csr.2016.12.008

Vlijm, R. J. (2011), Process-based modelling of morphological response to Submerged breakwaters, MSc Thesis, Delft University of Technology, The Netherlands.

Van D. M. et al. (2005). Wave transmission and reflection at low-crested structures: Design formulae, oblique wave attack and spectral change.Coastal Engineering 52(10-11): 915-929.

Womera, S. A.(2011), Experimental and Numerical Investigation on Wave Interaction with Submerged Breakwater. MSc Thesis, Department of Water Resource Engineering, BUET.

Walstra, D.J.R., et al. (2000) , “Calculation of wavedriven currents in a 3D mean flow model”. Edge, B. Coastal Engineering vol. 2. ASCE, New York, pp. 1050– 1063.

Whitham, G.B., (1974), Linear and nonlinear waves, Wiley, New York, 636 p.

Ye Yincan et al, (2017), Marine Geo-Hazards in China, eBook ISBN: 9780128128121

APPENDIX A

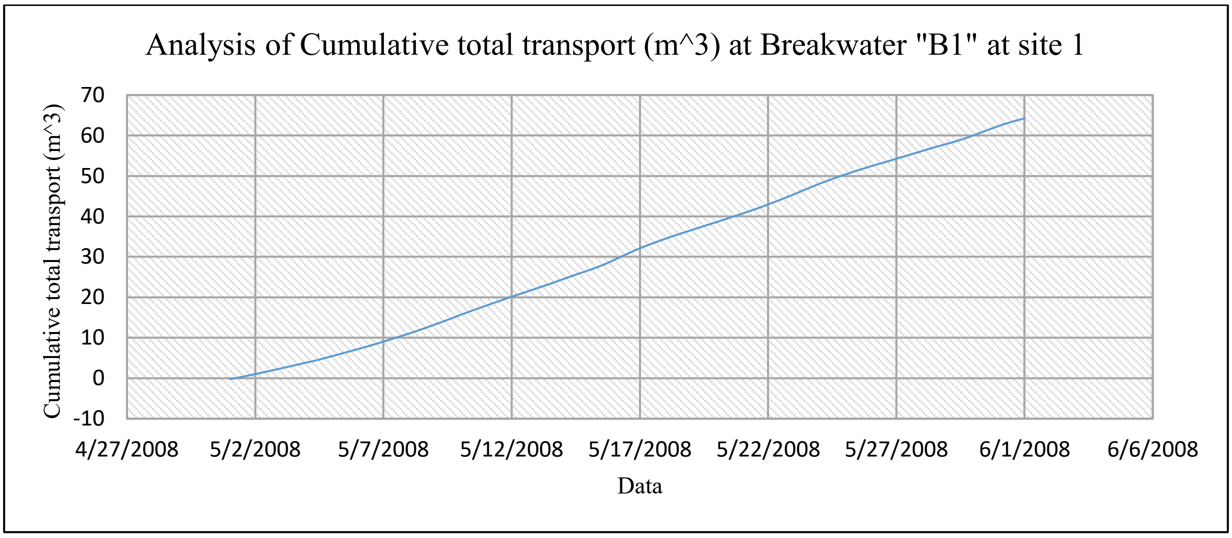

Analysis of Cumulative total transport (m^3) at Breakwater "B1" at site 1
Cumulative total transport (m^3)
70
60
50
40
30
20
10
0
-10
4/27/2008
5/2/2008
5/7/2008
5/12/2008
5/17/2008
5/22/2008
5/27/2008
6/1/2008
6/6/2008
Data

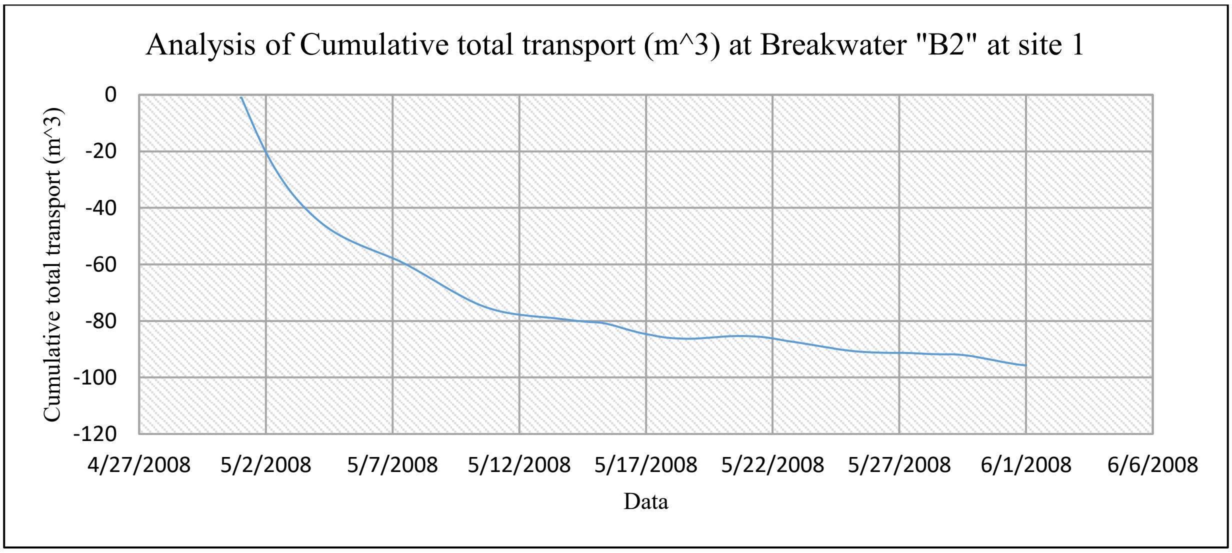

Analysis of Cumulative total transport (m^3) at Breakwater "B2" at site 1
Cumulative total transport (m^3)
0
-20
-40
-60
-80
-100
-120
4/27/2008
5/2/2008
5/7/2008
5/12/2008
5/17/2008
5/22/2008
5/27/2008
6/1/2008
6/6/2008
Data

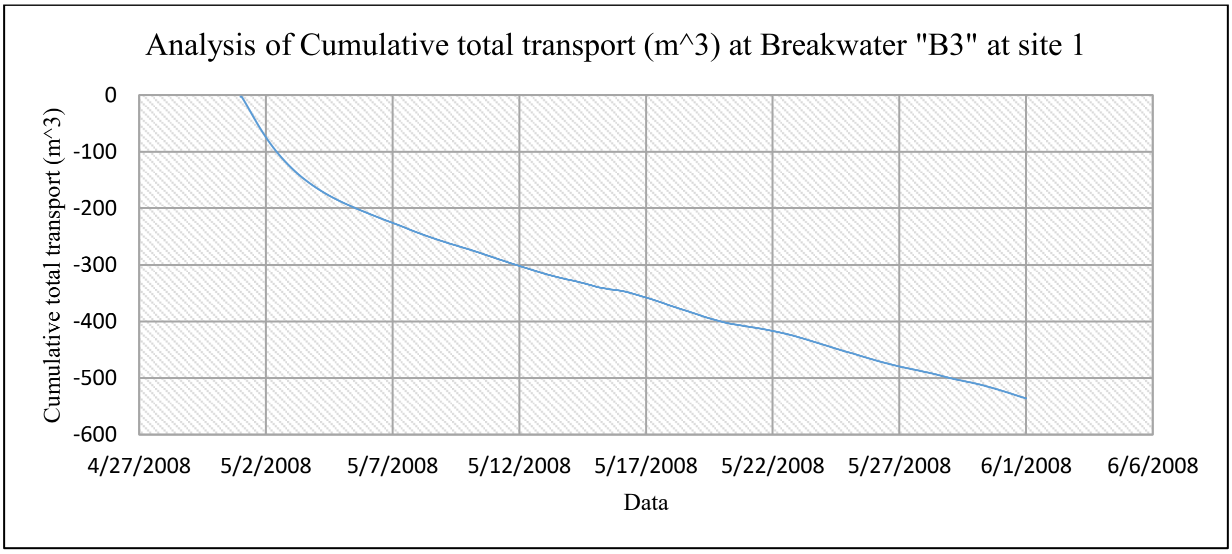

Analysis of Cumulative total transport (m^3) at Breakwater "B3" at site 1
Cumulative total transport (m^3)
0
-100
-200
-300
-400
-500
-600
4/27/2008
5/2/2008
5/7/2008
5/12/2008
5/17/2008
5/22/2008
5/27/2008
6/1/2008
6/6/2008
Data

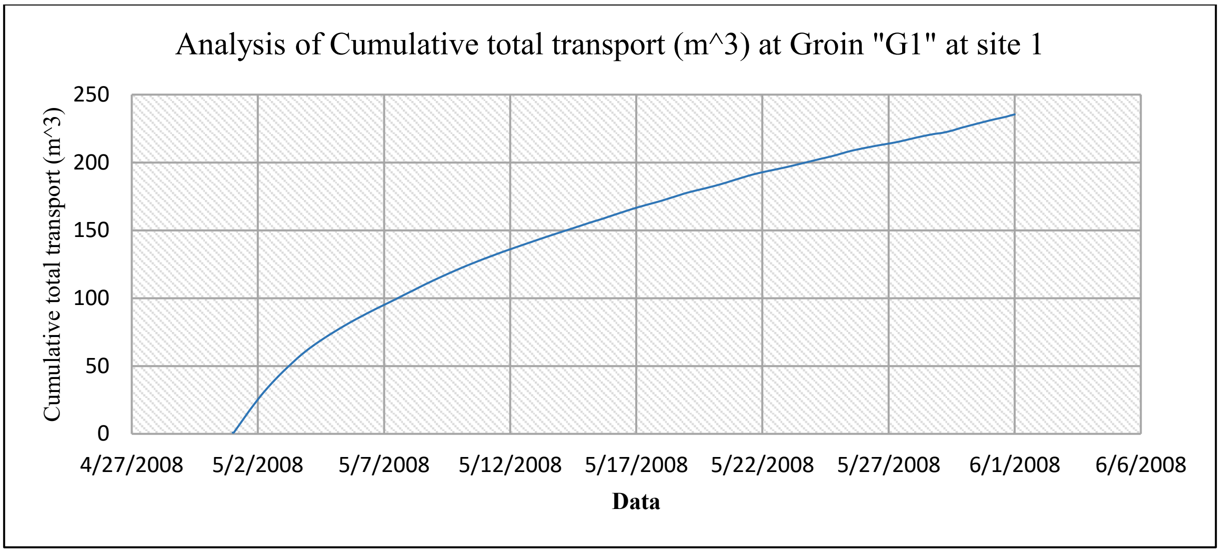
Analysis of Cumulative total transport (m^3) at Groin "G1" at site 1
Cumulative total transport (m^3)
250
200
150
100
50
0
4/27/2008
5/2/2008
5/7/2008
5/12/2008
5/17/2008
5/22/2008
5/27/2008
6/1/2008
6/6/2008
Data

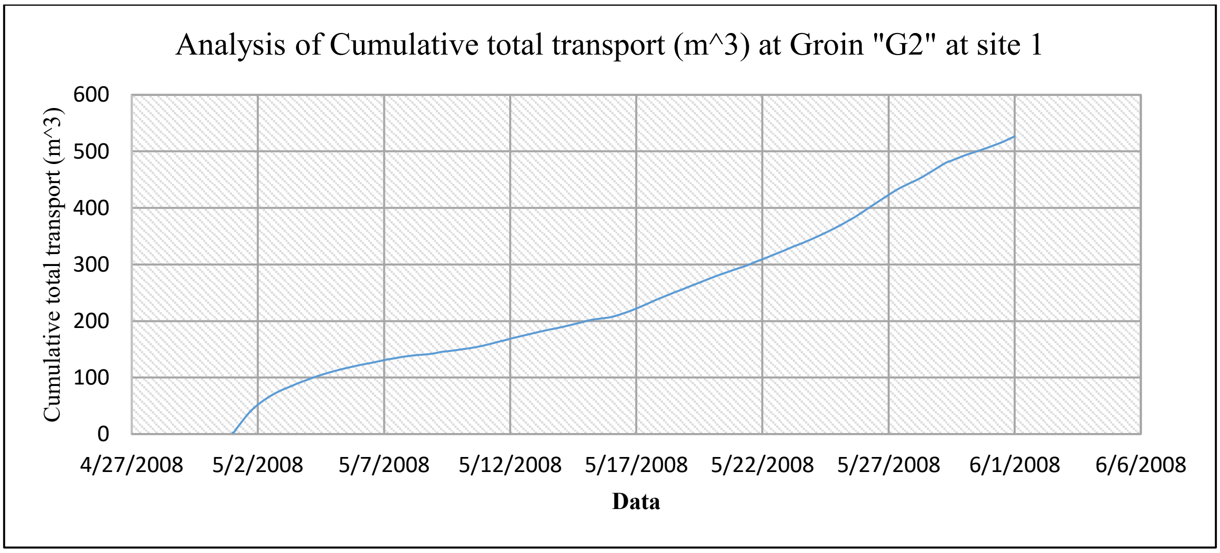
Analysis of Cumulative total transport (m^3) at Groin "G2" at site 1
Cumulative total transport (m^3)
600
500
400
300
200
100
0
4/27/2008
5/2/2008
5/7/2008
5/12/2008
5/17/2008
5/22/2008
5/27/2008
6/1/2008
6/6/2008
Data

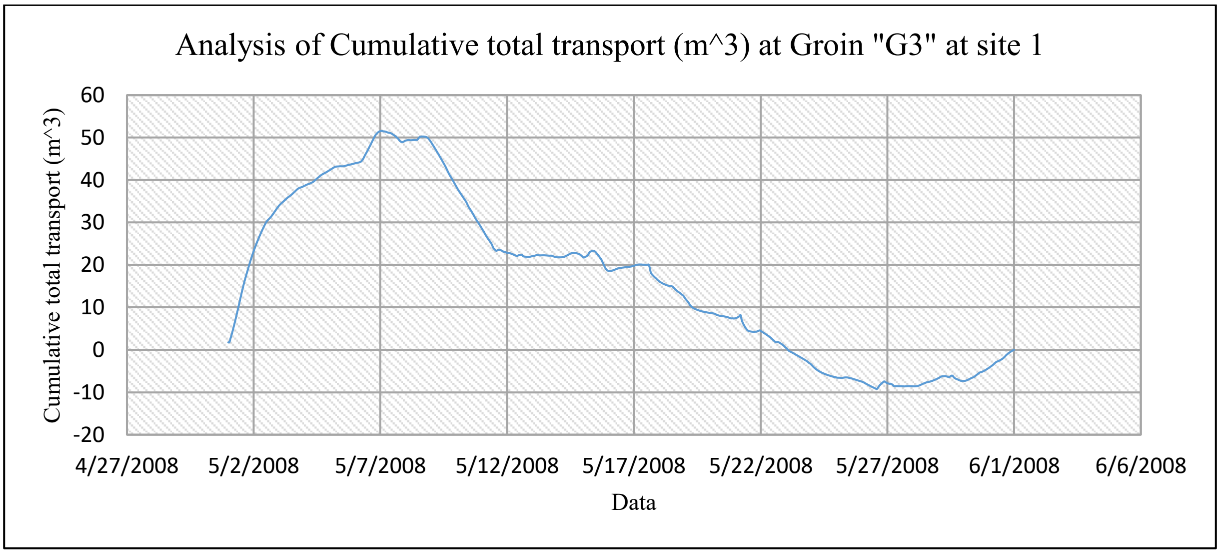
Analysis of Cumulative total transport (m^3) at Groin "G3" at site 1
Cumulative total transport (m^3)
60
50
40
30
20
10
0
-10
-20
4/27/2008
5/2/2008
5/7/2008
5/12/2008
5/17/2008
5/22/2008
5/27/2008
6/1/2008
6/6/2008
Data

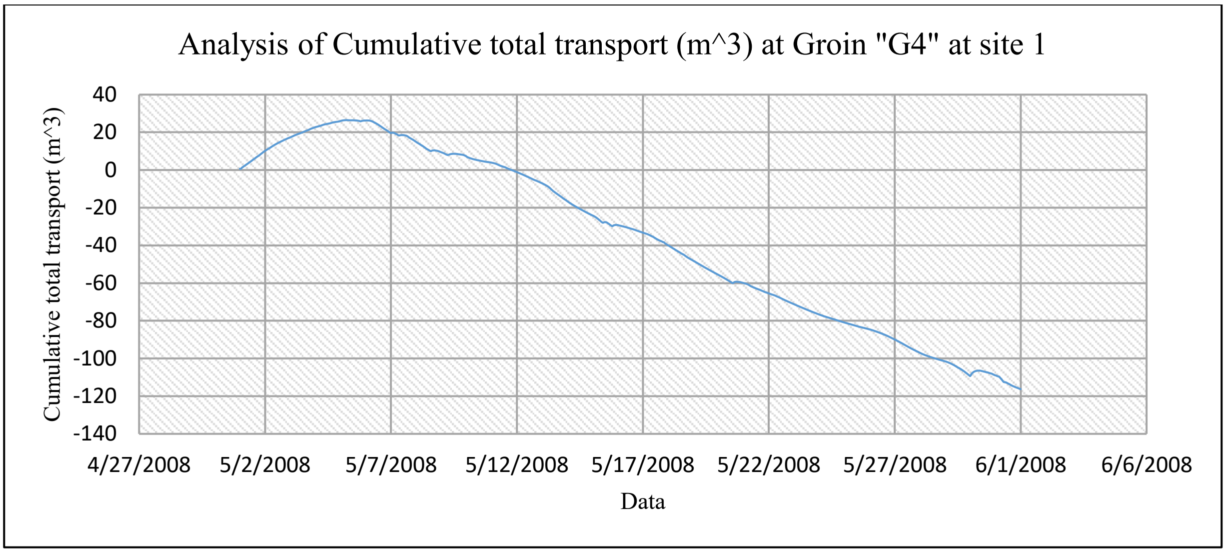

Analysis of Cumulative total transport (m^3) at Groin "G4" at site 1
Cumulative total transport (m^3)
40
20
0
-20
-40
-60
-80
-100
-120
-140
4/27/2008
5/2/2008
5/7/2008
5/12/2008
5/17/2008
5/22/2008
5/27/2008
6/1/2008
6/6/2008
Data

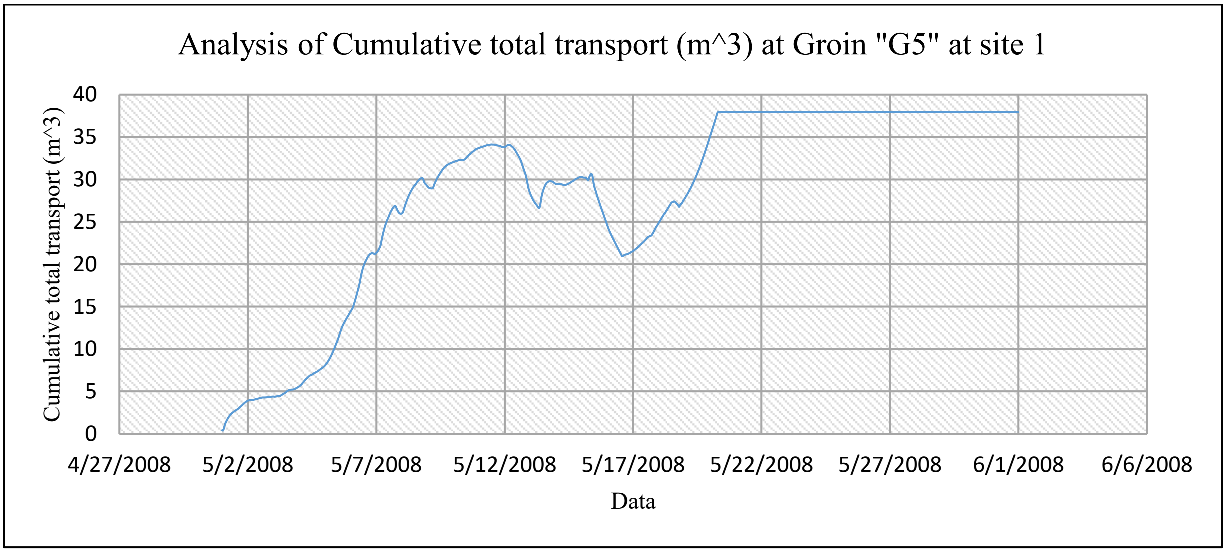

Analysis of Cumulative total transport (m^3) at Groin "G5" at site 1
Cumulative total transport (m^3)
40
35
30
25
20
15
10
5
0
4/27/2008
5/2/2008
5/7/2008
5/12/2008
5/17/2008
5/22/2008
5/27/2008
6/1/2008
6/6/2008
Data

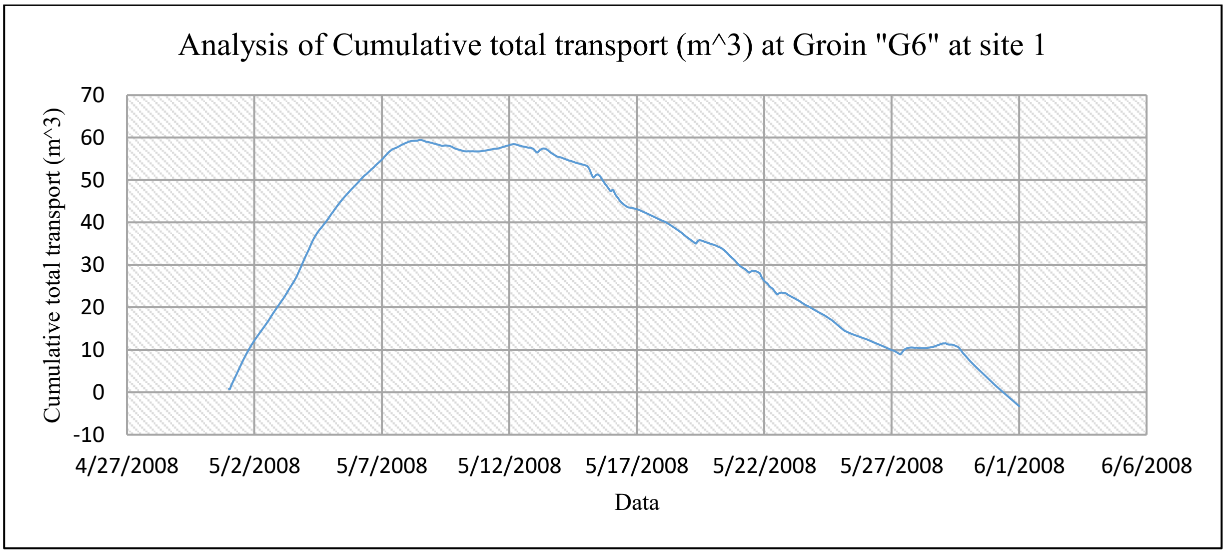

Analysis of Cumulative total transport (m^3) at Groin "G6" at site 1
Cumulative total transport (m^3)
70
60
50
40
30
20
10
0
-10
4/27/2008
5/2/2008
5/7/2008
5/12/2008
5/17/2008
5/22/2008
5/27/2008
6/1/2008
6/6/2008
Data

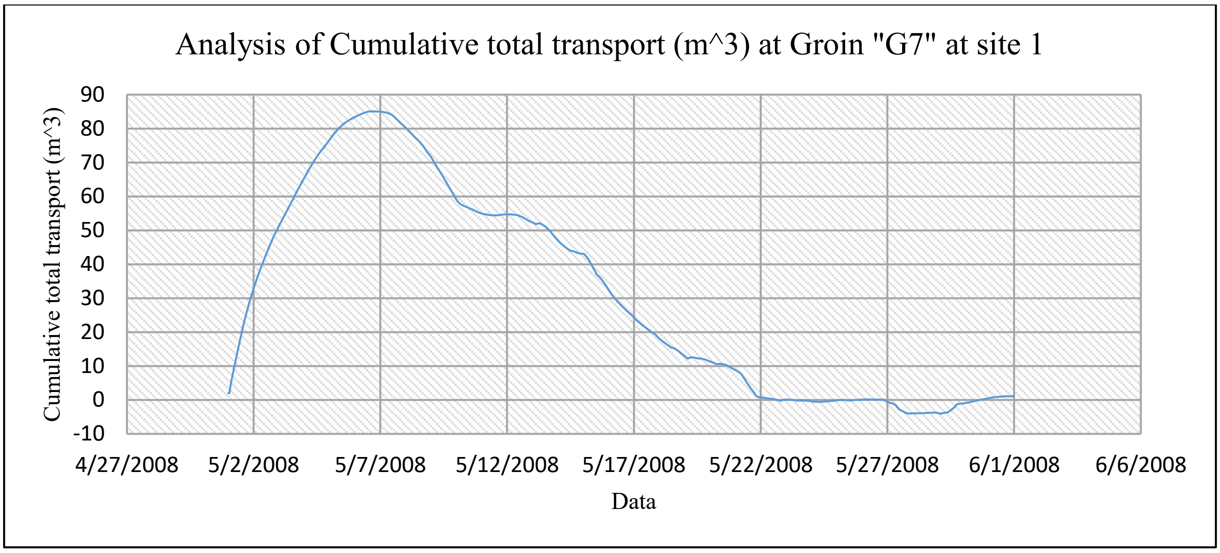
Analysis of Cumulative total transport (m^3) at Groin "G7" at site 1
Cumulative total transport (m^3)
90
80
70
60
50
40
30
20
10
0
-10
4/27/2008
5/2/2008
5/7/2008
5/12/2008
5/17/2008
5/22/2008
5/27/2008
6/1/2008
6/6/2008
Data

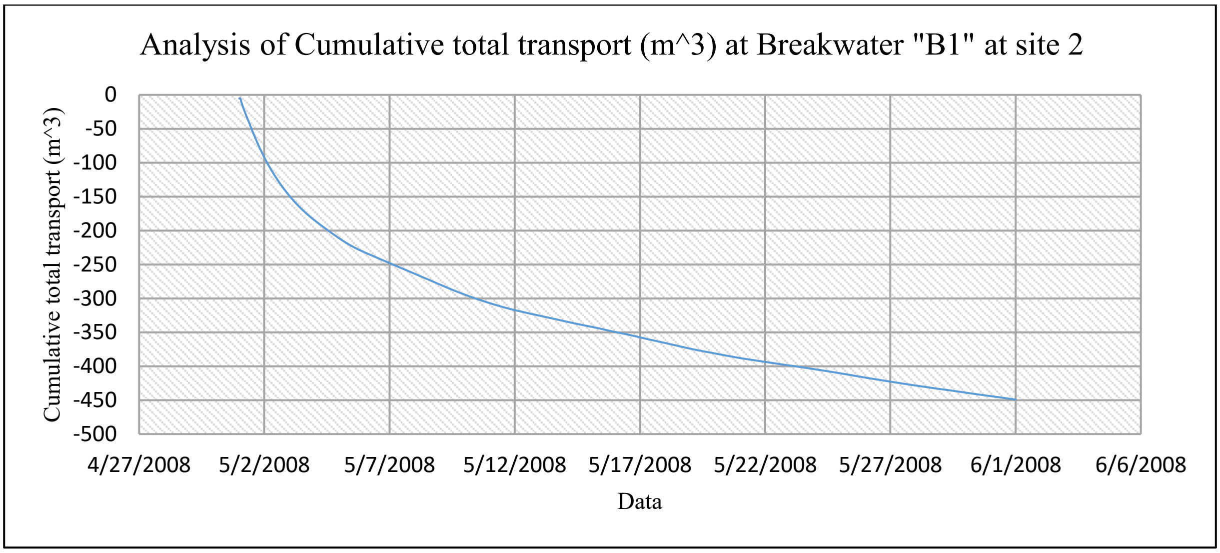
Analysis of Cumulative total transport (m^3) at Breakwater "B1" at site 2
Cumulative total transport (m^3)
0
-50
-100
-150
-200
-250
-300
-350
-400
-450
-500
4/27/2008
5/2/2008
5/7/2008
5/12/2008
5/17/2008
5/22/2008
5/27/2008
6/1/2008
6/6/2008
Data

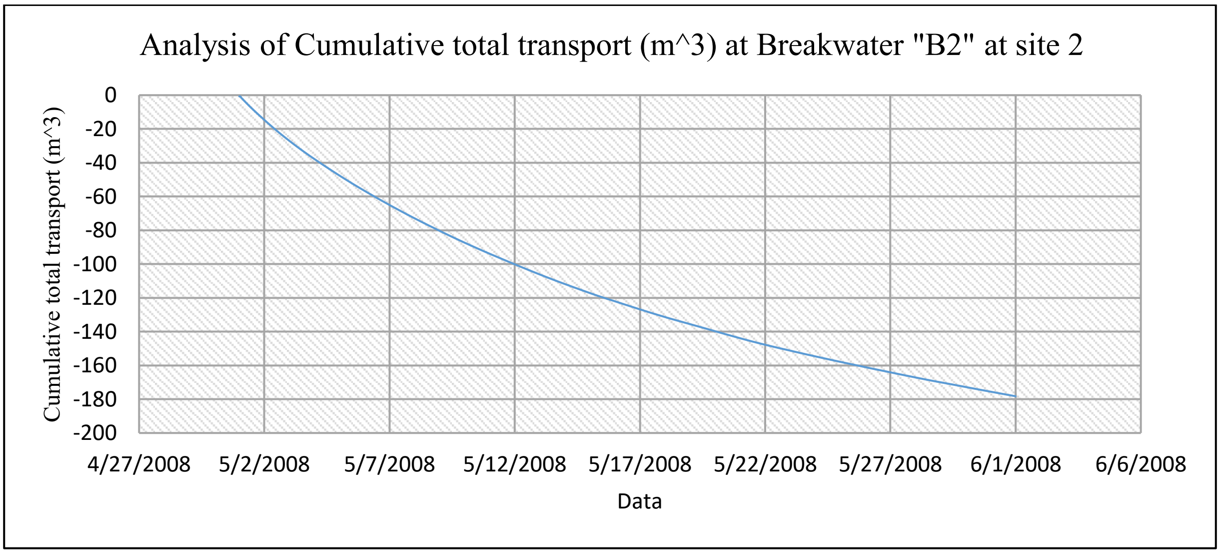
Analysis of Cumulative total transport (m^3) at Breakwater "B2" at site 2
Cumulative total transport (m^3)
0
-20
-40
-60
-80
-100
-120
-140
-160
-180
-200
4/27/2008
5/2/2008
5/7/2008
5/12/2008
5/17/2008
5/22/2008
5/27/2008
6/1/2008
6/6/2008
Data

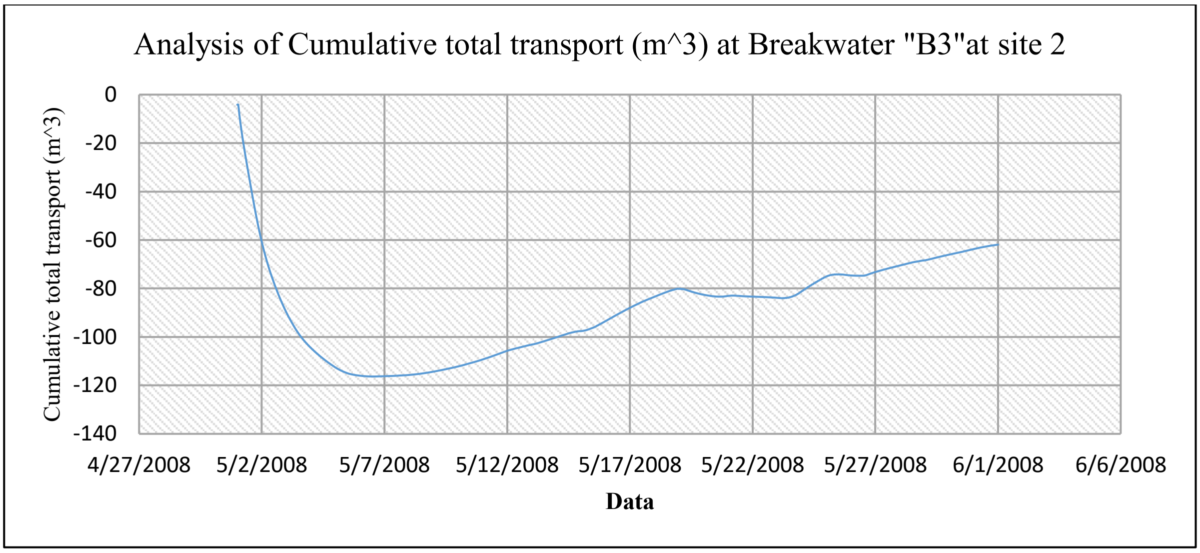
Analysis of Cumulative total transport (m^3) at Breakwater "B3"at site 2
Cumulative total transport (m^3)
0
-20
-40
-60
-80
-100
-120
-140
4/27/2008
5/2/2008
5/7/2008
5/12/2008
5/17/2008
5/22/2008
5/27/2008
6/1/2008
6/6/2008
Data

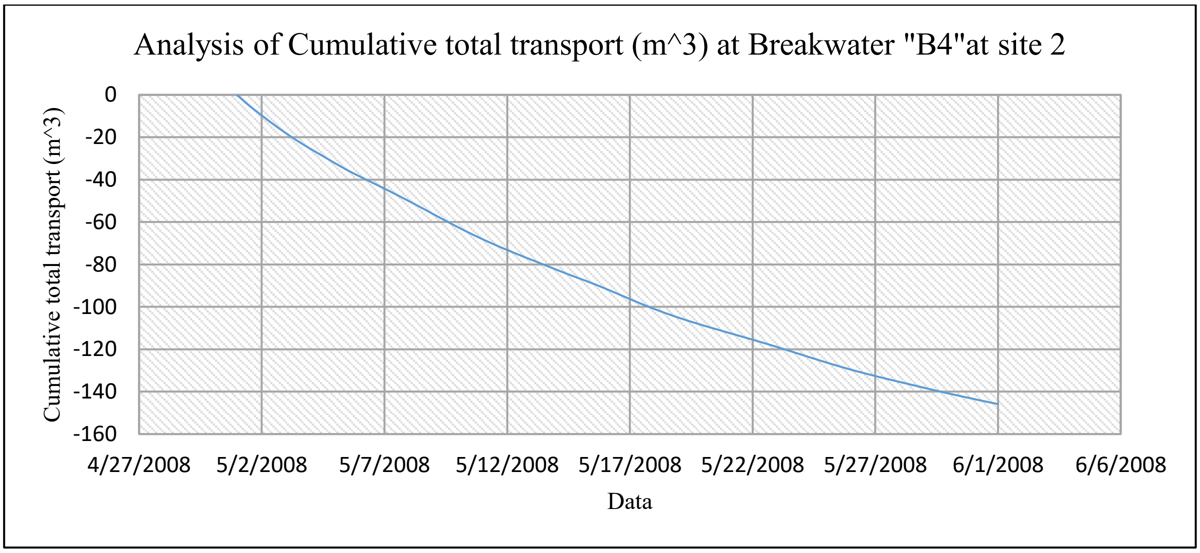
Analysis of Cumulative total transport (m^3) at Breakwater "B4"at site 2
Cumulative total transport (m^3)
0
-20
-40
-60
-80
-100
-120
-140
-160
4/27/2008
5/2/2008
5/7/2008
5/12/2008
5/17/2008
5/22/2008
5/27/2008
6/1/2008
6/6/2008
Data

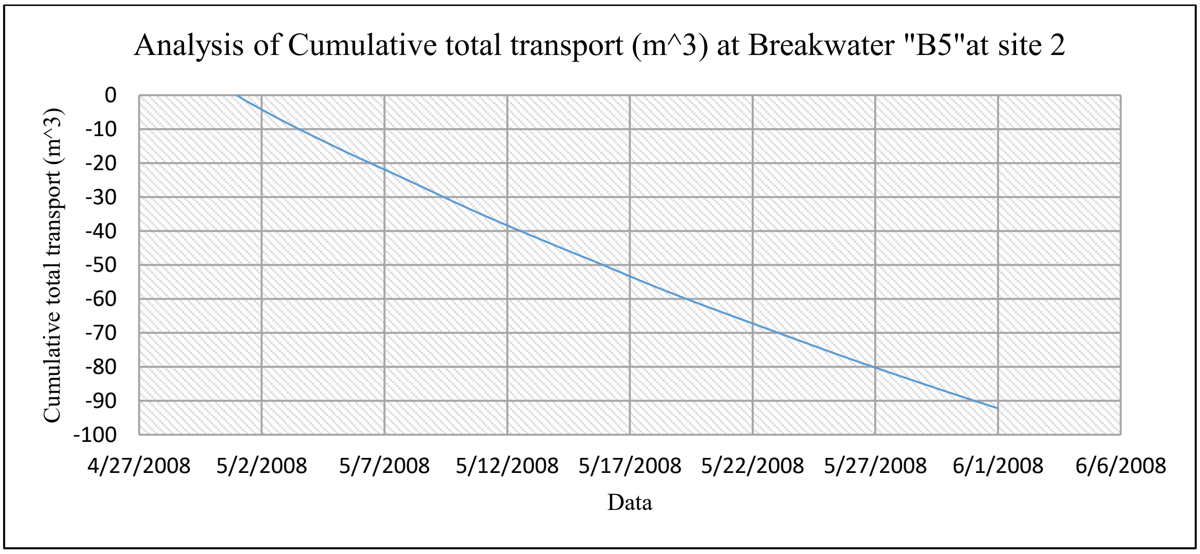
Analysis of Cumulative total transport (m^3) at Breakwater "B5"at site 2
Cumulative total transport (m^3)
0
-10
-20
-30
-40
-50
-60
-70
-80
-90
-100
4/27/2008
5/2/2008
5/7/2008
5/12/2008
5/17/2008
5/22/2008
5/27/2008
6/1/2008
6/6/2008
Data

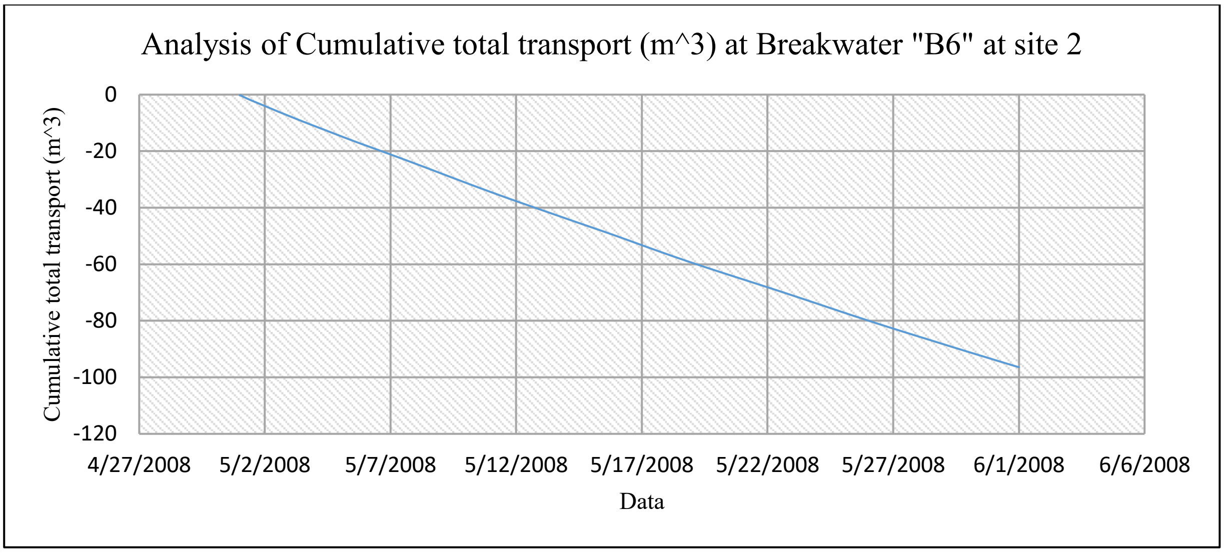
Analysis of Cumulative total transport (m^3) at Breakwater "B6" at site 2
Cumulative total transport (m^3)
0
-20
-40
-60
-80
-100
-120
4/27/2008
5/2/2008
5/7/2008
5/12/2008
5/17/2008
5/22/2008
5/27/2008
6/1/2008
6/6/2008
Data

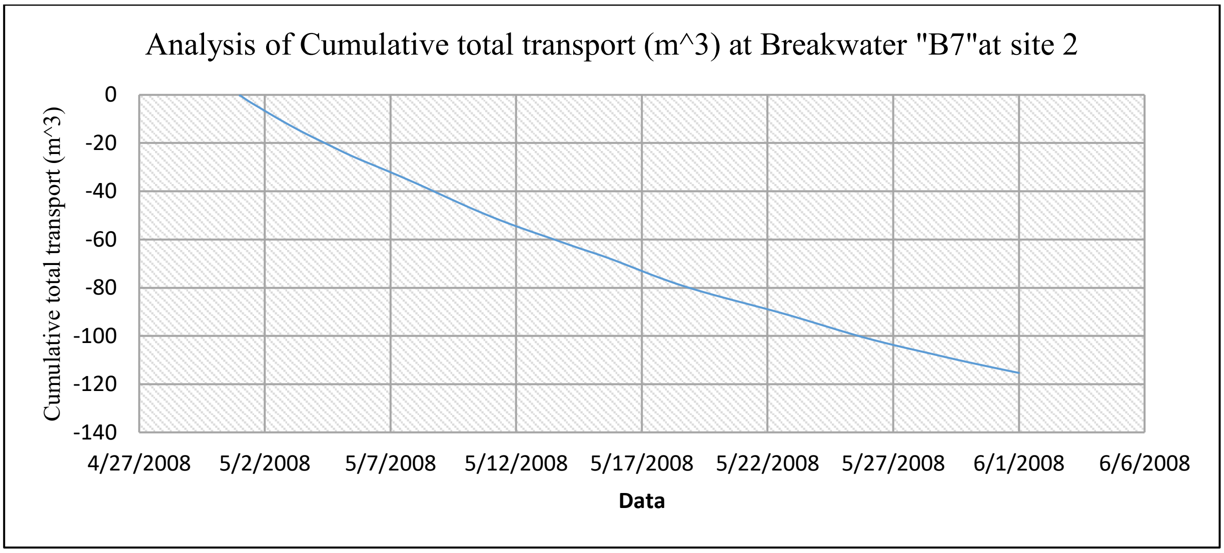
Analysis of Cumulative total transport (m^3) at Breakwater "B7"at site 2
Cumulative total transport (m^3)
0
-20
-40
-60
-80
-100
-120
-140
4/27/2008
5/2/2008
5/7/2008
5/12/2008
5/17/2008
5/22/2008
5/27/2008
6/1/2008
6/6/2008
Data

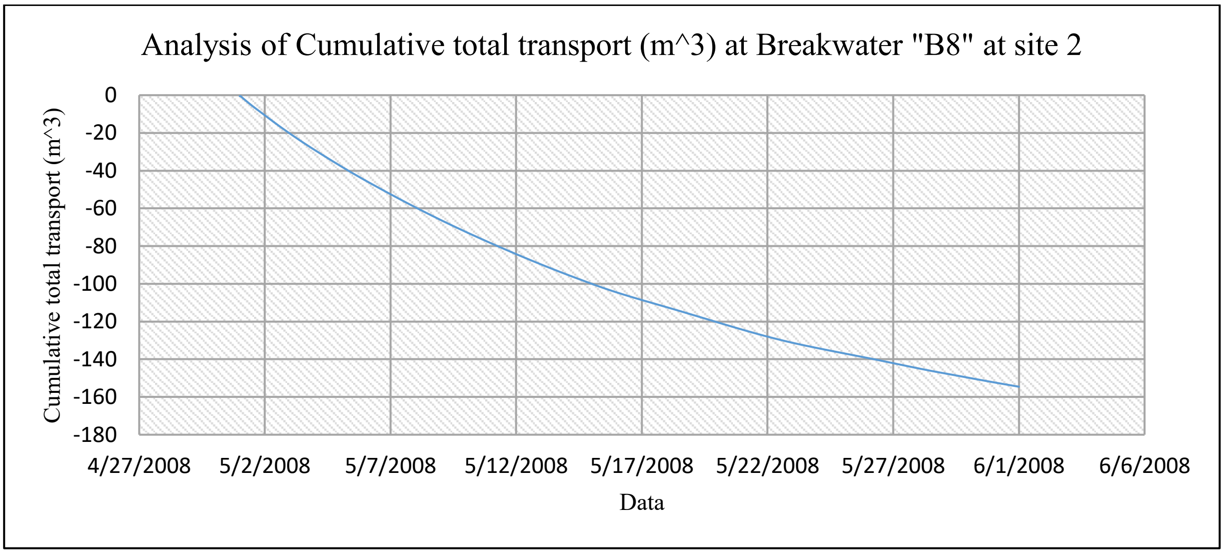
Analysis of Cumulative total transport (m^3) at Breakwater "B8" at site 2
Cumulative total transport (m^3)
0
-20
-40
-60
-80
-100
-120
-140
-160
-180
4/27/2008
5/2/2008
5/7/2008
5/12/2008
5/17/2008
5/22/2008
5/27/2008
6/1/2008
6/6/2008
Data

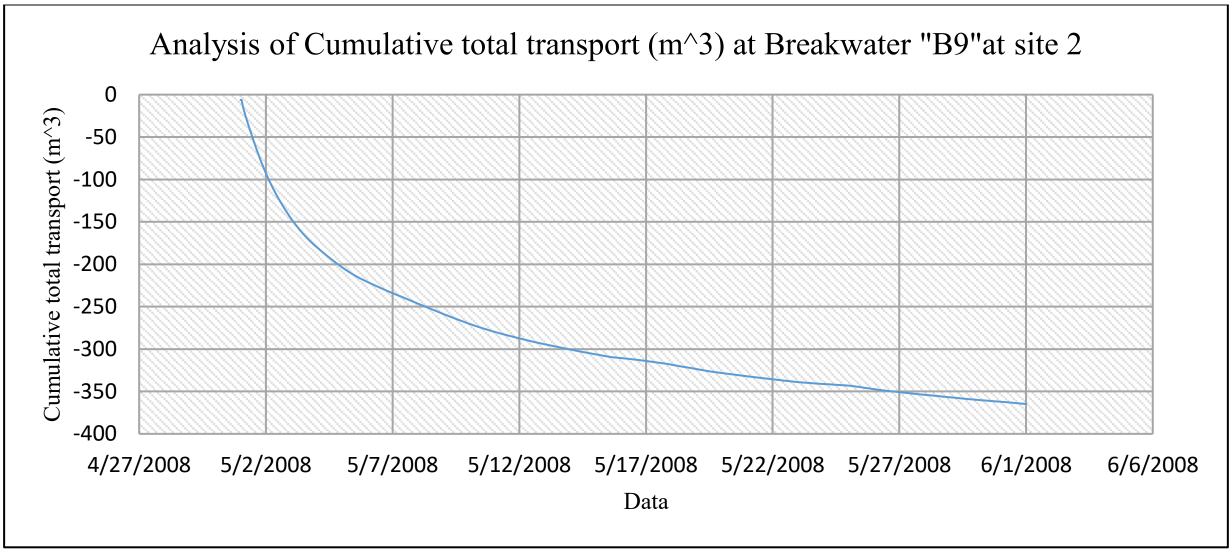
Analysis of Cumulative total transport (m^3) at Breakwater "B9"at site 2
Cumulative total transport (m^3)
0
-50
-100
-150
-200
-250
-300
-350
-400
4/27/2008
5/2/2008
5/7/2008
5/12/2008
5/17/2008
5/22/2008
5/27/2008
6/1/2008
6/6/2008
Data

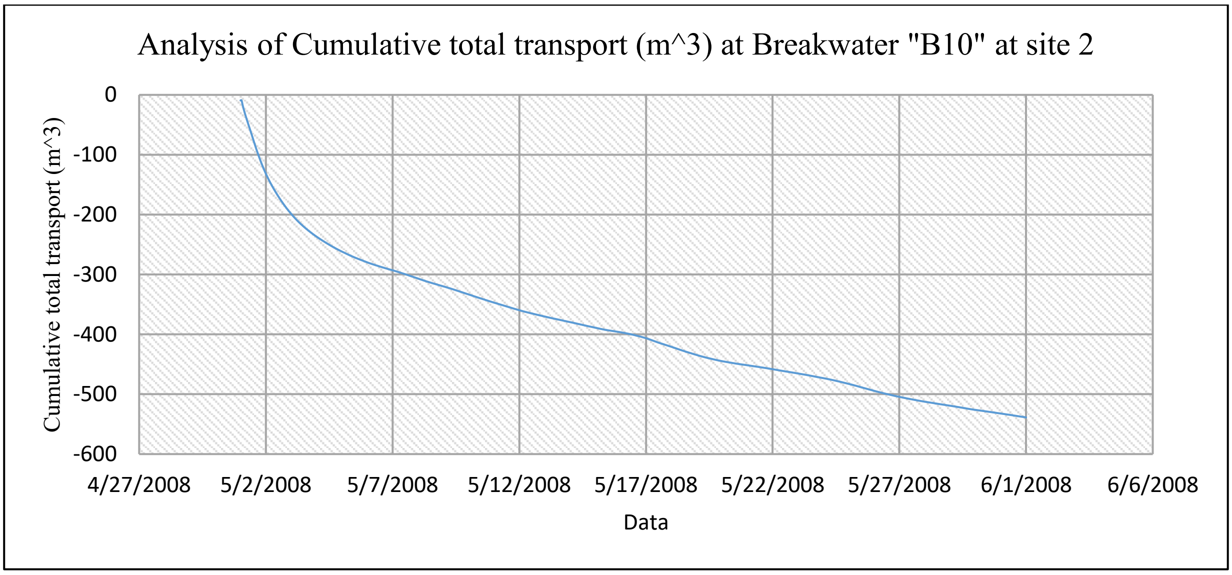
Analysis of Cumulative total transport (m^3) at Breakwater "B10" at site 2
Cumulative total transport (m^3)
0
-100
-200
-300
-400
-500
-600
4/27/2008
5/2/2008
5/7/2008
5/12/2008
5/17/2008
5/22/2008
5/27/2008
6/1/2008
6/6/2008
Data

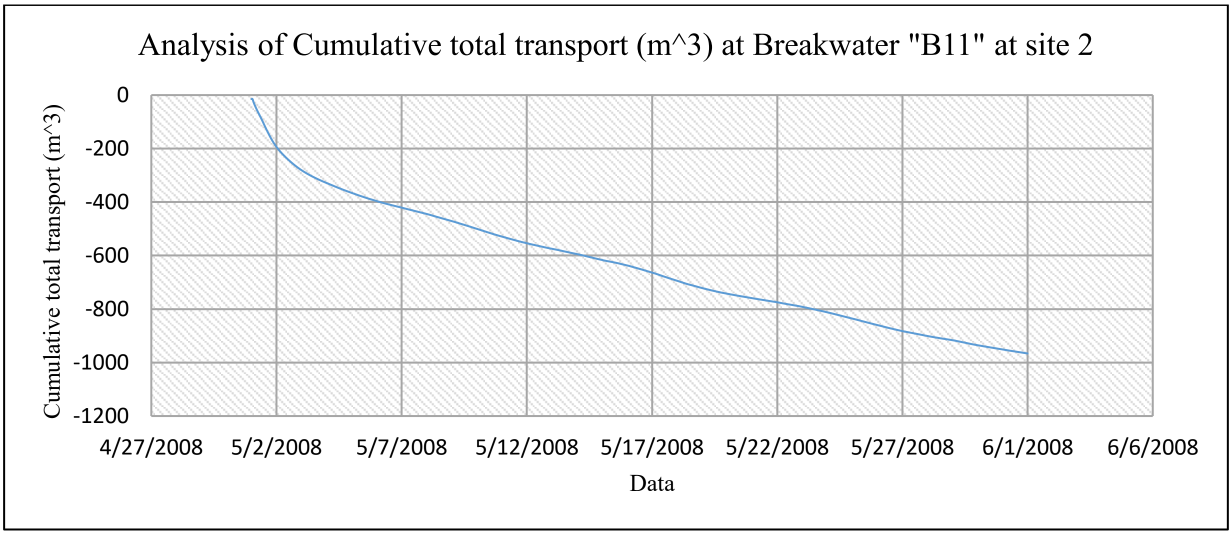
Analysis of Cumulative total transport (m^3) at Breakwater "B11" at site 2
Cumulative total transport (m^3)
0
-200
-400
-600
-800
-1000
-1200
4/27/2008
5/2/2008
5/7/2008
5/12/2008
5/17/2008
5/22/2008
5/27/2008
6/1/2008
6/6/2008
Data

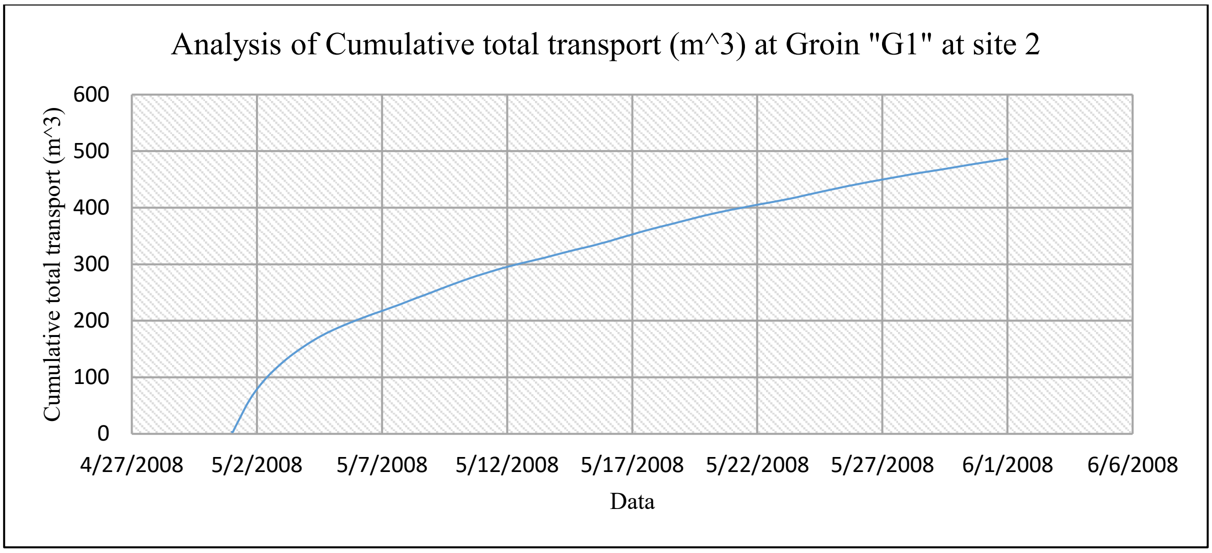
Analysis of Cumulative total transport (m^3) at Groin "G1" at site 2
Cumulative total transport (m^3)
600
500
400
300
200
100
0
4/27/2008
5/2/2008
5/7/2008
5/12/2008
5/17/2008
5/22/2008
5/27/2008
6/1/2008
6/6/2008
Data

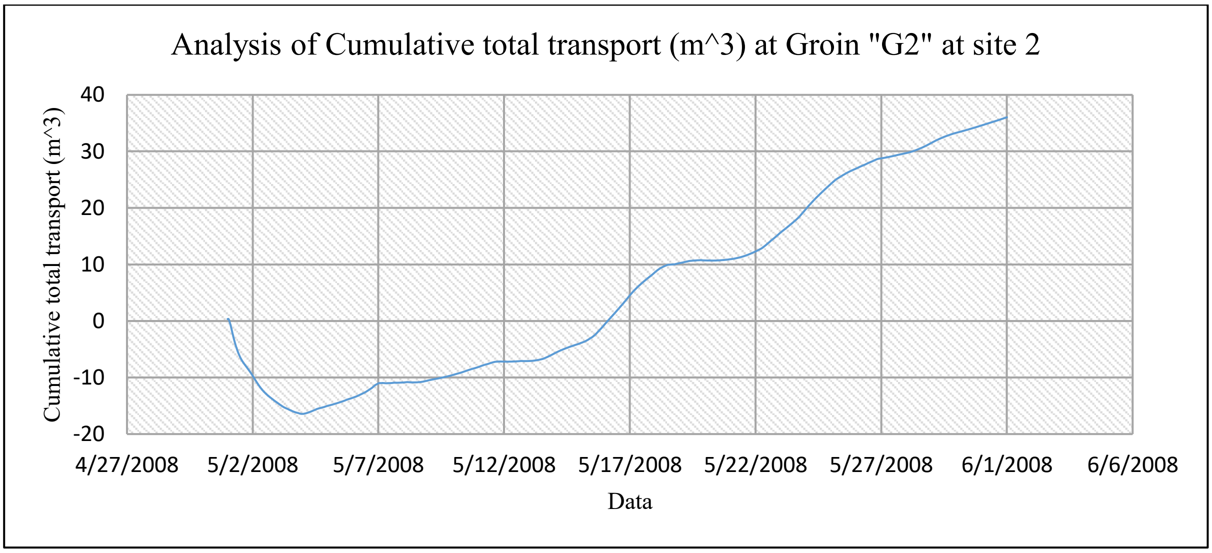
Analysis of Cumulative total transport (m^3) at Groin "G2" at site 2
Cumulative total transport (m^3)
40
30
20
10
0
-10
-20
4/27/2008
5/2/2008
5/7/2008
5/12/2008
5/17/2008
5/22/2008
5/27/2008
6/1/2008
6/6/2008
Data

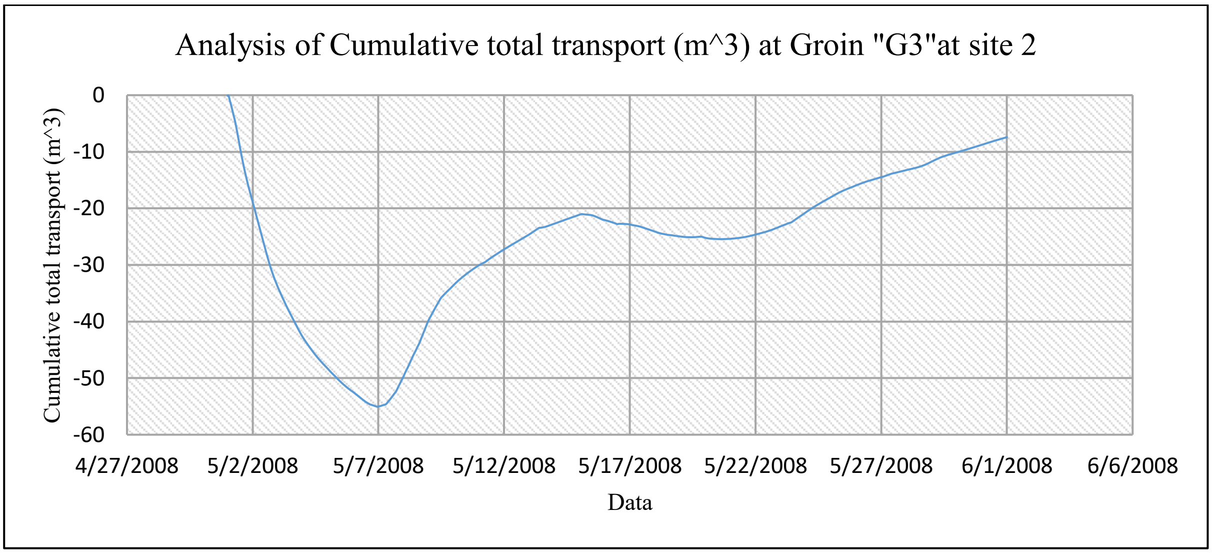
Analysis of Cumulative total transport (m^3) at Groin "G3"at site 2
Cumulative total transport (m^3)
0
-10
-20
-30
-40
-50
-60
4/27/2008
5/2/2008
5/7/2008
5/12/2008
5/17/2008
5/22/2008
5/27/2008
6/1/2008
6/6/2008
Data

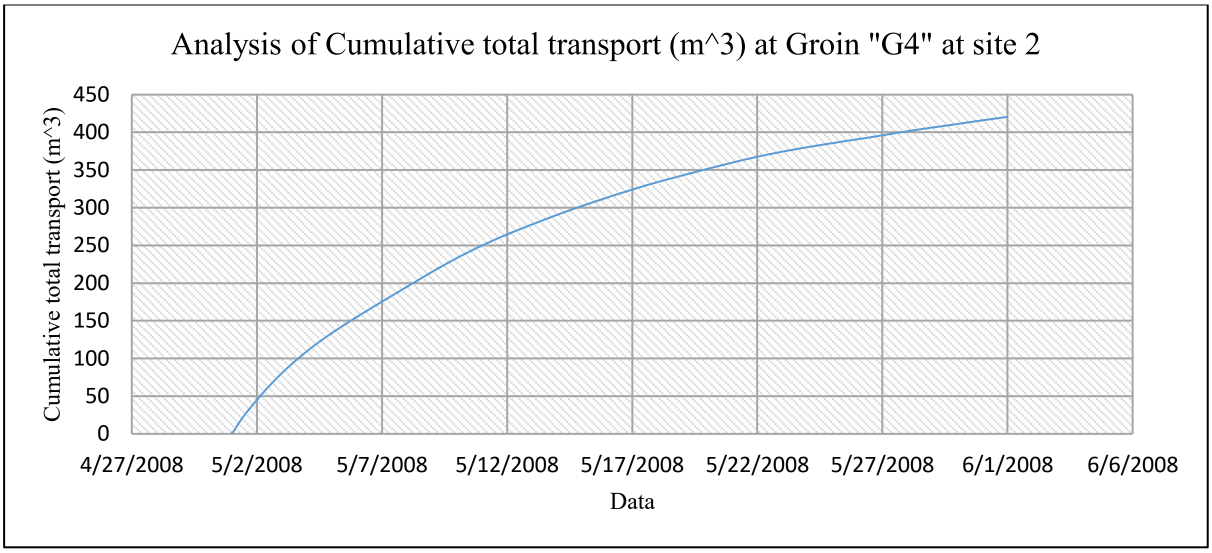

Analysis of Cumulative total transport (m^3) at Groin "G4" at site 2
Cumulative total transport (m^3)
450
400
350
300
250
200
150
100
50
0
4/27/2008
5/2/2008
5/7/2008
5/12/2008
5/17/2008
5/22/2008
5/27/2008
6/1/2008
6/6/2008
Data

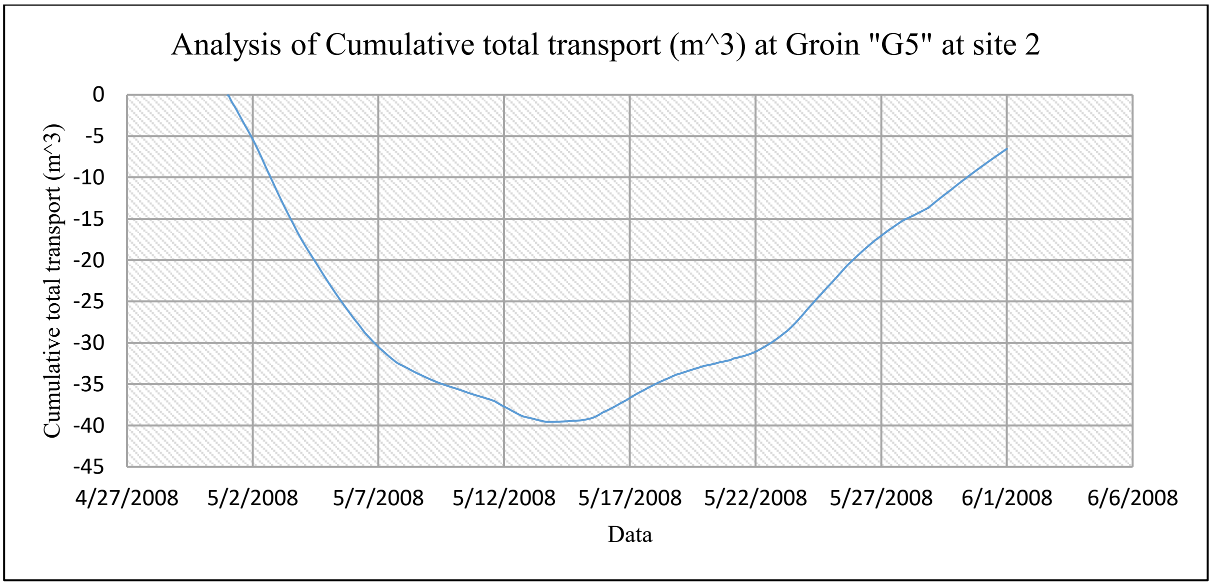

Analysis of Cumulative total transport (m^3) at Groin "G5" at site 2
Cumulative total transport (m^3)
0
-5
-10
-15
-20
-25
-30
-35
-40
-45
4/27/2008
5/2/2008
5/7/2008
5/12/2008
5/17/2008
5/22/2008
5/27/2008
6/1/2008
6/6/2008
Data

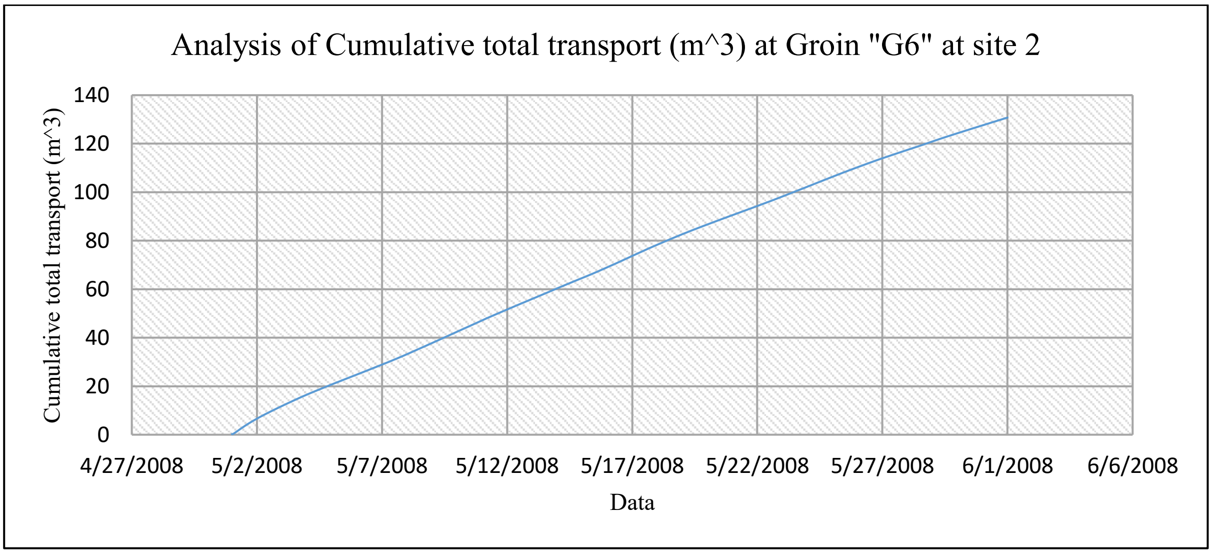

Analysis of Cumulative total transport (m^3) at Groin "G6" at site 2
Cumulative total transport (m^3)
140
120
100
80
60
40
20
0
4/27/2008
5/2/2008
5/7/2008
5/12/2008
5/17/2008
5/22/2008
5/27/2008
6/1/2008
6/6/2008
Data

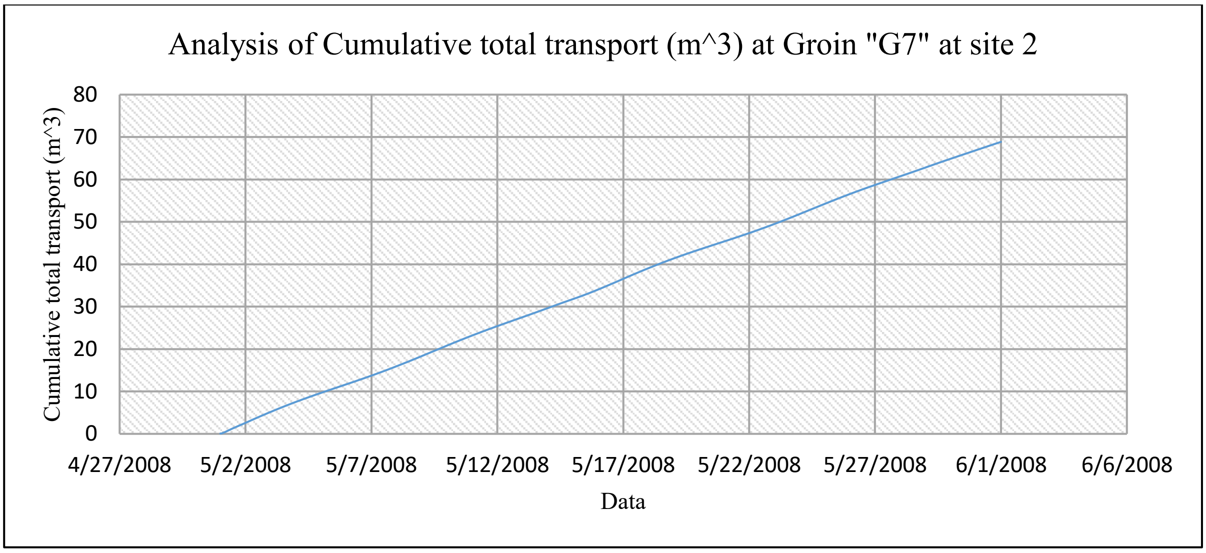

Analysis of Cumulative total transport (m^3) at Groin "G7" at site 2
Cumulative total transport (m^3)
80
70
60
50
40
30
20
10
0
4/27/2008
5/2/2008
5/7/2008
5/12/2008
5/17/2008
5/22/2008
5/27/2008
6/1/2008
6/6/2008
Data

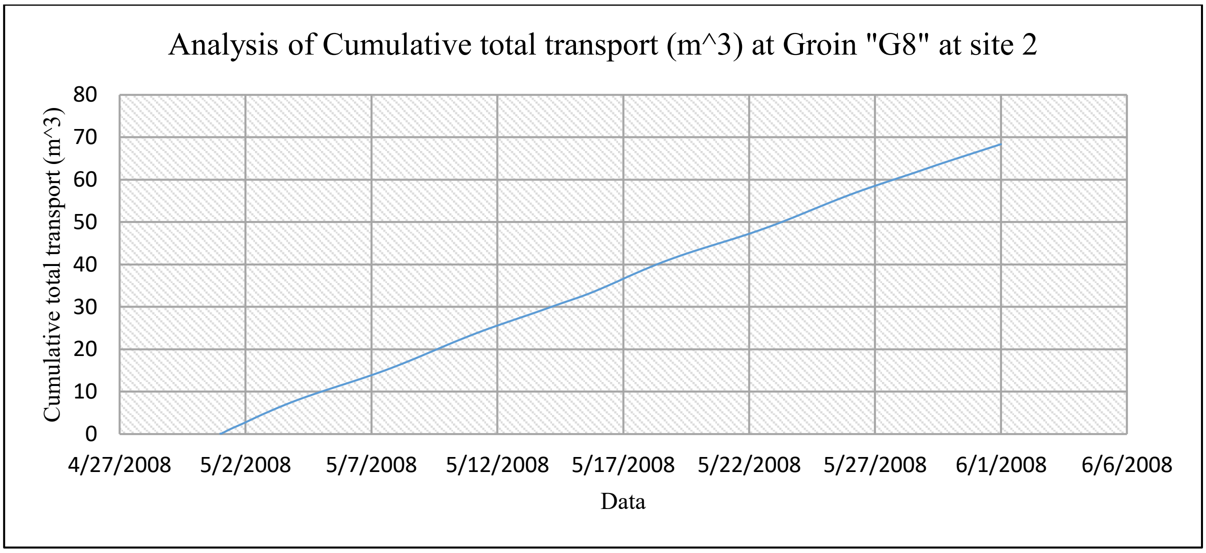

Analysis of Cumulative total transport (m^3) at Groin "G8" at site 2
Cumulative total transport (m^3)
80
70
60
50
40
30
20
10
0
4/27/2008
5/2/2008
5/7/2008
5/12/2008
5/17/2008
5/22/2008
5/27/2008
6/1/2008
6/6/2008
Data

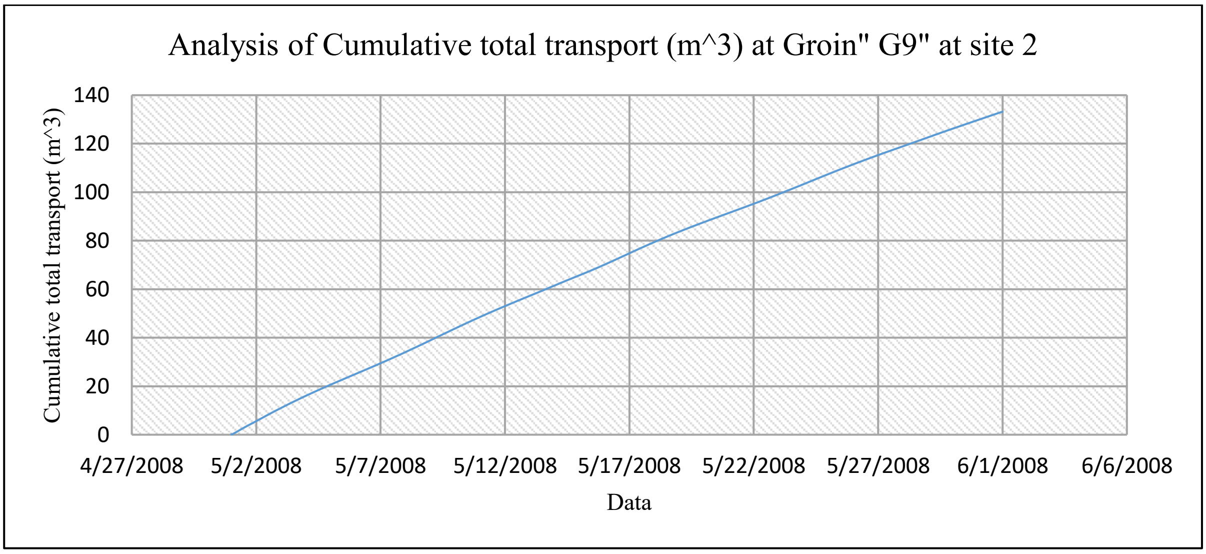

Analysis of Cumulative total transport (m^3) at Groin" G9" at site 2
Cumulative total transport (m^3)
140
120
100
80
60
40
20
0
4/27/2008
5/2/2008
5/7/2008
5/12/2008
5/17/2008
5/22/2008
5/27/2008
6/1/2008
6/6/2008
Data

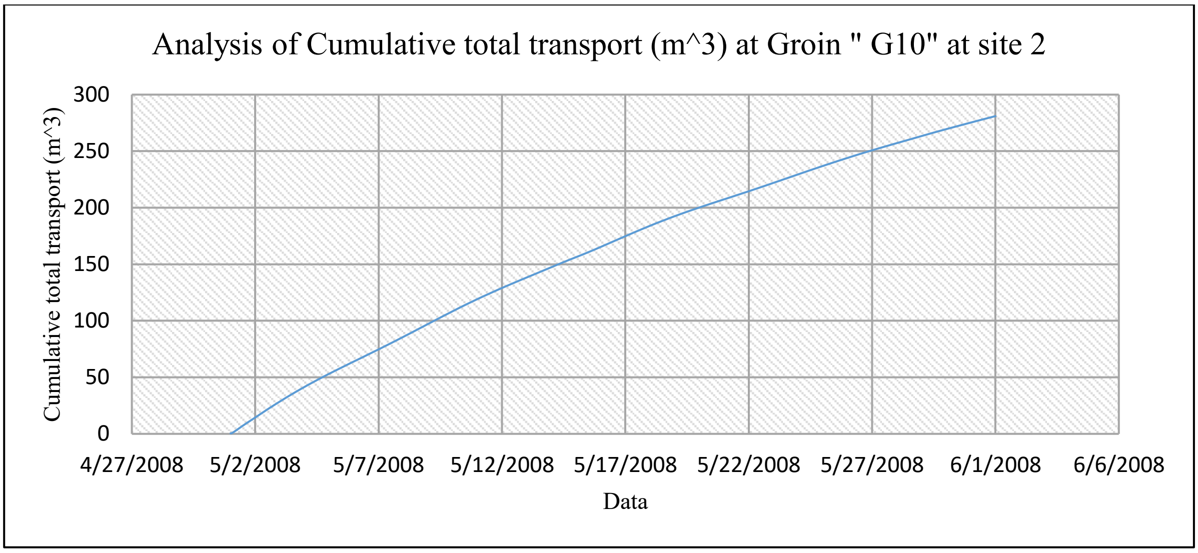
Analysis of Cumulative total transport (m^3) at Groin " G10" at site 2
Cumulative total transport (m^3)
300
250
200
150
100
50
0
4/27/2008
5/2/2008
5/7/2008
5/12/2008
5/17/2008
5/22/2008
5/27/2008
6/1/2008
6/6/2008
Data

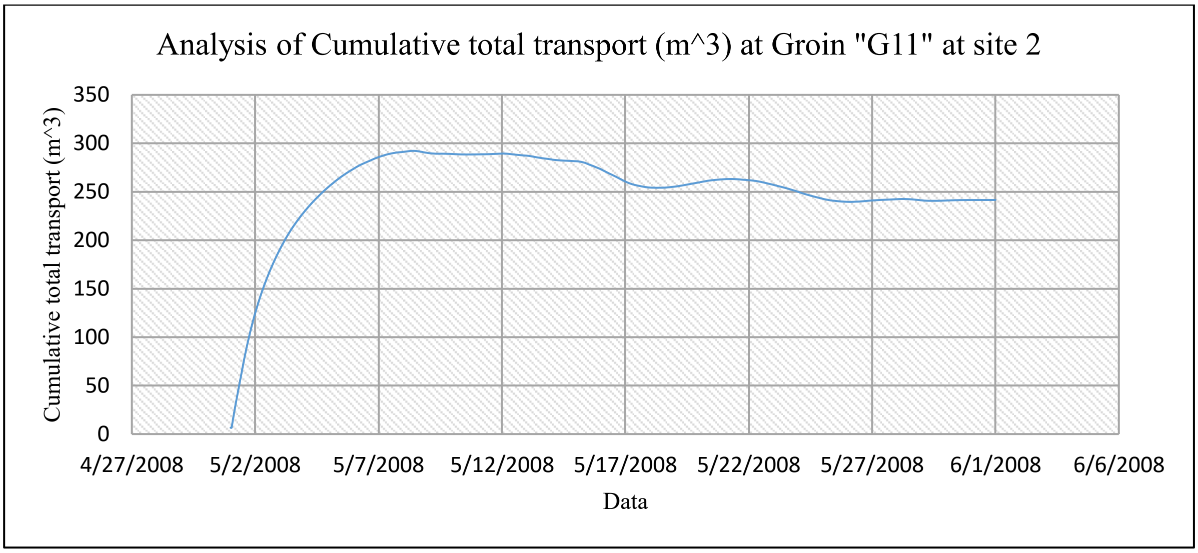
Analysis of Cumulative total transport (m^3) at Groin "G11" at site 2
Cumulative total transport (m^3)
350
300
250
200
150
100
50
0
4/27/2008
5/2/2008
5/7/2008
5/12/2008
5/17/2008
5/22/2008
5/27/2008
6/1/2008
6/6/2008
Data

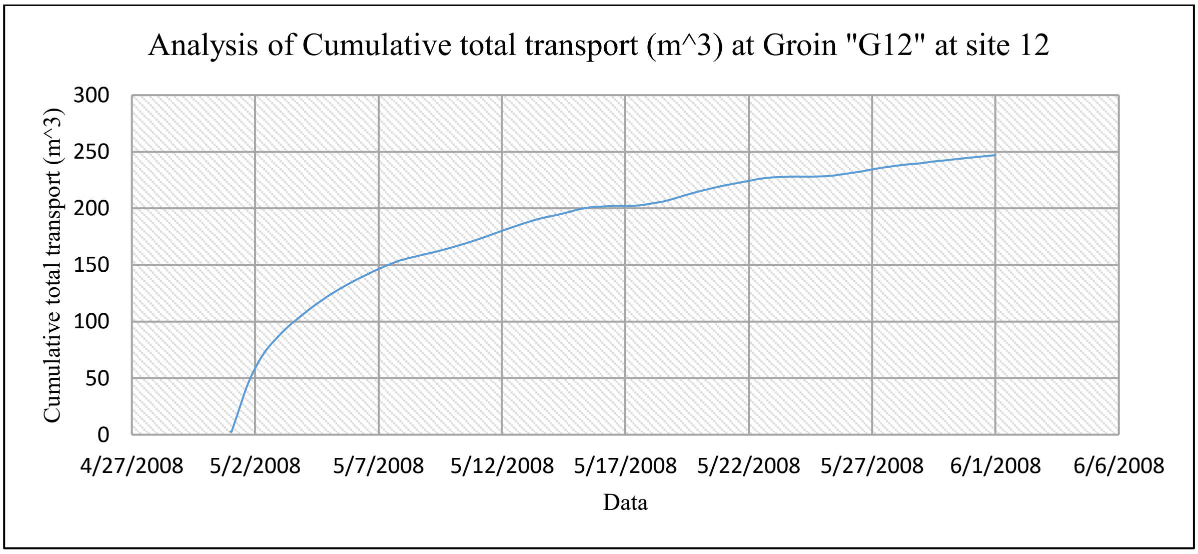
Analysis of Cumulative total transport (m^3) at Groin "G12" at site 12
Cumulative total transport (m^3)
300
250
200
150
100
50
0
4/27/2008
5/2/2008
5/7/2008
5/12/2008
5/17/2008
5/22/2008
5/27/2008
6/1/2008
6/6/2008
Data

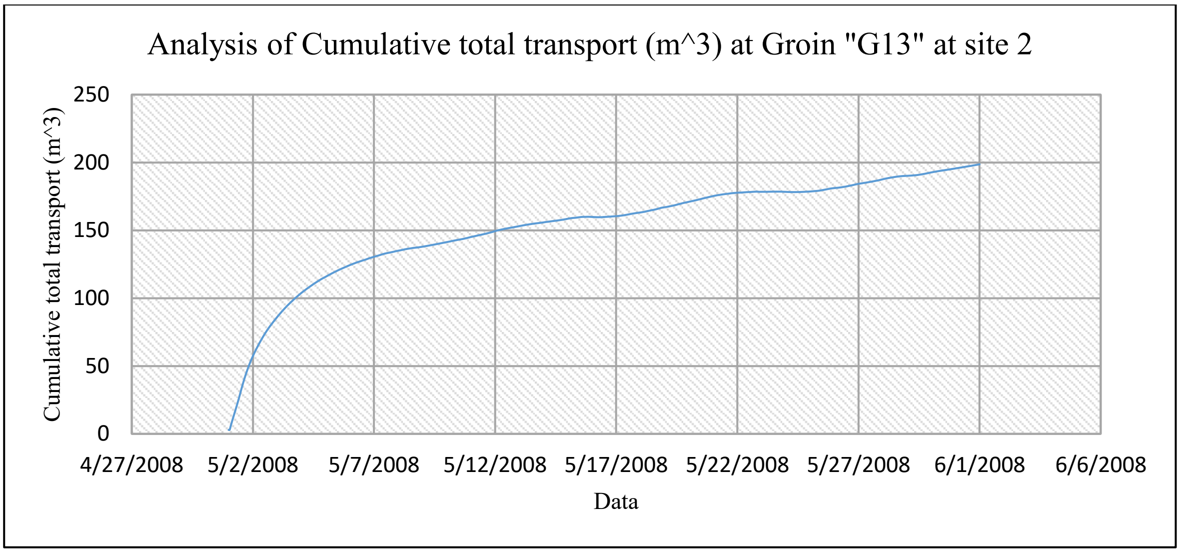
Analysis of Cumulative total transport (m^3) at Groin "G13" at site 2
Cumulative total transport (m^3)
250
200
150
100
50
0
4/27/2008
5/2/2008
5/7/2008
5/12/2008
5/17/2008
5/22/2008
5/27/2008
6/1/2008
6/6/2008
Data